**The Dissertation Committee for Rachel Marie Wypych certifies that this is the approved version of the following dissertation:**

# Thermodynamic Analysis of Protein-Ligand Interactions of Linear Tripeptide HCV NS3 Protease Inhibitors and Progress Toward the Total Synthesis of (±)-Arboridinine

**Committee:**

Stephen F. Martin, Supervisor

Eric V. Anslyn

Adrian T. Keatinge-Clay

Jonathan L. Sessler

Lauren J. Webb

# Thermodynamic Analysis of Protein-Ligand Interactions of Linear Tripeptide HCV NS3 Protease Inhibitors and Progress Toward the Total Synthesis of (±)-Arboridinine

**by**

**Rachel Marie Wypych**

**Dissertation**

Presented to the Faculty of the Graduate School of

The University of Texas at Austin

in Partial Fulfillment

of the Requirements

for the Degree of

**Doctor of Philosophy**

**The University of Texas at Austin**

**August 2017**

# Dedication

To my parents, my sister Jill, and Justin, for your unending love and support.

# Acknowledgements

First and foremost, I would like to wholeheartedly thank my advisor, Prof. Stephen F. Martin, for his unrelenting support and guidance, and also for teaching me to never be satisfied with results simply at face value and instead to constantly strive for a deeper and more thorough understanding. He has pushed me beyond what I thought I was capable of as a chemist. I would like to also thank my undergraduate advisor, the late Prof. Alan R. Katritzky, as well as my graduate mentor and friend Dr. Judit Beagle (Kovács) for their inspiration and encouragement in my early career.

To the Martin group members that I have had the privilege of working alongside over the last five years: your friendship, both professional and personal, is priceless. I especially want to thank Dr. Amy Bonaparte, Dr. Chao Fang, Dr. Alex Nichols, and Dr. Zhiguo Bian for welcoming me into the Martin group with open arms and serving as valuable mentors at the beginning of my tenure here. Thank you to Dr. John Clements and Dr. James Myslinski for helping me get my bearings in the bio projects and providing helpful ITC support and discussions. I want to thank Dr. Amy Bonaparte and Alicia Gravenstreter for their helpful discussions and for always providing a compassionate ear in times of trouble. I want to thank Zach White, Michael Wood, and Sam Etkind for all of their helpful discussions and for making Lab 3 a home over the years. I also would like to thank my undergraduate assistant Paul Bernard for his support as a colleague and friend during the year of my candidacy exam. I would especially like to thank Zach White, Alicia Gravenstreter, and Lance Lepovitz for editing sections of this dissertation. I also extend my thanks to the mass spectrometry and NMR facilities; specifically, Dr. Ben Shoulders, Angela Spangenberg, and Steve Sorey.

# Thermodynamic Analysis of Protein-Ligand Interactions of Linear Tripeptide HCV NS3 Protease Inhibitors and Progress Toward the Total Synthesis of (±)-Arboridinine

Rachel Marie Wypych, Ph.D.

The University of Texas at Austin, 2017

Supervisor: Stephen F. Martin

Interactions between proteins and small molecules dictate an overwhelmingly large number of biological processes, yet our knowledge of the effects of ligand structural changes on the thermodynamics of these interactions is fundamentally lacking. In an effort to expand our understanding of protein-ligand thermodynamics, the binding profiles of a series of linear tripeptide HCV NS3 protease inhibitors were analyzed by ITC. Substituents on the P2 proline residue were examined individually, and important trends were elucidated. The addition of a phenyl group to the 2-position of the heteroaryl subunit of the P2 residue resulted in more favorable binding entropy, which is possibly due to the desolvation of nonpolar surface area. Quinolines without a 2-phenyl substituent were found to bind in an alternate conformation with thermodynamic profiles that were dominated by favorable binding enthalpies rather than entropies. This could possibly be due to a favorable hydrogen bonding interaction between the quinoline nitrogen and Asp81 of the catalytic triad.

A series of analogs were prepared to examine the effect of incrementally increasing steric bulk at the P3 side chain of HCV NS3 inhibitors in order to preorganize the ligand

into the extended conformation. As steric bulk was increased, the binding affinities improved in turn, notably due to increasingly favorable binding enthalpies along with small gains in entropy. This could possibly attributed to a combination of factors including the entropic benefit derived from preorganization and an enthalpy-driven hydrophobic effect.

Several concise synthetic routes were designed toward the total synthesis of the pentacyclic indole alkaloid (±)-arboridinine. A novel Diels-Alder cycloaddition of an indole-3-glyoxamide with a diene to form a key tricyclic intermediate was attempted, but no reaction was observed under a variety of conditions. A second-generation attempt featured attempts at a challenging cascade reaction involving a conjugate addition of an indole-3-glyoxamide into an enone and subsequent attack of an enolate into the intermediate 3,3-disubstituted indolenine. The conjugate addition was successful, providing the first example of indole-3-glyoxamides as substrates for conjugate additions into enones. The resulting indolenine was found to be unreactive under acidic conditions and underwent a retro-Michael reaction to return the indole-3-glyoxamide under basic conditions.

# Table of Contents

## List of Tables

# List of Figures

## List of Schemes

# Chapter 1. Protein-Ligand Interactions

## 1.1 INTRODUCTION

Proteins play a critical role in nearly every biological process. Interactions between proteins and the small molecules that bind to them elicit biological responses ranging from modulation of chemical reactivity and intracellular transport to cell signaling and initiation of apoptosis. The ability to design small molecules that bind to targeted proteins with a high degree of both affinity and specificity is paramount to the development of efficacious drugs. Therefore, it follows that a thorough understanding of the relationship between structure and energetics of protein-ligand binding is key to rational drug design.

Owing to the limited understanding of the binding phenomena, current methods in drug design are carried out via high-throughput screening (HTS) methods and generation of massive libraries of derivatives.[1] These methods, while valuable for identifying hits and providing primitive structure-activity data, are time-consuming, costly, and inefficient. In addition, the mechanisms of action for these hit compounds are not known from HTS. The advent of virtual screening techniques and computer-aided drug design (CADD) have opened the door to faster and more efficient assays of vast commercial libraries of drug-like compounds. [2,3] Although this methodology is appealing due to its faster turnaround and lower synthesis load, computerized programs only work well when parametrized training sets are available, and no single program is successful across all systems.[4] CADD and other modern drug discovery assays do not provide information about the nuanced energetics of the binding event, namely changes in binding enthalpy ($\Delta H^\circ$) and entropy ($\Delta S^\circ$), and thus only superficial information pertaining to the binding affinity is available in the form of association constants ($K_a$), inhibition constants ($K_i$), and $IC_{50}$ values ($IC_{50}$ is

defined as the concentration of substrate needed to inhibit a certain biological process by 50 percent).

Few studies exist that seek to understand how incremental changes in ligand structure impact the energetics of binding to a biological receptor. [5-17] It is our view that systematic evaluations of the energetics of protein-ligand interactions as a function of specific changes in ligand structure will help uncover useful trends for optimization of binding affinity across a variety of proteins. A set of universally applicable guidelines for how specific changes in ligand structure affect the resulting binding affinity to a protein would greatly aid in improving the utility and reliability of CADD and remains a holy grail of rational drug design. This chapter will survey the fundamentals of protein-ligand interactions as well as outline successes and shortcomings of common strategies for ligand structural modification to improve protein-ligand binding.

## 1.2 THE ENERGETICS OF PROTEIN-LIGAND BINDING

Prior to the binding event, both the protein and ligand are solvated independently. Upon complexation, the solvent reorganizes around the complex and some water molecules are displaced into the bulk solvent (**Figure 1.1**).

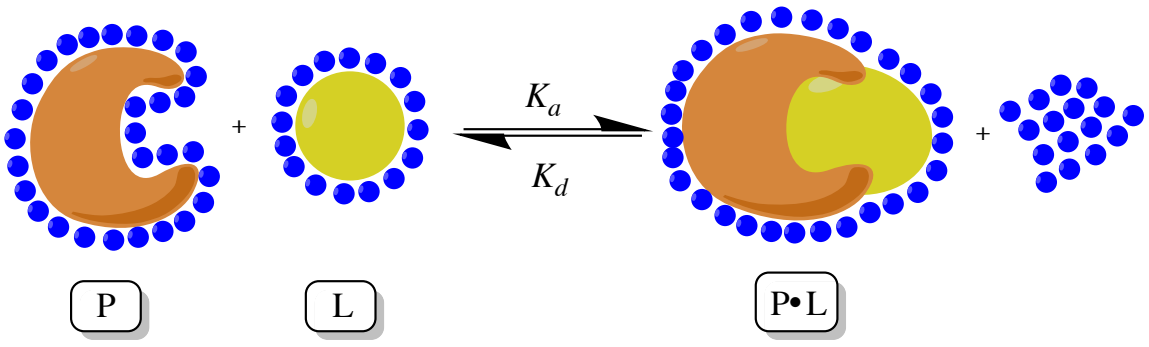


**Figure 1.1:** Cartoon representation of a protein-ligand binding event.

The protein-ligand binding event may be represented as an equilibrium between the free binding partners and the bound complex,

$$P + L \rightleftharpoons P \cdot L \tag{1.1}$$

where P represents the free protein, L is the ligand, and P·L is the bound protein-ligand complex. The association ($K_a$) and dissociation ($K_d$) constants are the corresponding thermodynamic equilibrium constants for the forward and reverse processes, respectively, and are related to the concentrations at equilibrium through equation 1.2.

$$K_a = K_d^{-1} = \frac{[P \cdot L]}{[P][L]} \tag{1.2}$$

The larger the value for $K_a$, the stronger are the binding interactions between the protein and the ligand. $K_a$ is mathematically related to the change in Gibbs free energy of binding ($\Delta G°$) at equilibrium as shown in equation 1.3,

$$\Delta G°_{obs} = -RT\ln(K_a) \tag{1.3}$$

where R is the universal gas constant (1.987 cal $mol^{-1}K^{-1}$) and T is the temperature in Kelvin. Negative values for $\Delta G°_{obs}$ are associated with favorable thermodynamic interactions. The Gibbs free energy of binding is a measurement of the difference in free energy between the bound and unbound states of the protein and ligand. The intrinsic standard free energy change between these two states is denoted as $\Delta G°_i$; however, this is not measured in practice. Experimental data yields $\Delta G°_{obs}$, which takes into account not

only differences in energy due to the binding event, but also changes in free energy due to differences in solvation states between the free binding partners P and L ($\Delta G°_{su}$) and the protein-ligand complex P·L ($\Delta G°_{sb}$), as shown by the Born-Haber cycle (**Figure 1.2**). Although it is impossible to determine $\Delta G°_{i}$ for the binding process, determination of the individual components that make up $\Delta G°_{obs}$ can provide valuable information about the nature of the interactions involved in the binding event.

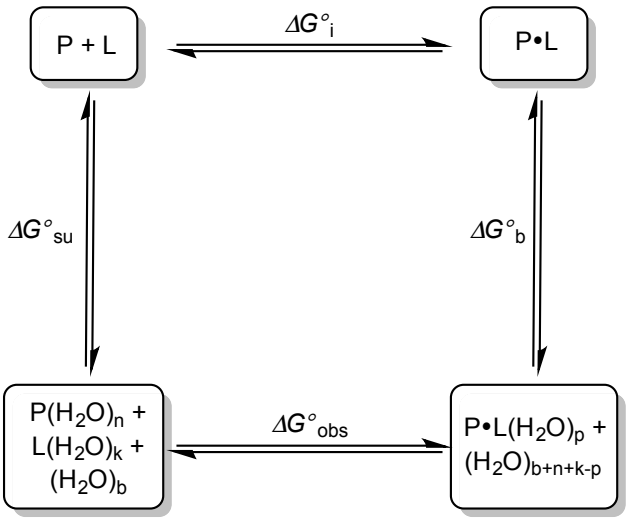


**Figure 1.2**: Born-Haber Cycle for protein-ligand interactions.[18]

$$\Delta G°_{obs} = \Delta G°_{i} + [\Delta G°_{sb} - \Delta G°_{su}] \tag{1.4}$$

The Gibbs free energy of binding is related to the enthalpy ($\Delta H°$) and entropy ($\Delta S°$) of binding through the standard Gibbs free energy equation (Equation 1.5).

$$\Delta G°_{obs} = \Delta H°_{obs} - T\Delta S°_{obs} \tag{1.5}$$

In theory, optimization of one or both of these terms would lead to a more favorable $\Delta G°_{obs}$, and thus $K_a$, although in practice this is quite difficult because it is often observed that efforts to optimize one thermodynamic term are countered by penalties to the other term. Such penalties in some cases completely offset any energetic gains. Optimization of specific non-covalent interactions between the protein and a ligand (in order to maximize binding enthalpy) requires assumption of even more highly ordered conformations in complexes, which can result in a less favorable entropy of binding. Modifications made to optimize binding entropy, which will be discussed later this this chapter, can disrupt key interactions with the protein, resulting in diminished binding enthalpy. This poorly understood phenomenon is known as "enthalpy-entropy" compensation is the topic of much debate. [19-23]

Compounds that bind to a protein with identical values for $\Delta G°_{obs}$ will have the same binding affinity. However, the individual enthalpic and entropic terms that make up the total binding energy arise from very different types of interactions with the protein and with the solvent. Thus, it is of paramount importance to evaluate and understand in order to make informed decisions about how to make changes in ligand structures for the purposes of maximizing binding affinity.

## 1.3 Methods for Thermodynamic Evaluation of Protein-Ligand Interactions

In order to attain a thorough understanding of the protein-ligand binding event, both the structural and corresponding energetic effects must be considered. X-ray crystallography and nuclear magnetic resonance (NMR) are the most commonly used techniques to study the structures of protein-ligand complexes. X-ray crystallography provides high-resolution maps detailing the orientation and positioning of both the ligand and receptor as well as ordered water molecules involved in hydrogen bonding systems.

This can provide crucial information pertaining to bond angles and interatomic distances that can help shed light on key interactions at the active site. However, crystal structures are static snapshots and protein-ligand binding is a dynamic event. Flexibilities in ligand and protein positioning are not readily observable in the crystal structure and thus the limited information about the range of available interatomic angles and distances may not be indicative of all of the interactions that are taking place. In addition, only ordered water molecules are visible in the crystal structure, and the invisibility of disordered water means that changes in solvation between the bound and unbound structures cannot be observed by x-ray structures.[6] This technique also falls short in the case of systems that are difficult to crystallize. NMR is a valuable tool for understanding changes in the dynamics and flexibility of the protein-ligand system. NMR gives valuable data about changes in protein conformational flexibility through the measurement of changes in order parameters. [24,25] Changes in chemical shifts can also provide qualitative insight in regards to hydrogen bonding strength, as stronger hydrogen bonds result in greater deshielding and thus more drastic downfield chemical shifts. [26-28]

No single technique exists that can measure all aspects of binding in its entirety, and thus energetic and structural techniques are often used complementarily to characterize the global binding event. Techniques such as UV-vis, fluorescence, and surface plasmon resonance (SPR) are widely employed in modern medicinal chemistry to evaluate binding affinities and obtain important kinetic data. However, these methods measure protein-ligand binding purely in terms of total binding affinity rather than via determination of the individual thermodynamic components. These affinities are often expressed in terms of $K_d$, $K_i$, or $IC_{50}$. These values are related through a modified Cheng-Prusoff equation[29] (Equation 1.6):

$$K_i = \frac{IC_{50}}{\left(1 + {C}/{K_d}\right)} \qquad K_d = \frac{C}{\left({IC_{50}}/{(K_i - 1)}\right)} \tag{1.6}$$

where C is the concentration of the inhibitor. $K_i$ will be approximately equal to the $IC_{50}$ when either the inhibitor concentration is small or $K_d$ is very large.[29] However, this equation was intended for use in studies on competitive inhibition of enzymatic reactions that operate under Michaelis-Menten kinetics, and the concentration is meant to be the free concentration of inhibitor rather than total concentration.[30] Corrections have been made to the equation in an attempt to account for this fact.[30] Even with these corrections, this type of analysis only provides information on whether one inhibitor binds more strongly than another; it says nothing of the *nature* of the binding event and provides minimal guidance for how modifications made to ligand structure might enhance or hinder binding affinity. Thus, further detailed evaluation of the thermodynamics of protein-ligand interactions is necessary.

Classical approaches for determining $\Delta H°$ and $\Delta S°$ relied on van't Hoff analysis. Substitution of Equation 1.3 into 1.5 yields Equation 1.7, which can then be rearranged to Equation 1.8.

$$-RT\ln(K_a) = \Delta H°_{obs} - T\Delta S°_{obs} \tag{1.7}$$

$$\ln(K_a) = -\left(\frac{\Delta H°_{obs}}{RT}\right) + \left(\frac{\Delta S°_{obs}}{R}\right) \tag{1.8}$$

A plot of $\ln(K_a)$ versus 1/T should result in a straight line if $\Delta C_p$ is zero for the process in question. The value of the slope for this plot would provide $\Delta H°$ for the reaction,

and the y-intercept would provide the value for $\Delta S°$. Since $\Delta C_p$ is not equal to zero in protein-ligand systems, this analysis becomes much more complicated. Van't Hoff analysis requires measurement of $K_a$ at multiple temperatures, which can cause significant error in measurement of $\Delta H°$.[31,32] Large amounts of protein are required to make the multitude of measurements needed, and the elevated temperatures required for this technique can also result in denaturation of sensitive proteins.

Isothermal titration calorimetry (ITC) stands as one of the most efficient methods for acquisition of energetic binding data pertaining to a binding event, generating all relevant thermodynamic parameters in a single experiment.[33] In a typical ITC experiment, a solution of one binding partner is placed in a sample cell that is thermocoupled to a reference cell containing solvent. A solution of the other binding partner is incrementally titrated into the sample cell, which will cause the temperature of the sample cell to either increase (for an exothermic process) or decrease (for an endothermic process). The power required to maintain an isotherm between the sample cell and the reference cell is measured. These data points are then integrated and modeled to a best-fit curve using the Wiseman isotherm (Equation 1.9): [33,34]

$$\frac{dQ}{d[X]_t} = \Delta H^{\circ} V_0 \left[\frac{1}{2} + \frac{1 - X_r - r}{2((1 + X_r + r)^2 - 4X_r)^{1/2}}\right] \tag{1.9}$$

where $\frac{dQ}{d[X]_t}$ is the change in heat of the system with respect to moles of ligand added per injection, $X_r$ is the mole ratio of the ligand to protein $\left(\frac{[L]_t}{[P]_t}\right)$, and

$$\frac{1}{r} = c = K_a[P]_t \tag{1.10}$$

This unitless parameter $c$ is commonly known as the Wiseman coefficient.[33] From the binding isotherm, $K_a$ and $\Delta H°$ can be determined directly (Figure **1.3**). Mathematical manipulations as shown in equations 1.3 and 1.5 can be used to generate $\Delta G°$ and $\Delta S°$ for the biomolecular association. In addition to the standard thermodynamic parameters, measuring $\Delta H°$ as a function of temperature can be used to determine $\Delta C_p$ (see section 1.5.2) of the system.[33]

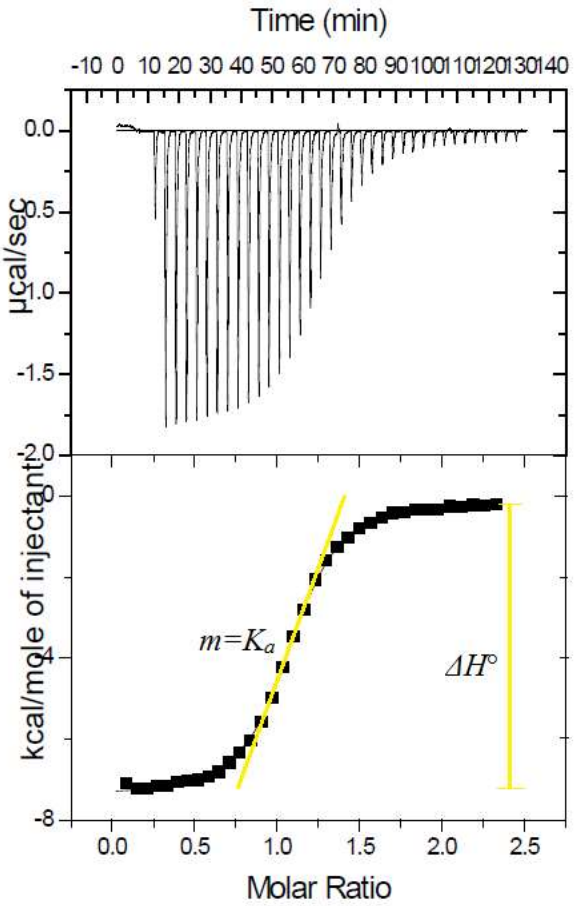


**Figure 1.3:** A sample ITC experiment and graphical representation of key parameters $K_a$ and $\Delta H°$.[35,36]

The Wiseman coefficient is important because it affects the shape of the resulting titration curves[34,37] (Figure **1.4**) and the accuracy of the values obtained for $K_a$ and $\Delta H°$.[34,38-40] At very low $c$ values ($c < 10$), the curve is ill-defined, and it is difficult to obtain accurate data for $\Delta H°$ because there is no clear distinction of the saturation point. As the $c$ value increases, the curves become more sigmoidal. However, once $c$ exceeds 1000 and increases further, the titration curve becomes a stepwise function, and the lack of data points near the inflection point results in an isotherm that can be assigned an infinite number of values for $K_a$. The optimal window for $c$ to obtain reliable data has been reported to be between 10 and 500.[34]

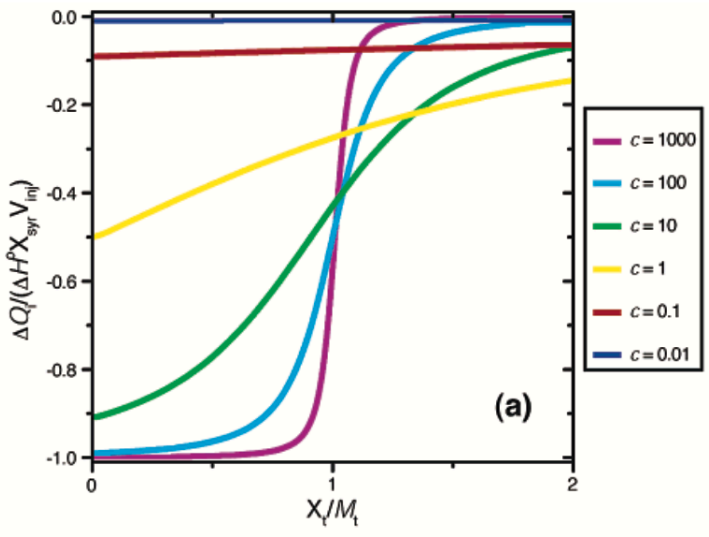


**Figure 1.4:** Graphical representation of ITC isotherms at different $c$ values.[34]

ITC functions over a wide range of systems from millimolar ($K_a = 10^3\ M^{-1}$) to nanomolar affinity ($K_a = 10^9\ M^{-1}$). The major drawback to ITC analysis is that the concentrations of both solutions must be known with great certainty. A report by Turnbull and Daranas showed that in the course of titration experiments between 18-crown-6 and

$Ba^{+2}$ ions, varying the ligand concentration by ±15% had little effect on the calculated value for $\Delta G°$, but gave rise to variations in $\Delta H°$ by as much as ± 1.5 kcal $mol^{-1}$ (± 20%).[34]

The increasing popularity of ITC as a technique for studying the energetics of protein-ligand binding interactions in detail has resulted in valuable information about the nature of protein-ligand interactions. However, these strategies for improving binding affinity are not always simple and straightforward. The remainder of this chapter is dedicated to the factors influencing both binding enthalpy and entropy, as well as successes and shortfalls of common strategies for optimization.

## 1.4 Enthalpic Contributions to Protein-Ligand Binding

The energetic difference between the non-covalent interactions that result from binding and those that occur between the unbound structures and the solvent determine both the sign and magnitude of $\Delta H°$.[41] Non-covalent interactions are typically weak but numerous, exhibiting a strong additive effect on the total binding energy. The most common non-covalent interactions observed in protein-ligand systems are electrostatic (charge-charge) interactions, hydrogen bonds, and van der Waals interactions.

Charge-charge interactions, more commonly known as "salt bridges", are the strongest noncovalent effects observed in biological systems. The high dielectric constant of water weakens the interaction between separated charges and thus salt bridges buried from solvent tend to be much stronger.[42] Charge-charge interactions are optimal at approximately 2.8 Å apart and can contribute anywhere from 3 to 12 kcal $mol^{-1}$ in energy.[43]

Hydrogen bonding results from electrostatic attraction between a hydrogen atom covalently bound to an electronegative atom (the "hydrogen bond donor") and a neighboring electronegative atom containing a free lone pair, (the "hydrogen bond acceptor"). Hydrogen bonds can be either *intra*molecular or *inter*molecular and vary in

strength depending on distance and angle between the donor and acceptor with the majority of hydrogen bonds in proteins occurring at a distance generally around 2.8-3.7 Å and angles between 30° and 180°.[43] Hydrogen bonds are considerably higher in energy than many other non-covalent interactions in biological systems and are valued anywhere from 0.5-2 kcal $mol^{-1}$ in energy.[43]

Van der Waals interactions (sometimes referred to as dispersive interactions or hydrophobic interactions) are considered the weakest non-covalent interactions. Since the distribution of electron density across a molecule is continually fluctuating, two molecules in close proximity can synchronize movement of charge in order to instantaneously generate dipoles, resulting in a transient attractive force between them. The energy of this attraction is related to the inverse sixth power of the distance between the molecules ($1/r^6$), and so these interactions are only significant at very close range.[43] These forces are estimated to contribute no more than 1 kcal $mol^{-1}$ in energy per non-hydrogen atom;[44] however, additive effects across large amounts of surface area can contribute significant energy to the overall binding event.[43]

Although optimization of $\Delta H°$ carries the potential to greatly enhance binding affinity through the strength of polar interactions, this is difficult to accomplish in practice because hydrogen bonds are distance and angle dependent, and the polarity and high dielectric constant of the surrounding water makes desolvation of polar surface area extremely unfavorable relative to nonpolar groups (Table **1.1**).[45] [46] Because interactions between polar groups and the solvent are so strong, these groups are often added to improve the solubility of extremely hydrophobic compounds.[46]

**Table 1.1**. Desolvation enthalpies of various structural subunits at 25 °C.[46]

| Group | $\Delta H°$ (kcal•mol$^{-1}$) | Group | $\Delta H°$ (kcal•mol$^{-1}$) | Group | $\Delta H°$ (kcal•mol$^{-1}$) |
|---|---|---|---|---|---|
| -$NH_2$ | 7.9 | -OH | 8.7 | -$CH_3$ | 0.57 |
| -NH | 9.4 | -SO | 12.7 | -$CH_2$ | 0.77 |
| -N | 9.3 | -CO | 5.5 | -CH | 0.73 |
| -$NO_2$ | 4.7 | -$CO_2$ | 5.4 | -$CH_{aromatic}$ | 0.7 |
| -O | 5.2 | -$CO_2H$ | 8.4 | -C | 1.1 |

In his work optimizing the affinity of plasmepsin II inhibitors for the purpose of generating new anti-malarial drugs, Freire noted that as the binding affinity improved, the range of observed binding enthalpies and entropies for the compounds narrowed. At maximum affinity, the binding enthalpy was –4.5 kcal mol$^{-1}$ and the binding entropy was –8.8 kcal mol$^{-1}$. He notes that compounds that have the same binding affinity can achieve this in very different ways from a thermodynamic perspective. Even compounds with the same number of polar groups do not necessarily bind with the same enthalpy. The quality, rather than quantity, of the interactions is of greatest importance to binding enthalpy, and these interactions have a ceiling when it comes to optimization. This phenomenon was elegantly coined the "optimization funnel" (Figure **1.5**).[46] He argues that all initial screening hits should undergo thermodynamic evaluation because at lower binding affinity an infinite number of possible enthalpy/entropy combinations exist. Those with intrinsically large values for $\Delta H°$ should be chosen as ideal candidates for further optimization because those key interactions with the protein are already established, and binding entropy ($\Delta S°$) is considered more straightforward (at least in theory) optimize. [45,46]

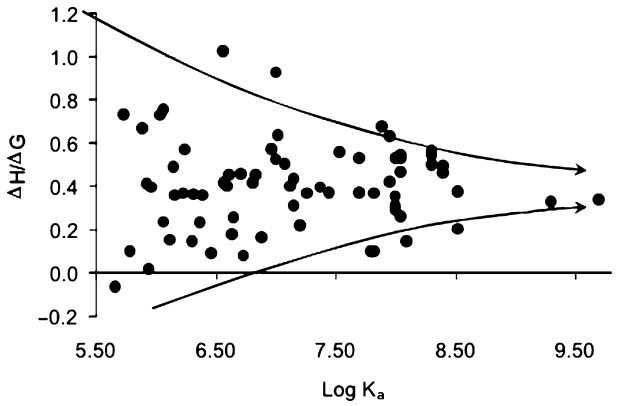


**Figure 1.5**. "Optimization funnel" of Freire's plasmepsin II inhibitors. Enthalpic contribution to $\Delta G^{\circ}_{obs}$ versus log ($K_a$).[46]

## 1.5 ENTROPIC CONTRIBUTIONS TO PROTEIN-LIGAND BINDING

The entropic ($\Delta S^{\circ}$) term measures the changes in rotational, translational, and conformational degrees of freedom as well as the ordering of water molecules between the bound and unbound states of the protein-ligand system.[41] In the uncomplexed solution state, both the protein and ligand are flexible resulting in a high degree of conformational entropy. However, the entropy of the solvent must consequently decrease as solvation of the hydrophobic surfaces of the protein and the ligand requires water molecules to assume more ordered structures (see section 1.5.2). Upon binding, these entropy terms switch signs. In order to assume the complementary shape necessary to facilitate polar interactions and hydrogen bonds with the protein, a ligand will often assume a bound conformation that is higher in energy than the solution-state conformation. This loss of freedom translates into an unfavorable change in conformational entropy; however, some of the ordered water molecules will be displaced from the surfaces of the protein and ligand upon binding and returned to the bulk solvent, and this desolvation process is entropically favorable. Binding entropy can theoretically be optimized by either minimization of the unfavorable changes in entropy due to conformational changes or maximization of the favorable entropy that

accompanies desolvation of the ligand. Both of these strategies for ligand optimization with be discussed in detail in the following sections.

### 1.5.1 Entropic Effects Associated with Conformational Changes

Some of the translational and rotational degrees of freedom available to the free ligand in solution will typically be lost upon binding, resulting an unfavorable entropy term. The exact degree to which this loss contributes to total binding energy is variable and difficult to measure,[47] though tables are available to provide rough theoretical approximations of the entropy change on restriction of various internal rotors.[48] Conformational changes in the protein before and after complexation of the ligand can also contribute to overall binding affinity.[47] In some cases, dynamic changes in remote regions of the protein can compensate for unfavorable changes in entropy at the binding site so the overall change in entropy with respect to degrees of freedom within the protein is zero, a phenomenon that has been coined "entropy-entropy compensation." [18,47,49-52]It has also been reported that some proteins are able to overcompensate resulting in a net *increase* in entropy following the binding event. [18,53]

One optimization strategy to circumvent this "entropic penalty" that results from conformational changes in the ligand upon binding is to introduce a constraint that "preorganizes" the ligand into a conformation identical to or similar to the bound state conformation.[54] Complete restriction of a rotatable bond has been found to increase the Gibbs free energy of binding by 0.7-1.6 kcal $mol^{-1}$ on average. [55-57] In order to understand why a constrained ligand should bind more favorably to a protein it is important to note that the binding free energy ($\Delta G°_{obs}$) can be divided into individual components which can be either favorable or unfavorable, as shown in equation 1.11.[58]

$$\Delta G^\circ_{obs} = \Delta G^\circ_{t+r} + \Delta G^\circ_{r} + \Delta G^\circ_{conf} + \Delta G^\circ_{h} + \Sigma \Delta G^\circ_{p} + \Delta G^\circ_{vdW} \quad (1.11)$$

$\Delta G^\circ_{t+r}$ is the free energy change associated with restriction of translational and rotational degrees of freedom as a consequence of the binding event, $\Delta G^\circ_{r}$ represents the restriction of internal rotors upon complexation with the protein, and $\Delta G^\circ_{conf}$ reflects the energy change associated with the conformational change of the ligand. [58] Because the loss of freedom is entropically unfavorable these terms are assumed to be detrimental to binding ($\Delta G^\circ_{t+r,h,conf} > 0$). However, each term for $\Delta G^\circ$ is itself comprised of individual terms for $\Delta H^\circ$ and $\Delta S^\circ$ and the corresponding $\Delta H^\circ$ term may be, in some cases, sufficiently large to overcome this entropic penalty. [58,59] $\Delta G^\circ_{h}$ represents the formation of hydrophobic interactions between water and nonpolar surface area as well as the release of water into bulk solvent. [58] The last two terms represent the free energy change associated with non-covalent interactions between the protein and ligand as well as interactions made in the bulk solvent, with $\Sigma \Delta G^\circ_{p}$ representing polar interactions and $\Delta G^\circ_{vdW}$ representing van der Waals contacts.[58]

If the constrained and flexible ligands are solvated in a similar fashion and bind to the protein in near identical conformations, then the values for $\Delta G^\circ_{t+r}$, $\Delta G^\circ_{h}$, $\Delta G^\circ_{p}$, and $\Delta G^\circ_{vdW}$ should be nearly identical between the two ligands. The values for $\Delta G^\circ_{r}$ and $\Delta G^\circ_{conf}$ which are detrimental to the flexible ligand due to unfavorable conformational changes should be minimized in the case of the constrained ligand, leading to an overall favorable value for $\Delta G^\circ_{obs}$. However, this analysis is somewhat shortsighted because conformational changes of the protein also impact the binding event. Proteins are dynamic, and proteins have been shown to undergo changes in flexibility both at the binding site as well as remote sites upon complexation with a small molecule. [60-64]

Peptide ligands can be conformationally constrained in a number of ways that can be classified as either local or global constraints. Local constraints are limited to a single residue or residues immediately adjacent to the site of the constraint and tend to restrict regions of the peptide. On the other hand, global constraints, such as macrocycles, cover the majority of the peptide backbone and constrain the ligand as a whole. Constraints can also be either non-covalent or covalent. Non-covalent constraints do not constrain the molecule into a ring, but rather induce spontaneous formation of secondary structures within the peptide, utilizing tactics such a steric repulsion or intramolecular hydrogen bonds. These are typically local constraints, and common modifications to induce this secondary structure include D-amino acids, *N*-methyl amino acids, and α-amino acids. [65,66] Covalent constraints most commonly involve cyclization tactics to constrain the entire peptide backbone and are typically achieved through lactamization, lactonization, ring-closing metathesis, and disulfide bridges. [10,65,67,68] Cyclopropanes have also been employed as local covalent constraints. [7,9,16,68-72] The most common tactics for introducing constraint are depicted in Figure **1.6**.

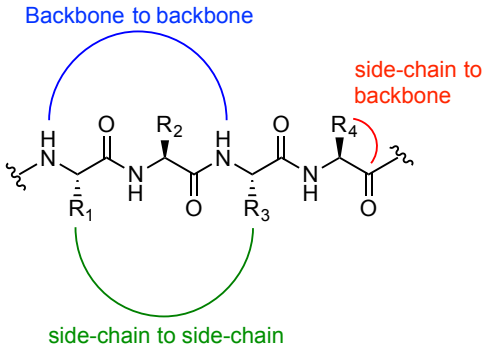


**Figure 1.6**. Common sites of conformational constraints for peptides.

### 1.5.1.1 Examples of Conformational Constraint Wherein Thermodynamic Parameters were not Determined

Freidinger was an early pioneer of using conformationally constrained peptides. In order to induce the β-turn that was computationally predicted to be adopted by leutenizing hormone-releasing hormone (LHRH, **1.1**),[73] he synthesized the constrained analog **1.2** by replacing a glycine residue with a lactam (Figure **1.7**).[74]When the compounds were administered in rats **1.2** was found to be nearly nine times more potent than the native LHRH **1.1**. No detailed thermodynamic studies were conducted on this system so the thermodynamic origin of the increase in potency is unclear. The addition of two hydrophobic methylene units as a result of lactamization also changes the number of van der Waals contacts available to the constrained ligand, which can have an impact on the thermodynamics of desolvation upon binding to the protein (see section 1.5.2), so this lactam may not serve solely as a conformational constraint. Although this work provided hope for the use of conformational constraint as a tool to achieve higher potency, the lack of thermodynamic data and appropriate controls can neither support nor refute the hypothesis that a more favorable binding entropy is the source of the observed increase in potency.

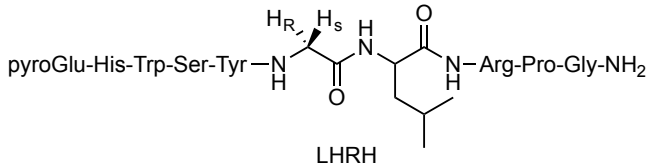


LHRH
**1.1**

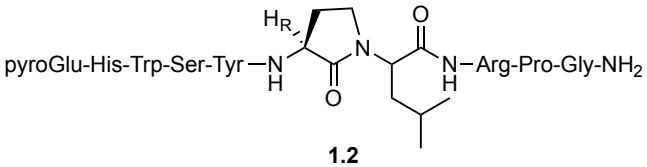


**1.2**

**Figure 1.7**. Native (**1.1**) and constrained (**1.2**) leutenizing hormone-releasing hormone.

Macrocyclic conformational constraints have also been utilized to improve the binding affinity of drug candidates. In the course of optimization of their linear tripeptide hepatitis C virus (HCV) NS3 protease inhibitors, Tsantrizos *et al.* noted that models of the enzyme-substrate complex showed the P1 and P3 residues of hexapeptide **1.3** to be close in proximity (Figure **1.8b**). [67,75] They hypothesized that a tether between these two residues would preorganize the ligand into the bound state conformation and result in a more potent inhibitor.

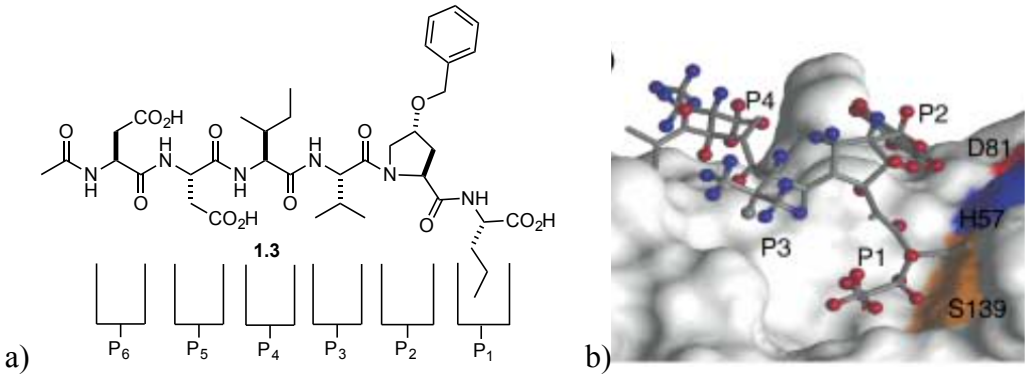


**Figure 1.8**. a) Inhibitor **1.3**. b) Model of **1.3** complexed with HCV NS3.[67]

Truncation to a tripeptide and optimization of the P1 residue[76] led to inhibitor **1.4**, from which they synthesized macrocyclic ligands **1.5**-**1.8**. The cyclic ligand **1.5** was shown to be significantly more potent than **1.4**. Substitution on the proline reside further enhanced the potency to give inhibitor **1.7**, with an $IC_{50}$ of 11 nM. Scission of **1.7** to the open chain analog **1.9** resulted in a 36-fold drop in potency, demonstrating that macrocyclization was key to the observed increase in binding affinity. No detailed thermodynamic studies were conducted on any of their inhibitors so whether this observed increase in binding affinity was due to more favorable binding entropy is unknown.

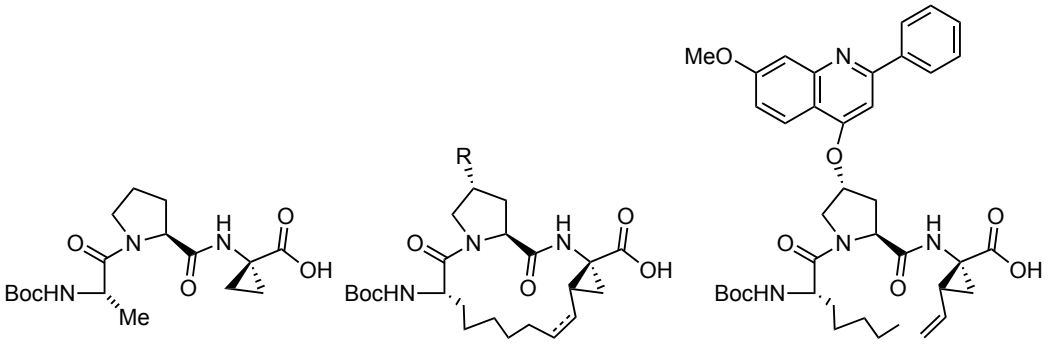


**1.4**

**1.5**: R = H, unsaturated bridge
**1.6**: R = $X^1$, unsaturated bridge
**1.7**: R = $X^2$, unsaturated bridge
**1.8**: R = $X^2$, saturated bridge

**1.9**

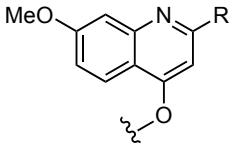


$X_1$: R = H
$X_2$: R = Ph

| Ligand | $IC_{50}$ (μM) |
|---|---|
| **1.3** | 7 |
| **1.4** | > 1000 |
| **1.5** | 400 |
| **1.6** | 0.024 |
| **1.7** | 0.011 |
| **1.8** | 0.028 |
| **1.9** | 0.400 |

**Figure 1.9**: $IC_{50}$ data for HCV NS3 inhibitors **1.3**-**1.8**.[67]

The Martin group initiated an endeavor to explore the effects associated with utilizing the cyclopropane motif as a conformationally constrained peptide mimic. The pioneering study involved introduction of a cyclopropane as a means to constrain the P3 residue of a potent renin inhibitor **1.10**.[71] This constrained peptide mimic **1.11** was approximately equipotent to the flexible counterpart **1.10**, while the diastereomeric cyclopropane **1.12** was nearly 300-fold less potent (Figure **1.10**).

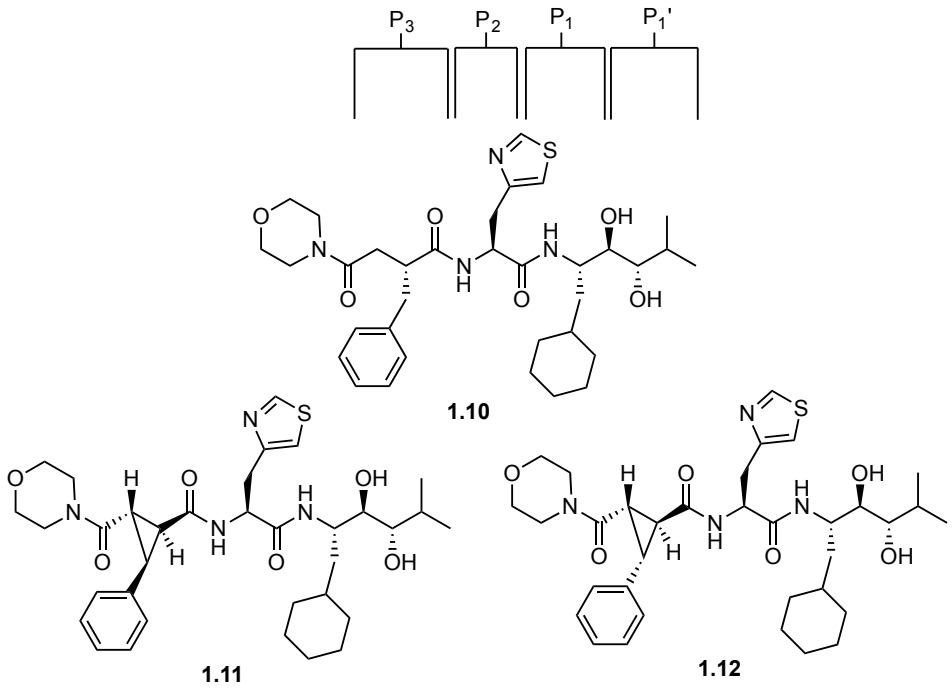


| Ligand | $IC_{50}$ (nM, pH 6.0) |
|---|---|
| **1.10** | 0.36 |
| **1.11** | 0.7 |
| **1.12** | 200 |

**Figure 1.10**. $IC_{50}$ data for flexible and constrained renin inhibitors **1.10**-**1.12**.

However, several other investigations by the Martin group also showed that binding of conformationally constrained ligands did not result in the expected increase in potency.[68,77] Studies of flexible and constrained analogs of the HIV-1 protease inhibitor **1.13** in particular were both illuminating and confusing. Given that the flexible and constrained renin inhibitors were equipotent, we reasoned that the two ligands likely bound in very similar conformations. We were then interested in answering the question of whether additional constraints could be introduced to further rigidify ligand structure and further stabilize the bound conformation. Constraints designed to mimic the β-strand conformation

of the known inhibitor **1.13** resulted in constrained ligands **1.14**-**1.17** that bound with equal potency (Figure **1.11**).

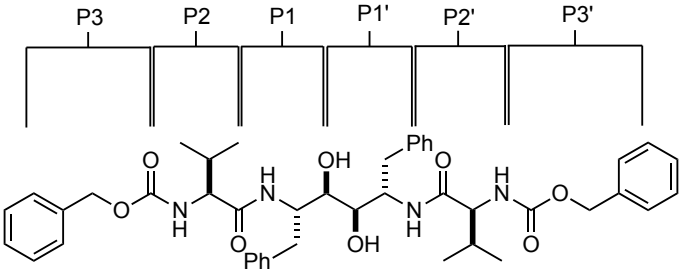


**1.13**

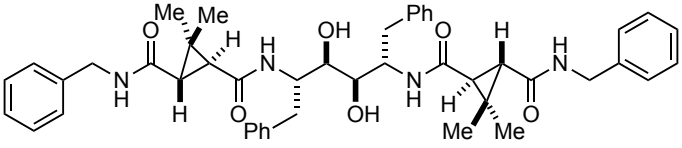

**1.14**

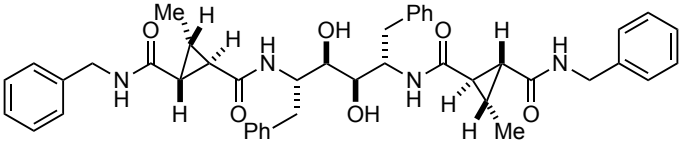

**1.15**

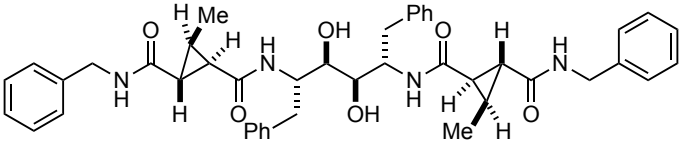

**1.16**

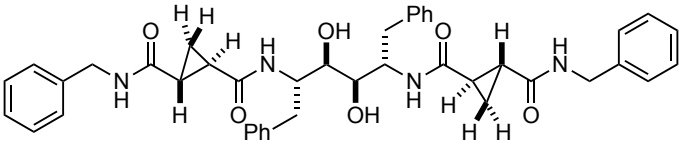

**1.17**

| Ligand | $IC_{50}$ (nM) |
|---|---|
| **1.13** | 0.22 |
| **1.14** | 0.31-0.35 |
| **1.15** | 0.16-0.21 |
| **1.16** | 0.47 |
| **1.17** | 0.17 |

**Figure 1.11**. Structures and $IC_{50}$ data for HIV-1 inhibitors **1.13**-**1.17**.[70]

X-ray crystallographic data of the protease complexed with **1.14** showed that the interaction of the central P2-P2' residues with the protein was analogous to the other bound ligands.[70] The NMR solution-state conformation of **1.15** was superimposed over the crystal structure of **1.14**, and the structures were found to be highly similar (Figure **1.12**).

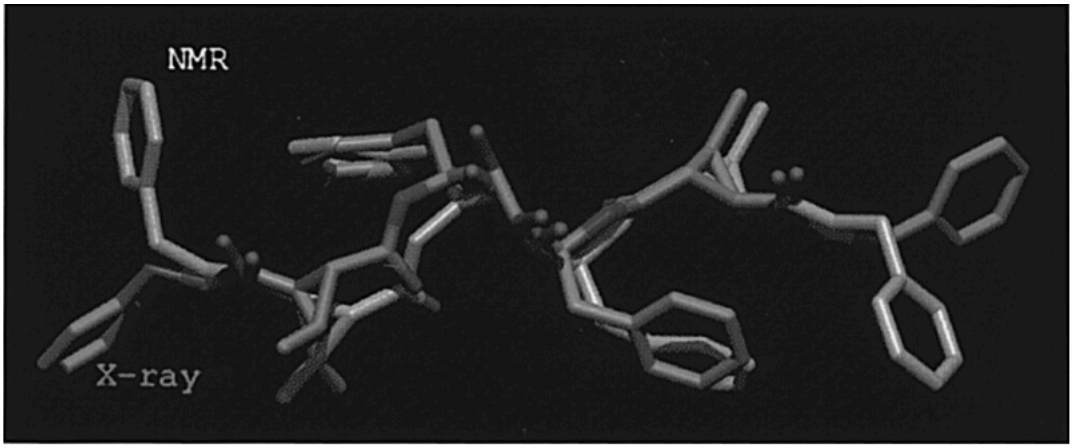


**Figure 1.12**. NMR structure of **1.15** overlaid with the crystal structure of **1.14**.[70]

The only notable differences were in the terminal benzyl groups; however, benzyl groups freely rotate in solution, and thus a variety of conformations are accessible. This study confirmed that constrained ligands can bind in a conformation similar to the into the native ligand and maintain potency. We also showed that the solution-state conformation of the flexible ligand was similar to the bound conformation of the ligand. This study begs the question: If the bound conformations of a flexible and constrained ligand were highly similar, why had the constraint not introduced a favorable change in binding affinity?

### 1.5.1.2 Thermodynamic Evaluations of Conformational Constraints

The unanswered questions from our study of HIV-1 protease inhibitors marked a turning point for our investigations, and we decided that thermodynamic data would be

necessary to understand why the cyclopropane constraints were not resulting in ligands with enhanced binding affinity. It was our view that calorimetric data pertaining to the differences in binding enthalpy and entropy of constrained ligands and their corresponding flexible controls would provide insight into subtle changes in interactions that may not be readily apparent in the crystal structures.

We sought out a well characterized model system with native ligands whose structures would be amenable to backbone constraint. The Src-homology-2 (Src SH2) domain seemed to be an especially ideal choice for this purpose as the protein is easily crystallized and there was a wealth of literature available pertaining to ligands that bind to the protein. [78-81] The tetrapeptide pYEEI (**1.18**, Figure **1.12**). has been shown to be the minimum scaffold for binding to Src SH2, and so we determined this to be an ideal starting point for the development of constrained analogs. [82,83] The ligand binds to the Src SH2 domain in an extended conformation, and key interactions with the protein active site occur at the *N*-terminal phosphotyrosine (pY) and *C*-terminal isoleucine (pY+3) residues. [81,82,84] The pY residue is known to be critical to binding, and so we introduced a *trans*-cyclopropane in order to constrain the backbone into the extended conformation and position the pY side chain into the necessary *gauche*(–) conformation.[16] The introduction of this constraint would require excision of the *N*-terminal amide. Although the N-H of the amide was not shown to be involved in any significant hydrogen bonding,[81] the carbonyl group is involved in two distinct hydrogen bonds, and thus would need to be conserved in order to avoid loss of interactions that would result in an enthalpic penalty. [16,81] The introduction of the constraint would also add a carbon atom to the backbone and the native pYEEI would no longer be a suitable control. Therefore, we prepared flexible control **1.20** with an additional carbon in the backbone to maintain the same number and types of atoms

between the constrained and flexible ligands. Flexible control **1.20** also contained a reversed amide to maintain the electronics of the *N*-terminal carbonyl group. (Figure **1.13**)

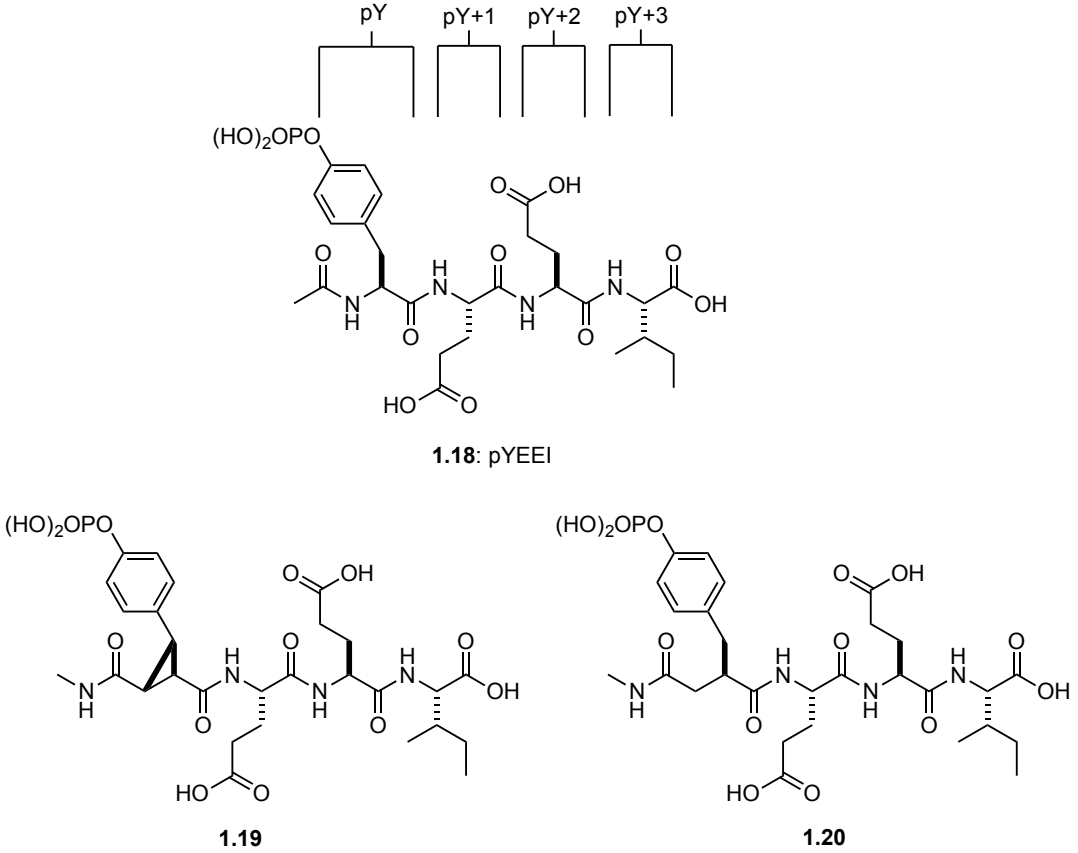


**Figure 1.13**. Native, constrained, and flexible Src SH2 inhibitors 1.15-1.17.[16]

The native pYEEI **1.38**, constrained analog **1.19**, and flexible control **1.20** were evaluated by ITC (Table **1.2**).[16] It was found that the constrained **1.19** and flexible **1.20** were nearly three fold more potent than the native ligand. It was satisfying to see that **1.19** did indeed exhibit a more favorable binding entropy over the flexible **1.20**, and this provides the first definitive support for our hypothesis that constraining ligands into the bioactive conformation imparts a more favorable binding entropy. However, this gain was

offset by an unexpected enthalpic penalty, resulting in similar overall binding affinities between the flexible and constrained ligands.

**Table 1.2**. ITC data for Src SH2 ligands **1.18**-**1.20**.[16]

| Ligand | $K_a$ ($M^{-1}$) | $\Delta G°$ (kcal•mol$^{-1}$) | $\Delta H°$ (kcal•mol$^{-1}$) | $\Delta S°$ (cal•mol$^{-1}$•K$^{-1}$) | $-\Delta C_p°$ (cal•mol$^{-1}$•K$^{-1}$) |
|---|---|---|---|---|---|
| **1.18** | 4.1 (± 0.1) x $10^6$ | –9.01 ± 0.01 | –6.06 ± 0.05 | 9.9 ± 0.2 | — |
| **1.19** | 1.0 (± 0.1) x $10^7$ | –9.55 ± 0.07 | –4.6 ± 0.2 | 17 ± 1 | –225 ± 9 |
| **1.20** | 1.7 (± 0.6) x $10^7$ | –9.8 ± 0.2 | –7.33 ± 0.03 | 8.3 ± 0.5 | –213 ± 7 |

In an attempt to identify the basis for the enthalpic penalty observed in the case of the constrained ligands, $\Delta C_p$ data was collected and found to be identical within experimental error, suggesting that desolvation did not play a significant role in the observed energetic differences. [85] The values for $\Delta C_p$ were found to be within experimental error, suggesting that desolvation did not play a role in the observed result.

A crystal structure of constrained ligand **1.19** complexed with the Src SH2 protein revealed two bound conformations.[16] Although there were some differences in positioning of the pY+2 glutamate side chain, the major binding residues pY and pY+3 were identical in both conformations. Unfortunately, crystal structures of flexible control **1.20** could not be obtained, and so the structures of **1.19** were compared with the known crystal structure of the previously reported 11-mer peptide containing the pYEEI motif.[81] Although not ideal for direct comparison, we believed this approach was valid since only the pYEEI residues interact with the protein, and the other residues were not expected to significantly influence the conformation. Differences were noted in the structures of the two complexes at the phosphotyrosine (pY) residue. The *N*-terminal amide N-H group and

the carbonyl group of the pY residue were both involved in hydrogen bonding with a water molecule in the structure of native ligand, and this conformation was not accessible to the constrained ligand **1.20** due to the *trans*-cyclopropane. These water-mediated hydrogen bonds resulted in the tilting of the aromatic ring and thus differences were noted in the positioning of the pY phosphate group in the SH2 binding pocket.

NMR and molecular dynamics studies were initiated in order to evaluate whether any differences in internal dynamics of the complexes of the flexible and constrained ligands might explain the observed enthalpy-entropy compensation that might not be adequately explained in the x-ray crystal structure. Molecular dynamics calculations showed no significant differences in chain fluctuations between **1.18**, **1.19**, and **1.20** that would explain the observed differences in binding enthalpy. Since $^{1}$H NMR is a powerful tool for measuring the extent of hydrogen bonding (see section 1.3), the chemical shift differences (CSDs) of Src SH2 bound with the three ligands were measured. It was noted that the CSDs of the complex with the constrained ligand **1.20** were significant relative to the other two complexes.[26] $^{1}$H-$^{15}$N HSQC experiments were conducted to measure chemical shifts of the N-H hydrogens involved in hydrogen bonds in the pY binding pocket, and the chemical shift perturbations were found to track well with the observed binding enthalpies (Figure **1.14**).

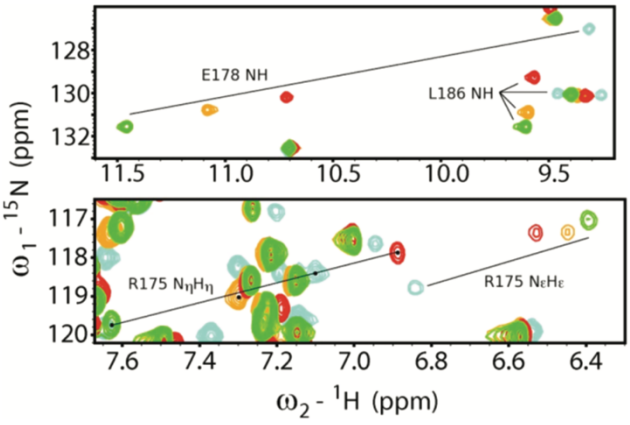


**Figure 1.14**: $^{1}H$-$^{15}N$ HSQC NMR data showing chemical shift differences (CSDs) of residues of Src SH2 bound to **1.18** (yellow), **1.20** (red), and **1.19** (green).[26]

The downfield shift of N-H hydrogens, as exemplified in this case by the Src SH2 E178 N-H and L186 N-H hydrogens, is typically indicative of progressively stronger hydrogen bonding, and these groups are known to make direct interactions with the phosphoryl group of the pY residue.[26] The CSDs of these residues provide reasonable evidence that small structural variations of the pY phosphoryl group can result in the differences in binding enthalpy between the three ligands. This pY residue is classified as a "hot spot" because it contributes approximately 52% of the total binding energy of the ligand. Although crystallographic structures appeared to be identical, the conformational constraint in **1.20** sufficiently altered the geometry of the protein-ligand complex so as to disrupt key hydrogen bonding interactions between the pY residue and the binding pocket, leading to the observed loss in enthalpy. Studies on the thermodynamic effects of introducing a conformational constraint at alternate locations of the Src SH2 tetrapeptide inhibitor in order to maintain the entropic benefit without disrupting key interactions are ongoing.[36,86]

In order to understand whether the lessons learned from Src SH2 domain were applicable to other protein systems attention turned to the Grb2 SH2 domain, another well characterized protein suitable for these investigations.[35] The tripeptide segment pTyr-Val-Asn (pYVN) of the heptapeptide $H_2N$-Lys-Pro-Phe-pTyr-Asn-Val-$NH_2$ has been shown to the minimum motif required for binding to the protein, analogous to the pyEEI motif for Src SH2. This tripeptide segment was chosen as a parent ligand for the development of constrained and analogs for structural and thermodynamic evaluation.[9] Modeling studies showed that *trans*-cyclopropane should be a suitable constraint at the pTyr residue of pYVN. [72] As was the case in the Src SH2 system, a flexible control with an additional carbon atom in the backbone and a reversed amide would be needed for direct comparison (Figure **1.15**).

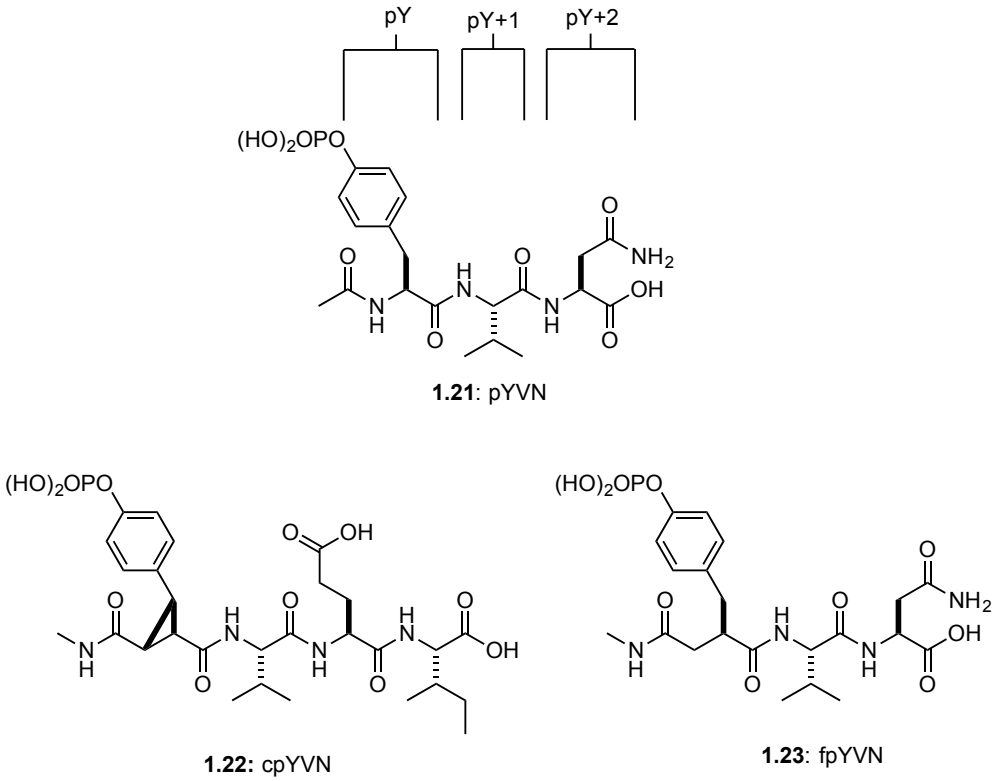


**Figure 1.15**: Constrained and flexible Grb2 SH2 inhibitors.[9]

When ligands **1.22** and **1.23** (pYVN) were evaluated by ITC, it was gratifying to see that the constrained ligand **1.22** bound approximately six-fold more favorably than the flexible control **1.23**. However, it was perplexing to note that unlike previously observed in the Src SH2 system, this increase in binding affinity was due to a more favorable binding *enthalpy*, and the binding of the constrained ligand was actually *less* favorable entropically. Because this was so contradictory to our established understanding of the effects of preorganization, a series of ligands **1.24-1.35** of known pYXaaN ligands were prepared and evaluated by ITC to determine whether this phenomenon was exhibited across other constrained/flexible ligand pairs. (**Figure 1.16**). The ITC data showed that all of the constrained ligands did indeed bind with higher affinity than their flexible counterparts. However, in every case, the conformational constraint provided a more

favorable *enthalpy*-driven binding effect at an entropic cost. This result is in direct contrast to the observations made in the Src SH2 system. Whether the binding entropy was favorable or unfavorable all together was shown to be dependent on the nature of the pY+1 side chain, with hydrophobic side chains showing favorable entropies of binding and polar and charged groups showing unfavorable entropies of binding. Further studies were conducted to evaluate possible changes in desolvation via measurement of $\Delta C_p$, but no significant differences in $\Delta C_p$ were observed between the flexible and constrained ligands. Thus, changes in desolvation were ruled out as a cause for the observed enthalpic effect.[9]

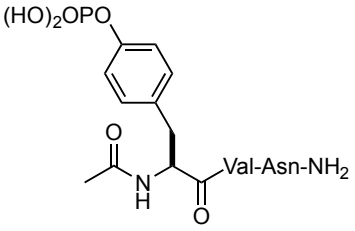


**1.21**

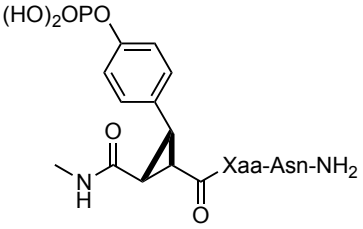


**1.24:** Xaa = Val (cpYVN)
**1.26**: Xaa = Ile (cpYIN)
**1.28**: Xaa = Leu (cpYLN)
**1.30**: Xaa = Gln (cpYQN)
**1.32:** Xaa = Glu (cpYEN)
**1.34**: Xaa = Lys (cpYKN)

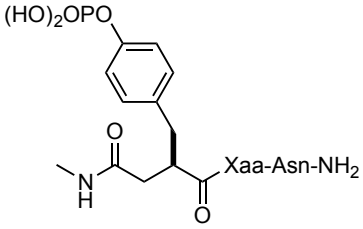


**1.25:** Xaa = Val (fpYVN)
**1.27**: Xaa = Ile (fpYIN)
**1.29**: Xaa = Leu (fpYLN)
**1.31**: Xaa = Gln (fpYQN)
**1.33** Xaa = Glu (fpYEN)
**1.35**: Xaa = Lys (fpYKN)

| Ligand | $K_a$ ($M^{-1}$) | $\Delta G°$ (kcal•mol$^{-1}$) | $\Delta H°$ (kcal•mol$^{-1}$) | $\Delta S°$ (cal•mol$^{-1}$•K$^{-1}$) |
|---|---|---|---|---|
| **1.24** | 2.8 (± 0.10) x $10^6$ | –8.8 ± 0.02 | –7.9 ± 0.29 | 3.0 ± 0.30 |
| **1.25** | 4.5 (± 0.12) x $10^5$ | –7.7 ± 0.02 | –5.4 ± 0.14 | 7.9 ± 0.22 |
| **1.26** | 2.1 (± 0.08) x $10^6$ | –8.6 ± 0.02 | –8.3 ± 0.30 | 1.3 ± 0.30 |
| **1.27** | 4.0 (± 0.15) x $10^5$ | –7.7 ± 0.02 | –5.5 ± 0.20 | 7.4 ± 0.30 |
| **1.28** | 7.1 (± 0.27) x $10^5$ | –8.0 ± 0.02 | –6.0 ± 0.22 | 6.6 ± 0.30 |
| **1.29** | 1.7 (± 0.06) x $10^5$ | –7.1 ± 0.02 | –4.6 ± 0.17 | 8.6 ± 0.30 |
| **1.30** | 1.2 (± 0.06) x $10^6$ | –8.3 ± 0.01 | –9.8 ± 0.20 | –5.2 ± 0.18 |
| **1.31** | 5.6 (± 0.15) x $10^5$ | –7.8 ± 0.02 | –8.7 ± 0.23 | –2.8 ± 0.22 |
| **1.32** | 3.6 (± 0.10) x $10^5$ | –7.6 ± 0.02 | –10.3 ± 0.27 | –9.0 ± 0.22 |
| **1.33** | 3.0 (± 0.08) x $10^5$ | –7.5 ± 0.02 | –8.8 ± 0.23 | –4.3 ± 0.22 |
| **1.34** | 5.5 (± 0.15) x $10^5$ | –7.8 ± 0.02 | –9.2 ± 0.24 | –4.6 ± 0.22 |
| **1.35** | 9.8 (± 0.23) x $10^4$ | –6.8 ± 0.02 | –7.7 ± 0.20 | –3.0 ± 0.21 |

**Figure 1.16**. ITC data for constrained and flexible Grb SH2 inhibitors **1.24**-**1.35**.[9]

Crystal structures were obtained for three pairs of constrained and flexible ligands (**1.24/1.25**, **1.26/1.27**, and **1.30/1.31**), and comparison of these structures revealed that there were no significant overall conformational differences between the constrained and flexible ligands or the backbone atoms of the protein. The flexible and constrained ligands bound to the domain in a $\beta$-turn-like conformation with an intramolecular hydrogen bond between the carbonyl group of the pY+1 residue and the *C*-terminal amide group. Comparison of contact diagrams found that the constrained ligands made more direct contacts and fewer water-mediated contacts with the domain than the flexible ligands, and the number of *direct* contacts correlated qualitatively with the observed binding enthalpies.[9] However, this analysis felt insufficient as the fixing of a water molecule into a water-mediated contact is considered entropically unfavorable, and a higher number of such contacts in the flexible ligands does not explain why the binding entropies are more favorable. Furthermore, the number of water mediated contacts was different for even multiple copies of the same complex in one asymmetric unit.[9] No significant difference in van der Waals contacts were reported.

Following the unsatisfactory results from the crystal structures, we initiated a collaboration with Dr. Pengyu Ren to conduct computational studies on the protein-ligand complexes.[87] Molecular dynamics simulations with a polarizable force field were performed, and the computational binding thermodynamics for the flexible and constrained ligands were largely consistent with the experimental ITC values. Interestingly, simulations showed significant differences in the solution state conformations of the flexible and constrained pYVN analogs **1.24** and **1.25**, respectively. The dominant conformation of fpYVN was reported to be a macrocyclic structure stabilized by an intramolecular hydrogen bond between the phosphate oxygen atoms and the pY+2 amide residue (Figure **1.17**). The rigid cyclopropane structure prevents the constrained ligand

from adopting this conformation. Thus, although the cyclopropane is an effective local constraint for the pY residue, the inability to assume the macrocyclic conformation makes the pY+1 an pY+2 regions *more flexible* in solution than those in the unconstrained ligands.

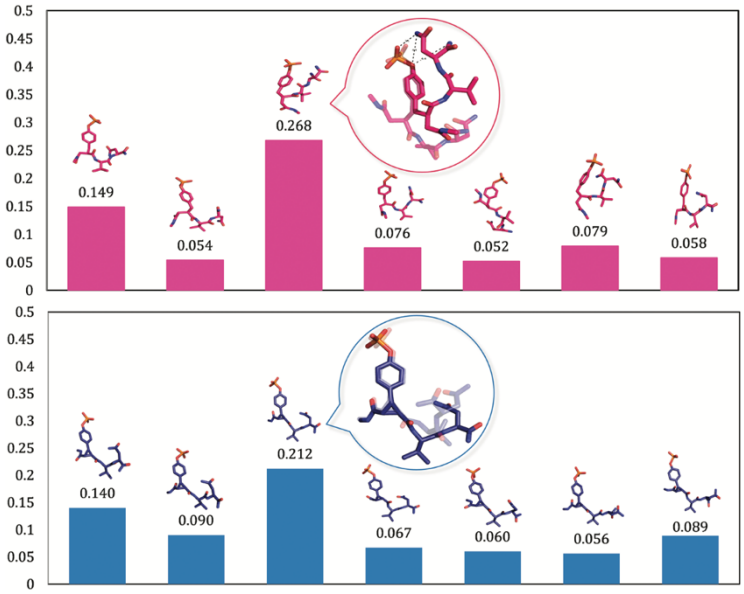


**Figure 1.17**. Solvated structures of fpYVN **1.25** (pink) and cpYVN **1.24** (blue). The most dominant structures are superimposed onto the observed crystal structure (transparent).[87]

No significant differences in the dynamics of the SH2 domain were reported that would explain the observed differences in binding entropy and, so this entropic penalty is a direct consequence of differences in ligand entropies. The computational analysis suggests that, due to the ability to for intramolecular hydrogen bonding interactions, the flexible controls have a lower absolute entropy than the constrained ligands. Thus, we have shown that simply introducing a conformational constraint as a general design strategy for optimizing the binding entropy of a ligand is shortsighted because the constraint may not necessarily lower the entropy of the ligand in solution. Although the cyclopropane was

shown to be an effective local constraint of the pY residue, as evidenced by the near identical binding modes and number of contacts observed in the crystal structures, the macrocyclic structure of the flexible ligands **1.24** and **1.26** reduced the overall flexibility in solution to a greater degree than the cyclopropane. We have learned that rather than focusing on preorganizing the ligand into its bound state conformation, design strategies that lower the overall entropy of a ligand while still allowing it to adopt its binding conformation should lead to a more favorable binding entropy.

Spaller and coworkers reported a systematic study on the thermodynamic effect of introducing conformational constraints into ligands known to bind the third PDZ domain of the mammalian postsynaptic density-95 (PSD-95) protein.[8] They rationalized that macrocyclization between the $P_{-1}$ and $P_{-3}$ residues would preorganize the peptide into the binding conformation without disrupting key interactions with the protein. Thus, constrained/flexible ligand pairs **1.36**/**1.37** and **1.38**/**1.39** were synthesized and evaluated by ITC (Figure **1.18**). The macrocycles were shown to be more potent than the flexible analogs, but only slightly so. Interestingly, the increased binding affinity of **1.36** compared to **1.37** originated from an enthalpic advantage, while the opposite was true in the case of **1.38** vs. **1.39**. However, questions arose over the appropriateness of the linear controls, in that ionizable anime and carboxylic acid groups were created that could alter the number and nature of polar interactions. Nonetheless, this apparent switch from enthalpy-driven binding to entropy-driven binding upon changing from a glutamate-derived bridge to an aspartate-derived bridge inspired Spaller to conduct further investigation using more ideal flexible controls.

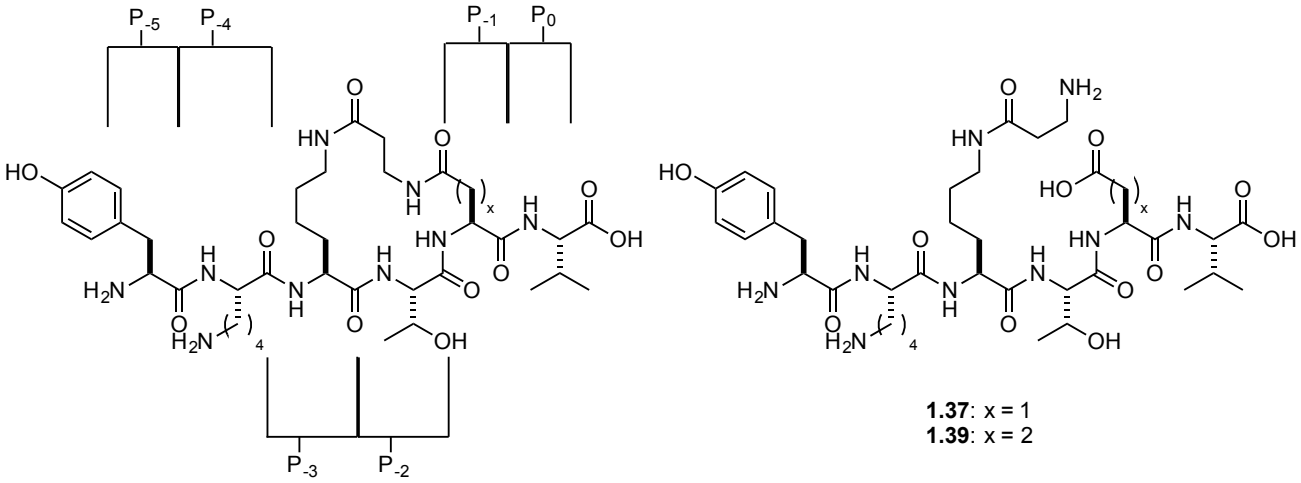


| Ligand | $K_d$ (μM) | $\Delta G°$ (kcal•mol$^{-1}$) | $\Delta H°$ (kcal•mol$^{-1}$) | $-T\Delta S°$ (kcal•mol$^{-1}$) |
|---|---|---|---|---|
| **1.36** | 34.5 | –6.08 | –2.45 | –3.64 |
| **1.37** | 44.1 | –5.94 | –1.38 | –4.57 |
| **1.38** | 4.47 | –7.29 | –2.29 | –5.01 |
| **1.39** | 5.54 | –7.17 | –4.77 | –2.04 |

**Figure 1.18**. ITC data for flexible and constrained PDZ3 inhibitors **1.36**-**1.39**.[8]

Spaller then decided to begin with a known macrocyclic ligand and design acyclic analogs rather an introduce a new cyclization to a linear molecule. In order to avoid generation of ionizable groups, they chose to construct linear analogs of macrocycle **1.40** via cleavage of a C-C bond on either side of the macrocycle, resulting in ligands **1.41** and **1.42** (Figure **1.19**).[17] In this case, the macrocyclic compound **1.40** was slightly more potent due to the expected more favorable binding entropy. It was not known whether the flexible controls had different binding conformations due to the differences in side chains; however, the affinities were found to be largely similar. This suggests that multiple control ligands could be synthesized for a given macrocycle at different scission points.

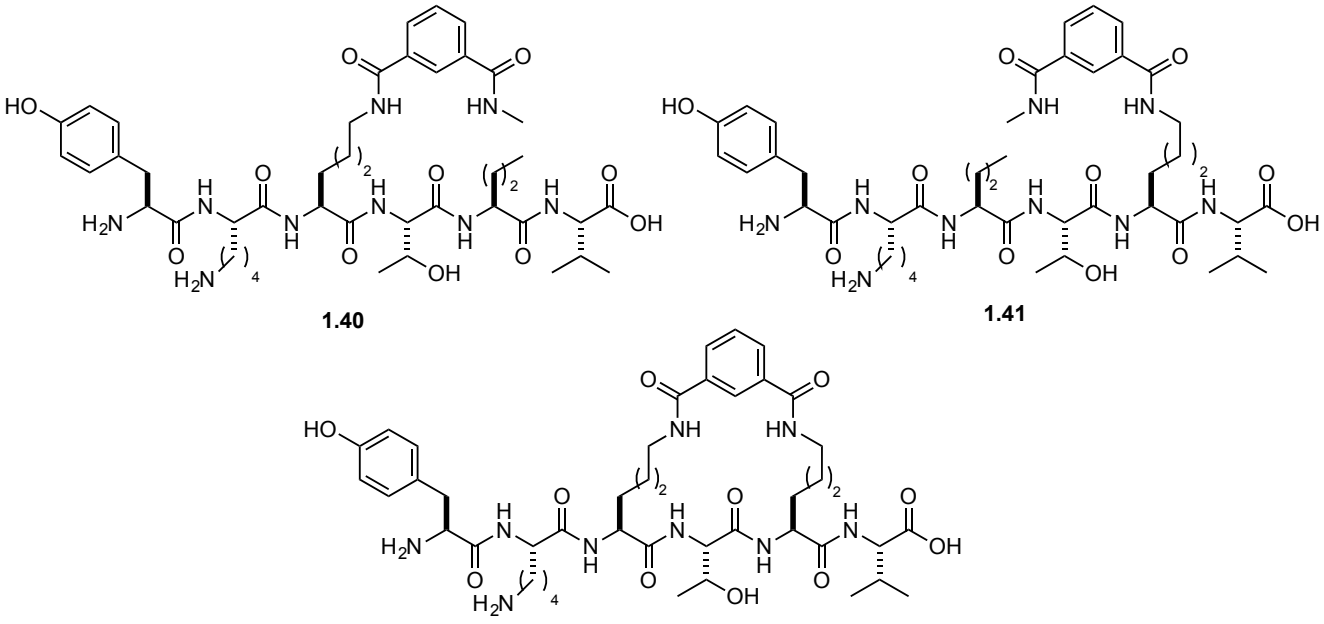

**1.40** **1.41** **1.42**

| Ligand | $K_d$ (μM) | $\Delta G°$ (kcal•mol$^{-1}$) | $\Delta H°$ (kcal•mol$^{-1}$) | $-T\Delta S°$ (kcal•mol$^{-1}$) |
|---|---|---|---|---|
| **1.40** | 4.4 | –7.3 | –2.6 | –4.7 |
| **1.41** | 4.7 | –7.3 | –3.1 | –4.2 |
| **1.42** | 3.8 | –7.4 | –1.9 | –5.5 |

**Figure 1.19**. ITC data for flexible and constrained PDZ3 inhibitors **1.40**-**1.42**.[17]

A third series of PDZ3 inhibitors consisting of macrocycle **1.43** and five distinct flexible controls **1.44-1.48** were also evaluated via ITC (Figure **1.20**).[17] Once again, the macrocycle **1.43** bound more strongly than all of the flexible analogs; however, the binding of **1.43** entropically *disfavored* compared to the control ligands. All of the flexible analogs demonstrated a highly similar thermodynamic profile suggesting that. provided the scission point is not one where significant changes in ligand polarity will be induced, a number of flexible control molecules may represent an unconstrained macrocycle. $\Delta C_p$ was evaluated for **1.43**, **1.45**, and **1.47** but no significant differences were found, suggesting desolvation did not play a role in the change in binding affinity between the constrained and flexible

ligands. No structural data was obtained, and so the cause of this difference in binding affinity remains unknown. Although in all cases the macrocyclic ligands bound more strongly than the flexible controls, the origin for the increase was highly variable. In one case, the increase in affinity was due to the more favorable binding entropy as expected based upon the prevailing paradigm of how preorganization affects ligand binding; however, other cases showed that the macrocycle imparted an *enthalpic* advantage, with the constraint even resulting in an entropic *penalty* at times. In the absence of structural data, it cannot be known whether conformational factors played a role in the observed differences.

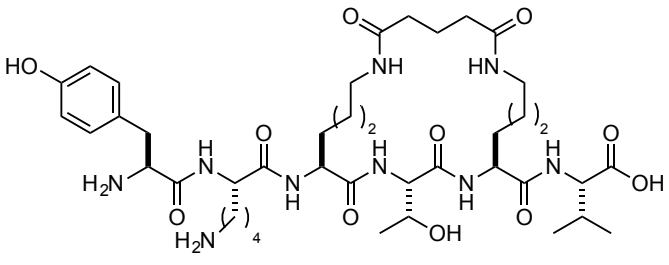

**1.43**

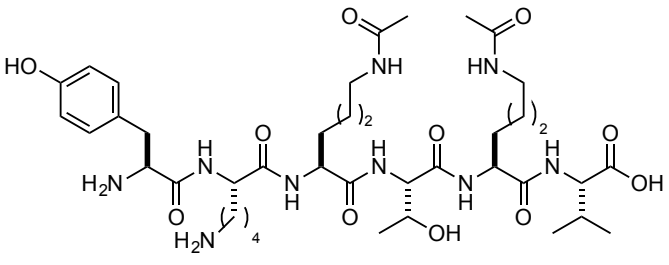

**1.44**

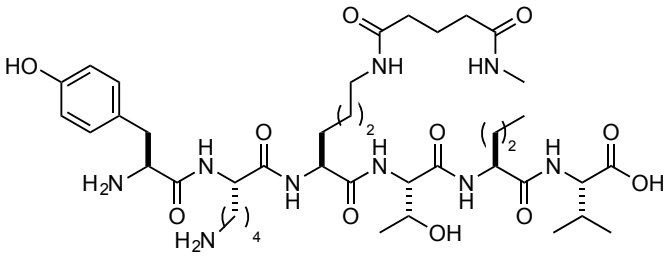

**1.45**

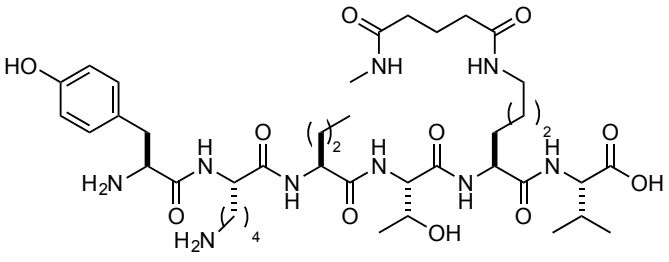

**1.46**

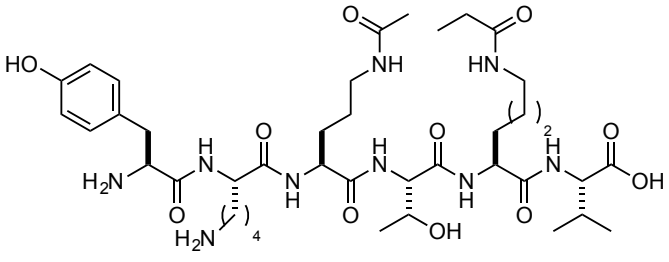

**1.47**

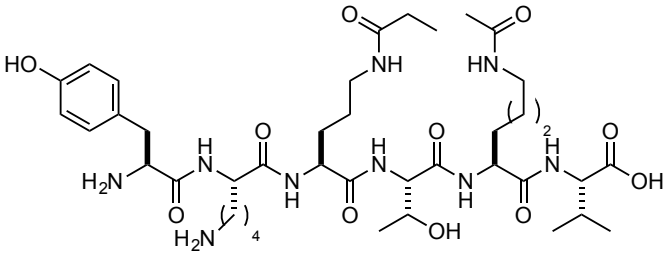

**1.48**

| Ligand | $K_d$ (μM) | $\Delta G°$ (kcal•mol$^{-1}$) | $\Delta H°$ (kcal•mol$^{-1}$) | $-T\Delta S°$ (kcal•mol$^{-1}$) |
|---|---|---|---|---|
| **1.43** | 4.9 | –7.3 | –3.9 | –3.4 |
| **1.44** | 9.6 | –6.8 | –2.5 | –4.3 |
| **1.45** | 5.7 | –7.1 | –2.6 | –4.5 |
| **1.46** | 6.9 | –7.1 | –2.4 | –4.7 |
| **1.47** | 10.1 | –6.8 | –2.0 | –4.8 |
| **1.48** | 8.1 | –7.0 | –2.2 | –3.8 |

**Figure 1.20**. ITC data for flexible and constrained PDZ3 inhibitors **1.40**-**1.42**.[17]

Macrocyclic constraints for a series of Grb2 SH2 inhibitors were also investigated by the Martin group.[10] It has been shown by us and others that peptide ligands containing the pYXN motif bind to the Grb2 SH2 domain in a $\beta$-turn-like fashion with an

intramolecular hydrogen bond between the carbonyl group of the pY+1 residue and the *C*-terminal amide group.[10] Ettmayer has shown that macrocyclization of peptides containing the pYVN subunit can enforce this conformation in solution, whereas the flexible controls adopted a random coil conformation.[88] In the same study, bioassay data showed that the macrocyclic ligand was approximately three-fold more potent than the corresponding flexible ligand. Subsequent studies showed that macrocycles of varying sizes bound to the Grb2 SH2 domain with high affinity;[10] however, due to the lack of thermodynamic data the energetics of this preorganization were not known in detail. We synthesized constrained and flexible ligands with pYVNG sequence **1.49**/**1.50** for ITC analysis. Since structural studies had shown that a valine side chain at the pY+3 site makes favorable van der Waals contacts with the protein[89] we also synthesized the pYVNV containing macrocycle **1.51** and flexible control **1.52** and evaluated both ligand pairs by ITC (Figure **1.19**). The macrocycle **1.49** was less potent than the flexible analog **1.50** by about an order of magnitude primarily due to both less favorable binding enthalpy and entropy terms. Compounds **1.51** and **1.53** were found to be roughly equipotent and equal in affinity from both an enthalpic and entropic standpoint, and both of these ligands were approximately five-fold more potent than the pyVNG-containing ligand **1.50** Crystal structures of the Grb2 SH2 domain complexed with ligand **1.50** showed that the pY-1 carbonyl oxygen atom only made one polar contact with Arg67, whereas all previously reported crystal structures of pYXN ligands bound to the Grb2 SH2 protein show two such contacts.[10] We rationalized that the 20-membered macrocycles may not be sufficiently large to achieve optimal interactions with the protein active site. ITC evaluation of the 23-membered macrocycle **1.53** and flexible ligand **1.54** showed a 20-fold higher binding affinity relative to the 20-membered analog **1.49** and comparable affinity to its flexible control (Figure **1.21**).

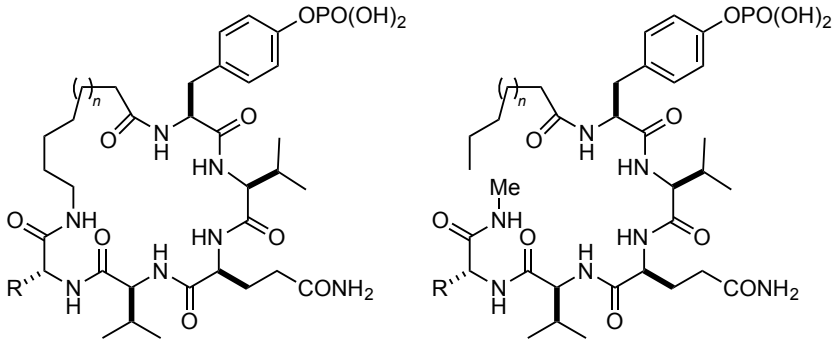

**1.49**: R = H, *n* = 1
**1.51**: R = *i*Pr, *n* = 1
**1.53**: R = H, *n* = 4

**1.50**: R = H, *n* = 1
**1.52**: R = *i*Pr, *n* = 1
**1.54**: R = H, *n* = 4

| Ligand | $K_a$ ($M^{-1}$) | $\Delta G°$ (kcal•mol$^{-1}$) | $\Delta H°$ (kcal•mol$^{-1}$) | $-T\Delta S°$ (cal•mol$^{-1}$) |
|---|---|---|---|---|
| **1.49** | 4.7 (± 0.11) x $10^4$ | –6.4 ± 0.01 | –3.5 ± 0.26 | –2.9 ± 0.06 |
| **1.50** | 4.1 (± 0.17) x $10^5$ | –7.7 ± 0.03 | –6.3 ± 0.40 | –1.4 ± 0.20 |
| **1.51** | 2.3 (± 0.21) x $10^6$ | –8.7 ± 0.06 | –4.3 ± 0.32 | –4.4 ± 0.16 |
| **1.52** | 2.3 (± 0.12) x $10^6$ | –8.7 ± 0.03 | –4.6 ± 0.23 | –4.1 ± 0.13 |
| **1.53** | 8.5 (± 0.03) x $10^5$ | –8.1 ± 0.07 | –6.3 ± 0.68 | –1.8 ± 0.12 |
| **1.54** | 5.7 (± 0.65) x $10^5$ | –7.9 ± 0.02 | –4.8 ± 0.57 | –3.1 ± 0.32 |

**Figure 1.21**. ITC data for constrained and flexible Grb SH2 inhibitors **1.49**-**1.54**.[10]

Larger 23-membered macrocycles of the pY+3 valine-type ligands were also synthesized but unfortunately solubility problems precluded any thermodynamic study. Inspired by the previous work of Ettmayer, we synthesized **1.55** and **1.56** for ITC analysis (Figure **1.22**). [10,88] From this, we found that the enhanced affinity of **1.55** relative to **1.56** was due to an enhanced binding enthalpy that dominated over an unfavorable binding entropy relative to the flexible ligand.

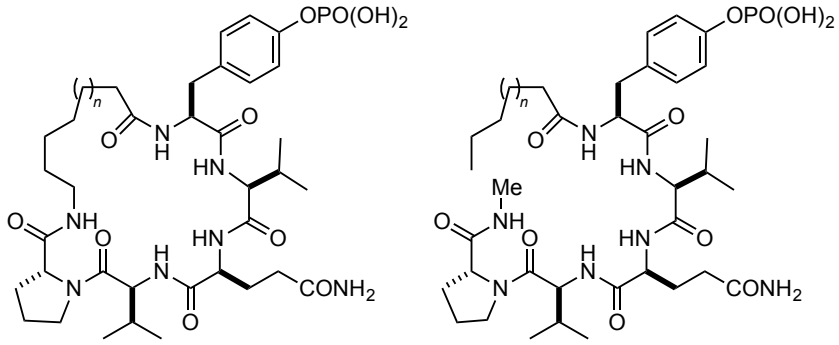


**1.55** **1.56**

| Ligand | $K_a$ ($M^{-1}$) | $\Delta G°$ (kcal•mol$^{-1}$) | $\Delta H°$ (kcal•mol$^{-1}$) | $-T\Delta S°$ (cal•mol$^{-1}$) |
|---|---|---|---|---|
| **1.55** | 1.0 (± 0.20) x $10^7$ | –9.6 ± 0.09 | –4.3 ± 0.57 | –5.3 ± 0.36 |
| **1.56** | 6.5 (± 0.13) x $10^6$ | –9.3 ± 0.01 | –6.3 ± 0.38 | –3.0 ± 0.06 |

**Figure 1.22**. ITC data for constrained and flexible Grb SH2 inhibitors **1.62**-**1.63**. [10,88]

It was interesting to observe that preorganization of these pYVN-containing ligands via macrocyclization can be either favorable or unfavorable in terms of binding entropy. It was also noteworthy that even for ligands that bound with comparable affinities, such as **1.50** and **1.54**, the individual enthalpic and entropic terms were very different. Small differences in $\Delta C_p$ between **1.53** and **1.54** suggest that this difference in enthalpy may be partly due to differences in desolvation; however, this does not seem to play a role in the differences between **1.55** and **1.56**. It is possible that although the linker does not interact directly with the protein, the nature and flexibility of the linker plays a role in the energetic outcome, as had been previously observed by Spaller. [8,17]

Crystal structures of the protein-ligand complexes of **1.55** and **1.56** showed that while the critical pYVN sequences aligned almost exactly between the two complexes, the termini of the flexible ligand **1.56** pointed away from each other in the crystal structure, thus affecting the relative positions of other atoms near either end of the peptide. There was no difference in the number of direct polar contacts and a difference of water-mediated

contacts between **1.55** and **1.56** of approximately ± 1, although the variance in the number of water-mediated contacts is due to differences in contacts present in the different isoenergetic conformations of **1.55**. There were also no reported differences in the number of van der Waals contacts.

One notable difference in the bound structures of **1.55** and **1.56** may make a key difference in the observed binding enthalpies. It was noted that there is a hydrogen bond between the pY carbonyl oxygen atom and the backbone nitrogen atom of the pY+3 residue in **1.56** that was not observed in any of the six isoenergetic structures of **1.55**. This intramolecular interaction is well known in the binding of pYXN ligands to the Grb2 SH2 protein. Since this interaction is not observed in the case of ligand **1.55**, this suggests that this ligand may bind in a higher energy conformation, and thus an unfavorable binding enthalpy is observed for the binding of **1.55** relative to **1.56**.

### 1.5.2 Entropic Effects Associated with Solvation

Changes in the degree of solvation also greatly impact binding entropy, and the addition of nonpolar surface area is another commonly used strategy to improve the binding affinity of a ligand to a protein. The entropy of solvation of small organic molecules in water is typically negative at room temperature,[90] and this is commonly referred to as the hydrophobic effect. Frank and Evans first proposed the "iceberg model," to rationalize the hydrophobic effect, postulating that upon solvation of a small nonpolar organic molecule, water molecules form series of increasingly disordered hydration shells around the solute, with those water molecules closest in proximity to the solute displaying the highest degree of order (this ordering of molecules is proposed to be similar to the crystal lattice of ice) (Figure **1.23**).[91] While this might be imagined to be accompanied by an unfavorable change in enthalpy due to disruption of hydrogen bonding networks in the bulk solvent, the

clathrate-like structures surrounding solute molecules exhibit stronger levels of hydrogen bonding such that the net enthalpy change is often near zero.[47] When nonpolar solute molecules aggregate fewer water molecules are needed to form these hydration shells, and many of the ordered "ice-like" water molecules are liberated into the bulk solvent, which is entropically favorable. As the temperature increases and these hydration shells "melt" and assume less ordered structures, and this "absorbance" of energy results in a more enthalpy-driven solvation effect, with the net entropy of solvation at higher temperatures approaching zero.[47]

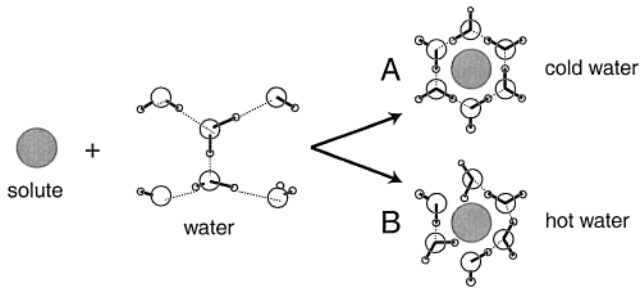


**Figure 1.23:** Iceberg Hydration model.[92]

The energetic effects of desolvation have been shown to be heavily dependent on the surface topography of a ligand.[92-94] Water molecules will be able to orient around small, convex surfaces in such a way as to form the four optimal hydrogen bonds to neighboring water molecules. However, this ordering intrinsically carries an entropic penalty, and the release of these water molecules to the bulk solvent should result in a favorable *entropy*.[92-94] In contrast, water molecules that form hydration shells around flat and concave surfaces will orient one of the four possible coordination sites toward the surface of the solute, and this non-optimal geometry hinders hydrogen bonding to that fourth site. As a result, when these surfaces are buried upon complexation with a protein the release of water

molecules to the solvent will restore optimal hydrogen bonding, and this process is considered to be *enthalpically* favorable. [93,94]

The change in heat capacity at constant pressure ($\Delta C_p$) for a system is classically considered to be an indicator of the hydrophobic effect in protein-ligand systems. $\Delta C_p$ is the amount of energy that is absorbed by a particular system as a function of temperature.[95] This value is obtained from the slope of a plot of $\Delta H°$ versus temperature (Equation 1.12).

$$\Delta C_p = \left(\frac{\partial \Delta H^\circ}{\partial \mathrm{T}}\right)_\mathrm{p} = \mathrm{T}\left(\frac{\partial \Delta S^\circ}{\partial \mathrm{T}}\right)_\mathrm{p} \qquad (1.12)$$

Heat capacity is considered to be entropically driven under physiological conditions and more enthalpically driven as temperature increases. The sign and magnitude of $\Delta C_p$ is indicative of the nature of the surfaces being solvated.[95]A negative value for $\Delta C_p$ is associated with the hydrophobic effect in that it suggests the burial of nonpolar surface area. The ordered solvent molecules around the nonpolar surface have a lower kinetic energy than those in the bulk solvent due to the rigid geometry and stronger bonding. Thus, the solution can absorb more thermal energy without a rise in temperature, leading to the observed sign of $\Delta C_p$.[96] The burial of polar surface area results in increased hydrogen bonding and molecular vibrations and is observed as a positive value for $\Delta C_\mathrm{p}$.[95] Although $\Delta C_p$ has been marked as an indicator of the hydrophobic effect, examples presented later in this chapter show that increased burial of surface area may not necessarily be accompanied by changes in $\Delta C_\mathrm{p}$.

A pivotal early study of the effects of increasing nonpolar surface area was conducted by García-Echeverría and coworkers in an effort to improve binding affinity of Grb2 SH2 inhibitors.[97] Working from the known pTyr-Xaa-Asn-$NH_2$ scaffold that had

been previously shown to adopt a $\beta$-turn upon binding,[98] they hypothesized that $\alpha,\alpha$-disubstituted amino acids could be used to improve binding affinity by preorganizing the ligand into this conformation for binding. Analysis of ligands **1.57**-**1.62** showed that the binding affinity steadily increased following incremental expansion of the ring at the pY+1 site up to a six-membered ring (Figure **1.24**). Although thermodynamic data were not examined, modeling studies on the number of van der Waals contacts within the binding pocket correlated well with the increases in binding affinity. From this, they rationalized that the increasing hydrophobicity of the $\alpha,\alpha$-disubstituted residue provided a set increase to binding affinity per methylene unit. However, no structural or energetic information was gathered and so whether this hydrophobic effect was enthalpy-driven or entropy-driven was unknown.

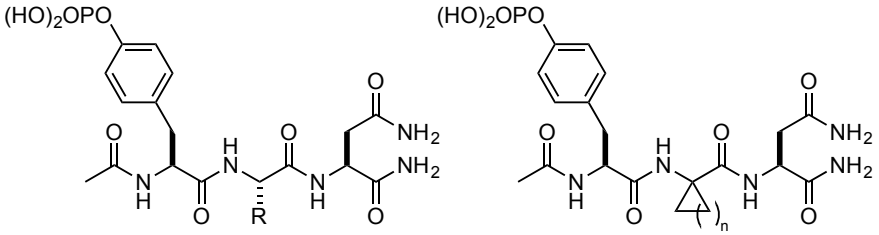

**1.57**: R = H
**1.21**: R = *i*Pr

**1.58**: n = 1
**1.59**: n = 2
**1.60**: n = 3
**1.61**: n = 4
**1.62**: n = 5

| Ligand | $IC_{50}$ ($\mu$M) | pY + 1 vdW contacts |
|---|---|---|
| **1.57** | 67.0 | 0 |
| **1.21** | 4.30 | 7 |
| **1.58** | 72.5 | 2 |
| **1.59** | 18.2 | 2 |
| **1.60** | 7.90 | 4 |
| **1.61** | 0.21 | 8 |
| **1.62** | 1.11 | 8 |

**Figure 1.24:** $IC_{50}$ data for Grb2 SH2 inhibitors with $\alpha,\alpha$-disubstituted amino acids at the pY+1 site.[97]

A study by Engberts provided early thermodynamic evidence for an entropy-driven hydrophobic effect across a series of benzamidinium-containing trypsin inhibitors (Figure **1.25**). Increasing the hydrophobicity of the ligands via adding sequential methylene units provided a more favorable entropy of binding that was offset to varying degrees by an enthalpic penalty. Increasingly negative values for $\Delta C_p$ correlated very strongly with the increasing hydrophobicity of the ligands, suggesting the burial of the nonpolar surface area on binding. Binding simulations were performed in an effort to understand why the enthalpic penalty occurred; however, no significant differences in conformation or interactions with the protein were observed. The origin of the enthalpic penalty was

unknown, and again highlights the necessity for deeper investigation into the effects of structural changes on binding energetics.

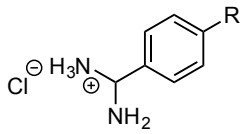


| Ligand | R | $K_a$ ($M^{-1}$) | $\Delta G°$ ($kJ•mol^{-1}$) | $\Delta H°$ ($kJ•mol^{-1}$) | $-T\Delta S°$ ($kJ•mol^{-1}$) |
|---|---|---|---|---|---|
| **1.70** | H | 4.5 (± 0.2) x $10^4$ | –26.6 ± 0.3 | –18.9 ± 0.4 | 7.7 ± 0.6 |
| **1.71** | Me | 6.9 (± 0.3) x $10^4$ | –27.6 ± 0.1 | –18.5 ± 0.3 | 9.1 ± 0.2 |
| **1.72** | Et | 2.9 (± 0.3) x $10^4$ | –25.4 ± 0.2 | –17.3 ± 0.5 | 8.2 ± 0.6 |
| **1.73** | *n*Pr | 3.1 (± 0.2) x $10^4$ | –25.7 ± 0.2 | –12.7 ± 0.5 | 13.0 ± 0.6 |
| **1.74** | *n*Bu | 3.8 (± 0.2) x $10^4$ | –26.2 ± 0.2 | –9.9 ± 0.5 | 16.3 ± 0.7 |
| **1.75** | *n*Pent | 5.8 (± 0.3) x $10^4$ | –27.2 ± 0.1 | –9.9 ± 0.4 | 17.3 ± 0.3 |
| **1.76** | *n*Hex | 1.3 (± 0.06) x $10^5$ | –29.2 ± 0.1 | –10.6 ± 0.4 | 18.6 ± 0.3 |

**Figure 1.25**: ITC data for trypsin inhibitors **1.70-1.76.**[61]

It is notable that increasing the nonpolar surface area in a molecule may lead to higher affinity ligands because of more favorable binding *enthalpies*. For example, in work with the mouse Major Urinary Protein I (MUP-I), the Homans group noticed that adding of a single methylene unit to **1.77** to give **1.78** resulted in an increase in binding affinity.[14] Examination of the thermodynamic data revealed that this was due to a more favorable binding *enthalpy*, with the entropy of the more hydrophobic ligand **1.78** displaying a slightly *less* favorable binding entropy than **1.77** (Figure **1.26**).

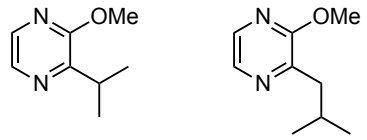


**1.77** **1.78**

| Ligand | $\Delta G°$ (kcal•mol$^{-1}$) | $\Delta H°$ (kcal•mol$^{-1}$) | $\Delta S°$ (cal•mol$^{-1}$•K$^{-1}$) |
|---|---|---|---|
| **1.77** | –8.1 ± 0.02 | –10.6 ± 0.02 | 2.5 ± 0.8 |
| **1.78** | –9.2 ± 0.02 | –11.5 ± 0.02 | 2.2 ± 0.1 |

**Figure 1.26:** ITC data for MUP-I ligands **1.77** and **1.78**.[14]

A similar observation had been reported by Stone who studied binding of a series of substituted thiazoles with MUP-I and found that favorable changes in binding enthalpy tracked with the addition of methylene groups.[99] This finding was surprising because it was contrary to the common assumption that burial of nonpolar surface area would lead to a more favorable binding entropy.

This *enthalpy*-driven hydrophobic effect was further examined in the course of another study by the Homans group involving the binding of aliphatic alcohols **1.78**-**1.83** to MUP-I.[15] As the hydrophobicity of the ligand increased, so too did the binding affinity by approximately –0.94 kcal mol$^{-1}$ per methylene group added. This was due to incremental increases in binding enthalpy of approximately –1.35 kcal mol$^{-1}$ per methylene, while the entropic term –T$\Delta S°$ because progressively more unfavorable by approximately 0.41 kcal mol$^{-1}$ per methylene group (Figure **1.27**).

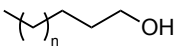


| Ligand | *n* | $\Delta G°$ (kcal•mol$^{-1}$) | $\Delta H°$ (kcal•mol$^{-1}$) | $-T\Delta S°$ (kcal•mol$^{-1}$) |
|---|---|---|---|---|
| **1.79** | 1 | –5.5 ± 0.02 | –9.8 ± 0.02 | 4.3 ± 0.8 |
| **1.80** | 2 | –6.8 ± 0.02 | –11.4 ± 0.02 | 4.6 ± 0.1 |
| **1.81** | 3 | –7.7 ± 0.01 | –12.8 ± 0.01 | 5.0 ± 0.1 |
| **1.82** | 4 | –8.5 ± 0.02 | –13.9 ± 0.02 | 5.4 ± 0.1 |
| **1.83** | 5 | –9.3 ± 0.05 | –15.2 ± 0.05 | 5.9 |

**Figure 1.27:** ITC data for MUP-I ligands **1.79**-**1.83**.[15]

Crystal structures for all the protein-ligand complexes were obtained for comparison.[15] The conformation of the protein was found to be the same for all of the ligands. The ligands were shown to bind in two different conformations, with **1.79** and **1.80** binding in a similar orientation and **1.81**-**1.83** binding in a perpendicular orientation, likely due to steric hindrance as a consequence of the increased chain length. Four of the five alcohols (**1.79**, **1.80**, **1.82**, and **1.83**) contained the same number of ordered water molecules, with additional ordered water molecules in the complex with **1.81**. Further calculations showed that there was no consistent trend between increases in chain length and reduction of water molecules in the binding pocket. It was proposed by Homans that because the MUP-I binding pocket was known to be suboptimally hydrated,[14] there were fewer interactions between the protein and the solvent that would be disrupted on binding.[100] Thus, the dispersive interactions made between the ligand and the protein on burial of the nonpolar surface area of the ligand would not be fully cancelled out by loss of protein-solvent interactions and a more favorable binding enthalpy would be observed. The unfavorable change in binding entropy could possibly be due to the larger solution-state entropy of the longer chain alcohols due to the increase in molecular rotors.

A study on thrombin inhibitors by Klebe highlights the energetic complications associated with even seemingly straightforward structural changes.[101] They expected that adding the methylene group from ligand **1.84** to **1.85** would correspond to an increase in Gibbs free energy of about 3-4 kJ $mol^{-1}$ (0.7-1.0 kcal $mol^{-1}$), as has been reported in the literature to be the energetic contribution for burial of a methylene across series of congeneric ligands. Much to their surprise, the two ligands bound with virtually identical affinities (Figure **1.28**). The thermodynamic data revealed that adding the methylene group resulted in a favorable change in the entropic term ($-T\Delta S°$) by –1.7 kcal $mol^{-1}$; however, this was almost completely offset by an enthalpic penalty of +1.5 kcal $mol^{-1}$.

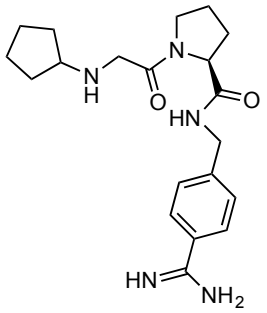

**1.84**

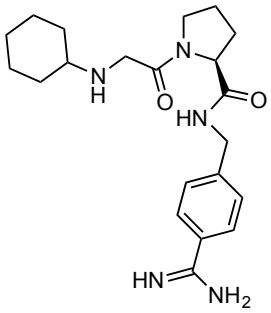

**1.85**

| Ligand | $K_a$ ($M^{-1}$) | $\Delta G°$ (kcal•$mol^{-1}$) | $\Delta H°$ (kcal•$mol^{-1}$) | $-T\Delta S°$ (kcal•$mol^{-1}$) |
|---|---|---|---|---|
| **1.84** | $1.54 \times 10^6$ | –8.46 | –4.03 | –4.43 |
| **1.85** | $2.8 \times 10^6$ | –8.64 | –2.51 | –6.13 |

**Figure 1.28:** ITC data for thrombin inhibitors **1.84**-**1.85**.[101]

Crystal structures of both complexes were obtained for comparison. While the cyclopentyl derivative **1.84** exhibited the expected bound conformation with the five-membered ring positioned within the S3/S4 pocket,[101] they were astonished to note that the cyclohexyl derivative **1.85** did not show a well-defined binding conformation for the six-

membered ring in this pocket. Molecular dynamics calculations showed that this six-membered ring is able to move freely in and out of the binding pocket. This enhanced binding entropy could be due to the increased freedom of the cyclohexyl ring on binding relative to the cyclopentyl ring. However, this increased freedom comes at a cost, as the cyclohexyl ring is unable to form the same breadth of dispersive interactions as the cyclopentyl ring. This study demonstrates how even slight changes in structure can alter the binding properties of two ligands.

Klebe also investigated the binding thermodynamics across a series of thermolysin inhibitors.[102] They explore the effect of increasing hydrophobicity in the side chain of phosphoramidite ligands **1.86**-**1.88** (Figure **1.29**). In all cases, they observed a more favorable binding enthalpy upon addition of nonpolar surface. This was also accompanied by an entropic penalty that in most cases resulted in only modest increases in affinity, and in one case resulted in a slight decrease in overall binding affinity. This observation was rationalized to be due to an expulsion of water molecules from the suboptimally hydrated binding pocket, a similar phenomenon observed in the MUP-I protein. The unfavorable change in binding affinity from **1.87** to **1.88** was attributed to the energy cost associated with conformational changes in the protein to accommodate the large benzyl side chain.

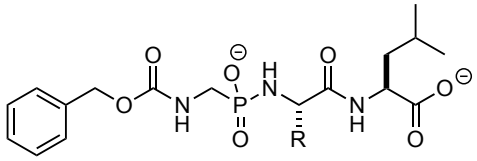

**1.86**: R = *i*Pr
**1.87**: R = *i*Bu
**1.88**: R = Bn

| Inhibitor (relative differences) | $\Delta\Delta G°_{Kd}$ (kcal•mol$^{-1}$) | $\Delta\Delta H°$ (kcal•mol$^{-1}$) | $-T\Delta\Delta S°$ (kcal•mol$^{-1}$) |
|---|---|---|---|
| **1.86-1.87** | 0.9 | 1.0 | –0.1 |
| **1.87-1.88** | –0.3 | 1.5 | –1.8 |
| **1.86-1.88** | 0.5 | 2.5 | –2.0 |

**Figure 1.29:** Relative ITC data for thermolysin inhibitors **1.86**-**1.88**.[101]

The Martin group has also reported on *enthalpy*-driven hydrophobic effects. We were intrigued by the report from García-Echeverría that increasing ring size of the pY+1 side chain of pYXN-derived Grb2 SH2 inhibitors and sought to determine whether this increased potency across ligands **1.58**-**1.62** was due primarily to favorable changes in binding enthalpy, entropy, or some combination of the two (Figure **1.30**). The binding affinity increased incrementally with increasing ring size up to n = 4, with the increase to a cycloheptyl ring (n = 5) showing no significant change in binding affinity. Surprisingly, this increase in binding affinity was the result of increasingly more favorable binding *enthalpies* rather than entropies, as might have been expected due to the hydrophobic effect. Although the negative sign for $\Delta C_p$ were in agreement with the burial of nonpolar surface area, the magnitude of $\Delta C_p$ did not track with the observed changes in binding affinity.

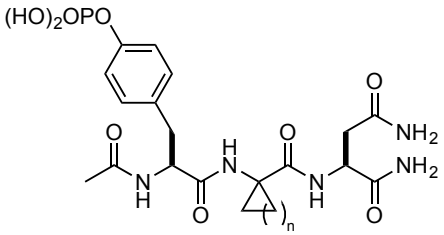

**1.58**: n = 1
**1.59**: n = 2
**1.60**: n = 3
**1.61**: n = 4
**1.62**: n = 5

| Ligand | $\Delta G°$ (kcal•mol$^{-1}$) | $\Delta H°$ (kcal•mol$^{-1}$) | $-T\Delta S°$ (kcal•mol$^{-1}$) | pY + 1 vdW contacts | $\Delta C_p$ (cal•mol$^{-1}$•K$^{-1}$) |
|---|---|---|---|---|---|
| **1.58** | –7.1 ± 0.1 | –3.3 ± 0.3 | –3.8 ± 0.1 | 4 | –116 ± 12 |
| **1.59** | –7.7 ± 0.1 | –5.4 ± 0.3 | –2.3 ± 0.2 | 5 | –185 ± 8 |
| **1.60** | –8.5 ± 0.1 | –6.3 ± 0.4 | –2.2 ± 0.2 | 9 | –141 ± 8 |
| **1.61** | –9.3 ± 0.1 | –8.5 ± 0.4 | –0.8 ± 0.4 | 13 | –181 ± 10 |
| **1.62** | –8.9 ± 0.1 | –6.8 ± 0.3 | –2.1 ± 0.2 | 14 | –173 ± 8 |

**Figure 1.30:** ITC data for Grb2 SH2 inhibitors with α,α-disubstituted amino acids at the pY+1 site.[11]

Crystallographic data showed that each of the bound ligands adopted the expected *β*-turn conformation with the characteristic hydrogen bond between the carbonyl oxygen of the pY residue and the *N*-terminal amide nitrogen.[11] No significant changes in binding conformation were reported and the number of direct polar contacts with the protein remained the same for all ligands, although the number of water-mediated contacts was slightly variable. It was noted that the increasing number of van der Waals contacts did indeed track well with the observed increase in binding affinity. Comparison of the thermodynamic values with the change in nonpolar Connolly surface area (CSA) showed a contribution to $\Delta G°$ of –56 ± 7 cal•mol$^{-1}$Å$^{-2}$, which is larger than the typically observed value of –12 ± 7 cal•mol$^{-1}$Å$^{-2}$.[11] The contribution to $\Delta G°$ as determined by the dependence on $\Delta CSA_{np}$ was –114 ± 25 cal•mol$^{-1}$Å$^{-2}$. This study also showcases the enormous

complexity associated with attempts to correlate ligand structural changes to binding energetics and challenges assumptions about $\Delta C_p$ as a barometer for the burial of nonpolar surface area.

Further studies were conducted to evaluate the effect of increasing nonpolar surface area for acyclic analogs of Grb2 SH2 inhibitors.[12] Linear tripeptides **1.84**-**1.89** were synthesized and the binding parameters were determined by ITC (Figure **1.31**). Although an increase in binding affinity was observed upon addition of the first methylene unit from **1.89** to **1.90**, subsequent additions provided no further improvement. All gains in enthalpy upon increasing the length of the alkyl chain were accompanied by equalizing entropic penalties. Upon crystallization of the protein-ligand complexes, it was noted that the *n*-propyl chain of **1.86** adopts a *gauche* conformation in the binding pocket. This conformation was also observed for **1.87-1.89**. It is possible that this unfavorable conformation is responsible for the observed entropic penalty, and further investigation is ongoing.

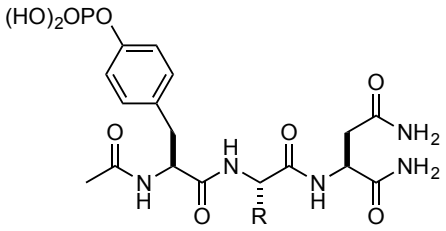

**1.89**: R = Me
**1.90**: R = Et
**1.91**: R = *n*Pr
**1.92**: R = *i*Pr
**1.93**: R = *n*-pentyl
**1.94**: R = 1-(*Z*)-propenyl

| Ligand | $\Delta G°$ (kcal•mol$^{-1}$) | $\Delta H°$ (kcal•mol$^{-1}$) | $-T\Delta S°$ (kcal•mol$^{-1}$) | pY + 1 vdW contacts | $\Delta C_p$ (cal•mol$^{-1}$•K$^{-1}$) |
|---|---|---|---|---|---|
| **1.89** | –7.3 ± 0.1 | –4.9 ± 0.3 | –2.4 ± 0.1 | 4 | –123 ± 9 |
| **1.90** | –8.1 ± 0.1 | –6.8 ± 0.3 | –1.3 ± 0.2 | 9 | –170 ± 15 |
| **1.91** | –8.0 ± 0.1 | –6.7 ± 0.4 | –1.3 ± 0.2 | 12 | –173 ± 13 |
| **1.92** | –8.1 ± 0.1 | –7.3 ± 0.4 | –0.8 ± 0.4 | 14 | –138 ± 12 |
| **1.93** | –8.0 ± 0.1 | –7.2 ± 0.3 | –0.8 ± 0.2 | 14 | –148 ± 7 |
| **1.94** | –7.9 ± 0.1 | –7.0 ± 0.3 | –0.9 ± 0.2 | 9 | –176 ± 7 |

**Figure 1.31:** ITC data for linear pYXN Grb2 SH2 inhibitors.[12]

## 1.6 SUMMARY

Although modern high throughput and virtual screening assays have afforded medicinal chemists the unprecedented ability to search vast libraries of structures in order to find drug candidates, this "shotgun approach" to drug discovery is time consuming, costly, and inefficient. These shortcomings in drug development are primarily due to our limited understanding of protein-ligand interactions. We still do not have the ability to predict the binding affinity of a ligand simply based on structural data, nor can we accurately predict how specific modifications to ligand structure will affect binding affinity. A thorough understanding of biomolecular interaction processes from both a structural and energetic perspective is key to furthering our ability to quickly develop and optimize safer, more specific and efficacious therapies. Strategies have evolved to optimize

specific thermodynamic parameters in order to improve ligand binding affinity; however, our incomplete understanding of protein-ligand binding energetics is underscored in the apparently paradoxical nature of the data uncovered in the scant thermodynamic evaluations available thus far.

Conformational constraints are conventionally thought to enhance binding affinity by reducing the inherent entropic penalty that is incurred by a ligand during binding with a protein. However, studies by the Martin group and others have shown that it is possible that a constraint may improve binding affinity through a more favorable change in binding entropy or *enthalpy*, or it may even be *detrimental* to binding affinity. Cyclopropanes were shown to be effective local constraints for a variety of protein-ligand systems, resulting in inhibitors with either equipotent[45,71] or improved binding affinity[9,16] over flexible controls; however, detailed thermodynamic studies revealed some of the subtle yet significant challenges of designing effective constraints.

Constrained derivatives of the native pyEEI peptide were shown to bind to the Src SH2 domain with higher affinity than flexible analogs due to a more favorable binding entropy; however, this was partially offset by an enthalpic penalty.[16] NMR studies revealed chemical shift differences in the protein that suggested that the flexible ligand was able to form stronger hydrogen bonds with key residues in the protein backbone.[26] Thus, even minor alterations in geometry resulting from introducing constraints in "hot spot" regions can result in loss of binding enthalpy.

Constrained pYXN-containing inhibitors of the Grb2 SH2 domain also bound with higher affinity than their flexible counterparts; however, in this case the constrained ligands bound with a more favorable *enthalpy* at an entropic cost.[9] Molecular dynamics calculations showed that the flexible ligands were able to adopt a macrocyclic structure in solution that was not possible for the constrained ligands, which resulted in a lower

solution-state entropy for the flexible ligands compared to the constrained analogs.[87] From this, we learned that preorganizing the ligand into the bound conformation may not necessarily result in a more favorable binding entropy if the constraint does not lower the solution-state entropy of the ligand relative to the unconstrained ligand.

Macrocycles have also been evaluated as conformational constraints. Reports by Spaller showed that macrocyclic constraints can impart a higher binding energy through either a more favorable binding entropy or enthalpy depending on the nature of the macrocyclic tether. [8,17] Spaller also showed that with careful consideration of scission points, multiple flexible controls could represent an unconstrained macrocycle.

Our investigation into macrocyclic inhibitors of the Grb2 SH2 domain showed that macrocycles can be either favorable or unfavorable in terms of binding energy.[10] We learned that the size of the macrocycle can be important in order for the constrained ligand to maintain all key interactions with the protein. We also showed that the constrained macrocyclic ligand developed by Ettmayer[88] bound with a higher affinity than the flexible control due to a more favorable binding entropy at an enthalpic cost. We also showed that this enthalpic cost could be due to an intramolecular hydrogen bond that is observed in the bound structure of the constrained inhibitor and not observed in the flexible analog.

These results reveal the importance of continued investigation into the enthalpic and entropic effects of ligand preorganization in order to better understand the complex effects that making changes to ligand structures has upon their binding affinities. In chapter 3.x we will discuss the thermodynamic effects associated with an acyclic conformational constraint.

Solvation is another key factor in protein-ligand binding. Solvation of the protein and ligand prior to binding is an entropically unfavorable process due to the ordering of water molecules around the surface. However, polar surfaces are able to establish

interactions with the solvent water molecules that makes subsequent desolvation of these surfaces very unfavorable enthalpically. Since nonpolar surfaces are unable to make such interactions with the solvent, the desolvation of these surfaces on binding should result in a more favorable binding entropy.

Adding nonpolar surface area to a ligand is a common strategy for optimizing binding affinity; however, this strategy is also not without its challenges. Engberts showed that increasing hydrophobicity of trypsin inhibitors resulted in the expected favorable increase in binding entropy, but this was offset by an unidentified enthalpic penalty.[61] Klebe showed that although addition of a methylene unit to a thrombin inhibitor resulted in a more favorable binding entropy, the new ligand was found to bind in an alternate conformation that weakened interactions with the protein, and thus binding enthalpy.

More examples are emerging in support of an *enthalpy*-driven hydrophobic effect.[12,14,15,99,103] This phenomenon, at least within the MUP-I system, was proposed by Homans to be due to suboptimal hydration of the binding pocket, and release of these water molecules lining the surface of the protein would be enthalpically favorable; however, whether or not this is broadly applicable to other systems is uncertain. Studies on phorphoramidite inhibitors of thermolysin by Klebe showed an analogous enthalpy-driven hydrophobic effect, and it suggested that this protein may also have a suboptimally hydrated binding pocket.[101]

Our studies of α,α-disubstituted pYVN ligands have also shown $\Delta C_p$ to be a poor indicator of the burial of nonpolar surface area.[12,103] As these studies continue to show, our knowledge of the intricacies of protein-ligand binding energetics is still highly superficial, and only through more systematic study across a wide variety of protein ligand systems can we come to understand and master the delicate act of optimizing binding affinity through balancing changes in conformation, solvation, and non-covalent interactions.

## 1.7 LOOKING FORWARD – A NEW PROTEIN-LIGAND SYSTEM

In order to elucidate correlations between ligand structure and binding affinity that can be broadly applicable to protein-ligand binding, we must continue to well-characterized systems through which to study protein-ligand binding energetics. It is important that several criteria are met in order for a protein to serve as a suitable model for this purpose. The protein-ligand system should be well studied and extensively characterized so that the key protein-ligand interactions have been identified. This provides valuable information about which structural changes may be appropriate for the ligand. The ligand should be simple enough that it can be synthesized readily, and the structure should be amenable to derivatization. Finally, the crystal structure of the protein should be known, and conditions should be available so that the various protein-ligand complexes can be crystallized for the purpose of obtaining structural information.

With these criteria in mind, the HCV NS3 protease captured our attention. As one of the most extensively studied proteins in the HCV genome, a sufficient knowledge of the structure of the enzyme active site and key interactions within was available to be suitable for our work. Crystal structures of several strains of the protein were known along with complexes with several inhibitors, and this led us to believe that crystallization should be straightforward. With the ongoing development of HCV inhibitors, there were also reports of ligand structural changes that resulted in significant changes in binding affinity. In particular, the work of Tsantrizos *et al*.[67] developing macrocyclic tripeptide inhibitors was of great interest to us (see section 1.5.1), as we had previously investigated the energetic effects of macrocycles as conformational constraints in another system.[10] Along the development pathway to clinical candidate BI 201335[104] several other ligand modifications were also of interest to us due to the significant impact on the affinity of the inhibitors, and these will be discussed in detail in the next chapter.

# Chapter 2. The Hepatitis C Virus and the NS3 Protease

## 2.1 The Hepatitis C Virus

The hepatitis C virus (HCV) stands as one of the preeminent global health concerns of the 21st century with an infected global population estimated at 170 million, making HCV infection five times as widespread as the human innumodeficiency virus (HIV-1).[105] First discovered in 1989, HCV was identified as the cause of non-A, non-B hepatitis infections. It is estimated that individuals born between 1945 and 1965 make up nearly 75% of all infected patients in the United States due to a lack of proper infection protocols regarding the handling of blood prior to 1990.[106] While heightened awareness of blood-borne diseases and subsequent screening measures have significantly decreased the risk of acquiring the virus via transfusion, new cases continually arise as a result of intravenous drug use.[105] Inability to culture HCV stifled early development of treatment, and many patients progressed to long-term complications including cirrhosis and hepatocellular carcinoma. A large number of patients infected with the disease suffer only mild symptoms or are completely asymptomatic, which results in delay of treatment until more advanced stages of the disease. As a result, HCV infection remains the leading cause of liver transplants in the United States.[105]

HCV is an RNA virus belonging to the *Flaviviridae* family of viruses with the hepatitis G virus, yellow fever virus, and dengue virus as the closest viral relatives.[105] HCV contains a single-stranded positive-sense RNA genome of approximately 9,600 nucleotides. The genomic RNA is composed of one open-reading frame flanked by a 5' and 3' noncoding region that is translated to a single 3,000 amino acid polyprotein (**Figure 2.1**). This polyprotein is then cleaved by a combination of viral and host proteases into three structural proteins (core, E1, and E2) and seven nonstructural proteins (p7, NS2, NS3, NS4A, NS4B, NS5A, and NS5B). The structural proteins are processed by host proteases,

whereas the protease domain of the NS3 protein is responsible for self-cleavage of the NS3/NS4A junction and cleavage of subsequent downstream proteins. [107-110]

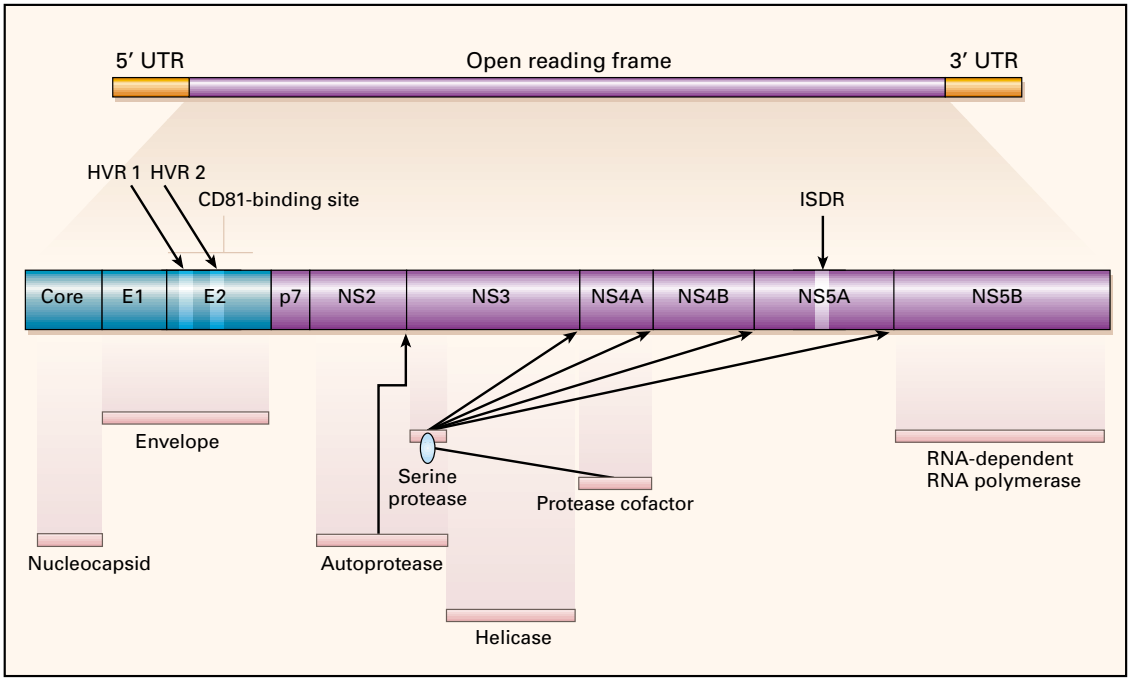


**Figure 2.1:** Diagram of the HCV genome and polyprotein.[105]

HCV has classically been difficult to treat. Six distinct genotypes of HCV have been identified and vary in prevalence across the globe. HCV genotype 1 is the most commonly observed genotype in the United States and western Europe, with lower incidences of genotypes 2 and 3.[111] Genotype 4 is most prevalent in Egypt, where an astonishing 6 to 28 (mean 22) percent of the population is estimated to be infected with the disease.[105] Genotype 5 is most commonly found in South Africa and genotype 6 primarily affects Southeast Asia.[105] Although the various genotypes are related, response to treatment varies and some therapies have been shown to be only effective against a few genotypes.[111] Replication occurs rapidly, and it is estimated that 10 trillion virion particles are produced

per day.[105] The RNA polymerase lacks proofreading capabilities, resulting in rapid evolution of the virus even within a single host, further complicating treatment. [105]

Before HCV received a separate classification, patients diagnosed with "non-A, non-B hepatitis" were treated with PEGylated interferon-α ($INF_{\alpha}$) and ribavirin (**2.1**).[112] Although incidences of successful treatment were reported as early as 1989, [113,114]more than half of patients relapsed, and various unpleasant side effects were also reported[105] thus necessitating the development of new treatments. The first major clinical breakthroughs in small molecule therapeutics for the treatment of HCV came with the 2011 approval of telaprevir (Vertex Pharmaceuticals)[115] (**2.2**) and boceprevir (Merck)[116] (**2.3)**, although boceprevir was later voluntarily withdrawn from the market by Merck in response to the release of the superior medicines simeprevir (Jenssen)[117] (**2.4**) and sofosbuvir/ledipasvir (Gilead) in 2015 (**2.5 a**nd **2.6**, respectively) (**Figure 2.2**). [118-120]

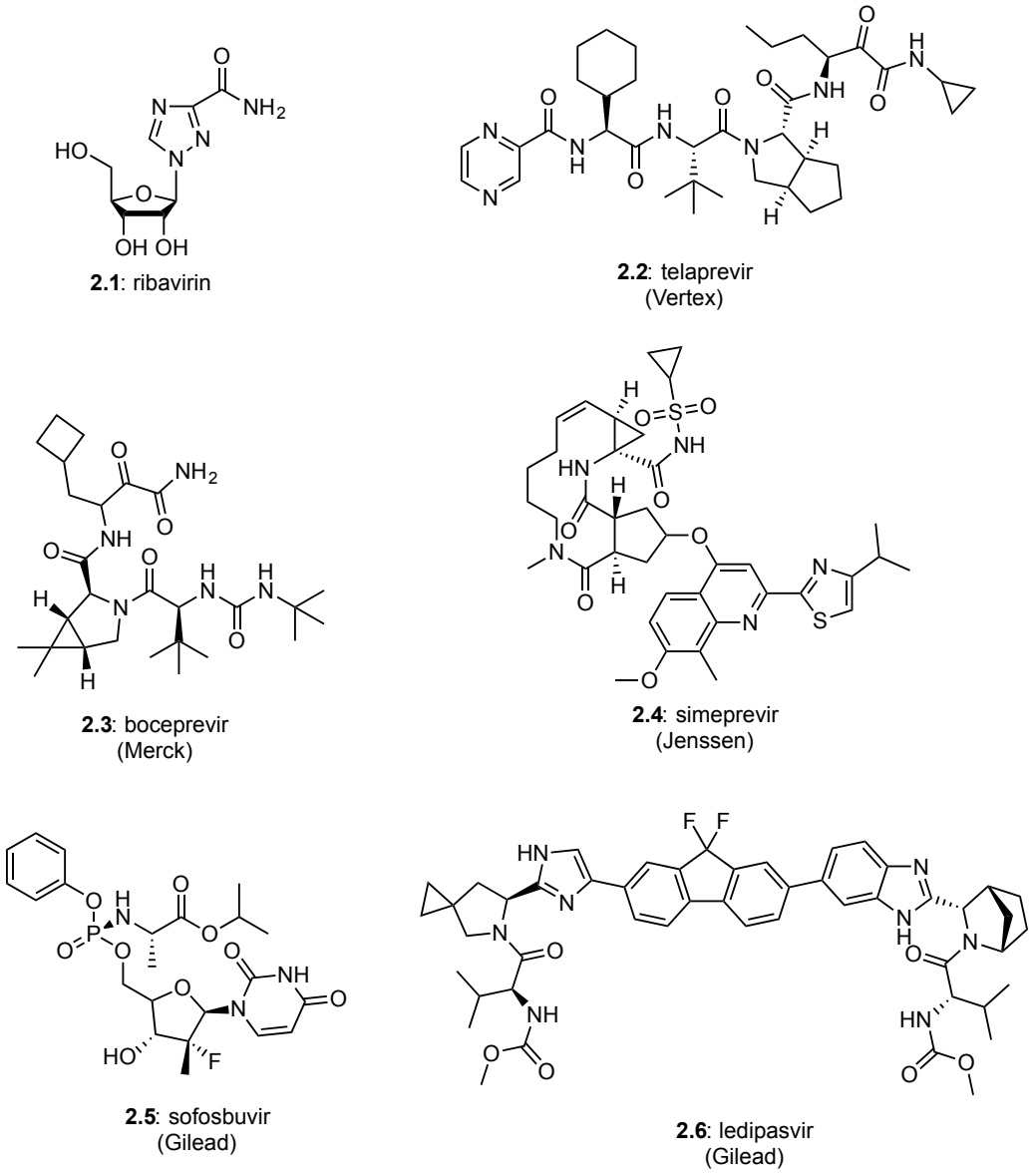


**Figure 2.2:** Current FDA approved therapies for HCV.

Current and developing therapies focus on inhibition of enzymatic activity. Inhibitors of the NS5B RNA polymerase are used in tandem with NS3 inhibitors as drug cocktails that are less prone to develop resistance. [121,122] The NS3 protease became the first target identified for therapeutic development when a clone containing a mutation in the

catalytic triad (S139A) was shown to lack infectivity, confirming the necessity of the enzyme for viral replication. [123] The protease remains one of the most well characterized and intensely studied enzymes in the HCV replicon.

## 2.2 HCV NS3 PROTEASE

The NS3 protease is located at the N-terminal third of the NS3 protein and consists of a chymotrypsin-like serine protease with a catalytic triad comprised of His57, Asp81 and Ser139 (His1083, Asp1107 and Ser1165 in the HCV polyprotein) [109,124]. Interestingly, other than the catalytic triad, the enzyme shares no sequence similarity to any other protease containing a trypsin-like fold.[125] The protease contains one zinc-binding domain[126] and functions as a heterodimer with a 54 amino acid cofactor known as NS4A via a hydrophobic 12-amino acid sequence at the center of the NS4A peptide (**Figure 2.3**). [127,128] Although sequence comparison shows similarities with other serine proteases, crystal structures of NS3 revealed several structure-defining loops that shape the N-terminal binding pockets of other proteases in this family are absent in the NS3 system, rendering the S1 specificity pocket as a shallow nonpolar groove consisting of the side chains of residues Phe154, Ala157, and Leu135. As a result, this enzyme displays a unique substrate specificity that renders classical serine protease inhibitors ineffective against NS3, suggesting that highly selective inhibitors could be developed.[129]

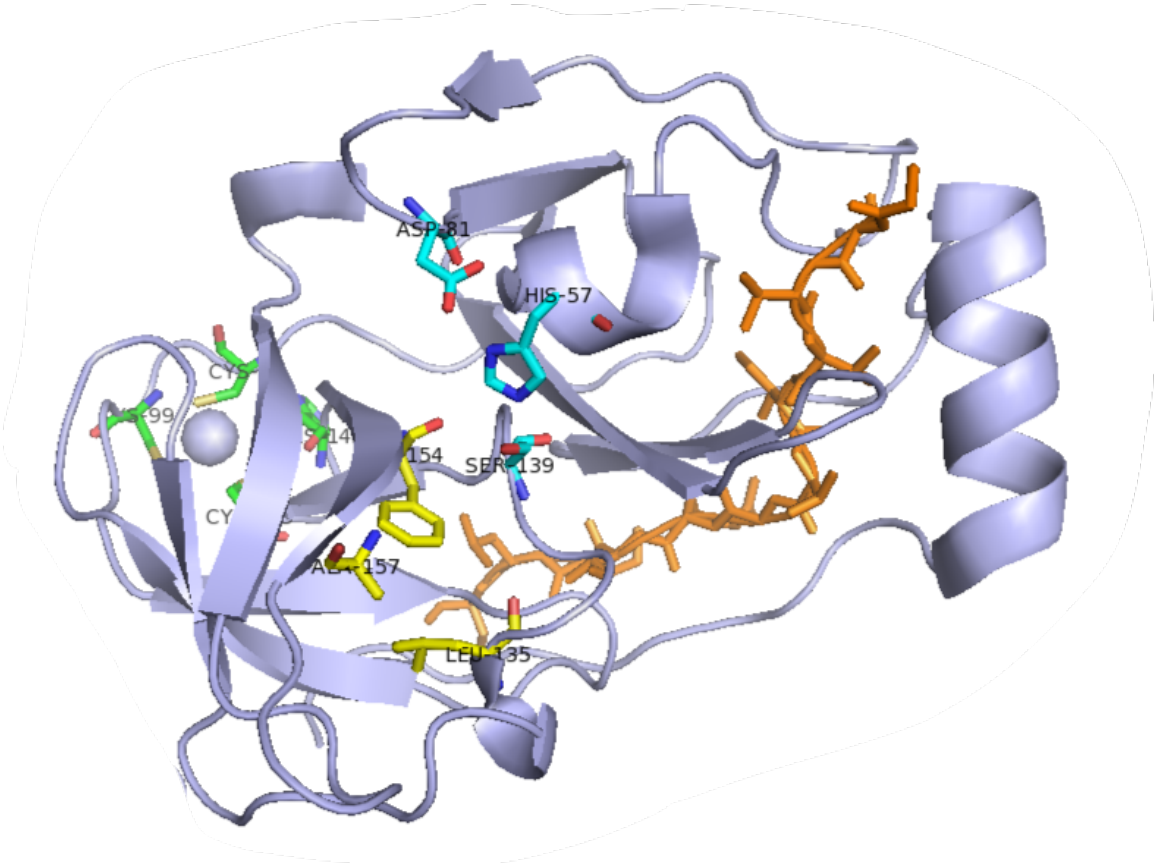


**Figure 2.3:** Crystal structure of the NS3/NS4A complex (PDB file 1DXP[130]) highlighting the catalytic triad (cyan), the S1 specificity pocket (yellow), the $Zn^{2+}$ binding domain (green) and the NS4A cofactor (orange).

## 2.3 Development of Linear Tripeptide HCV NS3 Protease Inhibitors

Given the unique structure and critical role of the NS3/NS4A complex in the processing of essential downstream proteins, the enzyme presented an attractive target for therapeutic development. Much of the groundbreaking work in the development of small molecule therapies for HCV was done by scientists at Boehringer Ingelheim. [67,76,104,131-141] At the outset of the work that is the focus of this dissertation there were no approved therapies for HCV, and the key developments in mapping the NS3 active site were made

in the course of their optimization studies. The remainder of this chapter will focus on the development of the first potent and specific linear tripeptide HCV inhibitors.

In 1998 Llinàs-Brunet *et al*. reported that the hexapeptide **2.7** (DDIVPC-OH), the N-terminal cleavage product of a substrate derived from the NS5A/5B cleavage site, [142] inhibits the NS3/4A complex with an $IC_{50}$ of 71 μM. (Figure **2.4**). Steinkühler *et al*. also reported that the NS3 protease was inhibited by N-terminal cleavage products of peptides corresponding to cleavage sites at the NS4A/NS4B, NS4B/NS5B, and NS5A/NS5B junctions. [143]

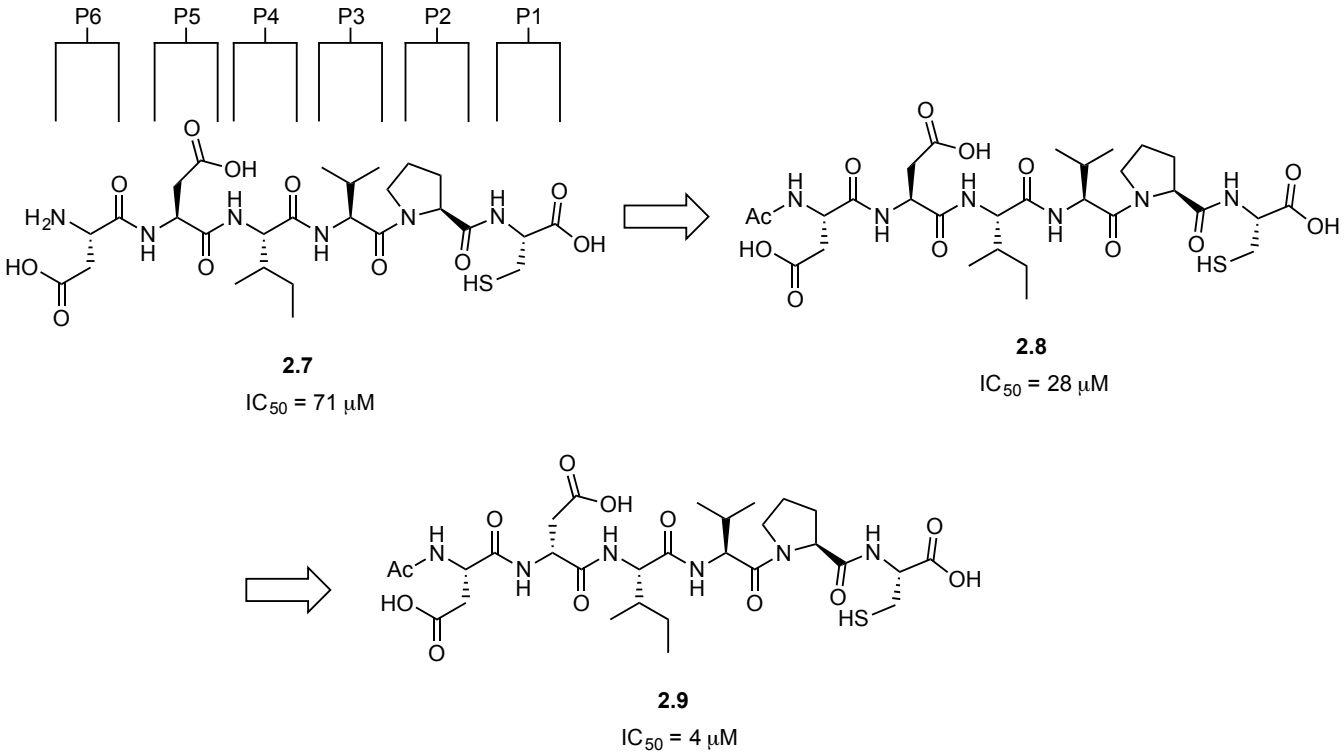


**Figure 2.4**: Early hexapeptide inhibitors of the HCV NS3 protease.[131]

Several *N*-terminal capping groups were screened with an acetyl group resulting in the largest increase in potency to give **2.8** with an $IC_{50}$ of 28 μM. Replacing each residue

with alanine and measuring the potency identified the P4 isoleucine, P3 valine, and P1 cysteine residues as most important to the binding affinity. Substitution at the P5 aspartate residue was well tolerated (**2.9**), suggesting that the side chain carboxylic acid is not important to potency. Interestingly, introduction of a D-aspartate residue at P5 resulted in a seven-fold increase in potency, however this increase was lost upon replacement of the P6 aspartate residue. The authors took this result to suggest that the P5 residue orients the P6 aspartate residue to form a more favorable interaction with the protein.

The importance of the P1 cysteine was thought to be due to interactions between the sulfhydryl group and the aromatic group of Phe154, which defines the bottom of the S1 specificity pocket of the enzyme. [125,144] Removal of the sulfhydryl group, methylation of the sulfur atom, and substitution to serine or methionine all resulted in substantial decreases in potency. [131]

Peptides **2.8** and **2.9** were chosen as the starting point for further optimization. Early efforts involving these hexapeptides focused on substitution of the P1 cysteine residue, which was prone to undergo dimerization reactions to form disulfides.[138] Although five-fold less potent than the cysteine residue of **2.7**, norvaline was determined to be the best cysteine replacement, resulting in low-micromolar inhibitor **2.10** (Figure **2.5**).[132] Replacement of the C-terminus with electrophilic carbonyl groups such as aldehydes and fluoro-carbonyl compounds is a common strategy for enhancing inhibition of serine proteases.[145] Unfortunately, these substitutions resulted in diminished potency against the protease. α-Ketoamide derivatives **2.10** and **2.11** were the strongest inhibitors of the NS3 protease. (Figure **2.5**).

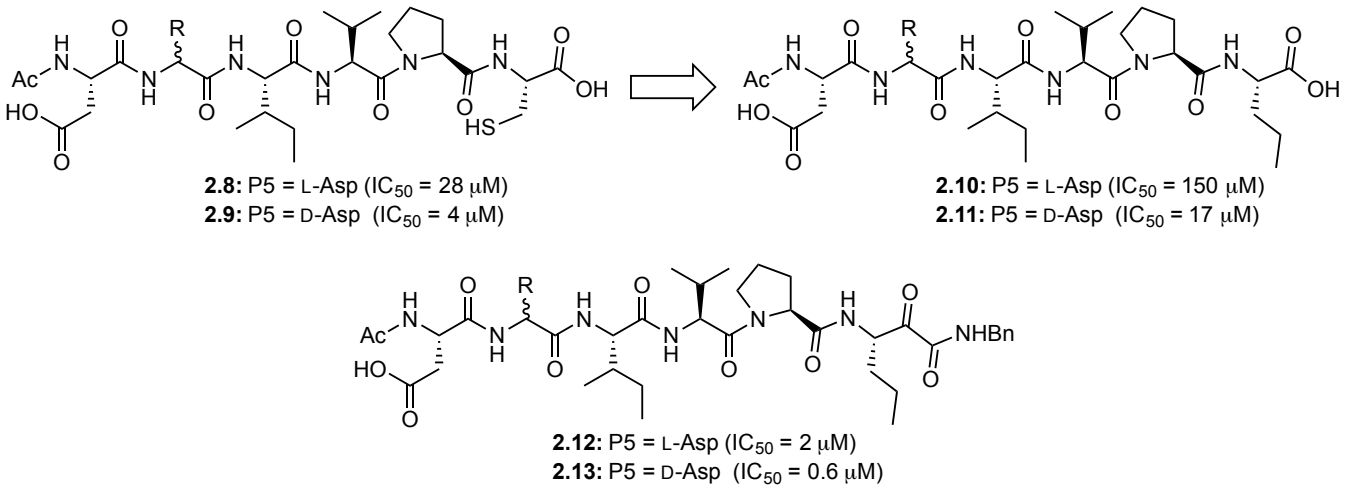


**Figure 2.5**: Hexapeptide HCV NS3 inhibitors **2.8**-**2.13**.[132]

The introduction of electrophilic carbonyls raised concerns about potential loss of specificity for the inhibitors. Although the. α-ketoamide **2.10** to **2.11** was the most potent, these inhibitors also displayed eroded selectivity against other serine proteases such as human leucocyte elastase (HLE) and porcine pancreatic elastase (PPE).[132] The original the C-terminal carboxylic acids appeared to impart the highest and specificity for the NS3 protease. Replacement of the carboxylic acid functionality with alcohols or amides reduced potency, although methyl and benzyl esters were found to be roughly equipotent, potentially due to hydrolysis by the enzyme.[132] When the *C*-terminal esters also showed off-target activity, the carboxylic acid was retained for further studies.

Substitution on the P2 proline ring with an (*R*)-benzyl or (*R*)-benzyloxy group resulted in a substantial gain in potency for inhibitor **2.14** as evidenced by the $IC_{50}$ (7 μM) (Figure **2.6**).[76] NMR and computational studies[75] provided key insights for further development of these inhibitors. Differential line broadening NMR showed that the P2 benzyloxy substituent is in direct contact with the protease resulting in the observed increase in potency. To increase van der Waals contacts with the protein naphthen-1-

ylmethoxy derivative **2.15**, which represents the first NS3 inhibitor with submicromolar potency. Further optimization with a P5 D-glutamate and a P4 cyclohexyl group provided nanomolar inhibitor **2.16**. NMR studies also showed the P5 and P6 residues were shown to be solvent exposed and only weakly interacting with the protease.[75] To reduce the peptidic nature of these compounds, these residues were then truncated. Replacing the *N*-terminal norvaline residue with a 1-amino-cyclopropylcarboxylic acid provided inhibitor **2.17**, a low micromolar, monocharged tetrapeptide inhibitor with good selectivity for NS3 over other proteases.[76]

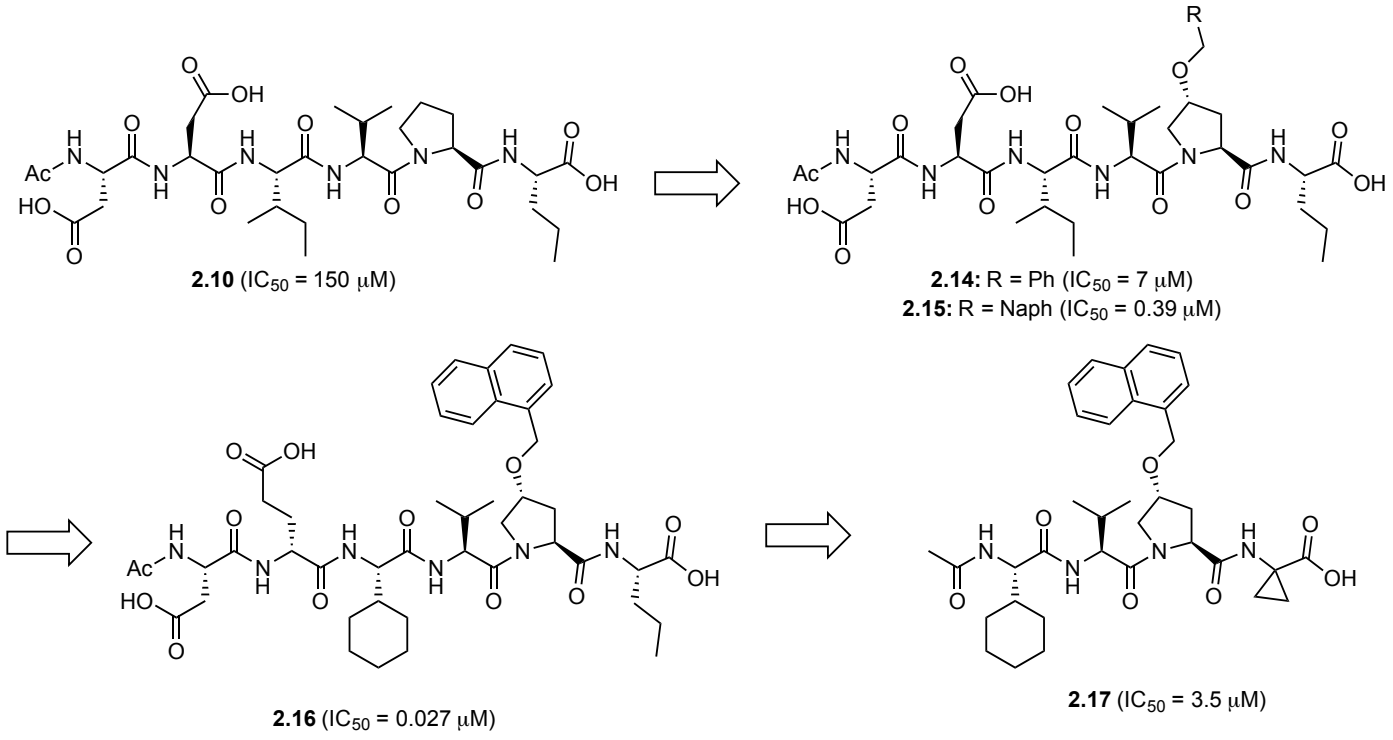


**Figure 2.6**: Hexapeptide HCV NS3 inhibitors **2.14**-**2.17**.[76]

The benefits of adding hydrophobic surface area suggested the presence of a lipophilic binding pocket within the enzyme active site. A variety of P2 subunits were

screened in order to probe the available surfaces and maximize dispersive interactions. *Para*-substituted phenyl groups afforded low micromolar inhibitors, with a tenfold increase in binding affinity observed from *p*-fluoro to *p*-iodo. They noted that the increase in binding affinity correlates with increasing polarizability of the halogen. A similar effect was also observed in the quinoline-containing ligands, leading them to rationalize that a dipole/quadrupole interaction may take place between the binding pocket and the aromatic ring.[133]

**Table 2.1**: $IC_{50}$ values for HCV NS3 inhibitors **2.18-2.27**.[76]

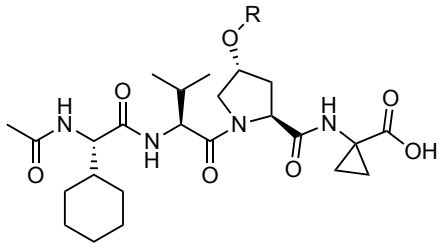

| Ligand | R | $IC_{50}$ (μM) | Ligand | R | $IC_{50}$ (μM) |
|---|---|---|---|---|---|
| **2.18** | 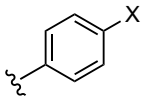 | 10-100 | **2.23** | 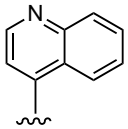 | 5 |
| **2.19** | 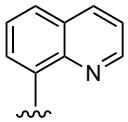 | 250 | **2.24** | 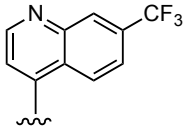 | 6 |
| **2.20** | 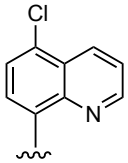 | 100 | **2.25** | 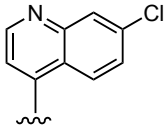 | 2 |
| **2.21** | 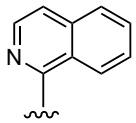 | 8 | **2.26** | 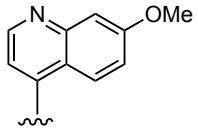 | 0.8 |
| **2.22** | 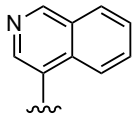 | 4 | **2.27** | 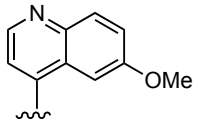 | 16 |

Computational models of inhibitor **2.14** bound to the enzyme showed the P1 and P3 residues in close proximity to one another.[67] They speculated that a hydrocarbon tether between these residues would result in a macrocyclic inhibitor that was preorganized into the bound conformation. They also hypothesized that additional interactions could be made between the hydrocarbon bridge and the binding pocket which should also increase binding affinity.

The tetrapeptide scaffold **2.28** without a P2 subunit was a poor inhibitor of the protease (< 20% inhibition at 1mM). Truncation to the tripeptide **2.29** also resulted in a poor inhibitor. However, when the P1 and P3 residues of **2.29** were tethered into a 15-membered macrocycle with a *Z*-olefin geometry provided a substantial increase in potency (Figure **2.8**). Substitution of the proline with the 4-hydroxy-7-methoxyquinoline moiety[138] resulted in a 16,600-fold increase in potency to give inhibitor **2.30**. Addition of a 2-phenyl group to give **2.31** resulted in a further doubling of potency. Scission of the macrocycle to linear analog **2.32** came with a large drop in potency, which supported their hypothesis that preorganization would lead to an increase in binding affinity.

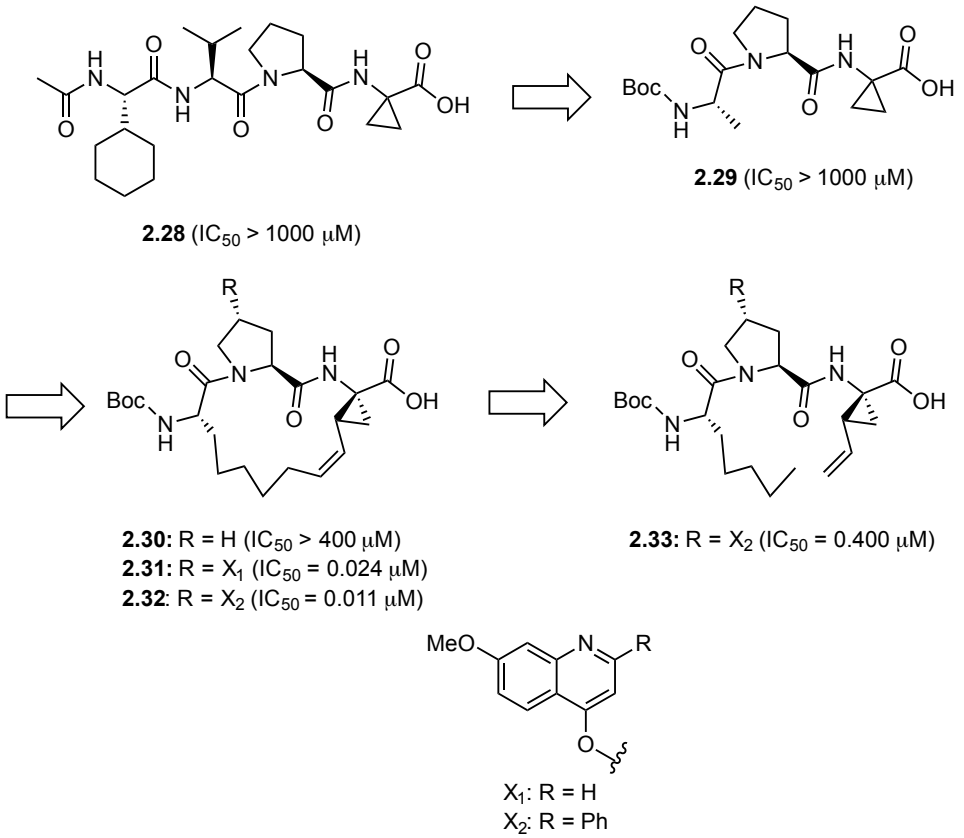


**Figure 2.7**: $IC_{50}$ values for HCV NS3 inhibitors **2.28-2.33**.[76]

Crystal structures of the NS3 protease complexed with **2.32** showed the macrocyclic P1-P3 bridge was shown in the X-ray structure to be within van der Waals distance of V132 and such interactions may contribute to overall binding. The macrocyclic compounds were relatively stable to metabolism in human and rat liver microsomes and shown to be cleared mainly through the liver.[67] Unfortunately, their most potent inhibitor **2.32** showed rapid clearance and a low steady state distribution.

Substitutions were made on the P2 subunit in order to improve the pharmacokinetic properties of the inhibitors. Substituting the 2-phenyl group with of the quinoline with a variety of 2-amino-4-thiazolyl groups resulted in low nanomolar inhibitors in both enzymatic and cell assays. The *N*-terminal Boc capping group was replaced with the more chemically stable cyclopentyl carbamate. Combining these optimizations resulted in macrocyclic inhibitor BILN 2061 (**2.34**) with an improved clearance and oral bioavailability of 42% (Figure **2.9**). The development of BILN 2061 is extremely significant in the development of HCV therapies, as BILN 2061 became the first proof-of-concept HCV inhibitor to reduce viral load in humans.[135]

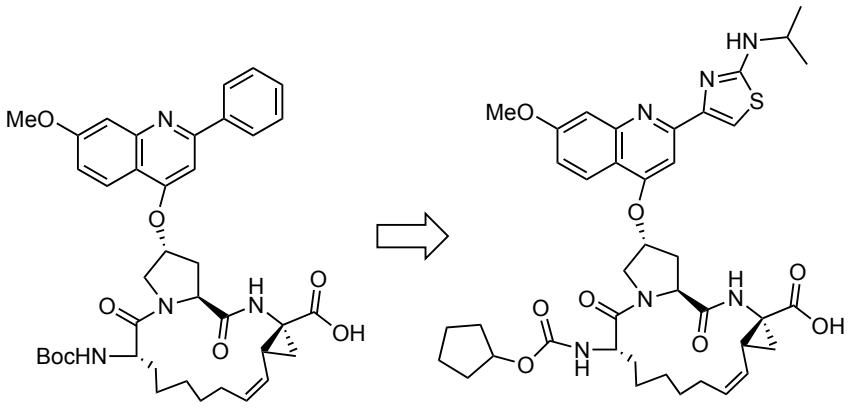


**2.32:** $IC_{50}$ = 0.011 μM

**2.34:** BILN 2061 (**$IC_{50}$** = 0.003 μM)

**Figure 2.8:** Development of BILN2061 (**2.15**).

Unfortunately cardiotoxicity associated with administration of **2.34** redirected attention away from the macrocyclic inhibitors and back toward linear analogs with the goal of truncation and modification to reduce the peptidic nature of the compounds and enhance bioavailability. [146] The P3 valine residue from previous inhibitors was substituted for the bulkier *tert*-butyl side chain in an effort to further rigidify and preorganize the compound into the bioactive conformation.[140] The previous 7-methoxy-2-phenylquinoline subunit was found to be optimal for these new linear compounds. Truncation of the P4 cyclohexyl glycine residue and capping of the *N*-terminus with a *tert*-butyl carbamate to maintain a key hydrogen bonding interaction between the capping group carbonyl and the NH of Cys159 afforded **2.35**, a linear tripeptide inhibitor with nanomolar binding both *in vitro* and *in vivo*. This tripeptide was further elaborated to generate the next clinical candidate from Boehringer Ingelheim, BI 201335 (**2.36**) (**Figure 2.10**).[104]

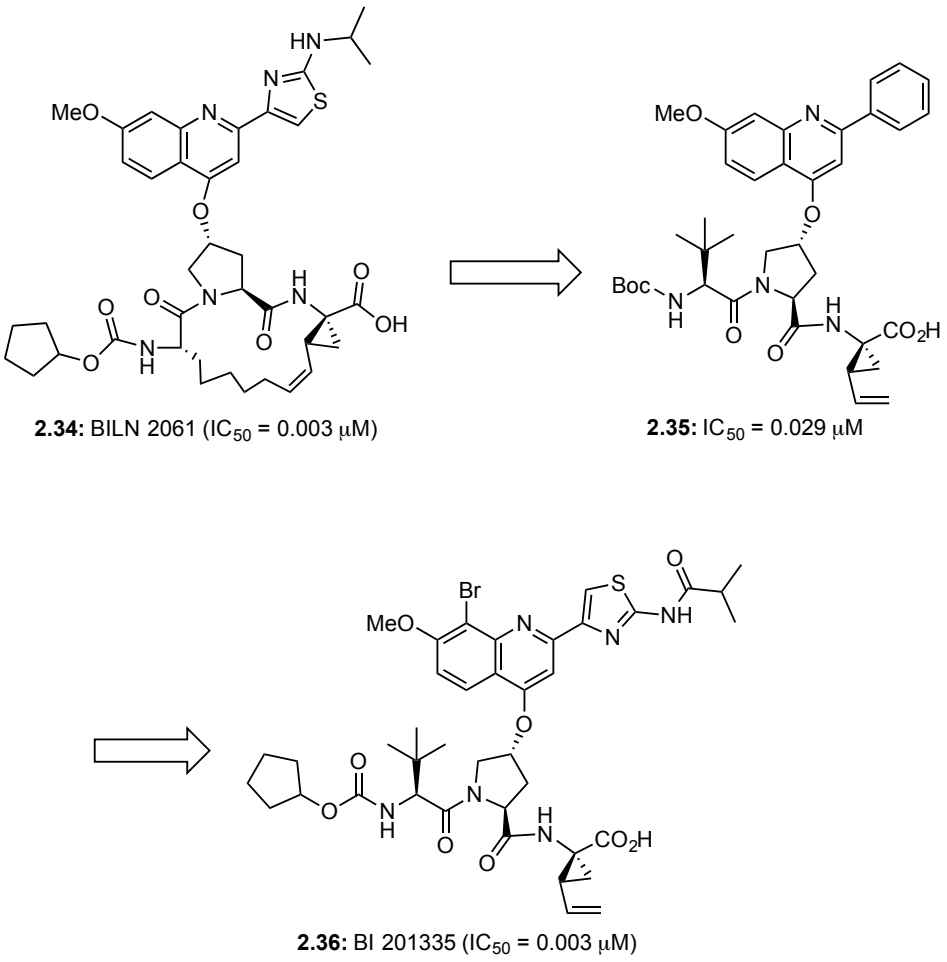


**2.34:** BILN 2061 ($IC_{50}$ = 0.003 μM)

**2.35:** $IC_{50}$ = 0.029 μM

**2.36:** BI 201335 ($IC_{50}$ = 0.003 μM)

**Figure 2.9:** Development of BI 201335 (**2.17**).

## 2.4 NS3 AS A MODEL SYSTEM FOR PROTEIN-LIGAND INTERACTIONS

The significant increases in binding affinity that accompanied structural changes to these ligands piqued our interest into the underlying thermodynamics of these interactions between the ligand and the enzyme active site. Due to our previous work investigating the thermodynamic effects of introducing conformational constraints on protein-ligand binding (see **Section 1.5.1.2**), we were eager to explore the energetics associated with conformational constraint related to the macrocyclic ligands **2.30**-**2.32** as well as the *tert*-butyl group in the linear tripeptide **2.35**. We were also greatly interested understanding the

energetics of interactions between the enzyme and the P2 heteroaryl subunit, as addition of a substituted 4-hydroxyquinoline moiety onto the oligopeptide scaffold resulted in substantial increases in potency (Figures **2.7** and **2.8**).

For our initial investigations into the energetics of binding between the NS3 protease and small peptide inhibitors, were particularly interested in ligand **2.35**. **t**he ease with which derivatives of this ligands could be prepared prompted us to seize this unique opportunity to conduct a detailed investigation of the enthalpic and entropic effects associated with incremental changes in ligand structure within the context of this medicinally important biological system. We speculated that the wealth of literature available with X-ray, NMR, and modeling structures provided a well-characterized binding pocket that would make collection and interpretation of structural data fairly straightforward. In the next chapter, we will discuss an evaluation the entropic and enthalpic contributions of several affinity-enhancing substituents on the P2 hereroaryl subunit. We will also explore the thermodynamic effects associated with incremental increases in steric bulk at the P3 site to understand the role that the *tert*-butyl group plays in improving binding affinity.

# Chapter 3. Thermodynamic Evaluations of Linear Tripeptide HCV NS3 Protease Inhibitors

## 3.1 INTRODUCTION

The profound increase in potency observed by introduction and subsequent substitution of the quinoline subunit on the P2 proline ring suggests the formation of key interactions within the enzyme active site. The ease with which derivatives of this P2 subunit could be prepared prompted us to seize this unique opportunity to conduct a detailed investigation of the enthalpic and entropic effects associated with incremental changes in ligand structure within the context of this medicinally important biological system. $IC_{50}$ data were collected for derivatives **3.1**-**3.6** by scientists at Boehringer Ingelheim (B.I.)[1] and provided to us along with estimated $\Delta G^\circ$ values.[2]

[1] Llinàs-Brunet, M. *Unpublished results*.

[2] Values for $\Delta G^\circ$ were calculated from Equation 1.3, under the assumption that $IC_{50} \approx 1/K_a$.

**Table 3.1**. $IC_{50}$ and calculated $\Delta G°$ values for ligands **3.1-3.6**.

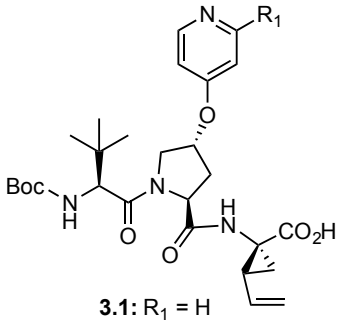

**3.1:** $R_1$ = H
**3.2:** $R_1$ = Ph

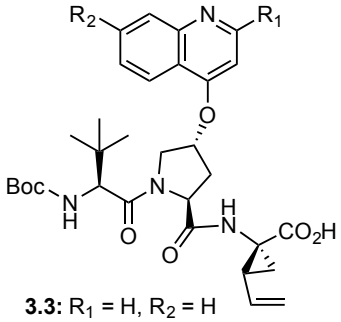

**3.3:** $R_1$ = H, $R_2$ = H
**3.4:** $R_1$ = Ph, $R_2$ = H
**3.5:** $R_1$ = H, $R_2$ = OMe
**3.6:** $R_1$ = Ph, $R_2$ = OMe

| Compound | $IC_{50}$ (μM) | $\Delta G°_{calc}$ (kcal•mol$^{-1}$) |
|---|---|---|
| **3.1** | 96 | –5.5 |
| **3.2** | 34 | –6.1 |
| **3.3** | 3 | –7.6 |
| **3.4** | 0.150 | –9.4 |
| **3.5** | 0.170 | –9.3 |
| **3.6** | 0.025 | –10.4 |

Although changes in the association constants ($K_a$) and free energies of binding ($\Delta G°$) across this series could be approximated from the $IC_{50}$ values, the individual enthalpic ($\Delta H°$) and entropic ($\Delta S°$) contributions of these changes were still unclear. It is hypothesized that a thorough understanding of both the enthalpic and entropic consequences of these structural modifications, with respect to interactions with the NS3 protease active site, could aid in guiding the development of novel, potent inhibitors with favorable properties as drugs. Thus, an investigation commenced in an effort to better understand these protein-ligand interactions.

### 3.1.1 The Double Mutant Cycle

A detailed thermodynamic analysis would allow for determination of the changes in enthalpy and entropy of binding resulting from introduction of each substituent as well as evaluation of the impact that one substitution may have on another region of the molecule. With this in mind, a double mutant cycle analysis was envisioned to be most appropriate. The concept of a double mutant cycle analysis was first proposed by Fersht in 1984 as a method to aid in the analysis of the secondary effects of side chain mutations in proteins. [147] While gross structural differences as a result of such modifications can be readily observed by x-ray crystallography, the magnitude of the distortion and subsequent impact on binding energetics is highly variable. A change of even 0.1 Å, observable at higher resolutions by x-ray crystallography, may contribute as much as 2-3 kcal $mol^{-1}$ if optimization of a hydrogen bond occurs.[147] Examination of the differences in crystal structure may not be sufficient to explain small changes in binding affinity. The double mutant cycle offers a simple solution-state complement to x-ray analysis that allows for investigation of interaction between residues.

In order to evaluate any potential interactions between residues, two distinct single mutants (A'B and AB') and a double mutant (A'B') were constructed for comparison to the wildtype (AB) (**Figure 3.1**). It was proposed that if side chain modifications introduce no significant structural changes to the apoenzyme or the enzyme-substrate complex, then the energetic consequences will be independent of one another.

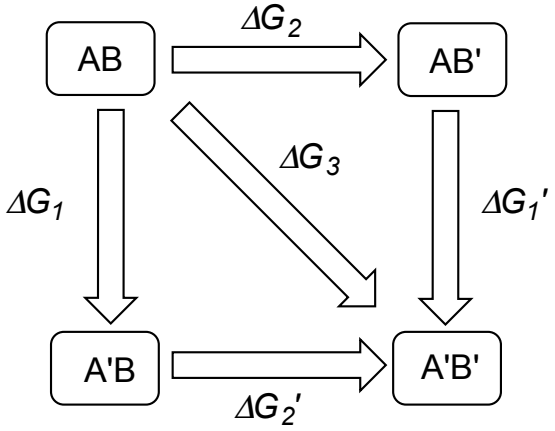


**Figure 3.1:** Basic double mutant cycle.[147]

$$\Delta G_1 = \Delta G_1' \tag{3.1}$$

$$\Delta G_2 = \Delta G_2' \tag{3.2}$$

As a result, the change in binding affinity between the wildtype and the double-mutant will simply be the sum of the corresponding energy differences of each of the single mutants.

$$\Delta G_3 = \Delta G_1 + \Delta G_2 = \Delta G_1' + \Delta G_2' \tag{3.3}$$

In the case where introduction of a mutation is accompanied by extensive structural changes, the change in free energy of the enzyme-substrate complex for one mutation may vary based on whether or not the other mutation is already present. For this situation, another set of equations can be generated:

$$\Delta G_1 \neq \Delta G_1' \tag{3.4}$$

$$\Delta G_2 \neq \Delta G_2' \tag{3.5}$$

$$\Delta G_1 - \Delta G_1' = \Delta G_2 - \Delta G_2' \neq 0 \tag{3.6}$$

The energy difference calculated in equation 3.6 is known as the "coupling energy" and measures the difference between the double mutant and the two single mutants taken separately. Cases in which one mutation has no impact on the affinity at a second site will exhibit a coupling energy of zero.

While studying the importance of three residues in the active site of tyrosyl-tRNA synthetase from *Bacillus stearothermophilus*, it was noted by Fersht that mutation of Thr51 to proline (as is observed in the *E. coli* enzyme) resulted in a massive improvement in the binding affinity for ATP.[147] It was hypothesized that rather than forming a direct interaction with ATP, the introduction of a proline residue to the backbone destabilizes the α-helix and repositions the side chain of His48 to provide stronger interaction with ATP. In order to probe the interaction between these two residues, binding affinities of the wildtype TyrTS(His48-Thr51) were compared to two single mutants (TyrTS(Gly48) and TyrTS(Pro51)) and a double mutant (TyrTS(Gly48-Pro51)).

A double mutant cycle was constructed to evaluate possible impacts of an H48G mutation on a nearby cysteine residue, as shown in **Figure 3.2**. The data suggest that the energetic consequences of mutations in these residues are independent of one another. The loss of binding energy between the wildtype and double mutant is the sum of the energy loss calculated for each of the single mutants Gly35His48 and Cys35Gly48 (+2.3 kcal $mol^{-1}$).

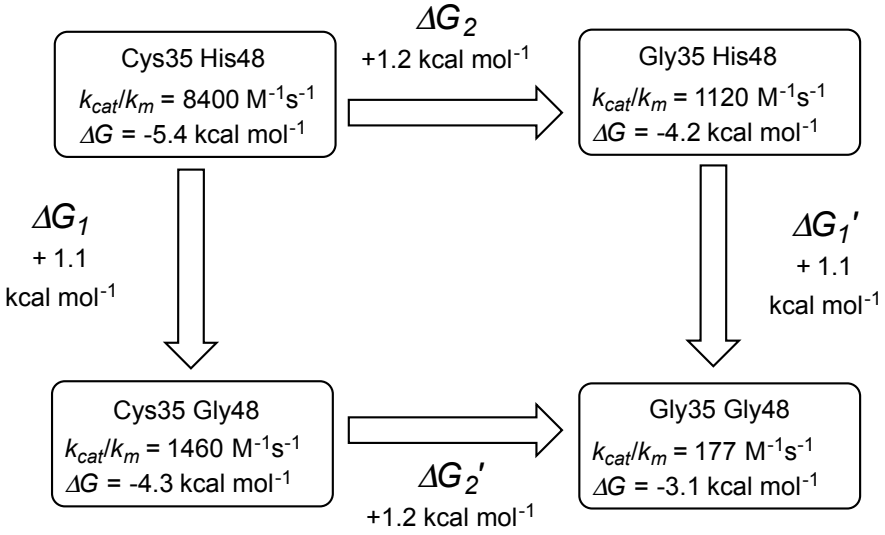


**Figure 3.2:** Double mutant cycle analysis of H48G mutation.[147]

A second double mutant cycle analysis was constructed to evaluate the energetic consequences of the H48G and T51P mutations (**Figure 3.3**). Were the two mutations in the of tyrosyl-tRNA synthetase enzyme non-interacting, the Gly48 Pro51 double mutant would be expected to exhibit a more favorable binding energy than that of the wildtype by –0.8 kcal mol$^{-1}$; however, the double mutant cycle analysis revealed that the observed binding energy was much *worse* (by 1.8 kcal mol$^{-1}$) than expected.

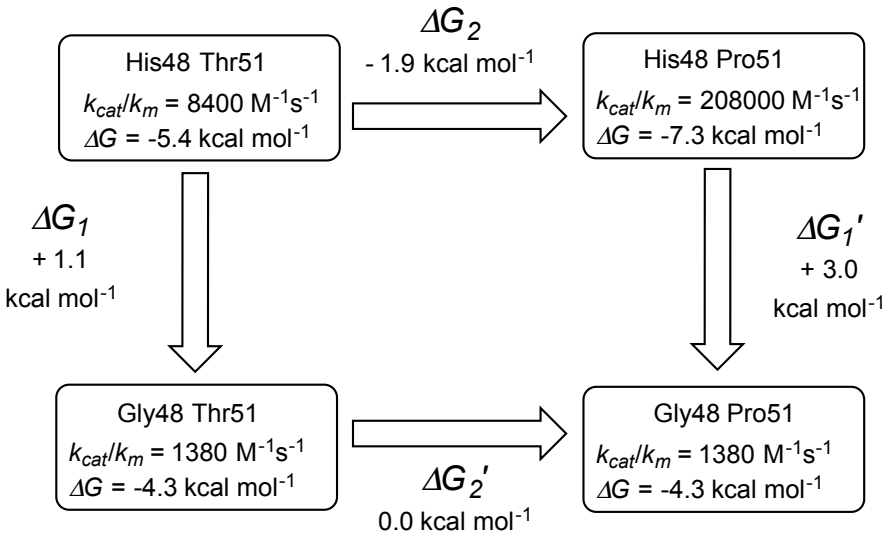


**Figure 3.3:** Double mutant cycle analysis of T51P mutation.[147]

No binding energy change was observed between the Gly48 Thr51 single mutant and the Gly48 Pro51 double mutant which precludes the possibility of a simple direct interaction with ATP and further highlights the interactions between these two residues. This finding supports the proposed hypothesis that the distortion in the backbone due to introduction of the proline residue results in an increase in the interaction of the histidine residue with ATP.

This methodology has been extended to the study of synthetic chemical systems to probe interactions within supramolecular complexes[148,149] as well as interactions between aromatic groups[150-154]. A novel DMC analysis has also been applied to the study of HCV NS3 tripeptide inhibitors.[141] This approach was utilized to further illuminate the binding event and provide valuable ligand structure-activity relationship (SAR) data.

The first DMC was constructed in an effort to understand the impact of the *N*-terminal Boc capping group and the P3 *tert*-butyl side chain (**Figure 3.4**). Noninteraction between these two groups would result in additive effects on the binding energy resulting

in a predicted $IC_{50}$ of 0.58 μM and a calculated $\Delta G°$ of –9.2 kcal $mol^{-1}$ for inhibitor **3.6**. The observed activity however is much greater at 0.080 μM ($\Delta G° = -10.4$ kcal $mol^{-1}$).

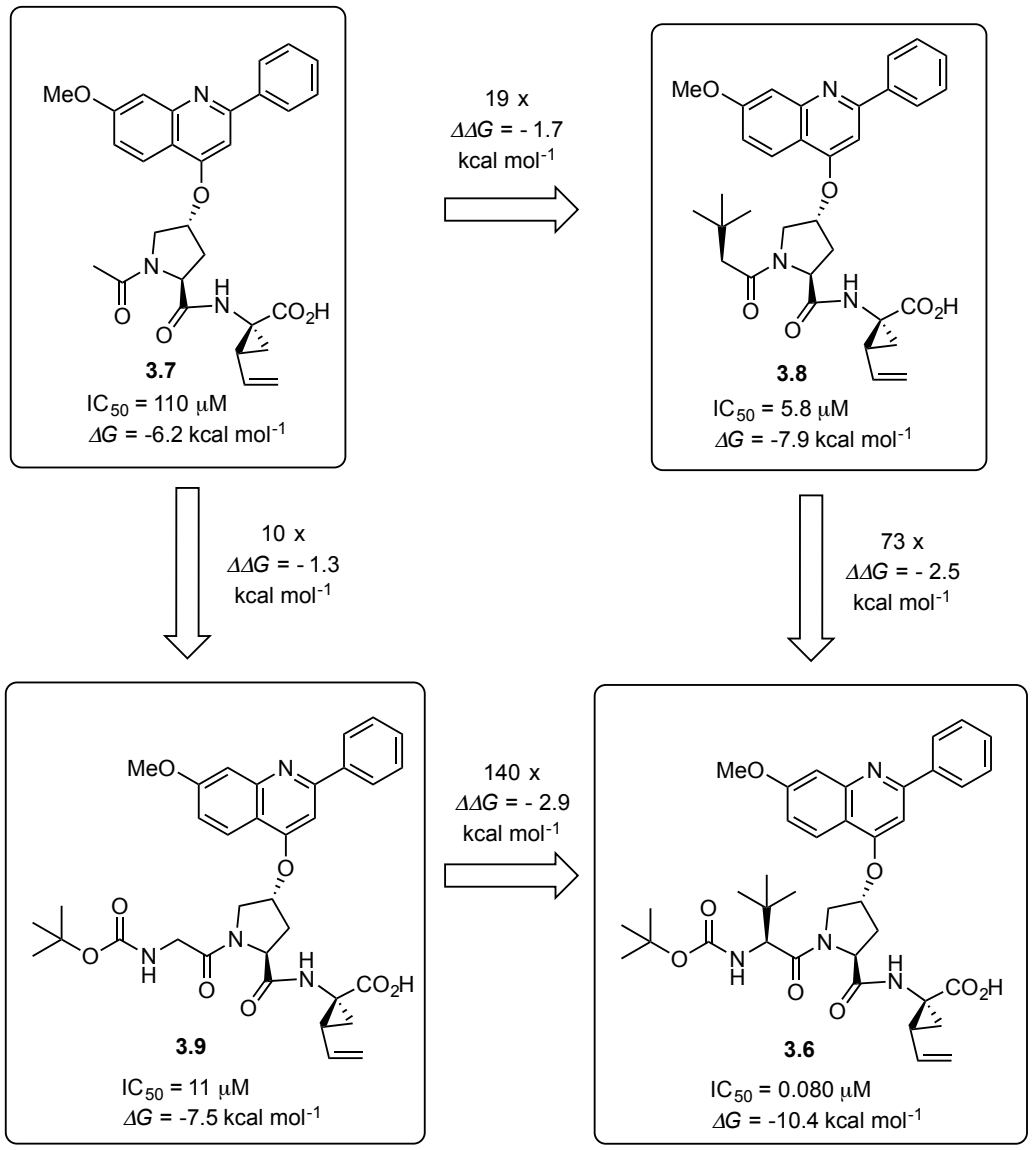


**Figure 3.4:** Double mutant cycle analysis of P3 capping group and *tert*-butyl side chain.[141]

The synergy between these two substitutions was hypothesized to originate from conformational factors. The global rigidification of the peptide upon introduction of the conformationally restricting *tert*-butyl group results in a forcibly extended peptide backbone that allows for the Boc-P3 region to form hydrogen bonds with the enzyme,[141] though the exact enthalpic and entropic contributions to the observed binding affinity are unknown.

The next DMC analysis investigated the contributions of the P2 quinoline B-ring and the thiazole moieties of **3.14**, an analog of BILN 2061 that is known to bind the HCV protease in a similar manner (**Figure 3.5**).[141] Beginning from the unsubstituted pyridine ligand **3.1**, addition of either substituent results in a substantial increase in potency, and the doubly substituted compound **3.11** exhibits a nearly 2500-fold increase in potency. However, the DMC analysis reveals an antagonistic effect, with the observed $IC_{50}$ of 0.039 μM falls 10-fold short of the expected $IC_{50}$ of 0.0039 μM.

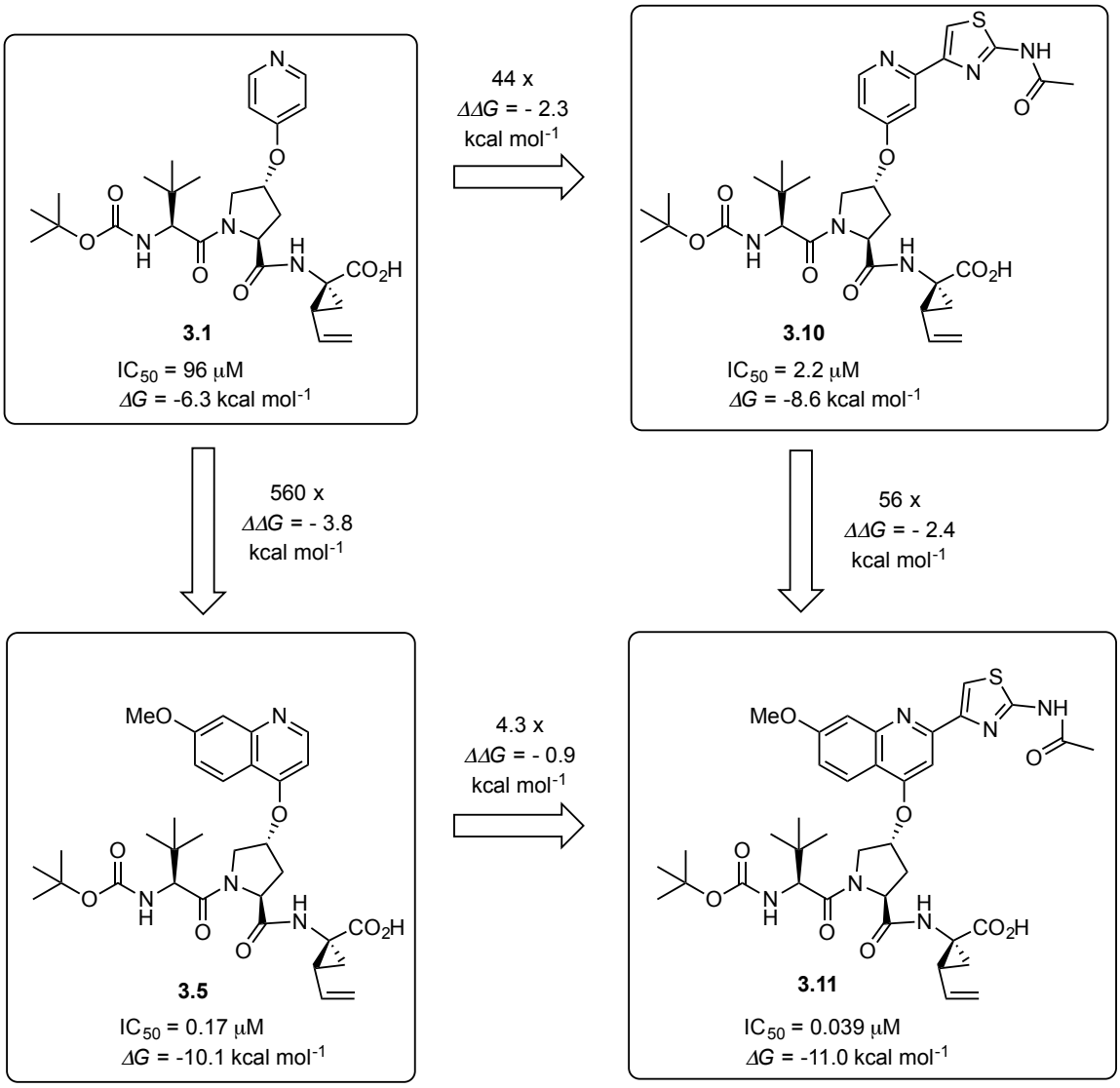


**Figure 3.5:** Double mutant cycle analysis of P2 substituents. [141]

Such an antagonistic effect was suspected to be the result of a change in the bound conformation of the inhibitor, as such a phenomenon had been previously observed for several pyridine and quinoline containing tripeptide NS3 inhibitors.[136] NMR studies were undertaken to determine the binding conformation of **3.11**. A molecular model generated from NOE data revealed that the thiazole moiety of **3.11** is oriented toward the N-terminal

end of the inhibitor, whereas the 2-phenyl substituent of the pyridine and quinoline-containing ligands are known to be oriented toward the C-terminus of the inhibitor. [136]

This literature study represents the first application of this methodology to the study of ligand structural modifications within the global context of a protein-ligand binding event. This type of SAR analysis when coupled with structural studies help to further understand the importance of understanding secondary interactions within protein-ligand binding events. Identification and subsequent optimization of favorable secondary interactions would prove useful to rapid development of more potent therapeutics. Although this methodology has been used to probe interactions between substituents and the subsequent effects on total binding affinity, this analysis has never before been extended to an evaluation of individual thermodynamic parameters. The research presented herein furthers this analysis for a series of related HCV NS3 inhibitors to examine the energetic contributions of each substituent through the lens of enthalpy and entropy changes upon binding.

### 3.2 Studies on Tripeptide NS3 Inhibitors: The P2 Heterocycle

With the large increases in binding affinity associated with the addition of the heteroaryl P2 subunit (see Chapter 2), we were interested in understanding the individual thermodynamic effects of the addition of the second aromatic ring to form the quinoline subunit as well as the addition of the 2-phenyl and 7-methoxy substituents. Thus, we set out to evaluate two separate double-cycles in an effort to examine the thermodynamic impact of each substituent individually (**Figure 3.6**).

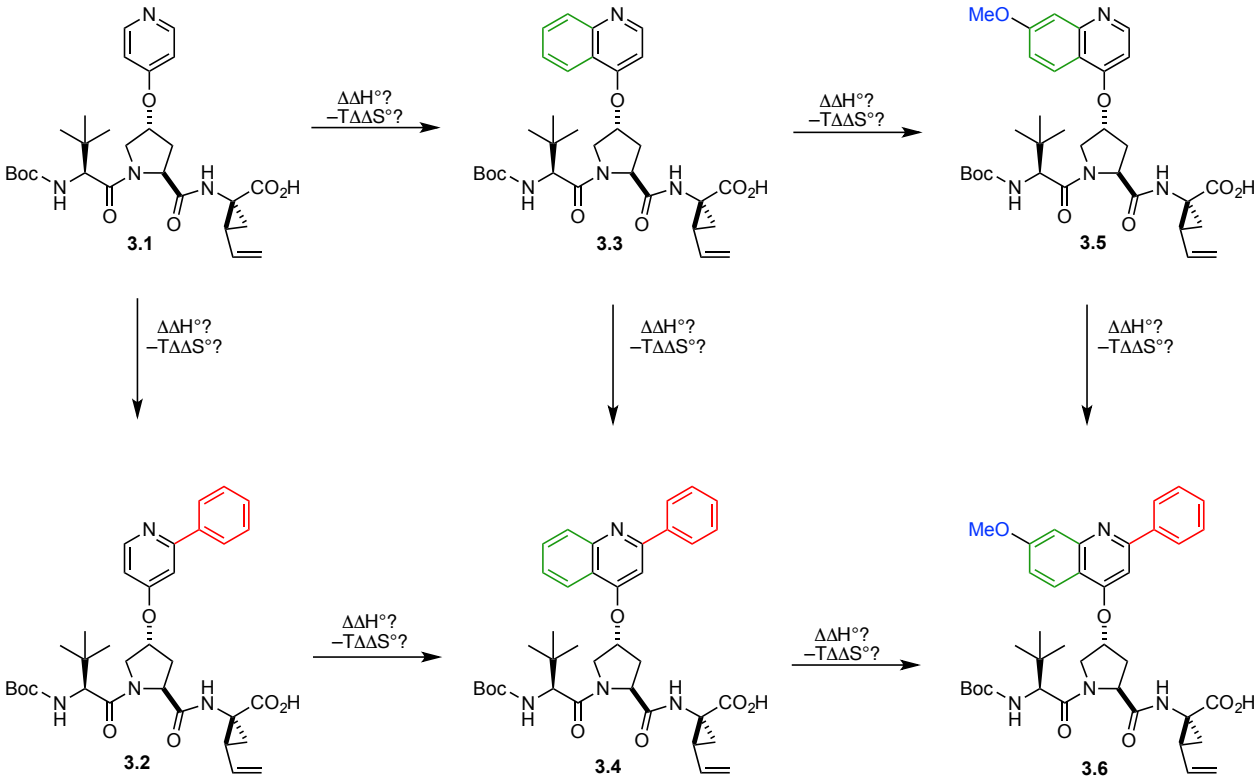


**Figure 3.6:** Proposed double mutant cycles for **3.1**-**3.6**.

For this purpose, we initiated a collaborative effort with Boehringer Ingelheim. In addition to providing us with valuable synthetic intermediates, we were also provided the plasmid DNA that encodes for the NS3-NS4A "single chain" fusion protein developed by B.I.[155]

The full-length NS3 protein is a 70kDa protein that contains both a protease domain and a helicase domain. However, only the protease domain, which makes up the *N*-terminal 180 amino acids of the protein, complexed with the NS4A peptide is necessary for proteolytic activity. The wildtype protein suffers from extremely low yields and poor solubility, which would make the full-length NS3 extremely difficult to obtain at the concentrations necessary for use in ITC experiments (30-70 μM). Furthermore, accurate ITC results would depend on the quantitative formation of a trimeric complex between

NS3, NS4A, and the ligand. For the sheer number of experiments necessary, the amount of the 17-mer NS4A peptide segment would also present a significant synthetic burden. Thus, it was determined that the single-chain construct would be more appropriate for this project.

During their investigations into the role of the helicase domain in proteolytic activity, B.I. scientists engineered a simpler "single chain" protease. This construct contains the central 17 residues of the NS4A peptide linked to NS3 protease domain (**Figure 3.7**). The NS4A peptide sequence is covalently linked to the *N*-terminus of the NS3 protease domain by a two-amino acid bridge (Gly-Asp). To aid in solubility, lysine residues were added to the termini of the NS4A segment, and five hydrophobic residues of the NS3 protease were mutated to alanine (L13A, L14A, I17A, I18A, and L21A). A poly-lysine tail was also introduced to the *C*-terminus of the construct for solubility purposes. The Cys16 residue of the protein was mutated to threonine, as this residue was prone to oxidation during the long incubation periods.

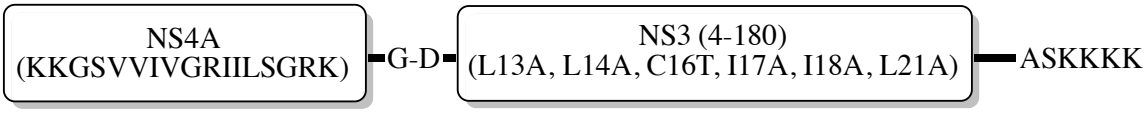


**Figure 3.7:** Schematic diagram of NS3/NS4A "single chain" protease.

This construct was well expressed in standard *E. coli* BL21 (DE3) (20 mg/L). Kinetic data obtained for the reaction between the NS3 protein and the peptide anthranilyl-DDIVPAbu[C(O)-O]AMY(3-$NO_2$)TW-OH, a substrate derived from the NS5A/NS5B cleavage site, showed highly similar values for $K_m$ and $k_{cat}$ between the single-chain construct (sc-protease) and the full-length protein (FL-protease) (Table **3.2**).

**Table 3.2**. Kinetic data for the single-chain NS3/NS4a protease (sc-protease), the NS3/NS4A complex ($NS3_{pr}$-$NS4A_{pept}$), and the NS3-NS4A Protein (FL-protease).[155]

| | sc-protease | $NS3_{pr}$-$NS4A_{pept}$ | FL-protease | FL-protease (M485A/V254A/Q256A) |
|---|---|---|---|---|
| $K_m$ (μM) | 2.9 ± 0.3 | 3.4 ± 0.5 | 2.1 ± 0.7 | 4.2 ± 0.1 |
| $k_{cat}$ ($min^{-1}$) | 150 ± 12 | 140 ± 13 | 69 ± 5 | 37 ± 1.1 |
| $k_{cat}/K_m$ (x $10^5$ $M^{-1}s^{-1}$) | 8.4 ± 0.5 | 6.9 ± 0.3 | 5.5 ± 1.8 | 1.5 ± 0.1 |

A survey of 25 different NS3 protease inhibitors, ranging from micromolar to sub-nanomolar in affinity, showed identical profiles between the single-chain and full-length proteases (**Figure 3.8**). From this, they determined that data obtained using the single-chain fusion construct would be representative of what would be obtained using the full-length wildtype protease. The improved expression and enhanced solubility allows for sufficient protein to be easily obtained for a wide variety of experiments. This single-chain protease is used in our experiments presented throughout the remainder of this chapter.

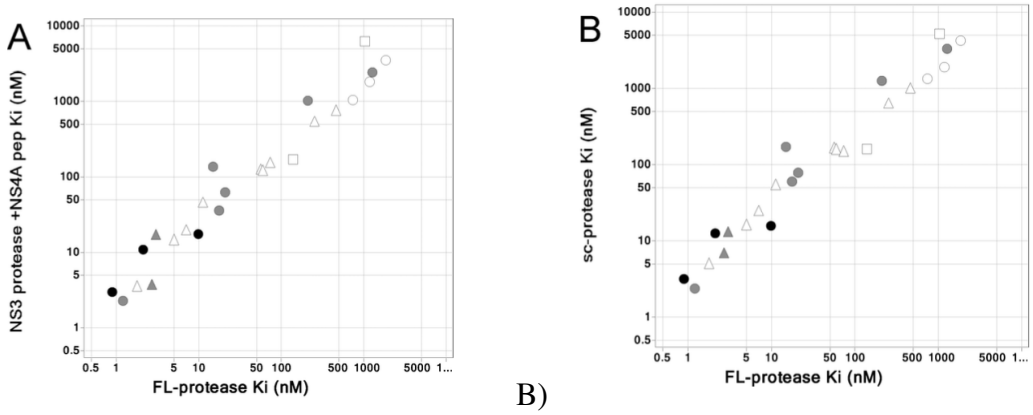


A) B)

**Figure 3.8:** Comparison of $K_i$ values for the a) full-length NS3/NS4A complex and B) single-chain NS3/NS4A construct.[155]

### 3.2.1 Preliminary Thermodynamic Data

Prior to my involvement in the project, preliminary ITC data was collected by Dr. John Clements (Table **3.3**). These data provide $\Delta G°$ values in agreement with those calculated from the $IC_{50}$ values. However, concerns quickly arose over the note that the stoichiometric ligand:protein ratio *n* was considerably higher than the expected value of 1.00 for all of the ITC experiments.

**Table 3.3**. Preliminary data for ligands **3.1-3.6**. [a]

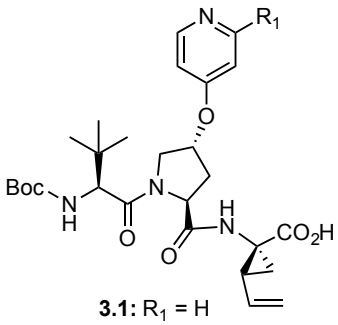


**3.1:** $R_1$ = H
**3.2:** $R_1$ = Ph

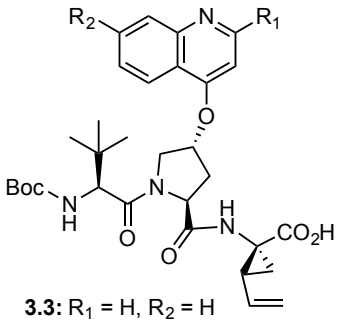


**3.3:** $R_1$ = H, $R_2$ = H
**3.4:** $R_1$ = Ph, $R_2$ = H
**3.5:** $R_1$ = H, $R_2$ = OMe
**3.6:** $R_1$ = Ph, $R_2$ = OMe

| Ligand | $K_a$ ($M^{-1}$) | $\Delta G°$ (kcal•mol$^{-1}$) | $\Delta H°$ (kcal•mol$^{-1}$) | $-T\Delta S°$ (kcal•mol$^{-1}$) | *n* |
|---|---|---|---|---|---|
| **3.1** | 4.0 (± 1.5) x $10^4$ | –6.2 ± 0.3 | –1.5 ± 0.6 | –4.7 ± 0.7 | 0.49 - 1.94 |
| **3.2** | N/A | N/A | N/A | N/A | N/A |
| **3.3** | 5.8 (± 1.5) x $10^6$ | –9.1 ± 0.2 | –2.8 ± 0.3 | –6.3 ± 0.4 | 1.32 - 2.20 |
| **3.4** | 8.1 (± 2.3) x $10^6$ | –9.4 ± 0.2 | –1.9 ± 0.1 | –7.5 ± 0.2 | 1.33 - 1.58 |
| **3.5** | 1.8 (± 0.2) x $10^7$ | –9.9 ± 0.06 | –4.5 ± 0.4 | –5.4 ± 0.4 | 1.09 - 1.58 |
| **3.6** | 5.4 (± 1.1) x $10^7$ | –10.4 ± 0.2 | –2.9 ± 0.1 | –7.5 ± 0.2 | 1.37 - 1.80 |

[a] Average of three trial per ligands, with *n* reported as the observed range over the trials.

Before any analysis of the data could begin, the abnormally high *n* values needed to be addressed, especially given the fact that the binding event was known from crystallographic evidence to occur with 1:1 stoichiometry with similar inhibitors.[156] Values

of *n* that deviate from the expected stoichiometry hinted at an error in concentration of either the protein or the ligand, and such concentration errors can have an impact on the resulting thermodynamic parameters.[34] An alternate independent method of determining concentrations of the ligand solutions was necessary.

### 3.2.2 The Model Chromophore System

In an effort to remedy the issues with the high *n* values, we speculated that UV spectroscopy could provide a more accurate measure of ligand concentration. However, since the purity of the ligand stock was questionable, standard solutions could not be prepared directly from the ligands. A simpler model system was employed for determination of molar extinction coefficients (**Figure 3.9**).

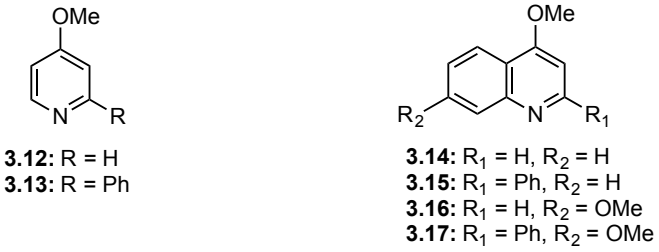


**3.12:** R = H
**3.13:** R = Ph

**3.14:** $R_1$ = H, $R_2$ = H
**3.15:** $R_1$ = Ph, $R_2$ = H
**3.16:** $R_1$ = H, $R_2$ = OMe
**3.17:** $R_1$ = Ph, $R_2$ = OMe

**Figure 3.9:** Model systems for ligands **3.12-3.17**.

4-Methoxyquinoline (**3.14**) was synthesized by former Martin group member Dr. Noah Benjamin. After determination of the extinction coefficient (6100 $M^{-1}$), the concentration of ligand **3.3** in the previous ITC trials was recalculated and the curves were refitted, resulting in a readjustment of *n* from 2.20 to 1.06.

With this promising result in hand, I entered the project and synthesized the rest of the model chromophores for the quinoline-containing ligands. Condensation of diethyl(ethoxy)methylenemalonate (**3.18)** with *m*-anisidine and subsequent cyclization with phenyl ether at 250 °C afforded ester **3.19** in 32% yield (Scheme **3.1**).[157]

Saponification of the ester and decarboxylation afforded the hydroxyquinoline subunit **3.20** in 45% yield.[157] Heating under reflux in $POCl_3$ provided chloro compound **3.21** in 84% yield.[157] Substitution with NaOMe furnished the desired chromophore **3.16** in 65% yield.

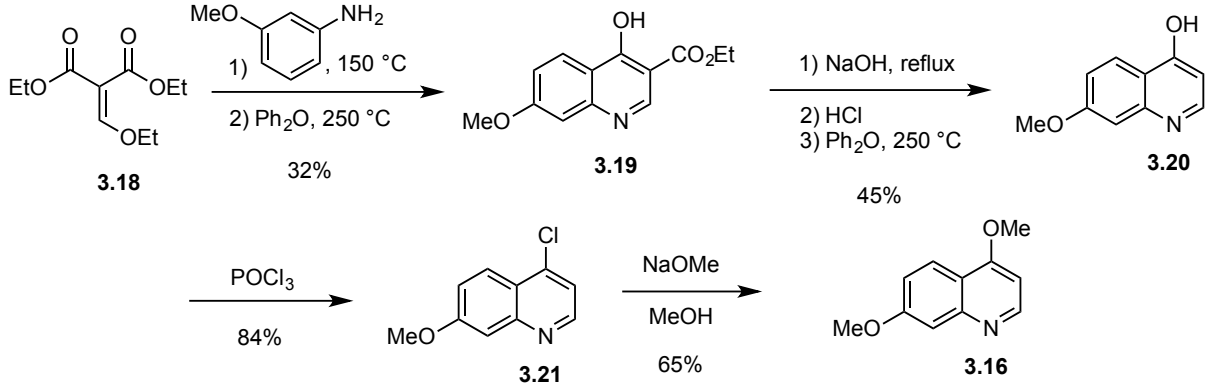


**Scheme 3.1**: Synthesis of **3.16**.

An analogous sequence was employed to synthesize 2-phenyl derivatives **3.15** and **3.17** (**Scheme 3.2**).[157]

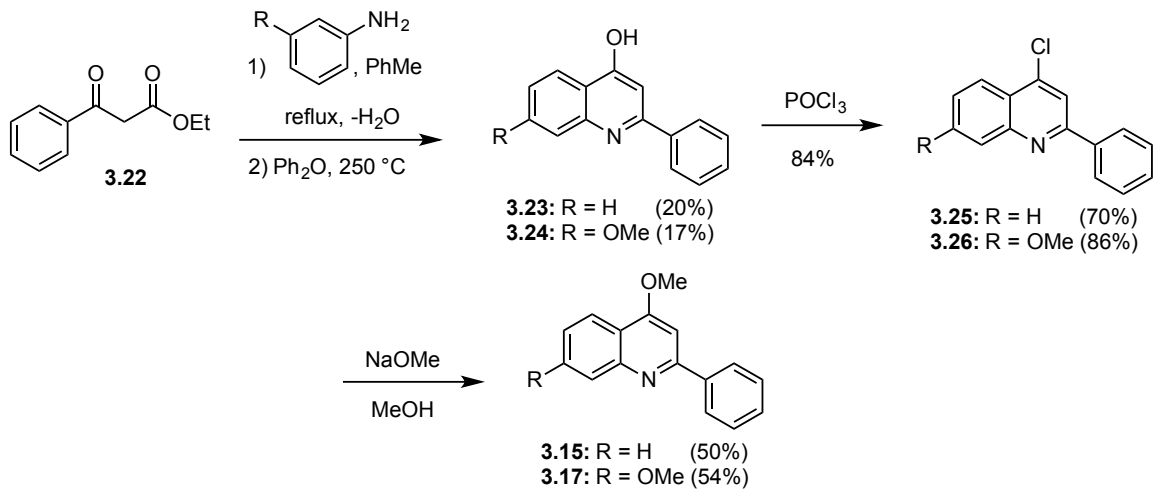


**Scheme 3.2:** Synthesis of **3.15** and **3.17**.

The molar extinction coefficient and $\lambda_{max}$ for **3.12** were obtained from the literature.[158] Due to solubility issues in the ITC buffer (50 mM HEPES, pH 7.5, 3% DMSO), extinction coefficients for **3.12**-**3.17** were measured in ethanol (Table **3.4**).

**Table 3.4**. Molar extinction coefficients of chromophores **3.12**-**3.17**.

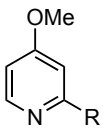


**3.12:** R = H
**3.13:** R = Ph

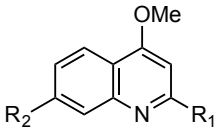


**3.14:** $R_1$ = H, $R_2$ = H
**3.15:** $R_1$ = Ph, $R_2$ = H
**3.16:** $R_1$ = OMe, $R_2$ = H
**3.17:** $R_1$ = Ph, $R_2$ = OMe

| Compound | $\lambda_{max}$ (nm) | $\varepsilon$ ($M^{-1}$) |
|---|---|---|
| **3.12** | 235 | 2200 |
| **3.13** | —— | —— |
| **3.14** | 284[a] | 6100[a] |
| **3.15** | 319 | 2899 |
| **3.16** | 295 | 8801 |
| **3.17** | 295 | 10101 |

[a] Benjamin, N. *unpublished results*.

With the molar extinction coefficients in hand adjustments were made to the available ITC data. Due to the fact that the ligand concentration by weight was initially assumed to be sufficiently accurate, many of the ITC experiments were conducted without collecting any UV absorbance data for the solutions, necessitating replication of those experiments. Unfortunately, even with the new molar extinction coefficients in hand, the same problems with the *n* values for some of the ligands persisted (**Table 3.5**). Trials using

ligand **3.6** also needed to be repeated because recalculation of the ligand solution concentration resulted in adjustment of *n* to 0.7, an equally troubling result.

**Table 3.5**. ITC data for ligands **3.1-3.6**. [a]

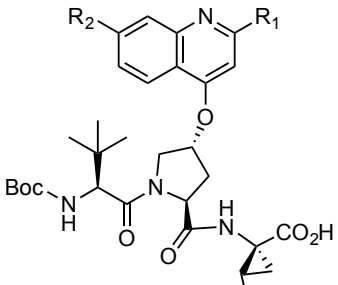


**3.4:** $R_1$ = Ph, $R_2$ = H
**3.5:** $R_1$ = OMe, $R_2$ = H
**3.6:** $R_1$ = Ph, $R_2$ = OMe

| Ligand | $K_a$ ($M^{-1}$) | $\Delta G°$(kcal•$mol^{-1}$) | $\Delta H°$(kcal•$mol^{-1}$) | $-T\Delta S°$(kcal•$mol^{-1}$) | *n* |
|---|---|---|---|---|---|
| **3.4** | 8.1 (± 2.3) x $10^6$ | –9.4 ± 0.2 | –1.9 ± 0.1 | –7.5 ± 0.2 | 1.33 - 1.58 |
| **3.4**[b] | 1.4 (± 0.5) x $10^7$ | –9.7 ± 0.3 | –2.6 ± 0.3 | –7.1 ± 0.4 | 1.01 - 1.06 |
| **3.5** | 1.8 (± 0.2) x $10^7$ | –9.9 ± 0.06 | –4.5 ± 0.4 | –5.4 ± 0.4 | 1.09 - 1.58 |
| **3.5**[b] | 2.3 (± 1.2) x $10^7$ | –9.9 ± 0.5 | –6.6 ± 0.4 | –3.3 ± 0.6 | 1.27 - 1.40 |
| **3.6** | 5.4 (± 1.1) x $10^7$ | –10.4 ± 0.2 | –2.9 ± 0.1 | –7.5 ± 0.2 | 1.37 - 1.80 |
| **3.6**[b] | 2.3 (± 1.2) x $10^7$ | –9.9 ± 0.5 | –6.6 ± 0.4 | –3.3 ± 0.6 | 0.60 - 0.72 |

[a] Average of three trial per ligands, with *n* reported as the observed range over the trials.
[b] Values corrected by replacing the ligand concentration by weight with the concentration by UV absorbance.

### 3.2.3 Ligand Synthesis and UV Evaluation

Given that UV absorbance data were not available for many of the ligands, the ITC experiments needed to be replicated. With the generous donation of the tripeptide brosylate **3.27** by B.I. and the availability of the necessary 4-hydroxy compounds from the chromophore synthesis, only two additional steps were necessary to prepare the ligands (Scheme **3.3**). Displacement of the brosylate group with the appropriate 4-

hydroxyquinoline provided tripeptide methyl esters **3.32-3.35** in good yield. Saponification of the ester furnished ligands **3.3-3.6** in modest yield.

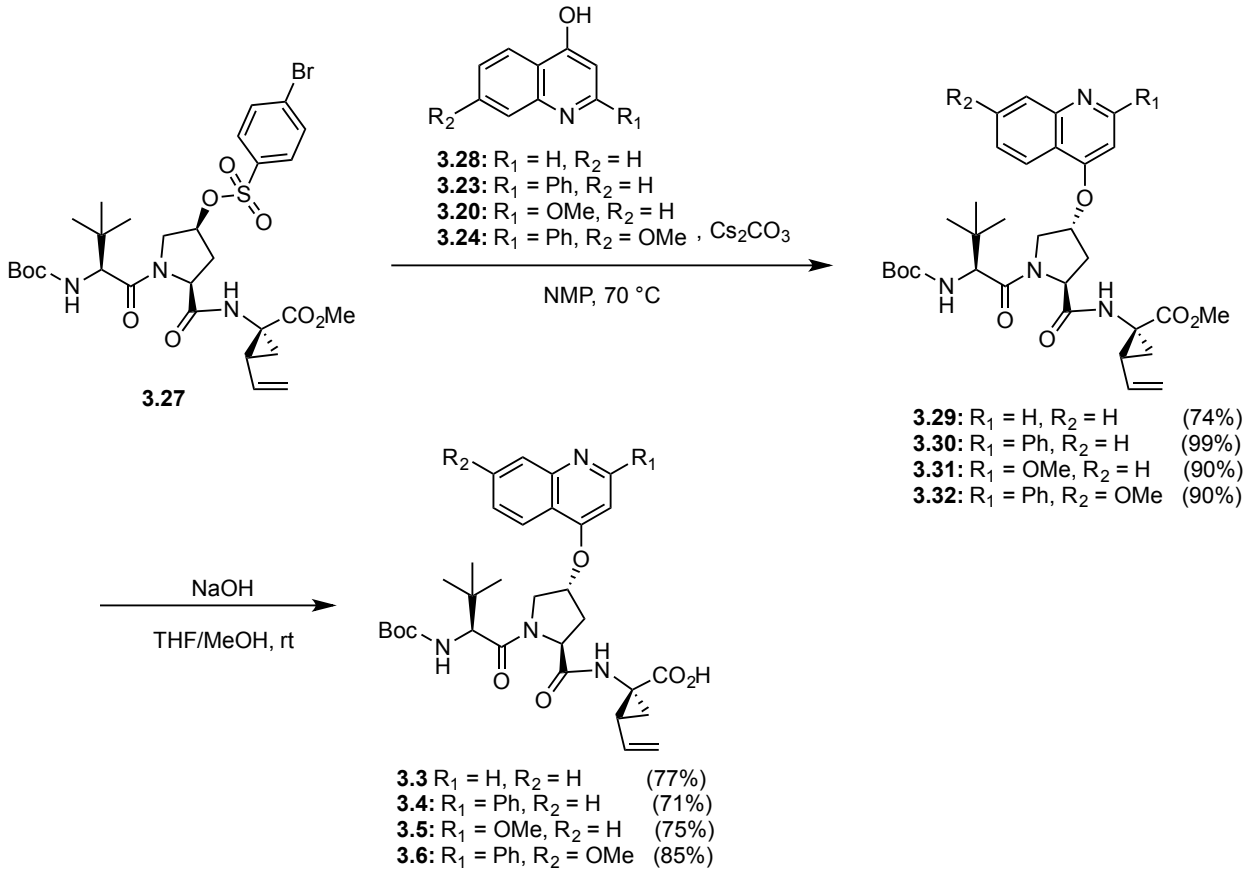


**Scheme 3.3:** Synthesis of ligands **3.3-3.6**.

Since 4-hydroxypyridine is commercially available and relatively inexpensive, attention was focused on the synthesis of the intermediate 4-hydroxy-2-phenylpyridine **3.37** necessary to synthesize the ligand **3.2 (Scheme 3.4**). The originally intended route would provide the desired compound in five steps from commercially available and inexpensive pyridine *N*-oxide (**3.33**), which was nitrated[159] to form **3.34** in 68% yield followed by nucleophilic substitution with NaOMe[160] to give **3.35** in 70% yield. Unfortunately, the Grignard addition/elimination sequence to furnish pyridine **3.36**[161] was

found to be highly irreproducible and plagued by the formation of mixtures of by-products that made purification difficult.

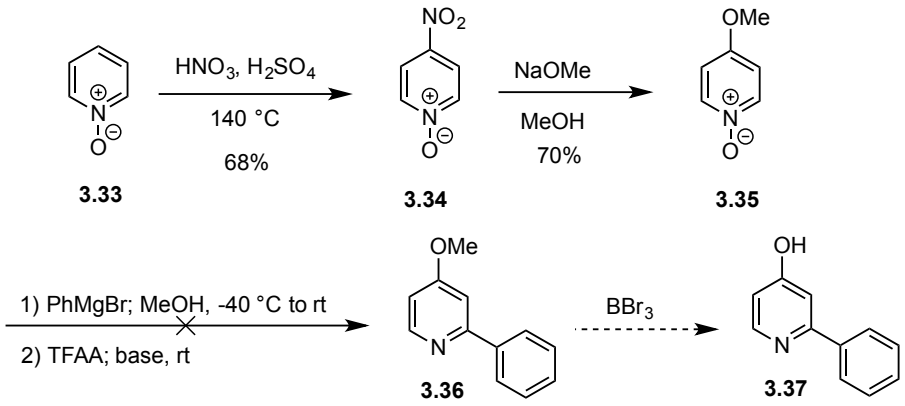


**Scheme 3.4:** Attempted synthesis of **3.37**.

Several sets of conditions were screened in an attempt to improve the yield of **3.36** (**Table 3.6**). Changing the base from NaOH to Hünig's base had minimal effect on the yield. Increasing the equivalents of TFAA to 2 did not seem to elicit any improvement. Lowering the temperature of the addition resulted in a decrease in yield to only 9%. Reversing the order of addition and attempting to acylate **3.35** with TFAA first before addition of the Grignard resulted in intractable mixtures of products.

**Table 3.6**. Addition/elimination sequence of **3.35**.

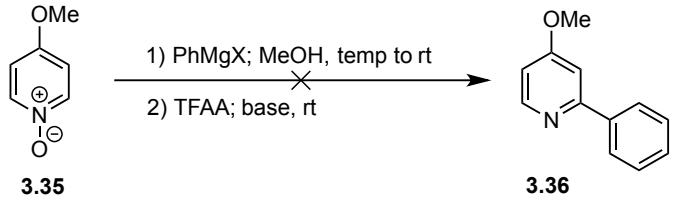


**3.35** **3.36**

| Temp (°C) | Base | eq. TFAA | % Yield |
|---|---|---|---|
| –40 | NaOH | 1.1 | 18 |
| –40 | *i*Pr$_2$NEt | 1.1 | 20 |
| –40 | NaOH | 2.0 | 20 |
| –78 | *i*Pr$_2$NEt | 1.1 | 9 |
| –40 | NaOH | 1.1[a] | intractable |

Pyridine *N*-oxides are reported to undergo ring open reactions to form dienal oximes (**2.54**) that can undergo further reaction (**Scheme 3.5**).[162] Although the by-products were inseparable, the presence of multiple peaks in the vinyl region of the crude $^1$H NMR spectrum suggested the possibility of ring opening.

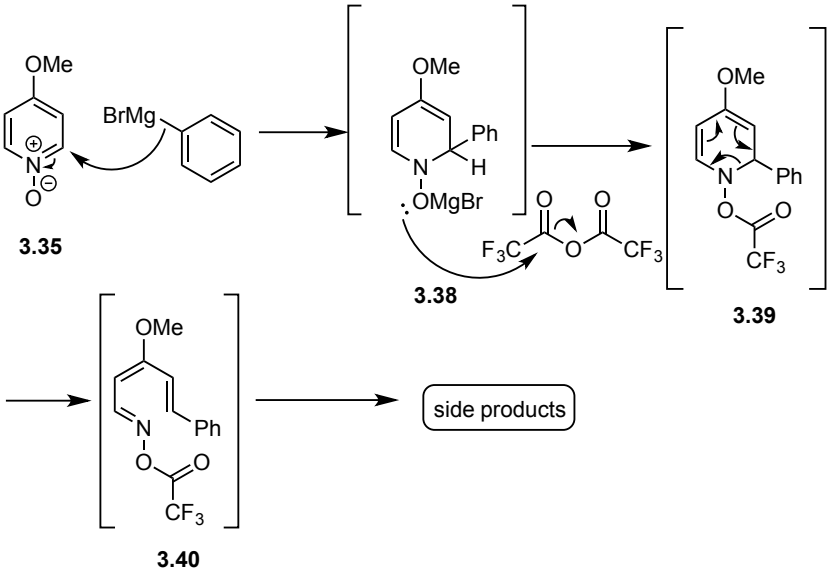


**Scheme 3.5:** Ring opening of pyridine **3.48**.

Due to the low yields and difficulty in purification, an alternate procedure was utilized to reach pyridone **3.47** (**Scheme 3.6**). Intermediate **3.33** was instead converted to 2-pyridone **3.41** in 68% yield,[163] followed by chlorination with $POCl_3$[157] to provide the 2-chloro compound **3.42** in 59% yield. Suzuki cross-coupling to install the 2-phenyl substituent[164] followed by demethylation with *p*TsOH and LiCl[165] provided pyridone **3.37** in good yield.

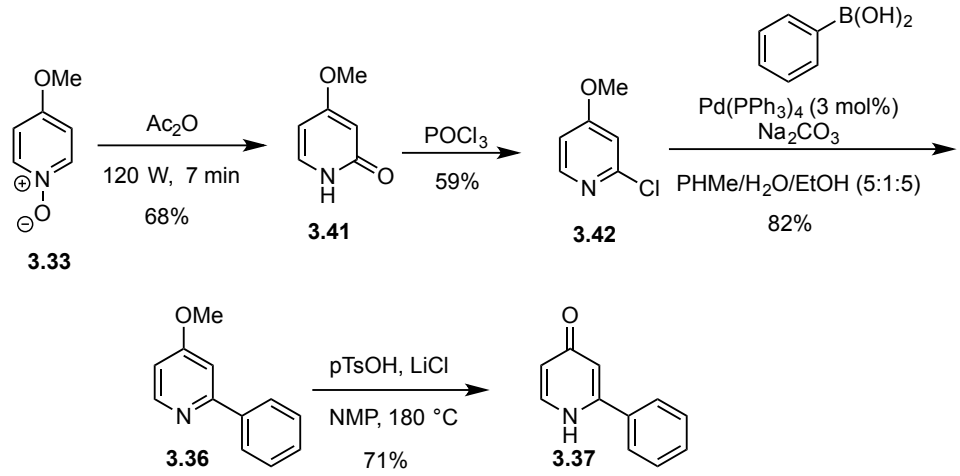


**Scheme 3.6:** Synthesis of **3.37**.

The tripeptide brosylate **3.27** was then subjected to an identical displacement/hydrolysis sequence to give pyridine ligands **3.1** and **3.2** in good yield.

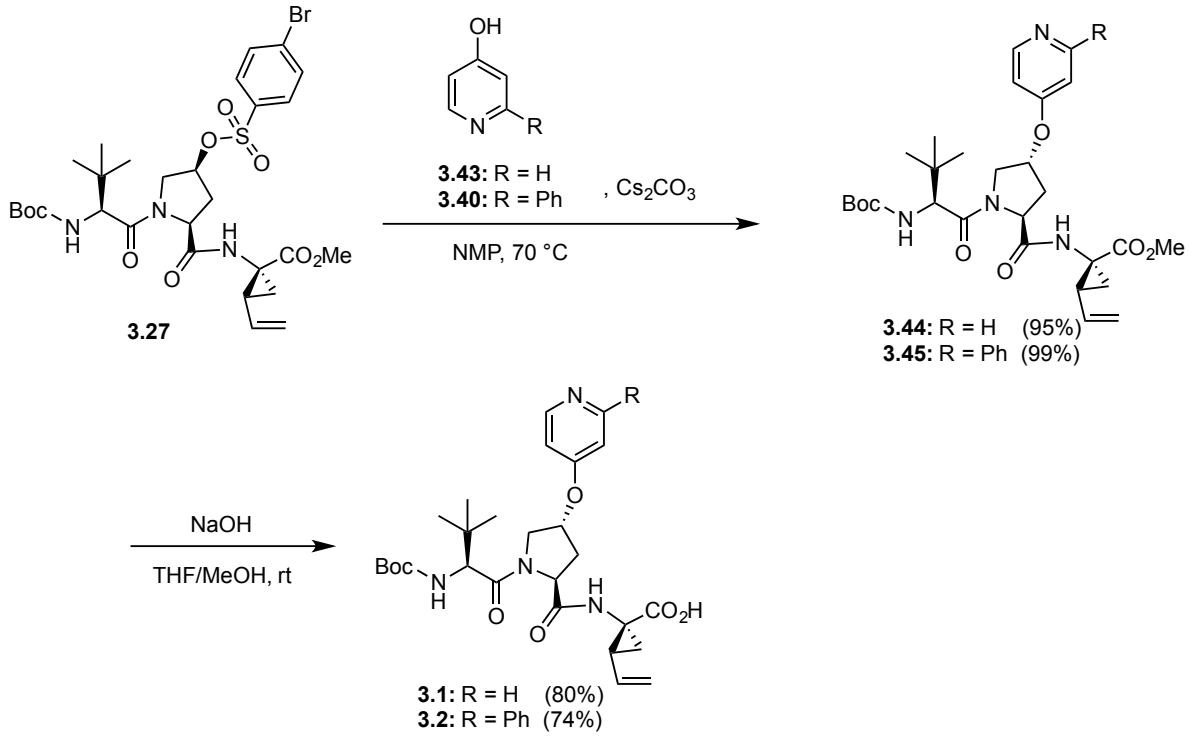


**Scheme 3.7:** Synthesis of **3.1-3.2**.

Upon completion of the synthesis, UV absorbance measurements were collected for ligands **3.1-3.6** and compared to those of the model chromophores (**Table 3.7**). Unfortunately, the unsubstituted pyridine ligand **3.1** did not absorb radiation at any wavelength that would provide a usable molar extinction coefficient ($\lambda > 250$ nm). Without a usable extinction coefficient, we would be unable to accurately determine the concentration of ligand **3.1**. We then reasoned that we would instead standardize these titrations based on the protein concentration. If that the titrations with the other ligands using the UV concentrations provided the appropriate *n* value of 1, we rationalized that we could then make the assumption that the concentration of properly folded protein in the sample cell was correct. If the protein concentration is known with certainty, then any issues with the value for *n* in titrations with ligand **3.1** could be remedied by normalizing the protein:ligand ratio with respect to the protein concentration; i.e., multiplying the ligand concentration by the observed *n* value to get a new concentration and refitting the curve to give an *n* value of 1.

**Table 3.7**. Molar extinction coefficients of ligands **3.1-3.6** and chromophores **3.12-3.17**.

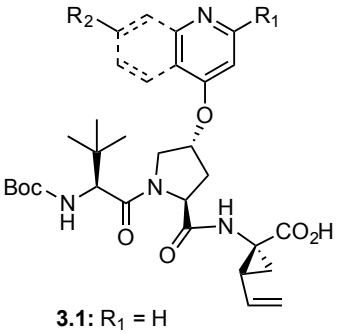

**3.1:** $R_1$ = H
**3.2:** $R_1$ = Ph
**3.3:** $R_1$ = H, $R_2$ = H
**3.4:** $R_1$ = Ph, $R_2$ = H
**3.5:** $R_1$ = OMe, $R_2$ = H
**3.6:** $R_1$ = Ph, $R_2$ = OMe

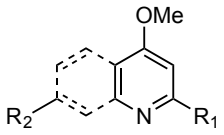

**3.12:** $R_1$ = H
**3.13:** $R_1$ = Ph
**3.14:** $R_1$ = H, $R_2$ = H
**3.15:** $R_1$ = Ph, $R_2$ = H
**3.16:** $R_1$ = OMe, $R_2$ = H
**3.17:** $R_1$ = Ph, $R_2$ = OMe

| Ligand | $_{max}$ (nm) | ($M^{-1}$) |
|---|---|---|
| **3.1** | —— | —— |
| **3.2** | 273 | 4685 |
| **3.3** | 284 | 5807 |
| **3.4** | 295 | 7330 |
| **3.5** | 319 | 3907 |
| **3.6** | 295 | 6429 |

| Model Compound | $_{max}$ (nm) | ($M^{-1}$) |
|---|---|---|
| **3.12** | 235 | 2200 |
| **3.13** | —— | —— |
| **3.14** | 284[a] | 6100[a] |
| **3.15** | 295 | 8801 |
| **3.16** | 319 | 2899 |
| **3.17** | 295 | 10101 |

### 3.2.4 Evaluating the breakdown of the model system

It was noted that the two ligands for which the model system had failed both contained a 7-methoxy substituent on the quinolone ring. Thus, it was speculated that the addition of this substituent could be altering the electronics of the ring in a manner that alters the UV absorption spectrum between the model and the ligand. Given that the ligand contains a proton source in the form of a free carboxylic acid that is not available to the model system, different protonation states of the two species could explain these discrepancies. In an effort to investigate this, UV absorbance measurements for three of the chromophores were measured in a 10% AcOH/EtOH solution and compared to those

collected for the ligands as well as those previously collected for the model compounds (**Table 3.8**).

**Table 3.8**. Molar extinction coefficients of chromophores **3.12**-**3.17** and ligands **3.4-3.6.**

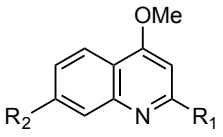


**3.15:** $R_1$ = Ph, $R_2$ = H
**3.16:** $R_1$ = OMe, $R_2$ = H
**3.17:** $R_1$ = Ph, $R_2$ = OMe

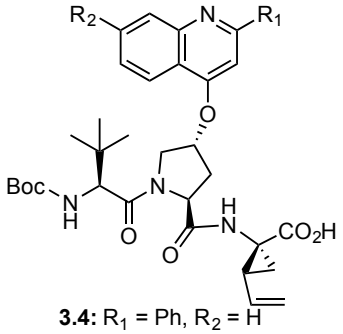


**3.4:** $R_1$ = Ph, $R_2$ = H
**3.5:** $R_1$ = OMe, $R_2$ = H
**3.6:** $R_1$ = Ph, $R_2$ = OMe

| Compound | $\lambda_{max}$ (nm)[a] | ε ($M^{-1}$)[a] | $\lambda_{max}$ (nm)[b] | ε ($M^{-1}$)[b] |
|---|---|---|---|---|
| **3.15** | 295 | 8801 | 295 | 10219 |
| **3.16** | 319 | 1925 | 319 | 4065 |
| **3.17** | 295 | 9040 | 295 | 6427 |

| Ligand | $\lambda_{max}$ (nm) | ε ($M^{-1}$) |
|---|---|---|
| **3.4** | 295 | 7330 |
| **3.5** | 319 | 3907 |
| **3.6** | 295 | 6429 |

[a] Values collected in EtOH.
[b] Values collected in EtOH with 10% AcOH.

The values for ε determined in 10% AcOH/EtOH for **3.15** and **3.17** tracked closely with those determined for the full ligands **3.4** and **3.5**, lending support to the hypothesis that the heterocyclic nitrogen atom may be protonated in the ligand solution. Compound **3.16** which does not contain a 7-methoxy substituent did display different behavior in the acidic solution, but this did not match the value obtained for the tripeptide ligand **3.4**, suggesting that the corresponding tripeptide ligand may not exhibit protonation of the heterocyclic nitrogen. The molar extinction coefficients for the ligands were thus used to evaluate concentrations for the ITC experiments.

### 3.2.5 Thermodynamic Data and Evaluations

Using the ligand molar extinction coefficients to measure concentration, ITC data collected for ligands **3.1**-**3.6** are presented in **Table 3.9**.

**Table 3.9**. ITC data for ligands **3.1-3.6**. [a]

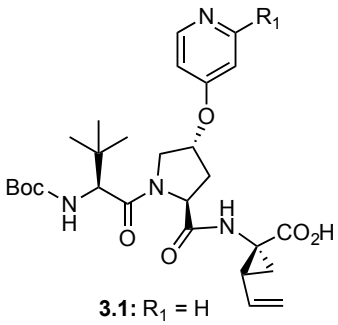


**3.1:** $R_1$ = H
**3.2:** $R_1$ = Ph

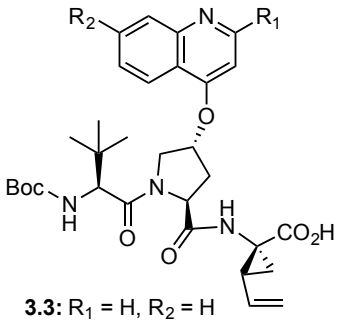


**3.3:** $R_1$ = H, $R_2$ = H
**3.4:** $R_1$ = Ph, $R_2$ = H
**3.5:** $R_1$ = OMe, $R_2$ = H
**3.6:** $R_1$ = Ph, $R_2$ = OMe

| Ligand | $K_a$ ($M^{-1}$) | $\Delta G°$ (kcal•mol$^{-1}$) | $\Delta H°$ (kcal•mol$^{-1}$) | $-T\Delta S°$ (kcal•mol$^{-1}$) | *n* |
|---|---|---|---|---|---|
| **3.1** | 7.4 (± 0.8) x $10^4$ | –6.7 ± 0.07 | –1.4 ± 0.1 | –5.3 ± 0.1 | 0.92 - 1.01 |
| **3.2** | 1.2 (± 0.2) x $10^6$ | –8.2 ± 0.1 | –2.1 ± 0.1 | –6.1 ± 0.2 | 0.94 - 1.09 |
| **3.3** | 5.1 (± 0.2) x $10^6$ | –9.2 ± 0.03 | –5.3 ± 0.2 | –3.8 ± 0.3 | 0.90 - 1.00 |
| **3.4** | 1.0 (± 0.03) x $10^7$ | –9.6 ± 0.02 | –2.6 ± 0.1 | –7.0 ± 0.1 | 0.98 - 1.17 |
| **3.5** | 5.6 (± 0.2) x $10^6$ | –9.2 ± 0.02 | –8.3 ± 0.5 | –0.9 ± 0.5 | 0.98 - 1.15 |
| **3.6** | 5.1 (± 0.4) x $10^7$ | –10.5 ± 0.05 | –3.3 ± 0.5 | –7.2 ± 0.5 | 1.00 - 1.02 |

[a] Average of three trial per ligands, with *n* reported as the observed range over the trials.

From these data, the effects of the individual substituents can be evaluated. If the addition of the second aromatic ring to form the quinoline and the addition of the 2-phenyl substituent were additive, the resulting ligand **3.4** would be expected to bind to the protease with a $\Delta G°$ value of –10.7 kcal mol$^{-1}$. From the ITC data, it is shown that although the actual binding profile falls slightly short of expected ($\Delta G°_{obs}$ = –9.6 kcal mol$^{-1}$), the expected and observed $\Delta G°$ values are within 1 kcal mol$^{-1}$ (**Figure 3.10**). However, when we dive deeper, this analysis immediately becomes much more complicated. Although

there are only small differences between the expected and observed free energies, the change in binding enthalpy for **3.4** ($\Delta H°_{obs}$ = –2.6 kcal mol$^{-1}$) is much less favorable than the expected –6.1 kcal mol$^{-1}$. On the other hand, the binding entropy, which would be expected to be –4.6 kcal mol$^{-1}$, is significantly more favorable (–T$\Delta S°_{obs}$ = –7.0 kcal mol$^{-1}$).

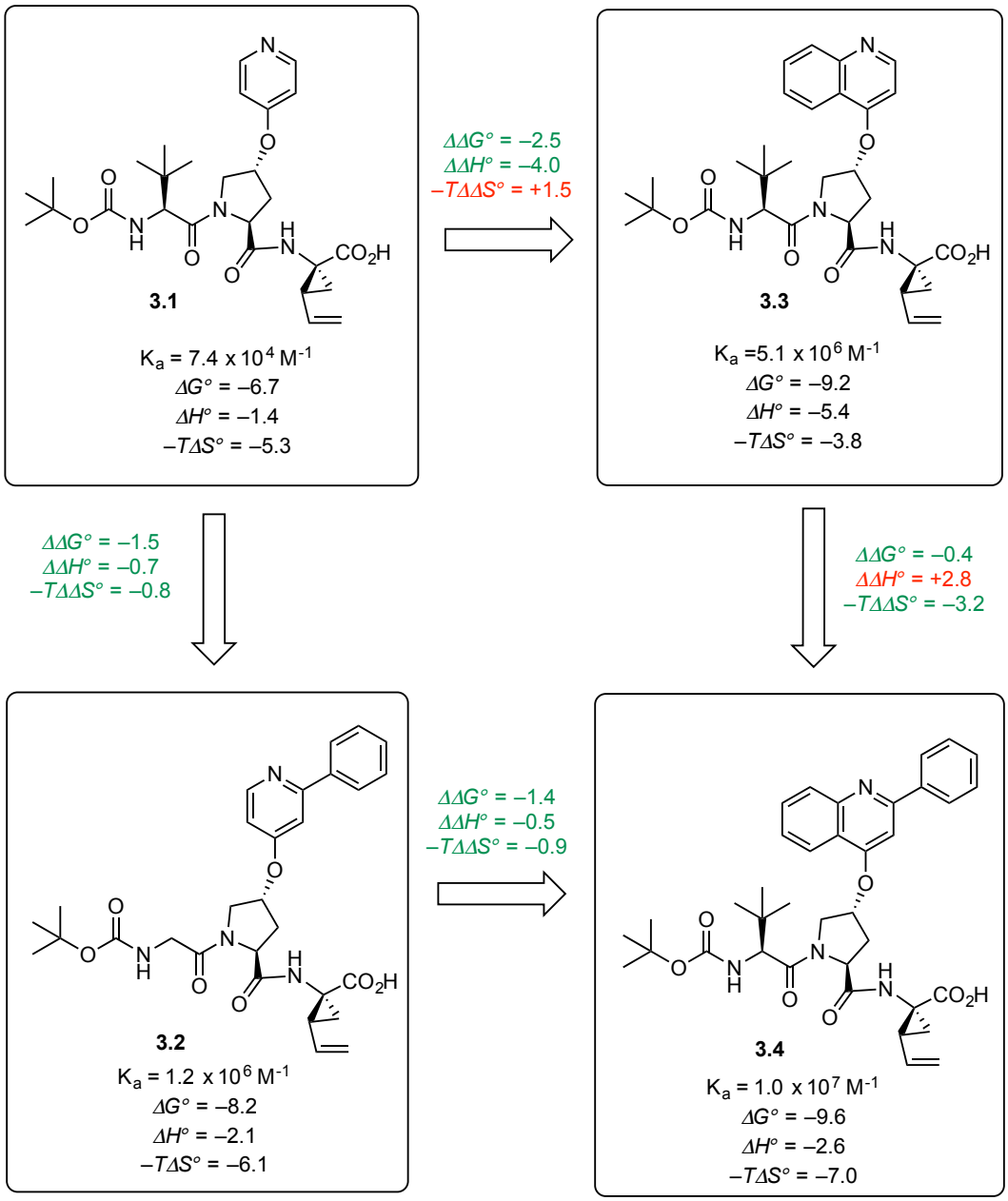


**Figure 3.10:** Double mutant cycle analysis for ligands **3.1**-**3.4**. Values expressed in kcal $mol^{-1}$.

The annulation of the benzenoid ring onto the pyridine of **3.1** to form the quinoline ligand **3.3** provides a sharp improvement in the binding enthalpy ($\Delta\Delta H°_{obs}$ = –4.0 kcal $mol^{-1}$), although this comes at an entropic cost ($-T\Delta\Delta S°_{obs}$ = +2.5 kcal $mol^{-1}$). Interestingly, the

addition of this same ring from the 2-phenylpyridine ligand **3.2** to the corresponding quinoline **3.4** results in a more favorable binding enthalpy ($\Delta\Delta H°_{obs}$ = –0.5 kcal mol$^{-1}$) *and entropy* (–T$\Delta\Delta S°_{obs}$ = –0.9 kcal mol$^{-1}$). The addition of the second ring nearly doubles the surface area of the heterocycle, and this large hydrophobic surface may be forming more dispersive interactions with the protein than with the solvent. Prior to the binding event, both the protein and the ligand are surrounded by solvent molecules. In addition to forming hydrogen bonding networks with other solvent molecules, dispersive interactions are also formed with the protein and ligand surfaces. It has historically been assumed that the differences in both the quality and quantity of these dispersive interactions before and after binding are zero, since dispersive interactions between the solute and the protein or ligand are simply replaced with solute-solute interactions and protein-ligand interactions upon binding. However, it has since been suggested that the topology of a hydrophobic surface influences the quality and quantity of hydrogen bonding networks between solvent molecules, with water molecules that solvate large flat surfaces (like aromatic groups) making fewer hydrogen bonds than those solvating concave surfaces (see **Section 1.5.2**). It therefore could be speculated that this suboptimal arrangement could result in fewer dispersive interactions between the surface and the solvent. Upon binding, replacement of these suboptimal solvent-solute interactions can be replaced with more optimal solvent-solvent and solvent-solute interactions, and this can have an impact on changes in binding enthalpy.[18] The origin of the entropic penalty in the case of the transition from ligand **3.1** to **3.3** is unknown at this moment, and investigation is ongoing.

The addition of the 2-phenyl substituent universally results in a favorable change in binding entropy, although the magnitude of this effect is highly dependent on which substituents are already present. From the simplest ligand **3.1** to **3.2**, the addition of this substituent results in both a more favorable binding enthalpy ($\Delta\Delta H°_{obs}$ = –0.7 kcal mol$^{-1}$)

and binding entropy ($-T\Delta\Delta S°_{obs}$ = –0.8 kcal mol$^{-1}$). It is worthy of note that the change in binding entropy between the pyridine ligands is substantially smaller than for the quinoline ligands. For the quinoline ligands, addition of the 2-phenyl group from **3.3** to **3.4** results in a favorable change in binding entropy ($-T\Delta\Delta S°_{obs}$ = –3.2 kcal mol$^{-1}$) at a nearly balancing enthalpic cost ($\Delta\Delta H°_{obs}$ = +2.8 kcal mol$^{-1}$). We hypothesize that the addition of the phenyl group contributes significantly to the binding entropy primarily through the desolvation of nonpolar surface area.

Working from quinoline ligand **3.3**, if the effects of the 2-phenyl and 7-methoxy substituents were additive, the combined ligand **3.6** would be expected to bind with a $\Delta G°$ value of –9.6 kcal mol$^{-1}$. We observed from the ITC data that the actual affinity was slightly higher than expected, with a $\Delta G°_{obs}$ value of –10.5 kcal mol$^{-1}$ (**Figure 3.11**), for a difference of –0.9 kcal mol$^{-1}$. Once again we see that although the overall binding free energy falls within 1.0 kcal mol$^{-1}$ of the expected value, the binding enthalpy for **3.6** ($\Delta H°_{obs}$ = –3.3 kcal mol$^{-1}$) is less favorable than the expected –5.5 kcal mol$^{-1}$. The binding entropy ($-T\Delta S°_{obs}$ = –7.2 kcal mol$^{-1}$) is likewise more favorable than the expected –4.1 kcal mol$^{-1}$.

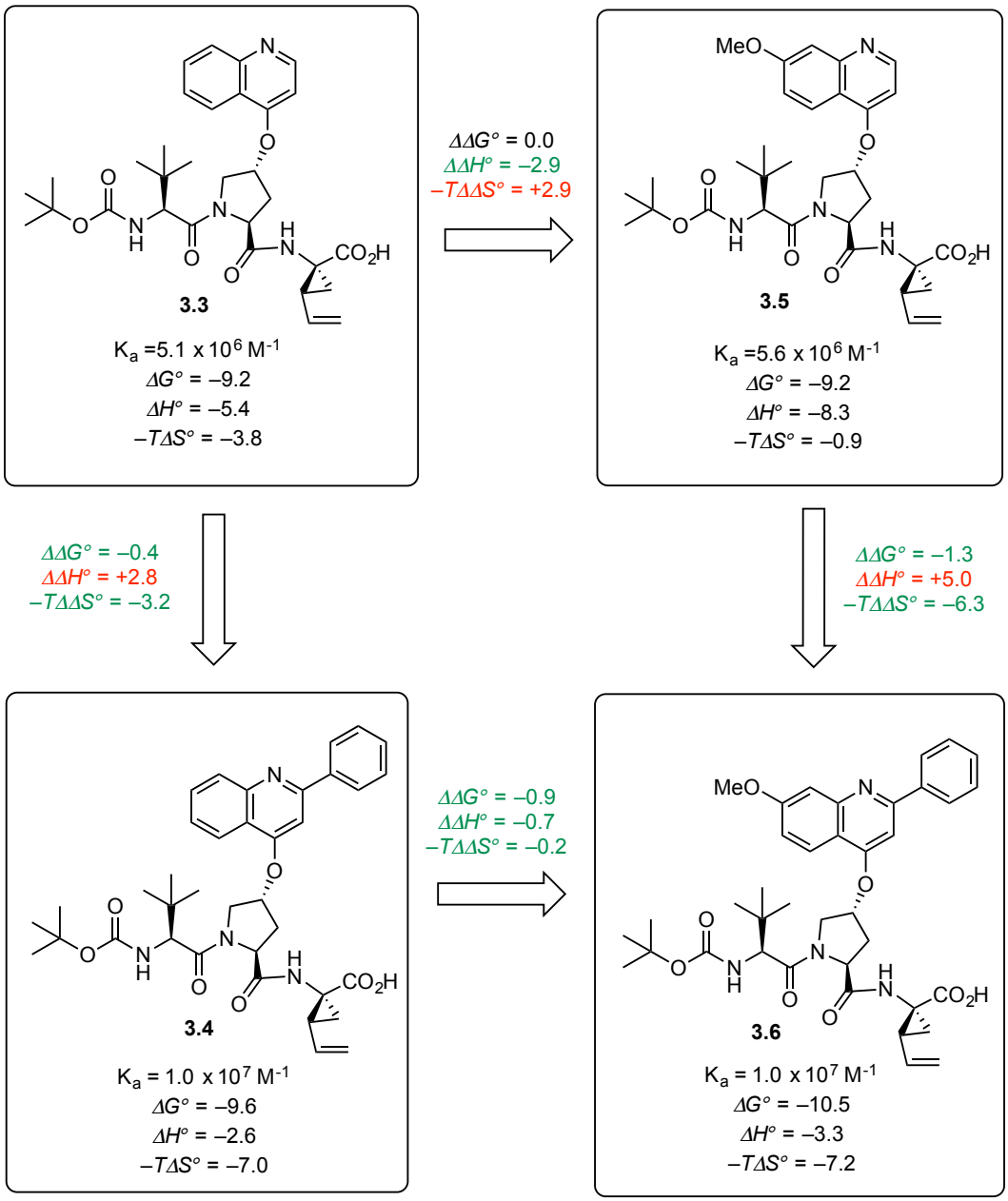


**Figure 3.11:** Double mutant cycle analysis for ligands **3.3**-**3.6**. Values expressed in kcal mol$^{-1}$.

As was observed previously in **Figure 3.10**, the addition of the 2-phenyl substituent going from ligand **3.5** to **3.6** improves the overall binding entropy ($-T\Delta\Delta S°_{obs}$ = –6.3 kcal mol$^{-1}$). Similar to the other quinoline ligands, this favorable change in binding entropy is

largely offset by a substantial enthalpic penalty ($\Delta\Delta H°_{obs}$ = +5.0 kcal mol$^{-1}$), which results in a small overall improvement to free energy ($\Delta\Delta G°_{obs}$ = –1.3 kcal mol$^{-1}$).

The 7-methoxy group improves the binding enthalpy of **3.5** compared to **3.3** ($\Delta\Delta H°_{obs}$ = –2.9 kcal mol$^{-1}$). Interestingly, no net change to the binding affinity is observed upon addition of this substituent, as all gains in binding enthalpy are subsequently balanced by an entropic penalty ($-T\Delta\Delta S°_{obs}$ = +2.9 kcal mol$^{-1}$). In the absence of structural data, we hypothesized that this methoxy group may be participating in an electrostatic interaction with the guanidine moiety of the Arg155 side chain, as had been previously noted in the literature.[140]

We then set out to obtain structural data for the various protein-ligand complexes in order to further explain these observations. Crystal structures of the full-length NS3 protein are known, as well as crystal structures of the isolated protease domain. However, crystal structures were never successfully obtained by scientists at B.I. with the "single-chain" fused construct (see **Figure 3.7**). We tried numerous commercial crystal screens as well as published conditions for crystallization of the full-length protein and the protease domain, but we only observed amorphous precipitation. Attempts to crystallize the protein by itself as well as co-crystallization attempts with each of the ligands **3.1**-**3.6** were all unsuccessful. It is possible that the amino acid mutations that help to improve the solubility of the construct (L13A, L14A, I17A, I18A, and L21A) were impeding crystallization. We also attempted to obtain crystal structures with a similar fused NS3/NS4 construct provided by B.I., which contains the same attachment of NS4A and terminal poly-lysine tail with only a single amino acid mutation (I17K). Unfortunately, this protein also failed to crystallize under a variety of conditions.

### 3.2.6 Computational Studies

With the failure to obtain crystallographic data, we turned our attention to preliminary computational modeling in order to obtain important structural data. All modeling studies were performed by our collaborators Jayadeepa Murugesan and Dr. Steven LaPlante (**Figure 3.12**-**3.13**). Starting from a known x-ray crystal structure of the NS3 protease[156], the tripeptides were modeled into the active site of the protein and the complex was energy minimized via the Quick Prep procedure as outlined in MOE (2016.0802). The complexes were minimized to an RMS gradient of 0.1 kcal $mol^{-1}$ with the MOE ligand interaction module with the receptor, ligand, and solvent atoms restrained. Crystallographic water molecules were kept, and hydrogen atoms were added using the MOE (2016.0802) Protonate 3D module. The Amber99 force field was applied with AM1-BCC charges for the ligand. The energy cutoff range was set between 10-12 Å and the Born solvation model was used for implicit solvation.

The molecular models for the tripeptide ligands show that the P2 region lies over the catalytic triad residues (Asp81, His57, and Ser139), and it has been reported that this orientation shields the catalytic triad from the solvent and facilitates two hydrogen bonding networks as shown in **Figure 3.12**.

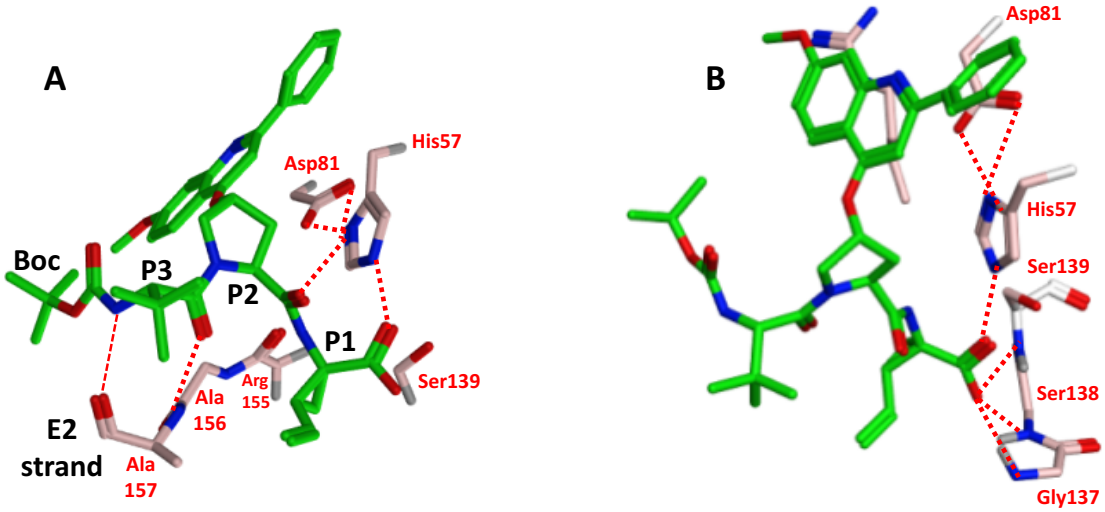


**Figure 3.12:** Bound conformation of ligand **3.6**. Two views are displayed.[3]

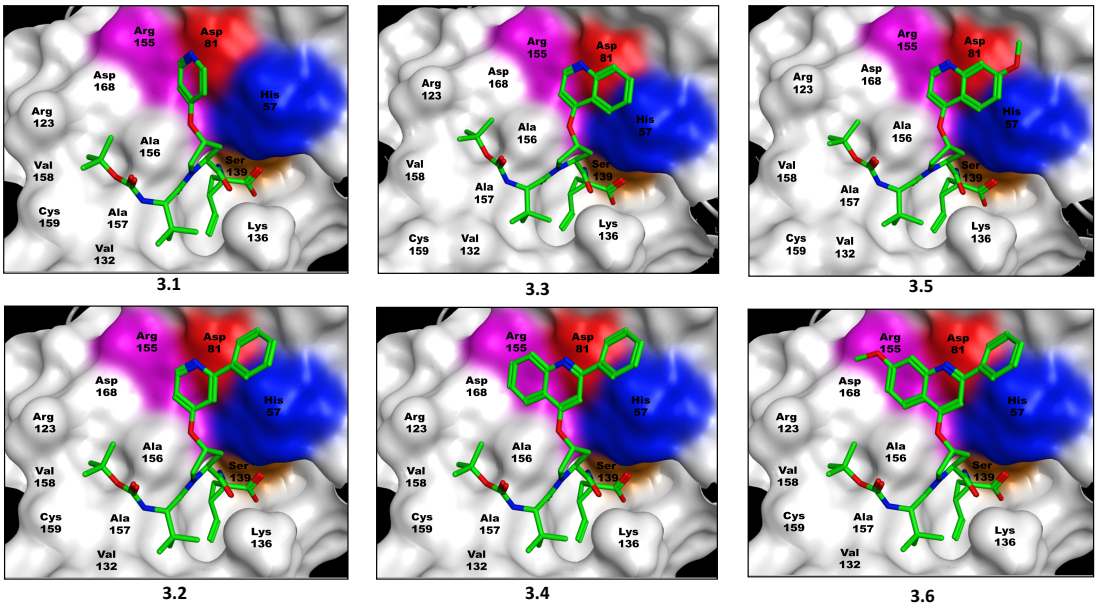


**Figure 3.13:** Modeled complexes of ligands **3.1**-**3.6** with the HCV NS3 protease.[4]

[3] Molecular docking and MD calculations were performed by Jayadeepa Murugesan and Dr. Steven LaPlante.

[4] Molecular docking and MD calculations were performed by Jayadeepa Murugesan and Dr. Steven LaPlante.

The most noteworthy observation from the computational data is that the quinoline ligands **3.3** and **3.5** bind in alternate conformations with the P2 quinoline ring flipped so that the benzenoid ring of the quinoline is positioned over the catalytic triad. This suggests that the 7-methoxy quinoline moiety of **3.5** is not interacting with the guanidine side chain of Arg155 as previously speculated. There may be some interaction between this group and Arg155 in the case of **3.6**, as the orientation of the heterocycle is such that these groups are in close proximity to one another (~2.6 Å).

This alternate binding mode is significant because of the six ligands investigated, the binding profiles of these two ligands were dominated by favorable binding *enthalpies* rather than entropies. This suggests that some significant non-covalent interaction may be occurring between the aromatic quinoline rings and the catalytic triad. As the binding mode shifts upon addition of the phenyl group from **3.3** to **3.4** and **3.5** to **3.6**, there is a significant enthalpic penalty of +2.8 kcal $mol^{-1}$ and +5.0 kcal $mol^{-1}$, respectively.

The proximity of the aromatic group of the P2 unit to His57 of the catalytic triad suggests the possibility of non-covalent interactions between the two aromatic groups. With both protonated and neutral forms, histidine is a versatile amino acid capable of participating in hydrogen bonds, π-π interactions, cation-π interactions, and hydrogen-π interactions.[166] Protonated histidine has been shown to be capable of forming cation-π interactions with aromatic groups in other amino acid residues ranging in energy from –7.8 kcal $mol^{-1}$ to –13.6 kcal $mol^{-1}$ in the gas phase.[166] The binding mode for the quinoline ligands **3.3** and **3.5** as illustrated by the modeled complexes in **Figure 3.12** and **Figure 3.13** suggests that the quinoline and the histidine residue could be positioned for possible π-π interactions in a "parallel-displaced" arrangement.[167] There is frustratingly little that is known about the detailed thermodynamics of interactions involving aromatic groups in the context of protein-ligand binding. [13,168,169] However, histidine has been shown to undergo

a variety of face-to-face (π-π) and edge-to-face (hydrogen-π/cation-π) interactions with the heterocyclic DNA bases with gas phase energies ranging from –4.7 to –10.7 kcal $mol^{-1}$ for neutral histidine and from –9.5 to –25 kcal $mol^{-1}$ for protonated histidine.[170] Although solvation effects are expected to decrease these energies, it has been argued that in nonpolar environments, these interactions are expected to be significant. These types of interactions contribute to a more favorable binding enthalpy, [167]. This type of interaction could explain the favorable binding enthalpies of **3.3** and **3.5**.

The proximity of the quinoline nitrogen atom to Asp81 of the catalytic triad (~2.6 Å) could also hint at a possible hydrogen bonding interaction. A separate investigation into a similar series of linear tripeptide NS3 inhibitors was conducted by Paul Bernard.[5] ITC data were collected for the naphthalene and 6-methoxynaphthalene derivatives **3.46** and **3.47**, respectively. An additional double mutant cycle can be constructed in order to illustrate the effects of the nitrogen atom and the 7-methoxy substituent (Figure **3.14**).

[5] Bernard, P. *unpublished results*.

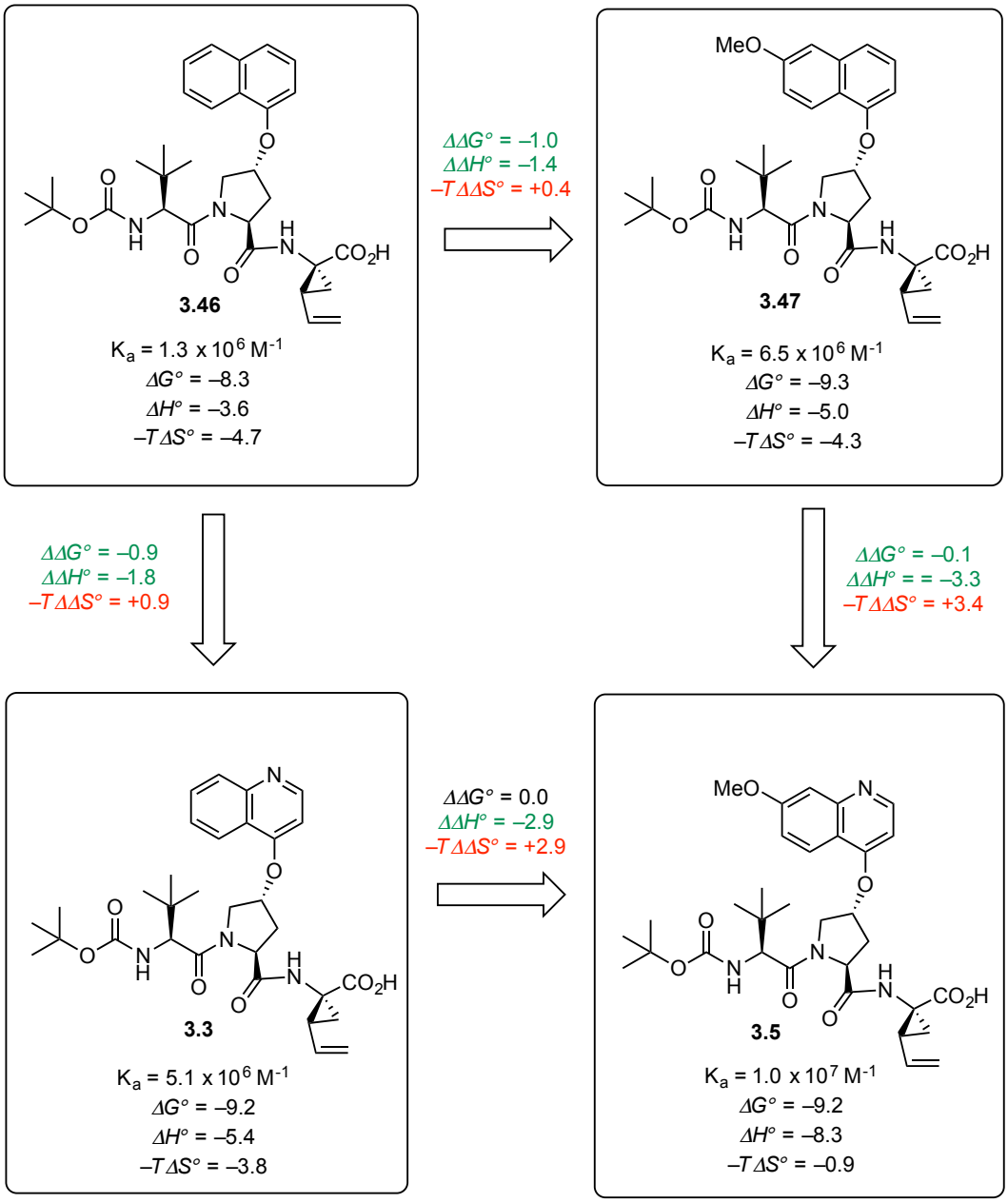


**Figure 3.14:** Double mutant cycle analysis for ligands **3.46**-**3.47** and **3.3**/**3.5**. Values expressed in kcal $mol^{-1}$.

Once again, the binding free energy for ligand **3.5** falls short of the expected value by only 1.0 kcal $mol^{-1}$, the observed binding enthalpy ($\Delta H°_{obs}$ = –8.3 kcal $mol^{-1}$) is more favorable than the expected value of –6.8 kcal $mol^{-1}$ if the enthalpic effects of these

substitutions were simply additive. Overall, the naphthalene derivatives exhibit less favorable binding enthalpies than the corresponding quinoline ligands, which would be expected to be the more electron deficient aromatic systems. Although this finding does not necessarily rule out a possible interaction between the π systems of the quinolines and His57, this suggests that a different interaction may be predominantly responsible for the observed enthalpies. Interestingly, incorporation of either the nitrogen atom or the methoxy group results in a near identical improvement in $\Delta H°_{obs}$ ($\Delta\Delta H°_{obs}$ = –1.4 to –1.8 kcal $mol^{-1}$). The preferred bound conformations of **3.46** and **3.47** are unknown, and so it cannot be said with certainty what interactions are responsible for the observed increase in enthalpy from **3.46** to **3.47**. However, regardless of which is incorporated first, addition of the second substituent results in a larger improvement in $\Delta H°_{obs}$. Thus, there is an observed synergistic effect between these two substituents. In conjunction with the UV data obtained from the 7-methoxy quinoline ligands (see **Table 3.8**), this finding lends support to the hypothesis that the addition of the methoxy group may enhance the basicity of the heterocyclic nitrogen. If the enhanced basicity of the heterocyclic nitrogen leads to protonation of the ligand at this site, then a favorable hydrogen bonding interaction with Asp81 could potentially be established.

Overall, these observations are significant in that they highlight the importance of collecting thermodynamic data during the early stages of lead optimization. Prior to this work, the individual thermodynamic parameters for these ligands were unknown. Following the principles of Freire's "enthalpy funnel" (see Section **1.4**), ligands with intrinsically more favorable values for $\Delta H°$ should be chosen as initial candidates for further elaboration, as strategies for optimization of binding entropy via preorganization or increasing hydrophobic surface area are more straightforward (at least in theory). The two ligands that bind with affinities that are dominated by binding *enthalpy*, **3.3** and **3.5**, are

speculated to bind in an alternate conformation relative to the other tripeptides. Had one of these ligands been chosen for further optimization by B.I. rather than **3.6**, an alternate set of analogs could have been developed, perhaps shortening the optimization process and exhibiting more favorable binding profiles.

### 3.2.7 Summary

In summary, we evaluated a series of linear tripeptide HCV NS3 inhibitors by ITC in order to better understand the individual thermodynamic contributions of a variety of substituents on the P2 proline residue. We had envisioned a double-mutant cycle-type of analysis in which we have shown that the binding affinities for four of the six ligands are predominantly due to a favorable binding entropy. Preliminary computational modeling studies suggest that that the two quinoline ligands that do not have a phenyl group at the 2-position of the aromatic ring appear to bind in an alternate conformation in which the quinoline ring is positioned over the catalytic triad. We have shown that although these ligands bind to the protein with similar affinity to the other quinoline ligands, this alternate conformation results in significantly different binding profiles that are dominated by favorable binding *enthalpies* rather than entropies.

It is difficult to compare changes in the thermodynamics upon addition of substituents if the two ligands bind in alternate conformations. Furthermore, although the observed binding enthalpies and entropies differed from those expected based upon additive energetic contributions, the overall binding free energies were measured within 1.0 kcal $mol^{-1}$ of the expected values. The nuanced web of factors that influence binding enthalpy and entropy are still not well understood, and as such this methodology may be inappropriate for this level of detailed thermodynamic investigation.

The addition of the 2-phenyl group to the quinoline ring systematically resulted in a more favorable entropy of binding. The magnitude of this effect was shown to be dependent on which substituents were already present, with values for $-T\Delta\Delta S°_{obs}$ ranging from –0.8 kcal mol$^{-1}$ for the transition from **3.1**-**3.2** to –6.3 kcal mol$^{-1}$ for the transition between **3.5**-**3.6**. The improvement in binding entropy is speculated to be due to an entropy-driven hydrophobic effect, and efforts to evaluate changes in desolvation via measurement of $\Delta C_p$ for these ligands is underway, although we have shown that $\Delta C_p$ is not necessarily an effective barometer for hydrophobic effects.[103] Addition of the 7-methoxy group was shown to impart a more favorable binding enthalpy, with values for $\Delta\Delta H°_{obs}$ of –2.9 kcal mol$^{-1}$ for the transition between **3.3**-**3.5** and –0.7 kcal mol$^{-1}$ for the transition from **3.4**-**3.6.** We originally speculated that the addition of 7-methoxy group resulted in the formation of an interaction with the guanidine moiety of Arg155; however, this does not appear to be the case for **3.5**, as this ligand binds in a different conformation. Rather, the increase in electron density of the aromatic ring of **3.5** may enhance the basicity of the heterocyclic nitrogen and thus facilitate a hydrogen bonding between the quinoline and Asp81 of the catalytic triad. This work showcases the value of thermodynamic evaluation of early hit compounds in the drug development process, as the transition from ligand **3.5**-**3.6** results in a large enthalpic penalty, suggesting the disruption of strong non-covalent interactions with the enzyme active site.

### 3.3 Studies on Tripeptide NS3 Inhibitors: The P3 Side Chain

Given our previous work investigating conformational constraints within the context of protein-ligand thermodynamics (see **Section 1.5.1.2**), we were also interested in understanding the role that the P3 *tert*-butyl side chain might play in the thermodynamics of binding between HCV NS3 and these tripeptide inhibitors.

### 3.3.1 The *tert*-butyl Group as a Conformational Constraint

Upon binding to a receptor, a flexible molecule will adopt a conformation that maximizes noncovalent interactions with the binding pocket. However, this conformation is often *less* energetically favorable than the solution state conformation due to the restriction of molecular rotors and accumulation of torsional strain, and thus an unfavorable change in entropy typically occurs on binding. Preorganizing a ligand so that the solution state conformation mimics that of the bound state conformation is a common strategy for improving the binding affinity of a ligand as it is thought to mitigate this entropic penalty, although we and others have shown that this is not necessarily the case (see section **1.5.1**).

It was known from the literature that the tripeptide inhibitors developed by B.I. bind to the NS3 protease in an extended conformation where the NH and CO groups of the P3 residue are involved in hydrogen bonding to the enzyme backbone.[140] Thus, it was presumed that the function of the P3 side chain was to rigidify the peptide into an extended conformation in solution, so a *tert*-butyl group was chosen for this purpose, leading to the development of **3.6** (see section **2.3**). We endeavored to investigate whether incremental increases in steric bulk up to the *tert*-butyl group of the P3 side chain improved the binding affinity of these tripeptides via favorable changes to binding enthalpy or entropy (**Figure 3.15**). The 4-hydroxy-2-phenylquinoline was chosen for the P2 subunit for this investigation because ligand **3.4** was shown to be a potent inhibitor of the NS3 protease and a well-behaved ligand in ITC experiments with a largely favorable binding entropy.

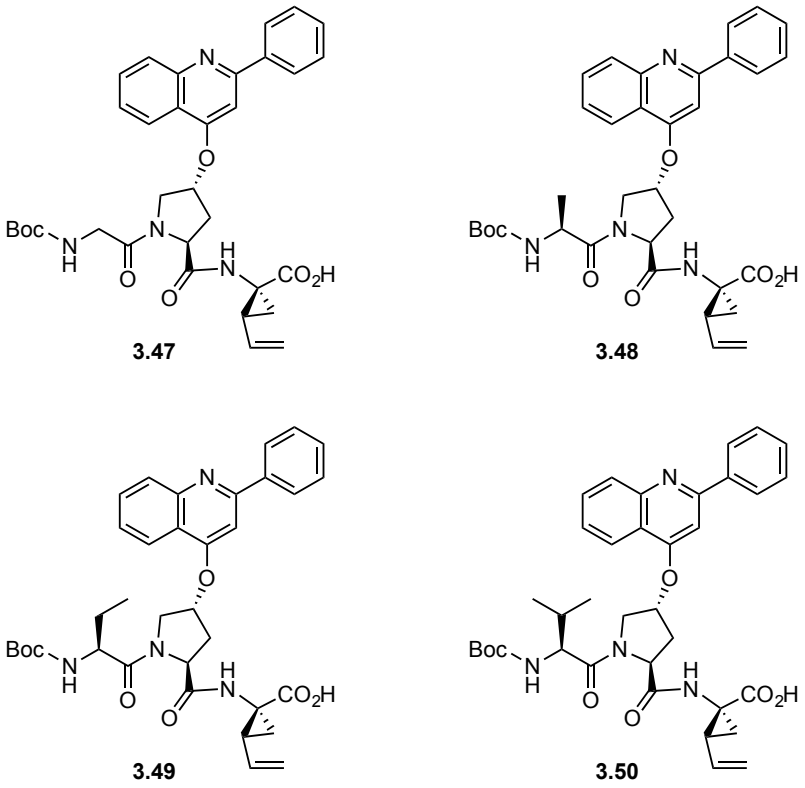


**Figure 3.15:** P3 side chain variants **3.47**-**3.50**.

### 3.3.2 Ligand Synthesis

The synthesis of these tripeptide ligands was straightforward, thanks to the generous donation of the dipeptide brosylate **3.51** by B.I. The previously synthesized hydroxyquinoline derivative **3.23** was substituted onto the dipeptide brosylate **3.51** in the same manner as the previous study to give Boc-protected dipeptide **3.52** in 96% yield (Scheme **3.8**). Deprotection with neat TFA provided dipeptide **3.53** in 93% yield. The dipeptide was coupled with the appropriate amino acid to give tripeptide esters **3.54**-**3.57**, which were then saponified to give ligands **3.47**-**3.50**.

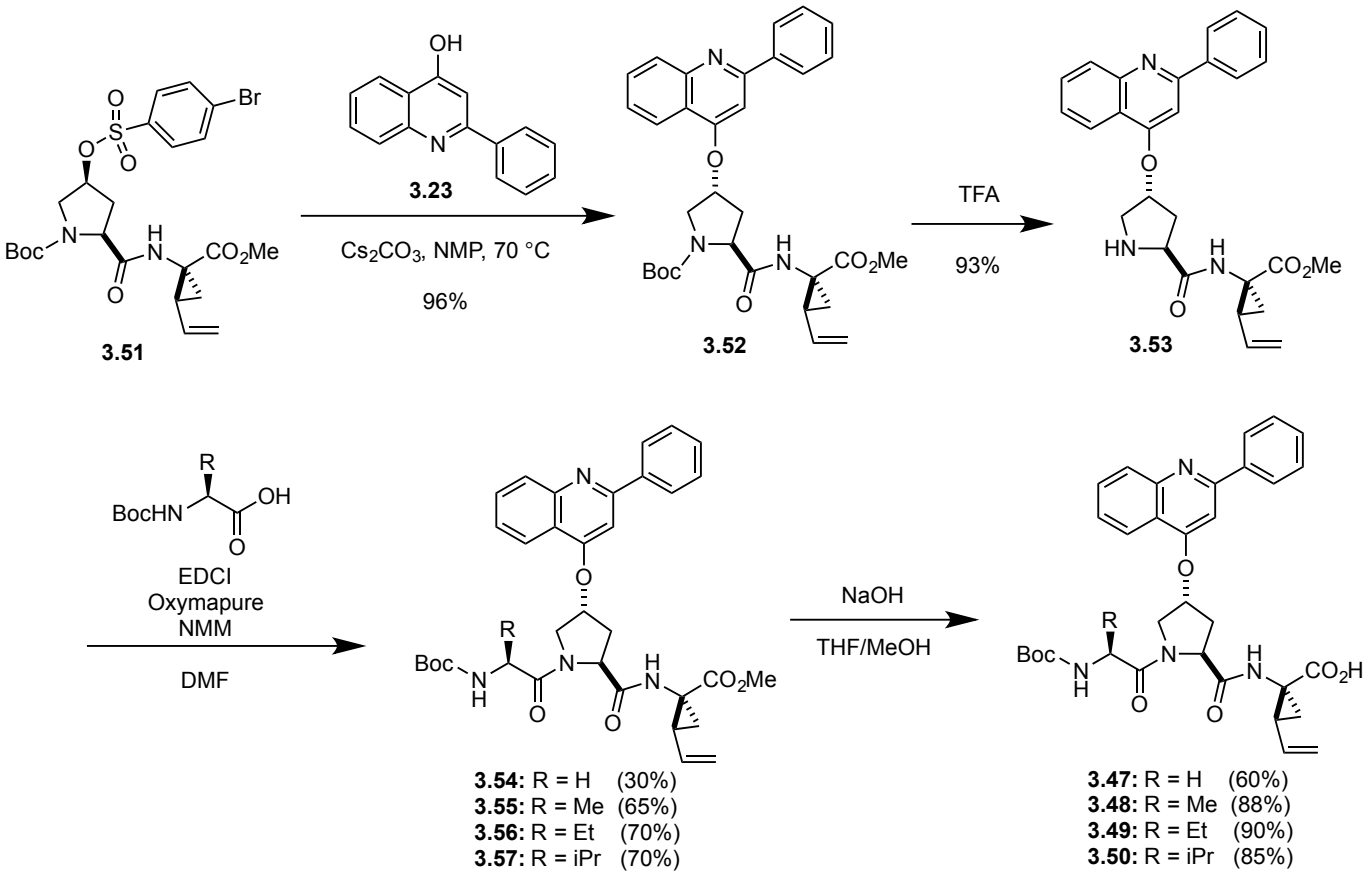


**Scheme 3.8:** Synthesis of ligands **3.46-3.49**.

### 3.3.3 Thermodynamic Data and Evaluations

ITC data was collected for ligands **3.46**-**3.49** and is presented in **Table 3.10**.

**Table 3.10**. ITC data for ligands **3.49-3.52**. [a]

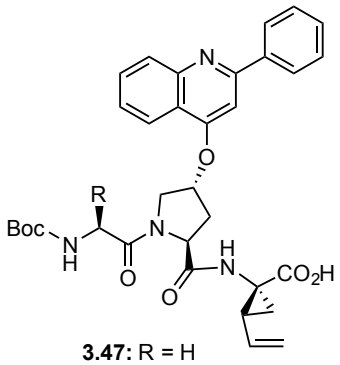

**3.47:** R = H
**3.48:** R = Me
**3.49:** R = Et
**3.50:** R = *i*Pr
**3.4:** R = *t*Bu

| Ligand | $K_a$ ($M^{-1}$) | $\Delta G°$ (kcal•mol$^{-1}$) | $\Delta H°$ (kcal•mol$^{-1}$) | $-T\Delta S°$ (kcal•mol$^{-1}$) | *n* |
|---|---|---|---|---|---|
| **3.47** | 1.3 x $10^4$ | –5.6 | –1.0 | –4.6 | 1.00 |
| **3.48** | 3.8 (± 0.4) x $10^5$ | –7.6 ± 0.06 | –1.1 ± 0.1 | –6.5 ± 0.1 | 0.96 - 1.02 |
| **3.49** | 1.1 (± 0.07) x $10^6$ | –8.2 ± 0.04 | –1.7 ± 0.1 | –6.5 ± 0.1 | 0.92 - 0.96 |
| **3.50** | 4.0 (± 0.8) x $10^6$ | –9.0 ± 0.1 | –2.3 ± 0.2 | –6.7 ± 0.3 | 0.94 - 0.99 |
| **3.4** | 1.0 (± 0.03) x $10^7$ | –9.6 ± 0.02 | –2.6 ± 0.1 | –7.0 ± 0.1 | 0.98 - 1.17 |

[a] Average of three trial per ligands, with *n* reported as the observed range over the trials.

The P3 glycine ligand **3.47** was a modest inhibitor of the protease with a $K_a$ of 1.3 x $10^4$ $M^{-1}$. Due to the low binding affinity (for ITC purposes) and binding enthalpy ($\Delta H°_{obs}$ = –1.0 kcal mol$^{-1}$), the ITC curves were difficult to fit, and only one well-defined isotherm was obtained. The P3 alanine ligand **3.48** was 30-fold more potent, and the net addition of the methylene unit to the P3 side chain resulted in a more favorable binding entropy by nearly 2 kcal mol$^{-1}$, as would be expected based on the conventional paradigm that conformationally restricting a ligand results in a more favorable binding entropy. Addition of the next methylene group to give ligand **3.49** resulted in a three-fold increase in potency

for an improvement of the binding free energy by 0.6 kcal $mol^{-1}$. It was surprising to observe that this increase was due solely to a more favorable binding *enthalpy*. Moving from the ethyl group to an isopropyl group resulted in a similar improvement in $\Delta G°_{obs}$ by 0.8 kcal $mol^{-1}$, again coming mostly from a more favorable $\Delta H°$. The parent ligand **3.4** with a *tert*-butyl side chain was a roughly three-fold more potent ligand than **3.50**, and the more favorable $\Delta\Delta G°_{obs}$ of 0.6 kcal $mol^{-1}$ was split evenly between favorable changes in enthalpy and entropy.

### 3.3.4 Computational Studies

As in the previous study, we turned to computational studies to obtain a clearer picture of the structure of the protein-ligand complex. Modeling studies were conducted by Japadeepa Murugesan and Dr. Steven LaPlante (Figure **3.16**). As in the previous study, starting from a known x-ray crystal structure[156], each of the compounds was modeled into the binding site of the protease and minimized using the Quick Prep procedure as implemented in MOE (2016.0802).

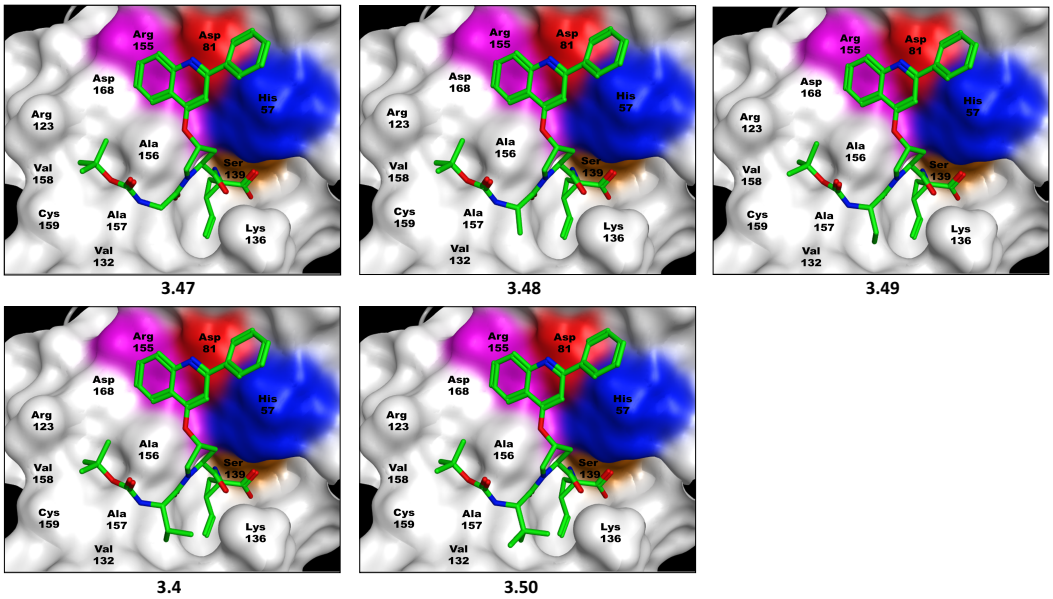


**Figure 3.16:** Modeled complexes of ligands **3.47**-**3.50** with the HCV NS3 protease.[6]

Based on the modeling data, the ligands **3.46**-**3.49** appear to bind in conformations identical to the parent ligand **3.4**. The side chain of the P3 residue does not appear to make any significant interactions with the enzyme surface. In the absence of any significant interaction, we can speculate that the observed increase in binding affinity potentially derives from an enthalpy-driven hydrophobic effect (see **Section 1.5.2**). Efforts are underway to evaluate differences in the number of van der Waals contacts between the ligands.

We observed that the change in binding free energy ($\Delta\Delta G°_{obs}$) resulting from increases in steric bulk at the P3 side chain ranges from –0.6 to –0.8 kcal mol$^{-1}$ per methylene unit incorporated. This finding is interesting in that these results are similar to a previous Martin group investigation into the effects of increasing nonpolar surface area of Grb2 SH2 inhibitors (See **Figure 1.30**). Myslinski *et al*. observed that expanding the ring size within a series of cyclic α,α-disubstituted pY + 1 analogs resulted in a $\Delta\Delta G°_{obs}$ of –

[6] Molecular docking and MD calculations were performed by Jayadeepa Murugesan and Dr. Steven LaPlante.

0.7 ± 0.1 kcal $mol^{-1}$ per methylene unit, which was attributed to an enthalpy-driven hydrophobic effect resulting in an increase in the number of van der Waals contacts. [11] These results are also similar to those reported by Homans, who observed an enthalpy-driven hydrophobic effect in two series of MUP-I inhibitors resulting in a favorable $\Delta\Delta G°_{obs}$ of *ca.* –0.9 kcal $mol^{-1}$ per methylene unit incorporated (see **Figure 1.26** and **Figure 1.27**). [14,15] There is, however, a notable difference between our work and that of others reporting on this phenomenon. In the literature reports detailing enthalpy-driven hydrophobic effects, adding nonpolar surface area resulted in increasingly less favorable binding entropies, whereas in our system, the binding entropy slowly improved alongside the binding enthalpy as nonpolar surface area was added from **3.46** to **3.4**. The rigidification of the tripeptide into its extended bioactive conformation as the P3 side chain increases in size should in theory impart a favorable $-T\Delta\Delta S°$. Thus, we can speculate that this effect may help mitigate the entropic penalty that is observed in other enthalpy-driven hydrophobic effects.

To further understand how steric bulk in the P3 side chain rigidifies the tripeptide motif, molecular dynamics (MD) simulations of the P3 ligands in the free (unbound) state were performed by Dr. Steven LaPlante (**Table 3.11**). In these calculations, the protein was removed and the carboxylic acid was made neutral. The P1 residue and the proline ring were kept rigid while the remaining atoms were allowed to rotate freely. Two torsion angles were recorded from the models of the bioactive conformations, as indicated by T1 (x1-x2-x3-x4) and T2 (y1-y2-y3-y4). These torsion angles were then extracted from the solution state conformations of the free carboxylic acids for comparison. LowModeMD was performed on each compound with up to 300 conformations. Each conformation was energy minimized to an RMS gradient of 0.1 kcal $mol^{-1}$. The RMSD limit was set to 0.1 Å and the energy window was set to 30 kcal $mol^{-1}$. These parameters were used to allow

sufficient sampling freedom. The percentages of the solution state conformations with torsion angles T1 and T2 within 20 degrees of the bioactive conformation for each of the ligands are reported in **Table 3.11**.

**Table 3.11**. Torsion angles for the bioactive conformation of ligands **3.4** and **3.46**-**3.49**.[7]

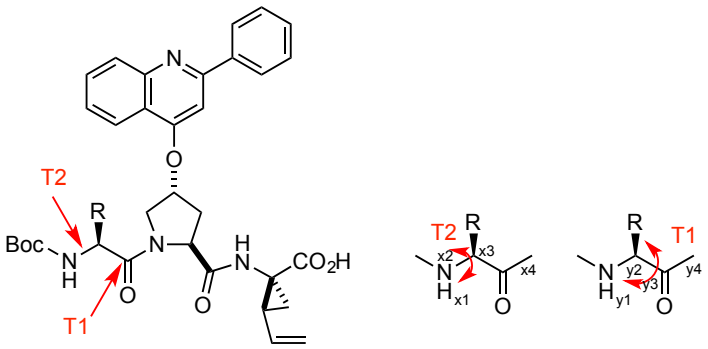


| Ligand | R | Bioactive Torsion (°) | | Free State Torsion, ± 20° from bioactive (%) | |
|---|---|---|---|---|---|
| | | T1 | T2 | T1 | T2 |
| **3.46** | H | 112 | –107 | 29 | 30 |
| **3.47** | Me | 112 | –108 | 42 | 42 |
| **3.48** | Et | 118 | –106 | 35 | 37 |
| **3.49** | *i*Pr | 125 | –110 | 40 | 36 |
| **3.4** | *t*Bu | 125 | –106 | 71 | 59 |

As is evidenced by the data presented in **Table 3.11**, the torsion angles T1 and T2 in the bound conformations of the P3 analogs are highly similar. This is to be expected, as the NH and CO groups of the P3 residue are known to form key hydrogen bonds with residues of the protease, and such interactions are distance and angle-dependent.[140] The angle T1 increases slightly as the side chain is increased from a methyl group (**3.47**) to an ethyl group (**3.48**) and again when the side chain is changed to an isopropyl group (**3.49**).

[7] MD calculations were performed by Jayadeepa Murugesan and Dr. Steven LaPlante.

This slight rotation of the P3 side chain may be necessary to avoid steric clashes with the enzyme backbone as the size of the side chain increases, although the extent to which these deviations in the angle T1 are significant is not immediately known.

The unsubstituted ligand **3.46** shows considerable flexibility in the solution state, with only 29 and 30 percent of solution-state conformations within 20 degrees of the bioactive conformation for torsion angles T1 and T2, respectively. Introducing a methyl group into the P3 side chain to give **3.47** rigidifies the structure and improves the similarities between the bound and unbound states of the ligand to 42%. This may provide some insight into the sharp improvement of the binding entropy between **3.46** and **3.47** ($-T\Delta\Delta S°_{obs} = -1.9$ kcal mol$^{-1}$); however, such a conclusion must be approached with caution, as only one data set was obtained for the glycine ligand **3.46**. The degree of similarity between the bound and unbound states of the ligands appears to decrease slightly when the side chain is further extended to an ethyl group (**3.48**), but no change in the binding entropy is observed between **3.47** and **3.48**. The fully substituted *tert*-butyl group shows a considerably higher degree of rigidity, with 71% of the solution state conformations within 20 degrees of the bioactive conformation for T1 and 59% of the conformations within 20 degrees for T2. This leads us to believe that the available solution state conformations for this ligand most closely match the bound state conformation, and this could be the origin of the favorable change in binding entropy from **3.49** to **3.4**, however there appears to be no direct numerical correlation between the changing torsional angles and either $-T\Delta\Delta S°_{obs}$ or $\Delta\Delta G°_{obs}$. The extent of any entropic penalty that may be incurred as a result of an enthalpy-driven hydrophobic effect and the degree to which this counteracts an entropic benefit that might be obtained from conformational constraint is difficult to untangle and warrants further study.

### 3.3.5 Summary

In order to understand the role of the P3 *tert*-butyl side chain in the thermodynamic binding profile of the linear tripeptide HCV NS3 protease inhibitor **3.4**, analogs **3.46-3.49** were synthesized wherein the steric bulk of the P3 side chain was incrementally increased from a glycine residue to a *tert*-leucine residue. The binding thermodynamics of these ligands were determined by ITC and structures of the protein-ligand complexes were generated by computational docking studies.

We hypothesized that as the size of P3 side chain increases, the subsequent rigidification of the tripeptide backbone would constrain the ligands into the bioactive conformation, and the binding affinity would improve because of more favorable changes in binding entropy. We discovered that as the bulk of the side chain incrementally increases, $\Delta G^{\circ}_{obs}$ became more favorable, with a $\Delta\Delta G^{\circ}_{obs}$ ranging from –0.6 to –0.8 kcal $mol^{-1}$ per methylene group incorporated, primarily through favorable increases in binding enthalpy ($\Delta\Delta H^{\circ}_{obs}$), although small gains were made in the binding entropies as well. The $\Delta\Delta G^{\circ}_{obs}$ values are in agreement with reports in other protein-ligand systems of incremental increases in nonpolar surface area contributing between –0.7 and –0.9 kcal $mol^{-1}$ per methylene group as a result of increasingly favorable binding enthalpies, which have been attributed to enthalpy-driven hydrophobic effects. While increasingly unfavorable binding entropies were observed in the other cases of enthalpy-driven hydrophobic effects, the binding entropies of the P3 analogs in this study remained largely consistent and improved very slightly. The entropic effects of preoganization due to the rigidity imposed by the P3 side chain may work to counteract an entropic penalty resulting from an enthalpy-driven hydrophobic effect, but our limited knowledge of the intricacies of these phenomena make detailed analysis difficult.

The modeled complexes show no significant differences in the bound conformations of the P3 analogs **3.46**-**3.49** and the parent ligand **3.4**. Computational analysis of key torsion angles related to the P3 residue also show highly similar results, suggesting that the key hydrogen bonding network between the tripeptide and the enzyme backbone is undisturbed. The torsion angle T1 was shown to increase slightly as the bulk of the P3 side chain increases. Comparison of the torsion angles in the bound and unbound conformations of the ligands revealed that the P3 glycine ligand **3.46** showed considerable flexibility in solution, whereas a majority of the solution state conformations of the constrained ligand **3.4** exhibited torsion angles within 20 degrees of the bound conformation. The intermediate ligands **3.47-3.49** showed similar degrees of similarity between the solution-state and bioactive conformations, and no direct correlations could be made between the level of similarity of the bound and unbound conformations and the thermodynamic values. Thus, the data suggest that the *tert*-butyl group is an effective group for conformational constraint of the ligand into its extended bioactive conformation, and incremental increases in steric bulk at the P3 side chain correspond to incremental increases in binding affinity; however, the effects of these modifications on the individual enthalpic and entropic terms is vastly more complicated due to the effects of both preorganization and a potential enthalpy-driven hydrophobic effect.

# Chapter 4. Progress Toward the Total Synthesis of (±)-Arboridinine

## 4.1 INTRODUCTION

Plants of the genus *Kopsia* (Apocynacae) are widely distributed throughout Southeast Asia, India, China, and Australia, with a majority of the species concentrated in Malaysia.[171] These plants are a rich source of a variety of indole alkaloids with unprecedented skeletons and interesting biological activities, with some compounds showing antitumor,[172] antimitotic,[173] antileishmanial,[174] and antitussive activities.[175] The newest addition to this family is the novel pentacyclic alkaloid (+)-arboridinine, which was isolated in 2014 by Wang and coworkers from *K. arborea* (Figure **4.1**).[176]

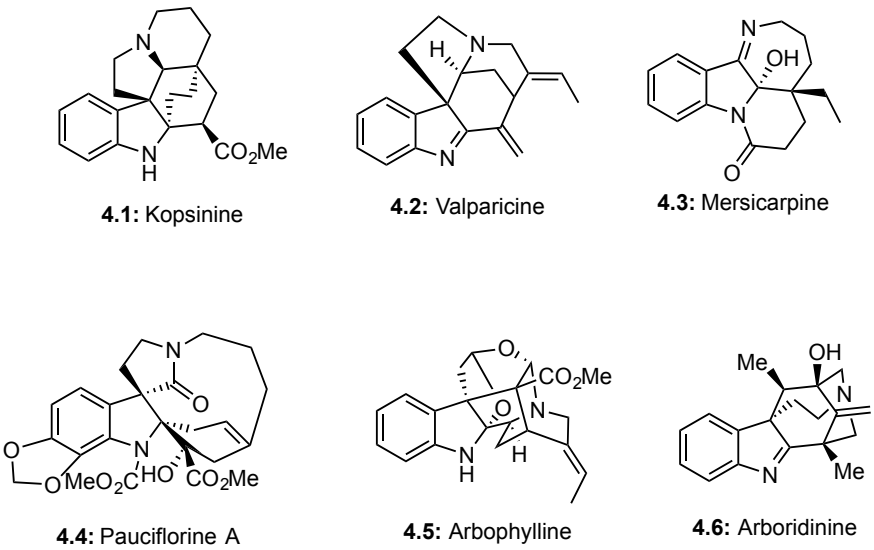


**Figure 4.1:** Representative members of the *Kopsia* alkaloids.

Arboridinine is a monoterpene indole alkaloid with a unique pentacyclic caged structure characterized by two azepane rings as well as a densely functionalized cyclohexyl ring fused to the indolenine moiety. A potential biosynthetic pathway was proposed starting from the related indole alkaloid pericine **4.7** (Scheme **4.1**).[176] Oxidation of the ethylidene

double bond forms epoxide **4.8,** which can be opened via nucleophilic attack by the indole moiety to furnish **4.9**. Conjugate reduction of the resulting imine provides enamine **4.10.** Once a suitable leaving group is installed on the tertiary amine nitrogen to give **4.11**, a Grob-type fragmentation would lead to a tetracyclic iminium **4.12**, from which attack of the enamine would generate arboridinine **4.6**.

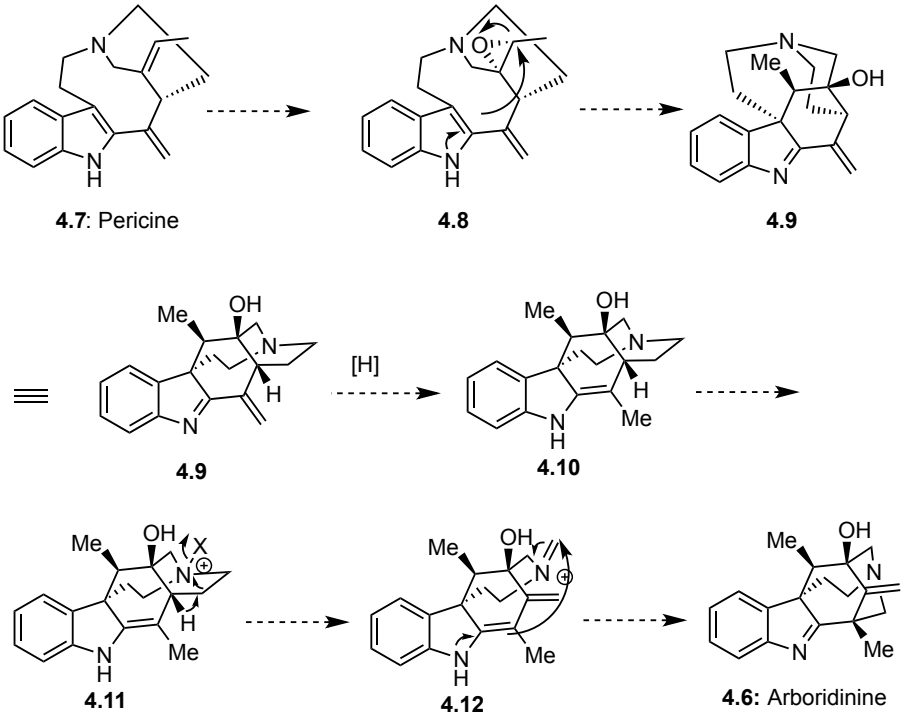


**Scheme 4.1:** Proposed biosynthesis of (+)-arboridnine.[176]

Biological testing by Wong and coworkers reported arboridinine to be inactive against drug-sensitive and vincristine-resistant KB cells; however, it was shown to have a moderate concentration-dependent relaxation effect on phenylephrine-induced contraction in isolated rat aortic rings with an $EC_{50}$ of 4.98 $\mu$M.[176] To date there are no reported syntheses or attempts toward arboridinine. The highly compact and complex structure

combined with its unique biological activity piqued the interest of our group and prompted us to develop a route toward a total synthesis of this unique natural product.

### 4.2 First Generation Approach

In designing a synthetic route toward arboridinine, it was envisaged that the exocyclic olefin would be installed near the end of the synthesis because ketone precursor **4.13** would provide a susbtrate that would ideally allow for closure of both azepane rings in a single step via a double Mannich reaction with two equivalents of formaldehyde (Scheme **4.2**). The α-silyloxyketone **4.14** could be made from oxidation of silyl enol ether **4.15**, which could be assembled by a Diels-Alder reaction of an *N*-protected indole-3-glyoxamide **4.15** and a diene **4.16**. We reasoned that the Diels-Alder reaction would be an ideal choice to quickly assemble the key tricyclic intermediate as three of the final four stereocenters could be set by the reaction in a single step. Utilizing any of the known derivatives of **4.15** and **4.16**, this synthesis could be completed in seven steps from known materials.

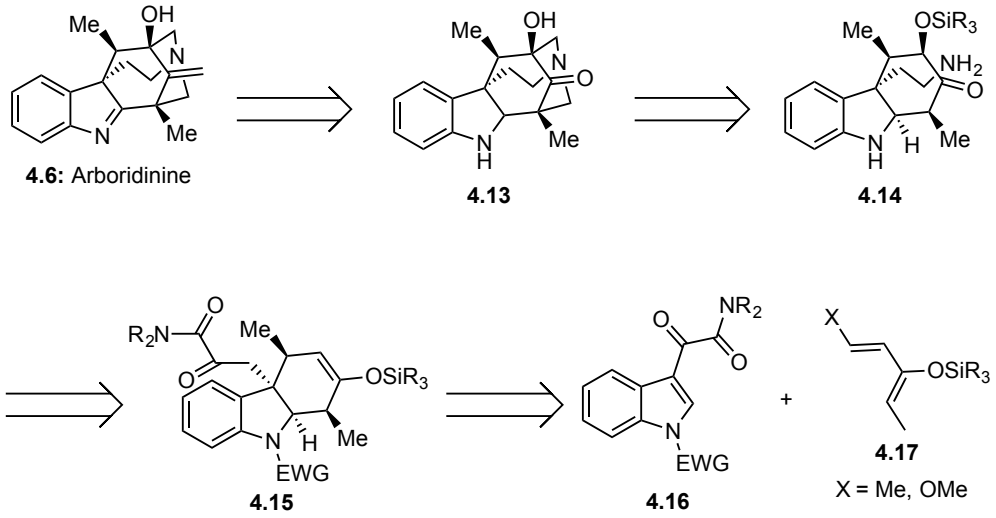


**Scheme 4.2:** Martin group retrosynthesis of **4.6**.

### 4.2.1 Diels-Alder Reactions of Indoles

The Diels-Alder reaction is one of the most powerful transformations in organic chemistry.[177] The reaction is stereospecific, diastereoselective, regioselective, and completely atom economical. The ability to form two new carbon-carbon bonds and set up to four contiguous stereocenters in a single step has cemented the role of the Diels-Alder reaction as a key transformation to quickly build complexity in natural product synthesis.[178,179] Given that indoles are typically electron-rich heterocycles, these compounds provide an ideal framework as electron-rich dienophiles in inverse-demand Diels-Alder reactions, which have been extensively characterized throughout the literature.[180-185] However, examples of electron-deficient indoles participating in normal-demand Diels-Alder reactions with electron-rich dienes, as would be needed in the case of our Diels-Alder reaction to form **4.15**, are sparse in comparison. The earliest example of such a transformation was reported by Wenkert, who showed that *N*-benzenesulfonyl indoles bearing a variety of electron-withdrawing substituents at the 3-position underwent reaction with isoprene **4.19** to give the regioisomeric adducts **4.20** and **4.21** (eq. 4.1).[186]

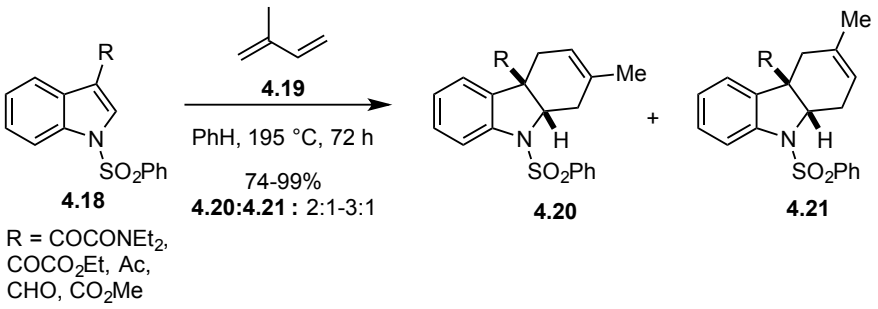


(4.1)

Similar yields were obtained using 1,3-butadiene as the diene under identical thermal conditions, albeit with lower conversion due to competing polymerization of the diene at elevated temperatures. The use of a Lewis acid catalyst enabled the reaction to

proceed at a lower temperature and with enhanced regioselectivity, albeit in a lower yield (eq. 4.2).[186]

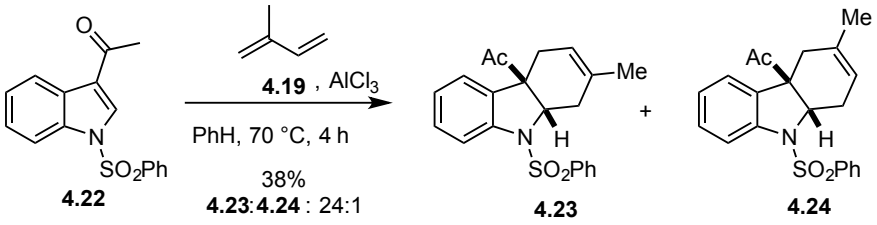


(4.2)

The ease of extrusion of $HNO_2$ following cyclization of the 3-nitrosubstituted derivative **4.25** also provided a new method to access dihydrocarbazoles **4.26** and **4.27** and carbazoles **4.28** and **4.29** (eq. 4.3).[186] Unfortunately, the elevated temperatures (195-270 ºC) and extended reaction times (48-72 h), combined with the competing polymerization of the diene has thus far precluded the typical thermal Diels-Alder reaction of these substrates from being of any synthetic utility.

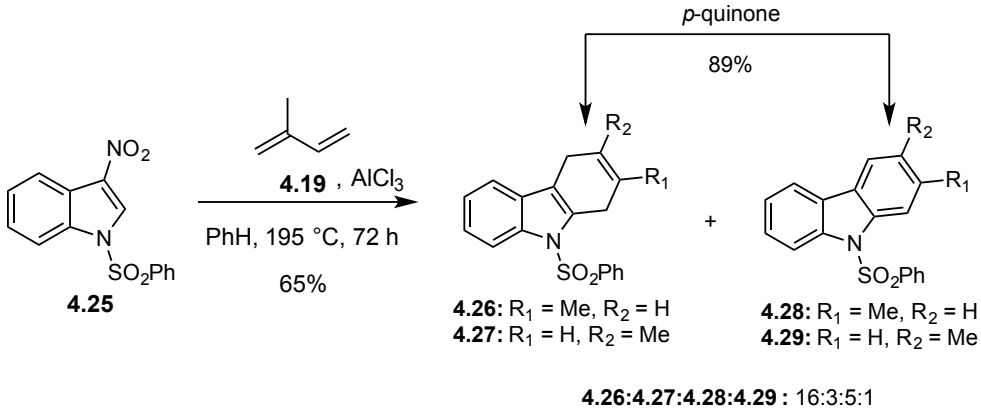


(4.3)

Pressure has been shown to have an impact on the rate of Diels-Alder reactions. The pressure dependence of the rate of a reaction can be defined as follows:

$$\frac{\partial \ln k}{\partial P} = -\frac{\Delta V^{\neq}}{RT} \tag{4.4}$$

where $k$ is the rate constant for the reaction and $\Delta V^{\neq}$ is the volume of activation.[187] Diels-Alder reactions have a negative volume of activation (that is, the transition state is more compact than the reactants), and thus $k$ increases as the pressure increases.[187,188] Piettre reported that performing the reaction of indole **4.30** and 1,3-cyclohexadiene (**4.31)** under high pressure allowed for lower reaction temperatures and reduced reaction times as well as increased conversion rates and product yields (**Table 4.1**).[189] The diastereoselectivity of the reaction was also enhanced to further favor the *endo*-adduct **4.32** from 80:20 under thermal conditions to 96:4 under hyperbaric conditions. The addition of 0.1 equivalents of $ZnCl_2$ under hyperbaric conditions led to further enhancement of the diastereoselectivity to >98:2 and allowed for the reaction to proceed at room temperature with complete conversion of the starting material after 48 h.

**Table 4.1:** Diels-Alder reaction of **4.30** and **4.31**.

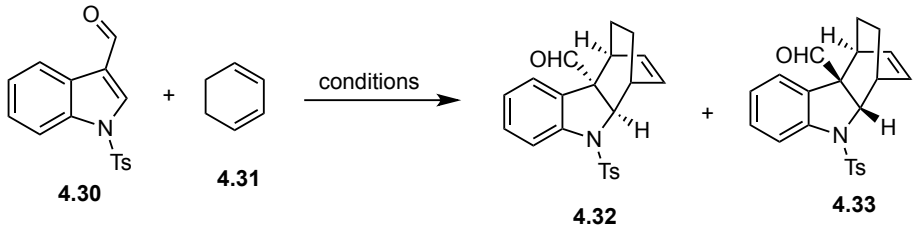


| Conditions | Conversion (%) | Yield (%) | Ratio **4.32:4.33** |
|---|---|---|---|
| 200 °C, 72 h | 25 | 25 | 80:20 |
| 50 °C, 16 kbar, 48 h | 86 | 50 | 96:4 |
| 25 °C, 16 kbar, $ZnCl_2$ (10 mol%), 48 h | 100 | 62 | >98:2 |

The addition of the electrophilic substituent at the C3 position allows the indole to be sufficiently electron-deficient to act as a dienophine in a normal demand Diels-Alder reactions. However, the use of carbonyl groups and nitriles at the C3 position of the indole ring is problematic in that these groups are also known to undergo hetero-Diels-Alder reactions with electron-rich dienes.[190,191] A subsequent report by Piettre shows the chemoselectivity in these Diels-Alder processes is dependent upon the nature of both the diene and the dienophile.[192] In this report, he shows examples of Diels-Alder reactions that occur on the carbon-carbon double bond of the indole or at the C3-carbonyl group of the indole to form hetero-Diels-Alder products. For example, switching the diene from 1,3-cyclohexadiene (**4.31**) to 2,3-dimethylbutadiene **(4.34)** in the Diels-Alder reaction with indole **4.30** affords the Diels-Alder adduct **4.35** with conventional heating; however, the use of hyperbaric conditions led to the formation of the bis-adduct **4.36** arising from a sequential cycloaddition first on the indole double bond followed by cycloaddition with the formyl group (**Table 4.2**).

**Table 4.2:** Diels-Alder reaction of **4.35** and **4.36**.

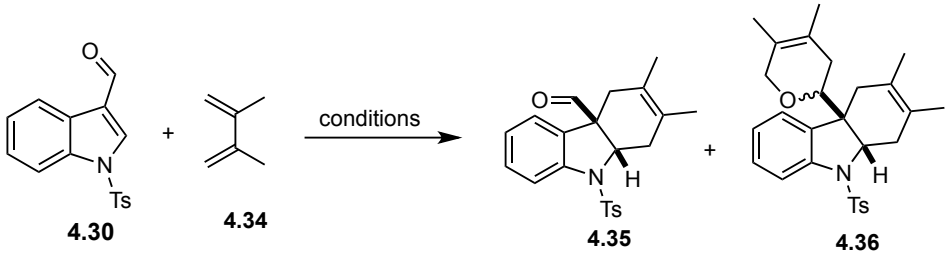


| Conditions | eq. **4.34** | Conversion (%) | **4.35:4.36** | Yield (%) **4.35:4.36** |
|---|---|---|---|---|
| 195 °C, 80 h | 12 | 85 | 100:0 | 83:0 |
| 25 °C, 16 kbar, $ZnCl_2$ (10 mol%), 48 h | 2 | 24 | 46:54 | nd |
| 25 °C, 16 kbar, $ZnCl_2$ (10 mol%), 24 h | 1.1 | 11 | 100:0 | nd |
| 25 °C, 16 kbar, $ZnCl_2$ (10 mol%), 24 h | 12 | 100 | 2:98 | 0:90 (2:1 d.r.) |

The higher reactivity of the aromatic double bond over the formyl group enables the formation of mixed bis-cycloadducts by isolating **4.35** and further reacting with a different diene, such as Danishefsky's diene (**4.37**) (eq. 4.5).[192]

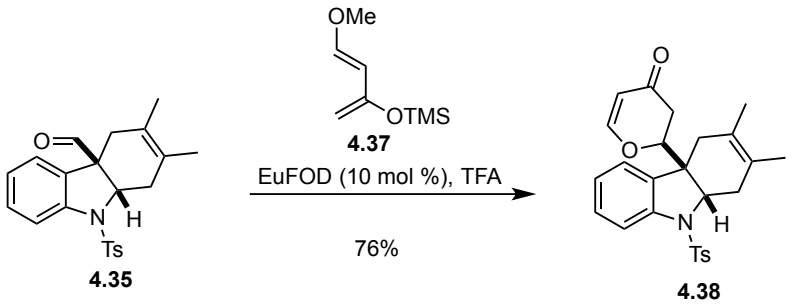


(4.5)

Interestingly, treatment of indole **4.30** with Danishefsky's diene resulted exclusively in the hetero Diels-Alder adduct **4.39** (eq. 4.6). Thus, once the first addition

occurs on the carbonyl group of the electron-withdrawing group at the 3-position, the indole is no longer sufficiently activated to participate in further cycloadditions.[192]

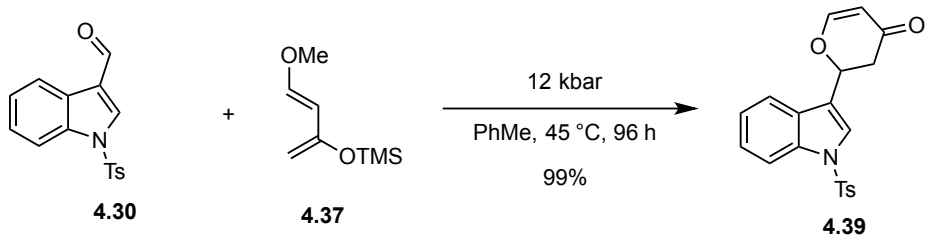


(4.6)

A similar result was obtained with ketoester **4.40** (eq. 4.7). The hetero Diels-Alder reaction removes the electron withdrawing group at the C3 position of the indole and again prevents the formation of any bis-cycloadducts.[192]

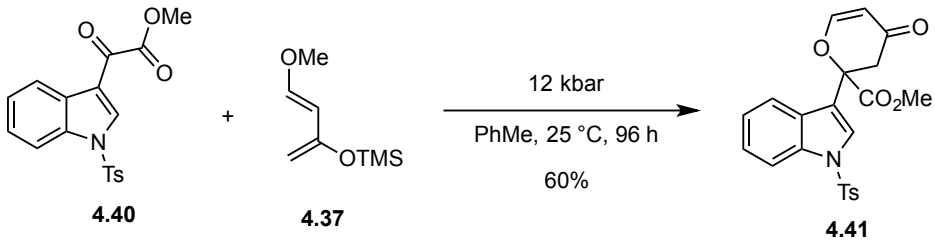


(4.7)

Changing the electron-withdrawing group at the C3 position from a glyoxylate to the *N,N,*-diethyl glyoxamide **4.42** resulted in a reversal in chemoselectivity and provided complete conversion to a separable mixture of diastereomeric cycloadducts **4.43** and **4.44**, with the major diastereomer **4.43** bearing a *trans*-relationship between the ketoamide and the methoxy substituents (**Table 4.3**).[192]

**Table 4.3**: Diels-Alder reaction of **4.42** with Danishefsky's diene (**4.37**).

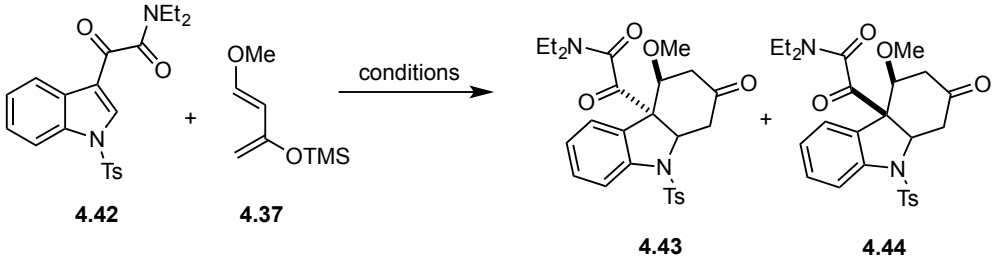


**4.42** **4.37** **4.43** **4.44**

| Conditions | Conversion (%) | Yield (%) | **4.43:4.44** |
|---|---|---|---|
| 180 °C, 48 h | 100 | 55 | 4:1 |
| 45 °C, 12 kbar, 48 h | 100 | 60 | 4:1 |
| 25 °C, 16 kbar, EuFOD (10 mol%), 38 h | 100 | 100 | 4:1 |

With this promising result with tertiary glyoxamide substituents, they then attempted to utilize a chiral secondary glyoxamide in order to effect a diasteroselective Diels-Alder reaction. When they treated indole **4.45** with **4.37** similar conditions, they were surprised to note that the compound underwent a hetero-Diels-Alder reaction to give **4.46** (eq. 4.8).[192]

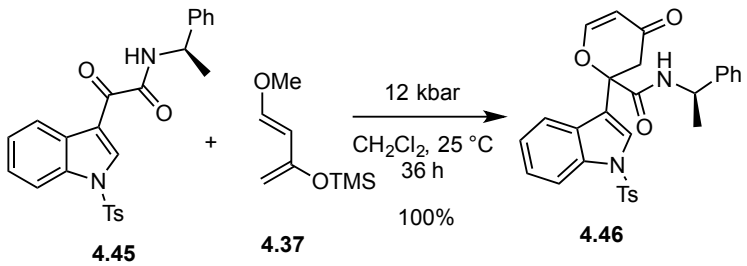


**4.45** **4.37** **4.46** (4.8)

The observed difference in reactivity between the secondary and tertiary glyoxamide substituents was hypothesized to arise from an intramolecular hydrogen bond

that shifted the ketoamide group out of conjugation with the indole (Figure **4.2**).[192] Two possible hydrogen bonding modes exist depending on the conformation of the dicarbonyl unit, either bridging the amide nitrogen with the ketone oxygen atom or one of the sulfur oxygen atoms.

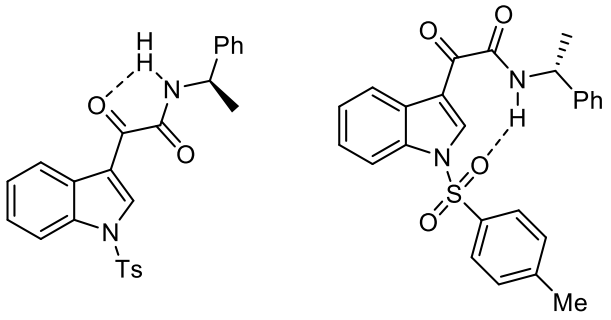


**Figure 4.2:** Possible hydrogen bonding conformations of glyoxamide **4.45**.

In summary, with careful choice of substituents, indoles can participate as dienophiles in normal demand Diels-Alder reactions with electron-rich dienes. In order to generate a sufficiently electron-deficient dienophile, electron withdrawing substituents are required at the indole nitrogen (usually a sulfonamide), and the C3 position (usually a nitro group or a carbonyl-containing group). Even with these substitution patterns, the reaction is often sluggish and requires high temperatures, which can cause problems with competing diene polymerization.[186] It has been reported that high pressure can be used to circumvent the temperature requirement and allow for the reaction to occur under much milder conditions, due to the negative activation volume of the Diels-Alder reaction. [189,192]

When carbonyl groups are placed at the 3-position of the indole ring, competing hetero Diels-Alder reactions can occur between the diene and the carbonyl double bond.[192] Piettre showed that the nature of the diene is important in reactions of 3-formylated indole derivatives. For example, Danishefsky's diene preferentially reacted with the carbonyl

group over the indole double bond, and 2,3-dimethylbutadiene preferentially reacted at the indole double bond.[192] However, he also showed that the nature of the C3 substituent is relevant to the outcome of the reaction, as indole 3-glyoxylates primarily reacted with Danishefsky's diene at the C3 carbonyl group, whereas tertiary indole 3-glyoxamides reacted at the carbon-carbon double bond of the indole ring. Secondary glyoxamides reacted similarly to the glyoxylate derivatives, and it was suggested that conformational and hydrogen-bonding factors could result in deconjugation of the system.

### 4.2.2 Diels-Alder Strategy for the Total Synthesis of Arboridnine

With these literature reports in mind, we felt that a Diels-Alder reaction between an electron-deficient indole **4.16** and a silyl enol ether **4.17** would generate tricycle **4.15** as the relative stereochemistry of the two methyl groups would be determined by the geometry of the diene (eq. 4.9). Based on the results by Piettre, [189,192] (see section **4.2.1**), we felt that the major diastereomer would have the desired *trans*-relationship between the C3 substituent of the resulting indoline and the adjacent methyl group. Thus, three of the four stereocenters present in the natural product would be set in a single step. The glyoxamide could then be easily reduced to unmask the ethylamine group.[193]

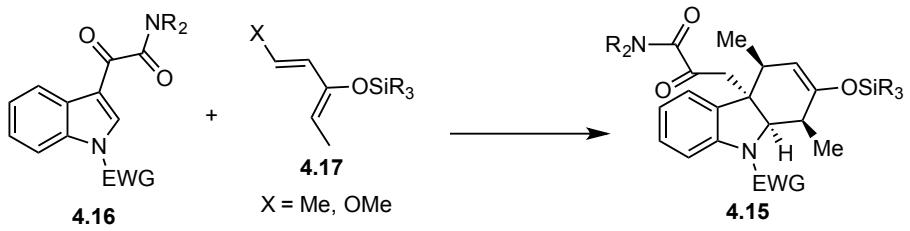


(4.9)

The silyl enol ether of **4.15** would already be in position for oxidation to the α-hydroxyketone, and the final stereochemical configuration of the hydroxyl group would be set by the configuration of the ethylamine chain during the key double-Mannich reaction.

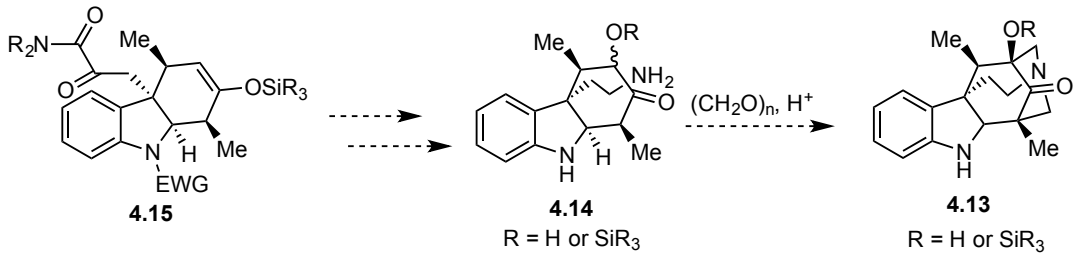


(4.10)

The shortest route to arboridinine that we envisioned would rely on using the primary glyoxamide **4.48** in the Diels-Alder reaction; however, given that secondary amides were shown to undergo hetero Diels-Alder reactions at the ketone carbonyl group,[192] we hypothesized that this reaction with a primary glyoxamide could also lead to the undesired hetero-Diels-Alder adduct **4.49** (eq. 4.11).

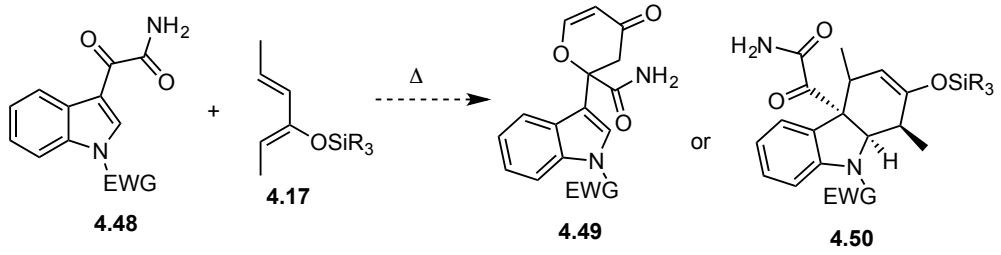


(4.11)

We decided that a tertiary glyoxamide would be more appropriate for the reaction, as Piettre had shown that tertiary glyoxamides underwent Diels-Alder reactions at the indole double bond.[192] We wanted substituents on the amide nitrogen atom that could be easily removed to unmask the primary amine in preparation for the double-Mannich reaction. It was hypothesized that an *N,N,*-dibenzyl derivative **4.51** should serve as a suitable substrate for this purpose (eq. 4.12).

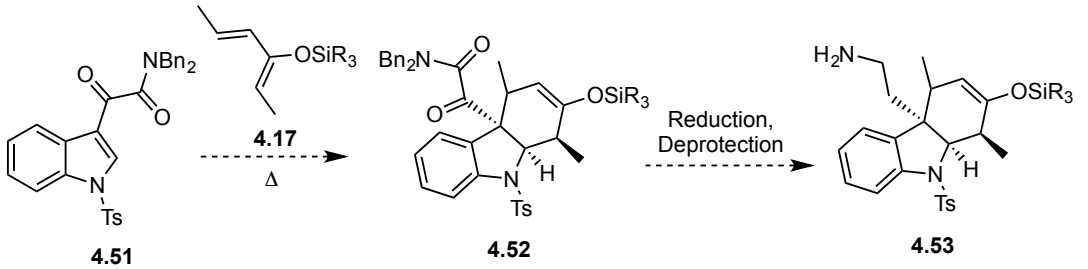


(4.12)

The nature of the indole was not the only reactant that needed to be considered. The only relevant examples of reactions with these indole systems were with 2,3-butadiene and Danishefsky's diene as the cycloaddition partners. When an indole-3-glyoxamide was reacted with 2,3-butadiene, the cycloaddition was observed on the indole ring; however, reaction with Danishefsky's diene resulted in a hetero-Diels-Alder reaction on the ketone carbonyl group (**Table 4.3**).[189,192] Since diene **4.17** should be more electron rich than 2,3-dimethylbutadiene but less electron rich than Danishefsky's diene, it was unclear whether the Diels-Alder product **4.52** or the hetero Diels-Alder product **4.54** would be favored (eq. 4.13).

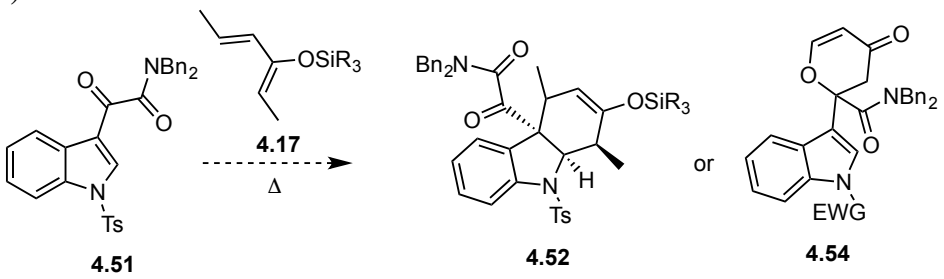


(4.13)

With this in mind, we decided that using an *N*-*N*-dimethyl glyoxamide as a model system for these Diels-Alder reactions would simplify the NMR spectra of the cycloaddition products and make identification and characterization of the cycloadducts easier.

### 4.2.3 Attempted Diels-Alder Cyclizations

As the first step toward examining the feasibility of the key Diels-Alder reaction, indole (**4.55**) was treated with oxalyl chloride followed by $Me_2NH$ to afford the *N*,*N*-dimethyl amide **4.57** in good yield. [194,195] The indole nitrogen atom of **4.57** was derivatized with a variety of different electron withdrawing groups to provide **4.58-4.61**.

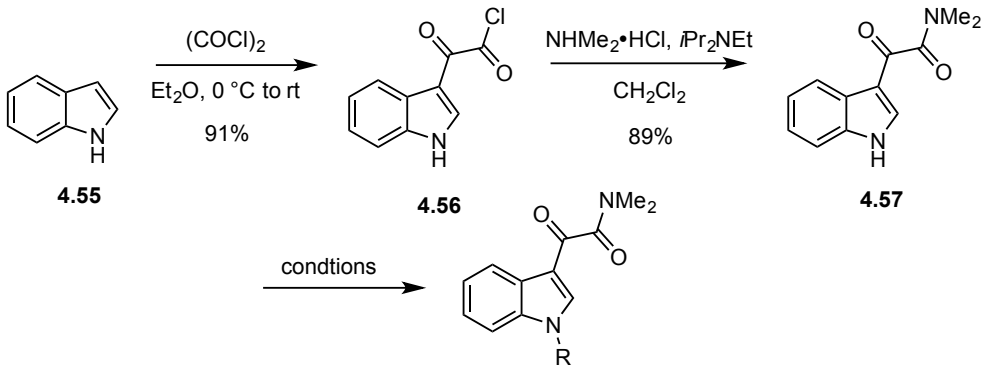


| Conditions | Compound | R | Yield (%) |
|---|---|---|---|
| NaH, TsCl, DMF | **4.58** | Ts | 50 |
| DMAP, DIPEA, NsCl, $CH_2Cl_2$ | **4.59** | Ns | 77 |
| $Boc_2O$, DMAP, $CH_2Cl_2$ | **4.60** | Boc | 82 |
| $Et_3N$, $Tf_2O$, DMAP, $CH_2Cl_2$ | **4.61** | Tf | 82 |

**Scheme 4.3:** Synthesis of indoles **4.58-4.61**.

The silyl enol ether **4.65** was prepared from commercially available crotonaldehyde (**4.62**) (**Scheme 4.4**). Addition of ethylmagnesium bromide to **4.62** provided alcohol **4.63** in 89% yield. Oxidation of **4.63** with PCC on celite then afforded enone **4.64** in 60% yield.[196] Treatment of **4.64** with $Et_3N$ and TBSOTf under the conditions reported by Yamamoto provided **4.65** in a 52% yield as an 88:12 mixture of regioisomers, which was

in agreement with the literature result.[197] Quenching the reaction after 4 h resulted in slightly elevated yield (60%) and selectivity (96:4). Thus, presumably **4.65** is the kinetically favored silyl enol ether, and after extended reaction times a slow equilibration process occurs between the regioisomeric silyl enol ethers.

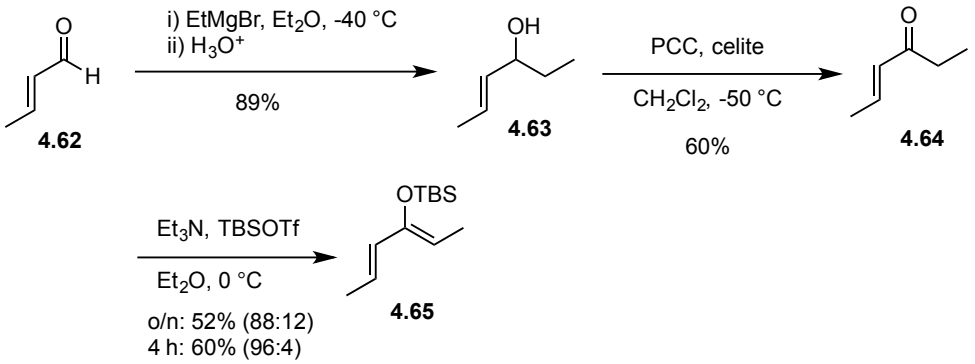


**Scheme 4.4:** Synthesis of **4.65**.

The extended reaction times reported in the literature for these types of Diels-Alder reactions under conventional oil bath heating conditions prompted us to investigate using microwave heating. Unfortunately, a number of attempts to induce the Diels-Alder reaction of **4.58** and **4.65** were unsuccessful with microwave heating (Table **4.4**). We hypothesized that, given the nature of the solvent, the reaction mixture may not be achieving the appropriate internal temperature. Nonpolar solvents such as toluene are transparent to microwave radiation, and if the reactants are not sufficiently polar, then the mixture will not adequately absorb the radiation.[198] With this in mind, we then tried adding DMF as a co-solvent; however, this also failed to induce a reaction.

**Table 4.4**: Diels-Alder reaction of **4.58** and **4.65**.

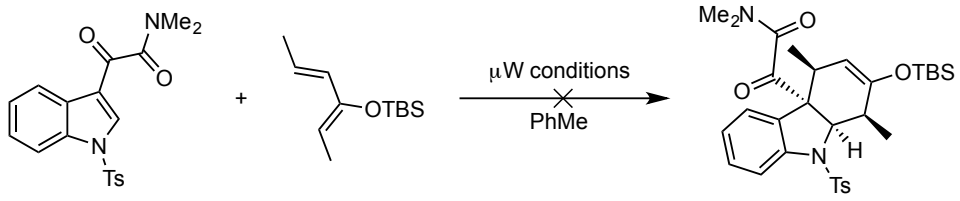


**4.58** **4.65** **4.66**

| Temperature (°C) | Power (W) | Time (h) | Result |
|---|---|---|---|
| 150 | 300 | 1 | RSM |
| 150 | 300 | 2 | RSM |
| 150 | 300 | 1 | RSM |
| 180 | 300 | 4 | RSM |
| 180[a] | 300 | 1 | RSM |
| 195 | 300 | 1 | RSM |
| 195 | 300 | 4 | RSM |

[a]Conducted using a 3:1 mixture of PhMe/DMF.

In order to increase the electrophilicity of the indole π-bond, the *N*-nosyl indole derivative **4.59** was subjected to similar conditions (Table **4.5**). As with the *N*-tosyl derivative, microwave irradiation in toluene returned only the starting materials. We then explored alternate solvent systems. For example, conducting the reaction in DMF resulted in decomposition of the starting material while NMP resulted in loss of the nosyl group to return indole **4.57**. Use of *o*-dichlorobenzene as a solvent also returned only the starting materials. We found that similar results were obtained for each of the solvents with conventional heating methods. After extending the reaction time to 120 h in several solvents, not even a trace of cycloaddition product was observed by $^1$H NMR or LCMS.

**Table 4.5**: Thermal and microwave Diels-Alder reactions of **4.59** and **4.65**.

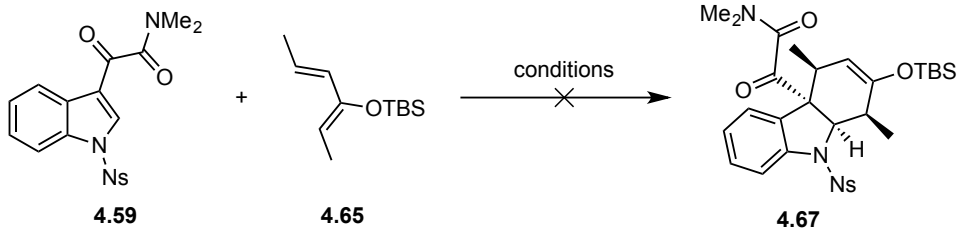


**4.59** **4.65** **4.67**

| Temperature (°C) | Conditions | Time (h) | Result |
|---|---|---|---|
| PhMe | 180 °C, 300 W | 2 | RSM |
| DMF | 180 °C, 300 W | 2 | decomp |
| NMP | 180 °C, 300 W | 2 | -Ns group |
| *o*-dichlorobenzene | 180 °C, 300 W | 1 | RSM |
| DMF | 180 °C | 48 | decomp |
| NMP | 200 °C | 48 | -Ns group |
| PhMe | 200 °C | 120 | RSM |
| *o*-dichlorobenzene | 200 °C | 120 | RSM |

We then began to explore tactics that would accelerate the reaction. Water has been shown to greatly accelerate the rates of some Diels-Alder reactions.[199] As mentioned previously, the Diels-Alder reaction has a negative volume of activation, so conditions such as high pressure that force reactants together enhance the rate of Diels-Alder reactions (see section **4.2.1**). When water is used as the solvent for Diels-Alder reactions, the hydrophobic effect can be exploited to the same end. In the initial report, Breslow showed that the rate of the Diels-Alder reaction between cyclopentadiene and butenone is accelerated 740-fold in water relative to 2,2,4-trimethylpentane.[200] When LiCl was added to further amplify the hydrophobic effect, an additional threefold acceleration was observed relative to water alone. Since then, numerous examples have been published using water as a solvent to enhance reaction rates of Diels-Alder reactions, particularly with very hydrophobic molecules such as aromatic compounds.[199]

When we used water as the solvent, both the indole and the diene were completely insoluble, even at elevated temperatures, and unfortunately when the biphasic mixture was heated, only decomposition was observed (Table **4.6**). We then tried ethylene glycol as a solvent, which can encapsulate hydrophobic molecules through a similar hydrogen bonding network as water while providing a higher degree of solubility. Unfortunately, this also resulted in decomposition of the starting materials under the reaction conditions. Running the reaction without any solvent also led decomposition of the starting material.

**Table 4.6**: Thermal Diels-Alder reactions of **4.59** and **4.65**.

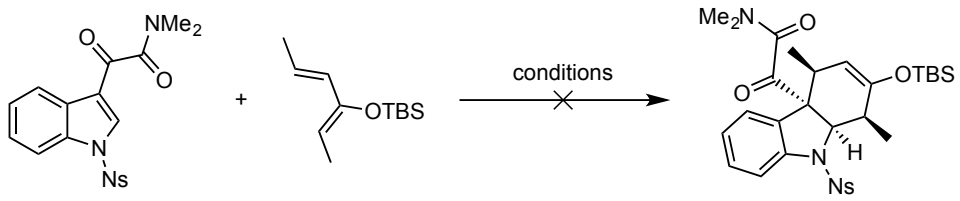


**4.59** **4.65** **4.67**

| Temperature (°C) | Conditions | Time (h) | Result |
|---|---|---|---|
| $H_2O$ | 200 °C | 120 | RSM |
| neat | 200 °C | 120 | decomp |
| ethylene glycol | 200 °C | 120 | decomp |

We next explored the effects of Lewis acid catalysis on the reaction of **4.59** and **4.65** (**Table 4.7**). [201,202] Use of $AlCl_3$ returned only the starting materials after 24 h, whereas $Cu(OTf)_2$, TMSOTf, and $ZnCl_2$ returned unreacted indole and desilylated diene.

**Table 4.7**: Lewis-Acid catalyzed Diels-Alder reactions of **4.59** and **4.65**.

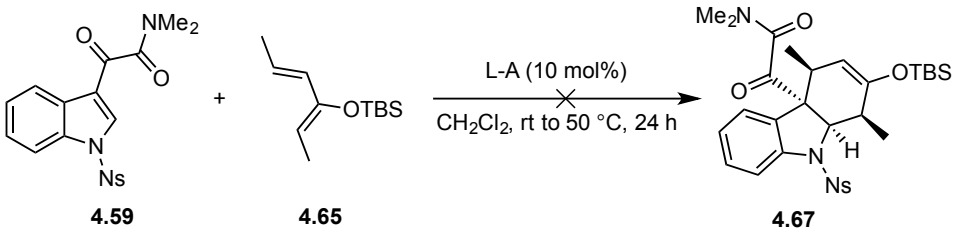


**4.59** **4.65** **4.67**

| L-A | Result |
|---|---|
| $AlCl_3$ | RSM |
| $Cu(OTf)_2$ | RSM (indole) |
| TMSOTf | RSM (indole) |
| $ZnCl_2$ | RSM (indole) |

Based upon these failures, it appears that the *N*-nosyl indole glyoxamide derivative **4.59** was not sufficiently activated to react with **4.65** at normal pressure. We believed that the nosyl group was the most electron-withdrawing indole substituent of the derivatives **4.58**-**4.61**, as the C2 proton of the indole was the most deshielded in the $^1$H NMR spectra. We did not have the necessary apparatus to conduct the reaction under high pressure and felt the procedure would not be amenable to the scale necessary for such an early step in the total synthesis. Thus, in a last-ditch effort to conduct the Diels-Alder cyclization we focused on utilizing a more electron-rich diene. However, the reaction of **4.59** with Danishefsky's diene (**4.37**), which was synthesized according to literature procedures[203] provided only an intractable mixture of unidentifiable products (eq. 4.14).

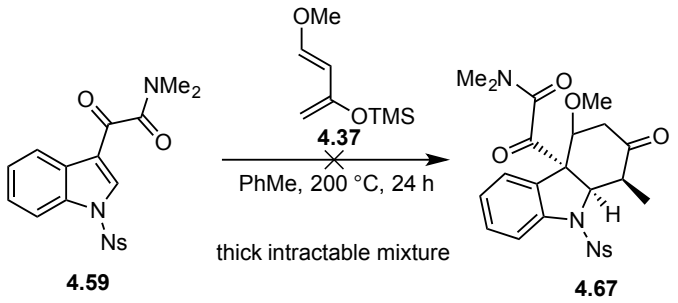


(4.14)

$Et_3N$ was added to prevent acid-catalyzed polymerization of **4.37**, but no Diels-Alder reaction was observed after 72 hours of heating (eq. 4.15).

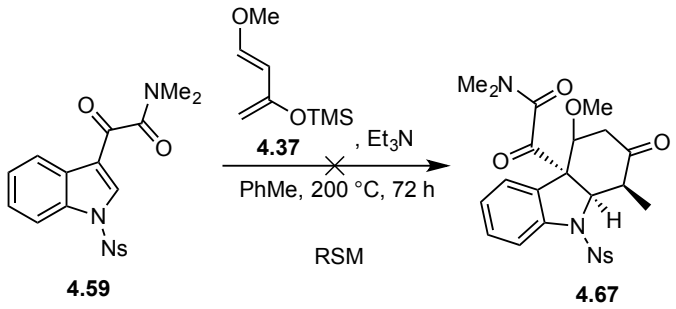


(4.15)

In summary, a number of Diels-Alder reactions were attempted in order to induce cyclization of indole-3-glyoxamides and diene **4.65**. Conventional heating conditions and microwave irradiation failed to induce the desired reaction. Varying the solvent resulted in either return of the unreacted starting materials, decomposition of the reaction mixture, or loss of the protecting group on the indole nitrogen atom. Efforts to accelerate the rate of the Diels-Alder reaction involving hydrophobic effects and Lewis acid catalysis also did not result in the desired cycloaddition. Without the ability to attempt the reaction under high pressure, we decided that alternate method to produce the desired tricyclic scaffold must be developed.

## 4.3 Second Generation Approach

With the failure to accomplish a concerted cycloaddition, we considered a stepwise approach to formation of a key tricyclic intermediate. We focused on a sequence involving addition of a tryptamine derivative **4.69** into enone **4.64** in order to generate an intermediate indolenine **4.70** (**Scheme 4.5**). This indolenine could then be captured by either the enol tautomer of the ketone or the enolate, depending on the reaction conditions, to give the desired tricyclic scaffold **4.70**. Using known tryptamine derivatives, **4.68** could be converted to **4.6** in the same number of steps as the first-generation approach.

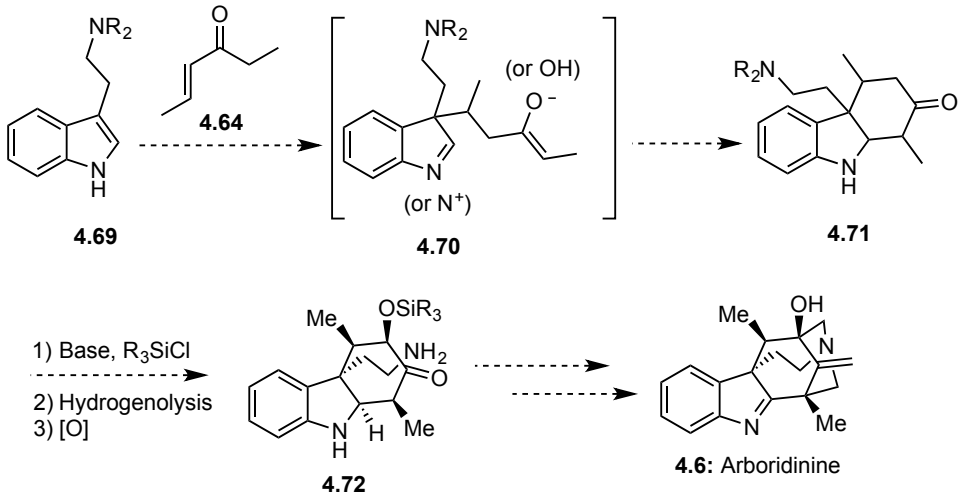


**Scheme 4.5:** Revised synthesis of **4.6**.

### 4.3.1 Substitution Reactions Involving 3-Substituted Indoles

Because they are electron-rich heterocycles, indoles serve as excellent nucleophiles in electrophilic aromatic substitution (EAS) reactions to give 3-substitued indoles.[204] Indoles already bearing substituents at the 3-position can also serve as nucleophiles in substitution reactions to give 3,3-substituted indolenines. However, these indolenines are unstable, and under acidic conditions they undergo rearomatization by 1,2-rearrangement

to give 2,3-substitued indoles.[205] This is perhaps most well-known in the case of spirocyclic indolenines, as exemplified by the famous Pictet-Spengler reaction (Figure **4.3**).[206]

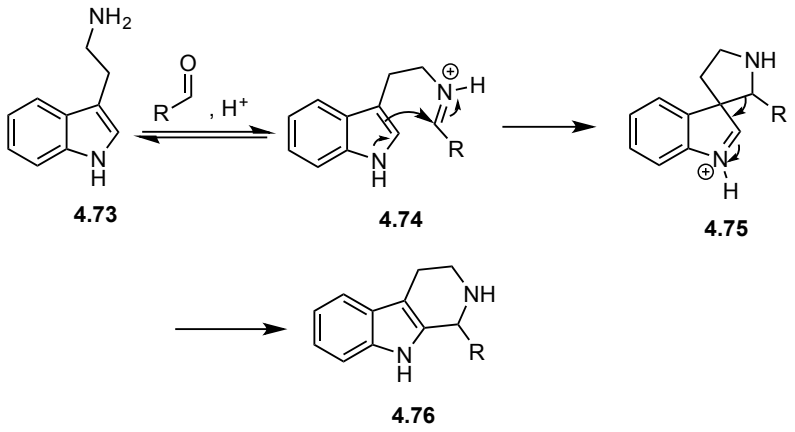


**Figure 4.3:** Mechanism of the Pictet-Spengler reaction.

Using a pendant nucleophile to trap a 3,3-disubstituted indolenine that is generated *in situ* is a strategy that has been widely employed to form complex polycyclic scaffolds in natural product synthesis. Danishefsky showed that when treated with *N*-phenylselenophthalimide (N-PSP), bis(Boc)tryptophan methyl ester **4.77** will undergo electrophilic addition to the double bond (Eq. 4.16).[207] The resulting *N*-acyl iminium ion is then intercepted by the *N*-methyl carbamate to give the pyrroloindoline scaffold **4.78**. This transformation was the first step in the total synthesis of amauromine.

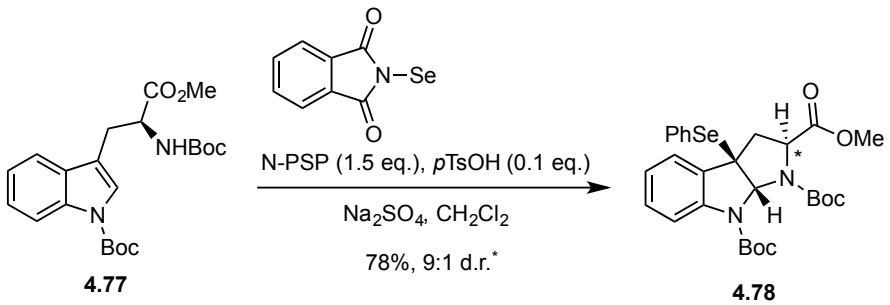


(4.16)

In Corey's synthesis of aspidophytine (**4.84**), the tryptamine derivative **4.79** was condensed with dialdehyde **4.80** to give the iminium ion **4.81**, which was attacked by the indole resulting in indolenine **4.81** (Figure **4.4**). This indolenine was then captured by the allylsilane to give **4.83**, which was further elaborated to aspidophytine (**4.84**).[208]

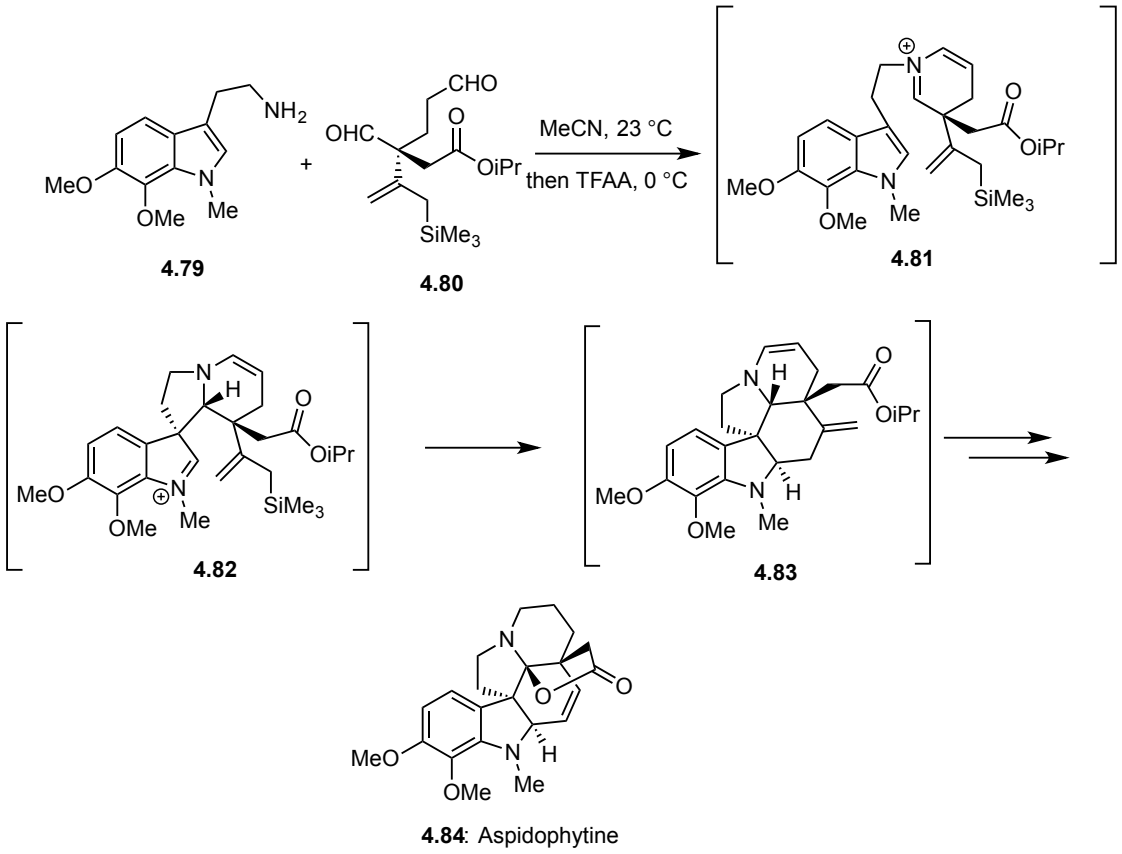


**Figure 4.4:** Polycyclization cascade in Corey's synthesis of aspidophytine.

Under acidic and Lewis acidic conditions, or if the indole nitrogen atom is substituted, the intermediate indolenine exists as a highly reactive iminium ion and thus is immediately trapped; however, under milder conditions it is possible to isolate the 3,3-disubstituted indolenine. These compounds can then be reacted with external nucleophiles to form 2,3,3-trisubstituted indolines, although this methodology is relatively uncommon.

Cheng and Tian reported that the spirocyclic indolenine **4.83** could be reacted with ketone **4.84** under proline catalysis to generate the indole **4.85** in 85% yield and 99% ee (eq. 4.17).[209]

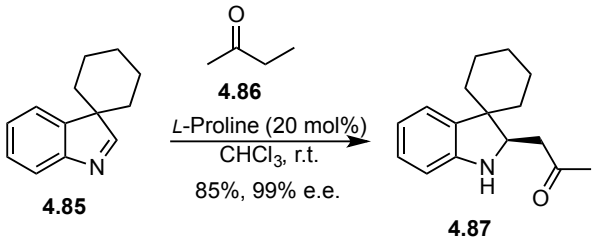


(4.17)

A similar result was reported by Dhankher *et al*.[210] Following a bis-allylation of indoles **4.88** to give 3,3-substituted indolenines **4.89** (Scheme **4.6**), an equivalent of acetone was added into the imine **4.89** under proline catalysis to give trisubstituted indolines **4.90a-c** in good yield and enantioselectivity. Additions of nitriles[211] and indoles[212] to these types of electrophiles under specialized conditions have also been reported.

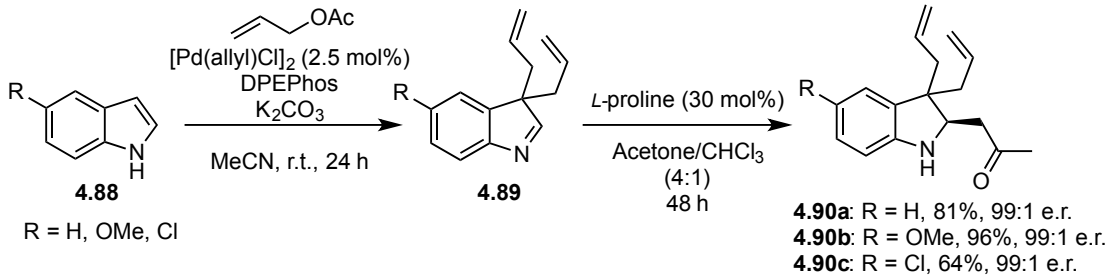


**Scheme 4.6:** Asymmetric Mannich reaction of 3,3-diallylindolenines **4.90a-c**.

### 4.3.2 3-Substituted Indoles as Nucleophiles in Conjugate Additions

3-Substituted indoles can also act as nucleophiles in conjugate additions into α,β-unsaturated aldehydes and ketones. A report by Garnick et al. showed that under strongly acidic conditions, *N*-methylskatole (**4.92**) can undergo a conjugate addition onto mesityl

oxide (**4.93**), and subsequent cyclization to give **4.95** in 60% yield (eq. 4.18).[213] However, the substrate scope reported in this study was limited to only 3-methyl indoles, and reaction with the unsubstituted skatole (**4.91**) resulted in complex mixtures of *C*- and *N*-alkylation.

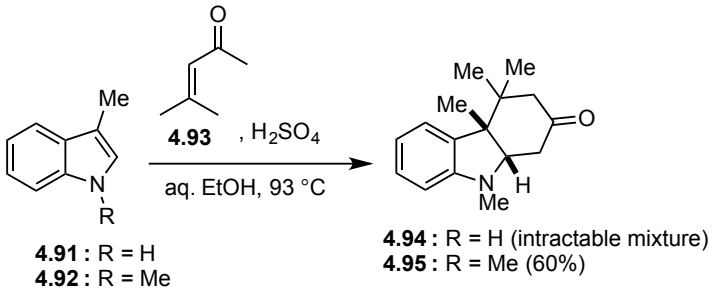


(4.18)

Conjugate additions of 3-substituted indoles into α,β-unsaturated aldehydes can be accomplished via organocatalysis. For example, Macmillan reported an imidazolinone **4.98** that efficiently catalyzes the conjugate additions and subsequent cyclizations of tryptamine derivatives **4.96** onto aldehydes **4.97** (eq. 4.19).[214] However, no reports were made on the utility of this catalyst with regard to ketones. As seen previously, the intermediate iminium ion (not shown) is captured by the carbamate to give pyrroloindoline **4.98**.

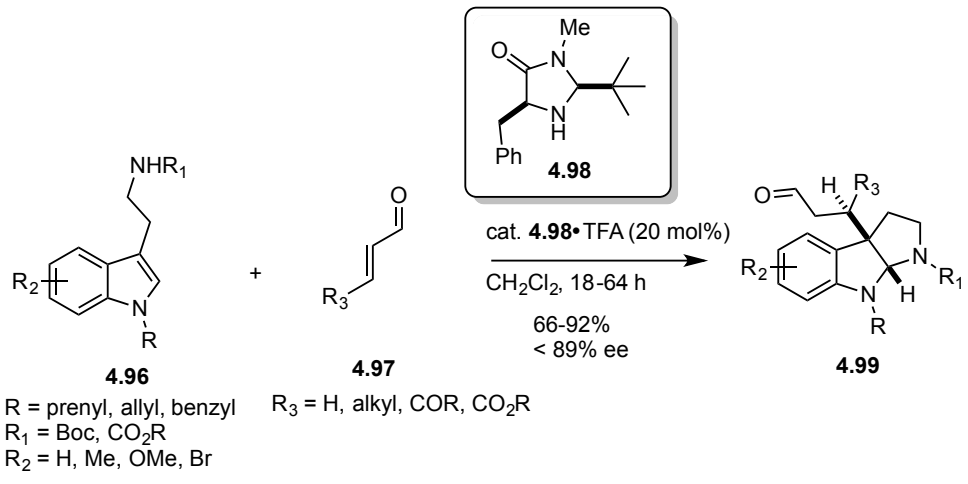


(4.19)

A similar tricyclic structure was synthesized via a conjugate addition/cyclization strategy under Lewis acid-mediated conditions by Piersanti en route to the total synthesis of esermethole (**4.103**) (Scheme **4.7**).[215] Following conjugate addition of indole **4.100** into the α,β-dehydroamino ester **4.101**, the intermediate *N*-methyl iminium ion was trapped by the carbamate group to give **4.102**. Depending on substituents on the indole ring, diastereomeric ratios ranging from 3:1 to 9:1 were reported, with the major diastereomer as exemplified by **4.102**.

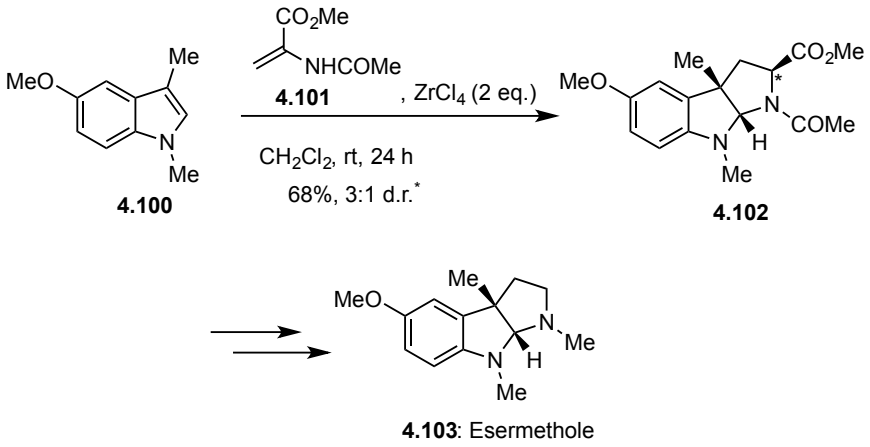


**Scheme 4.7:** Cyclization in the Piersanti synthesis of Esermethole.

Recently, intramolecular addition/cyclization sequences have been employed to rapidly assemble more complex polycyclic structures from simple starting materials. Cai *et al*. reported an intramolecular Michael/Mannich cascade reaction of **4.104** to form the tetracycle **4.106**, a scaffold present in several classes of natural products (eq. 4.20).[216] Screening of various chiral primary amine catalysts revealed that 9-amino-9-deoxyepiquinine (**4.105**) (20 mol %) used in tandem with 2-nitrobenzoic acid (40 mol %) catalyzed the desired polycyclization in high yield and enantioselectivity.

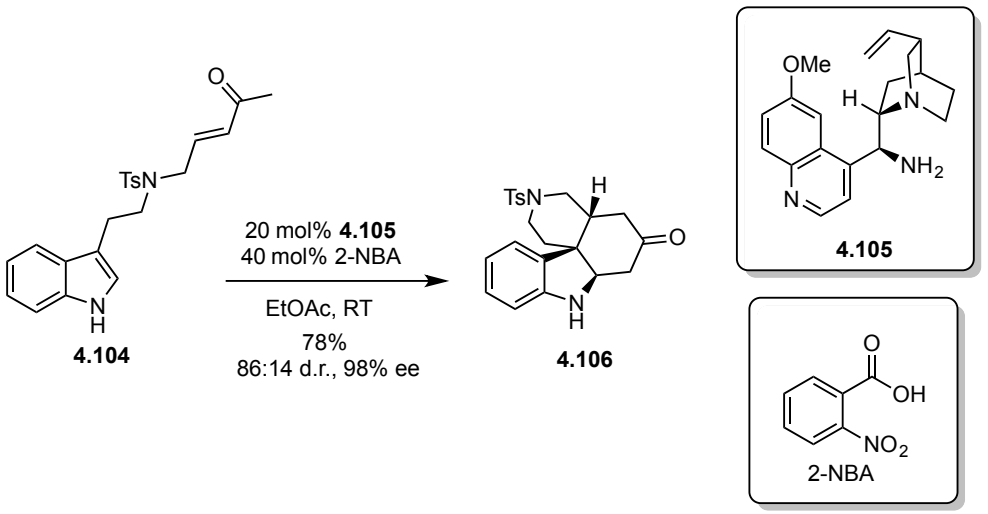


(4.20)

Zhang *et al*. showed that cyclization can occur under acidic conditions.[217] Coupling of tryptamine (**4.73**) with the carboxylic acid **4.107** provided adduct **4.108** in 95% yield (**Scheme 4.8**). The Michael/Mannich reaction of **4.108** proceeded smoothly under acidic conditions to give the tetracycle **4.109**, that was then transformed to the amide **4.110** and subsequently hydrolyzed to give **4.111**. Elaboration of **4.114** led to tetracycle **4.112**, which comprises the core structure of complex *Vinca* indole alkaloids.

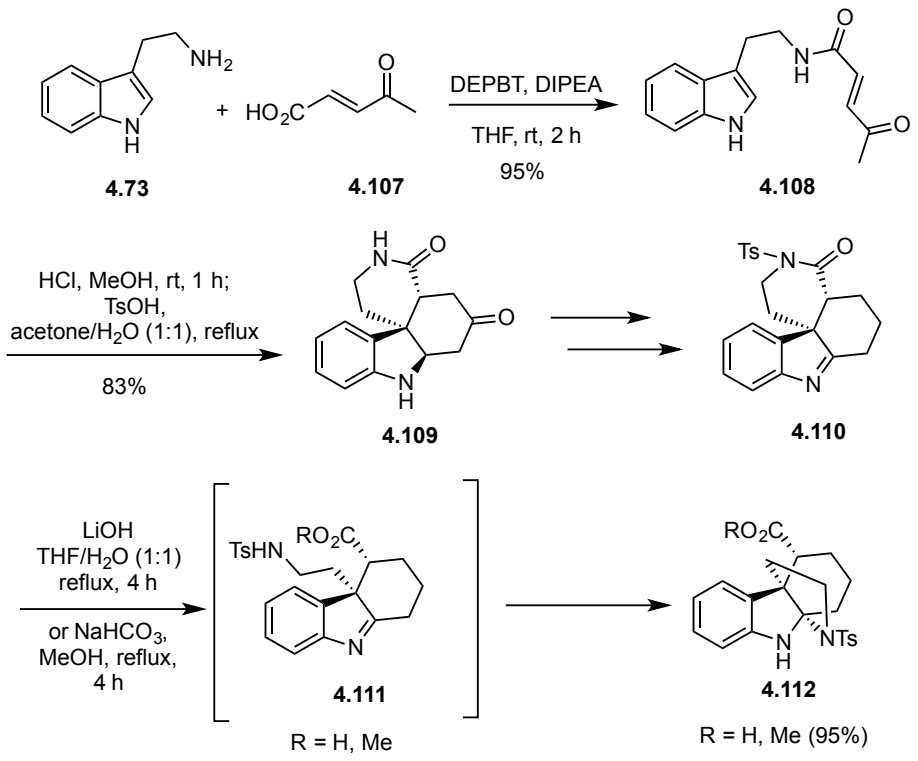


**Scheme 4.8:** Polycyclization cascade in the synthesis of the vincorine core **4.112**.

Recent reports also suggest that these intramolecular cascades can be accomplished under basic conditions. In an effort to develop an expedient route toward the core of the manzamine-type alkaloids, Markó showed that substituted gramines **4.113** may be treated with a base such as KOtBu to induce an anionic polycyclization cascade resulting in tetracycle **4.114** in moderate yield (Eq. 4.21).[218] In all reported examples, the tetracycle was isolated as a single diastereomer with a *trans*-fusion at the A/B ring junction (manzamine ring nomenclature).

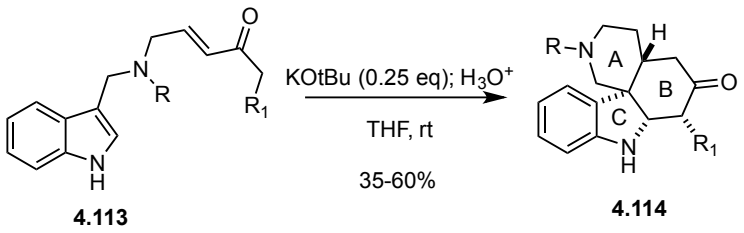


(4.21)

In a subsequent report, Markó attempted to exploit this methodology in the synthesis of Büchi's ketone (**4.125**).[219] Condensation of *N*-benzyl tryptamine (**4.115**) with 3-butyn-2-one afforded adduct **4.116** in 98% yield (eq. 4.22). Unfortunately, **4.116** failed to cyclize under a variety of conditions, including Brønsted bases and combinations of Brønsted bases with Lewis acids.

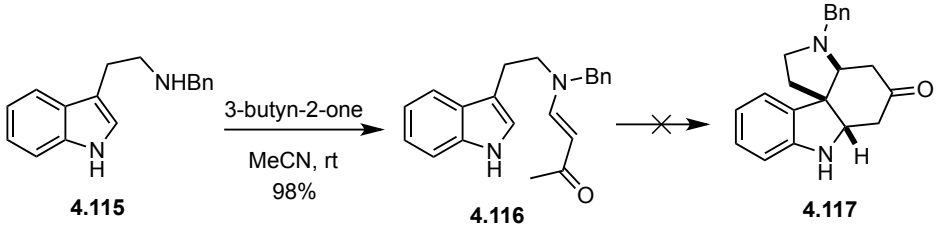


(4.22)

In order to increase the electrophilicity of the Michael acceptor, a carbonyl group was introduced between the nitrogen atom and the enone. When **4.118** was subjected to anionic polycyclization cascade conditions similar to those previously reported,[218] tetracycle **4.119** was isolated in 14% yield from **4.115**, along with numerous unidentified side products (Scheme **4.9**) . When **4.122** was treated with silica gel overnight in $CH_2Cl_2$, the spirocyclic indolenine **4.120** was isolated in 79% yield over two steps. Treatment of this intermediate with KO*t*Bu furnished **4.119** in 85% yield.

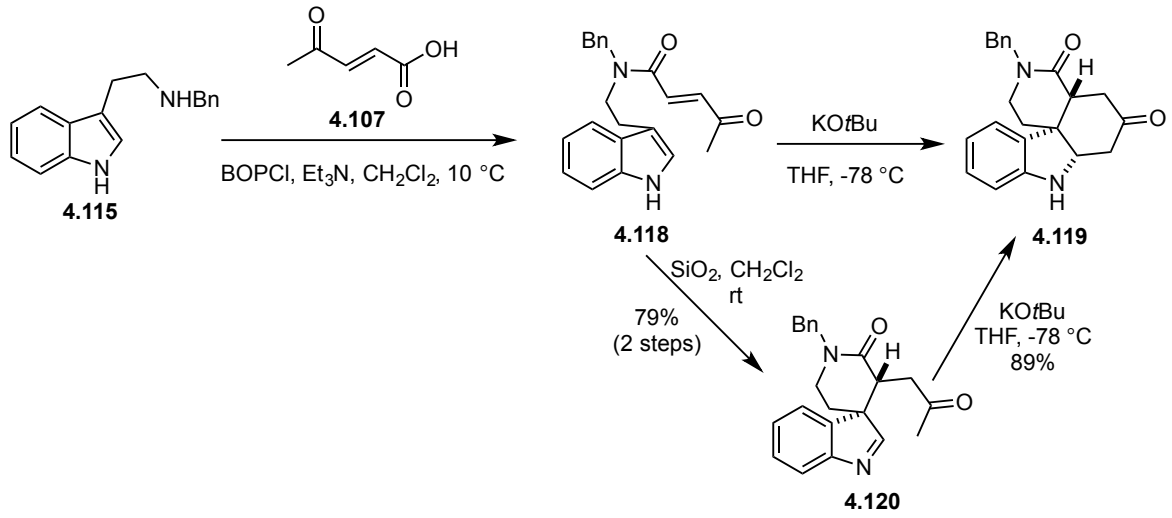


**Scheme 4.9:** Polycyclization cascade in the synthesis of **4.123**.

The introduction of the carbonyl group allowed for hydrolysis of the amide moiety to form tricycle **4.123** (**Scheme 4.10**). A decarboxylation/conjugate addition process then formed the pyrrolidine ring of **4.124**, which was then converted to **4.125** in two additional steps.

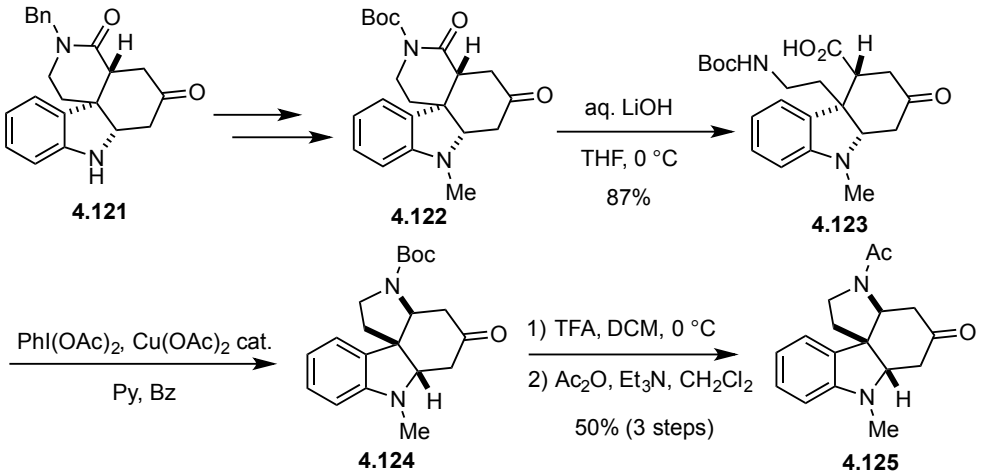


**Scheme 4.10:** Synthesis of Büchi's ketone **4.125**.

In summary, these reports collectively show that 3-substitued indoles can be used as nucleophiles in addition/cyclization cascades that can efficiently build complex polycyclic structures. [208,217,220] Under acidic and Lewis acidic conditions, or if the indole nitrogen atom is substituted prior to the reaction, the resulting iminium ion is prone to capture by nucleophiles.[207,208,213,215,217,218] For example, carbamates often serve as nucleophiles in this fashion to form pyrroloindoline scaffolds. [207,214,215] With careful choice of conditions, the indolenine can be isolated and reacted with exogenous nucleophiles to form diverse 2,3,3-trisubstituted indole scaffolds. [209,210]

### 4.3.3 Conjugate Addition/Cyclization Strategy for the Total Synthesis of Arboridinine

Since the anionic conjugate addition/cyclization cascade sequence reported by Markó represented the closest literature precedent for the transformation we needed,[218] we set out to attempt a conjugate addition/cyclization cascade utilizing a tryptamine derivative **4.126** and enone **4.64** under basic conditions. We also envisioned the possibility of using the known α,β-epoxyketone **3.127** as the electrophile to install the necessary α-hydroxyketone moiety without the need for a separate oxidation step (eq. 4.23).

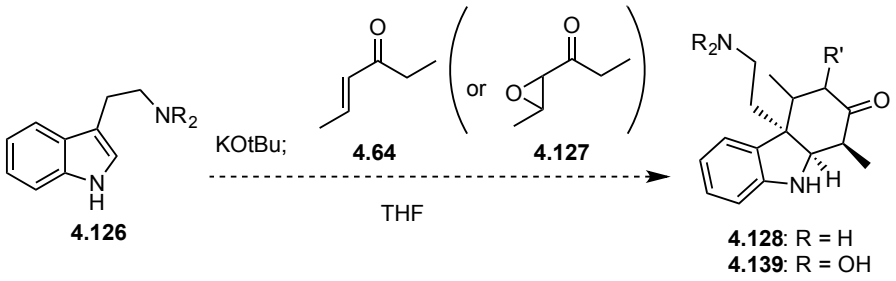


(4.23)

Although the most efficient route for the total synthesis in terms of overall step count would be to use tryptamine (**4.73**) as the indole derivative, we decided to protect the

amine side chain to prevent side reactions where the amine might act as a nucleophile into the enone (eq. 4.24).

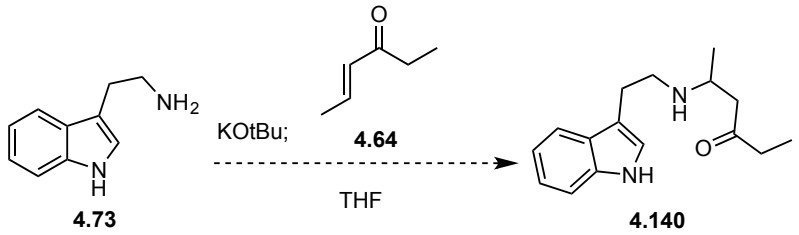


(4.24)

Although a pendant carbamate nitrogen had been shown in the literature to act as a nucleophile and add into the intermediate iminium ion when this reaction was conducted under acidic and Lewis acidic conditions,[207,214,215] we speculated that since the imine would be less reactive than the iminium ion this would be less likely to occur (eq. 4.25). Rather, we believed that the enolate would be able to capture the imine as had been observed by Markó.[218,219]

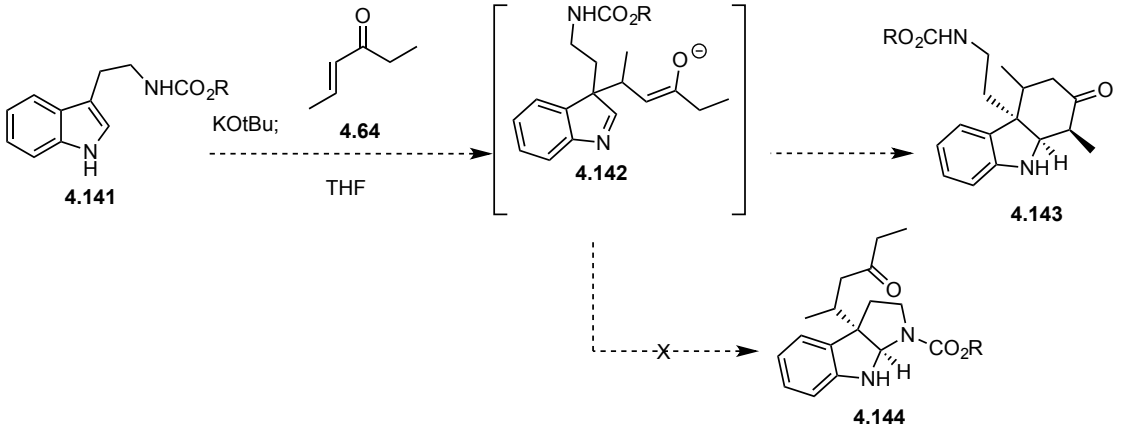


(4.25)

### 4.3.4 Attempted Conjugate Additions

To commence this version of the synthesis, tryptamine (**4.73**) was protected with Boc anhydride to give **4.145** in 82% yield (eq. 4.26).[221]

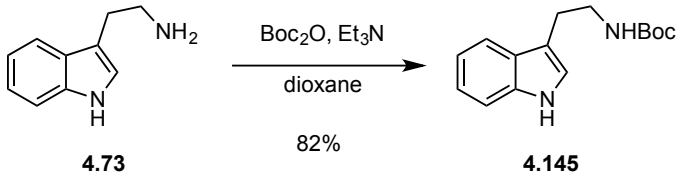


(4.26)

We first screened a variety of bases, however no reaction was observed between Boc-tryptamine (**4.145**) and enone **4.64** (eq. 4.27). Conditions identical to those reported by Markó returned the unreacted starting materials. We then tried gradually increasing the equivalents of KO*t*Bu, but only the starting materials were isolated from the reaction mixture. It was noted that on treatment of **4.145** with lithium bases, the lithium salt of the indole anion simply precipitated. Elevating the temperature with either KH or KO*t*Bu as the base resulted in consumption of the enone by TLC; however, only the returned boc-tryptamine was isolated following workup. We thought that the consumption of the enone could have been due to a polymerization of the enone, but no indication of the formation of this product was observed by $^{1}$H NMR or LCMS.

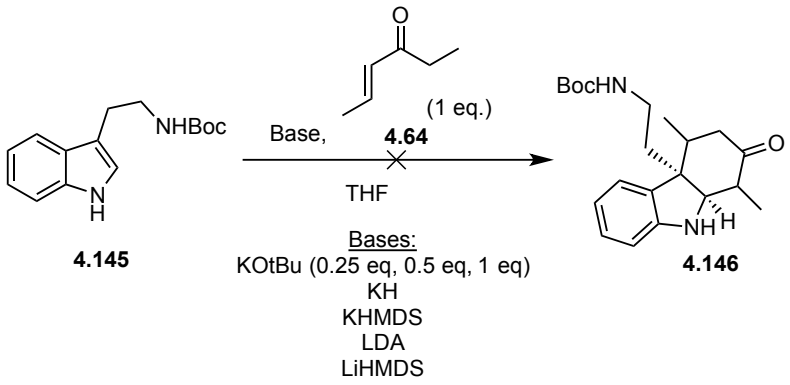


(4.27)

We next screened a variety of solvents in an attempt to induce a reaction. Unfortunately, only returned starting material was observed (Equation 4.28).

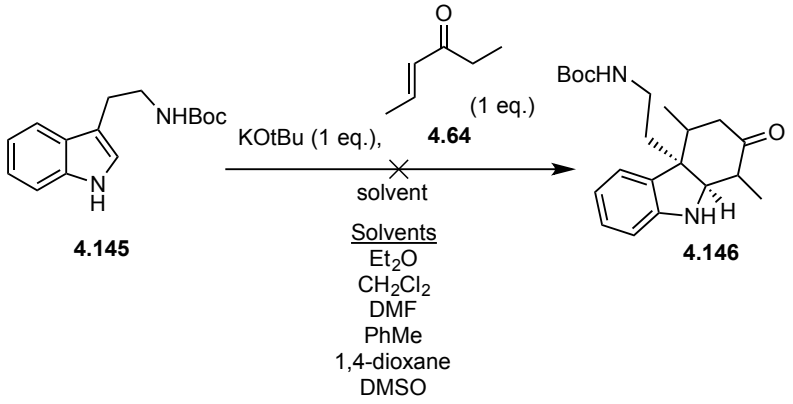


(4.28)

We then decided to switch from a Boc-protected amine to a Cbz-protected amine, as a CBz group would allow us to explore acidic conditions under which the Boc group would be unstable. Cbz-protection of **4.73** afforded **4.147** in 72% yield (eq. 4.29). Treatment of **4.147** with LiHMDS also resulted in precipitation, while use of potassium bases gave no reaction.

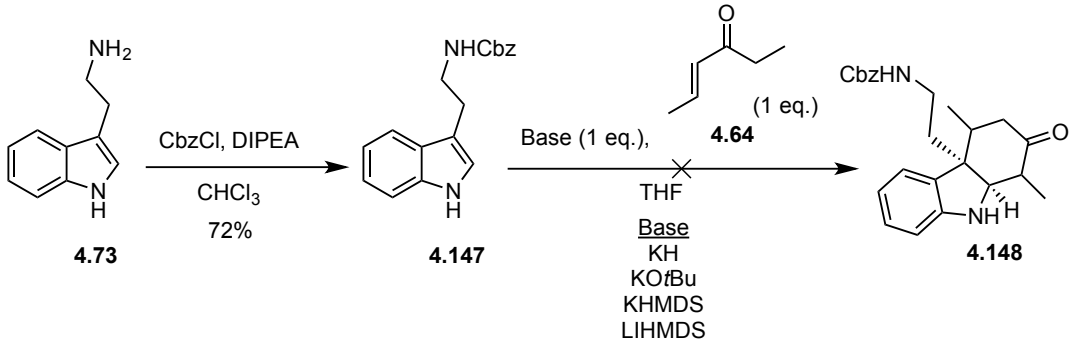


(4.29)

We then attempted to enhance the nucleophilicity of the indole ring. For example, Lin *et al*. reported that addition of triethylborane facilitates the alkylation of 2,3-disubstituted indoles to form quaternary indolenines (eq. 4.30). They proposed that the

coordination of the triethylborane to the indole nitrogen aom enhances the π-nucleophilicity of the resulting anion and drives alkylation to the 3-position.

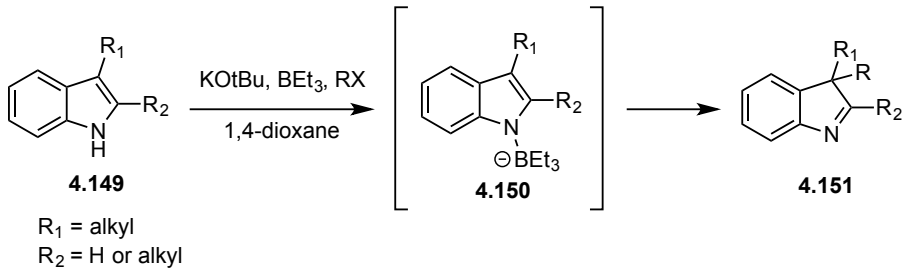


(4.30)

Unfortunately, when we subjected indoles **4.145** and **4.147** to these conditions with enone **4.64**, no reaction was observed (eq. 4.31).

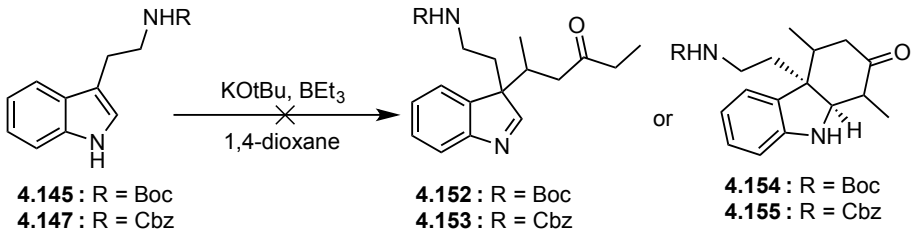


(4.31)

We next decided to explore using an α,β-epoxyketone as an electrophile. Oxidation of **4.64** with *tert*-butyl hydroperoxide and KF/alumina provided epoxyketone **4.156** in 78% yield (Equation 4.32).[222] Unfortunately, the epoxyketone was completely unreactive toward **4.145** and **4.147** under a variety of conditions (eq. 4.33)

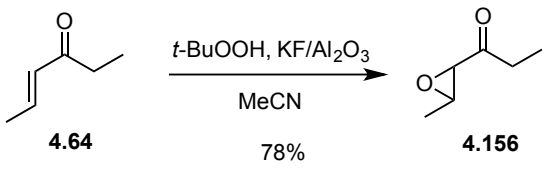


(4.32)

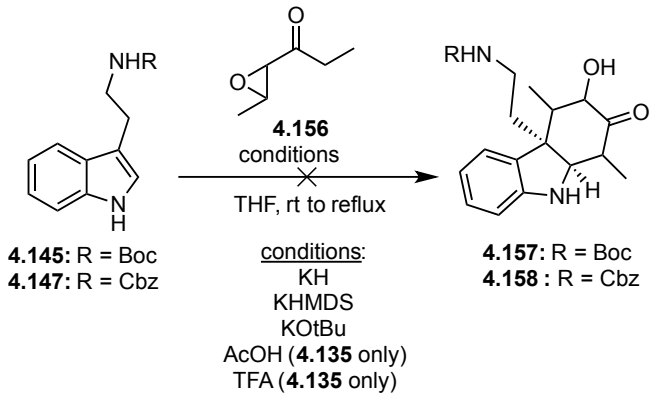


(4.30)

Following our inability to unite tryptamine derivatives with either enone **4.64** or epoxyketone **4.156**, we speculated two reasons for the failures: either **4.64** and **4.156** were not sufficiently electrophilic to react with the indole anion under the reaction conditions, or the indole anion was not being formed. Although the the $pK_a$ value of indole (~21) is lower than that of a typical secondary carbamate (~24), the presence of an inductively donating alkyl group at the 3 position of the indole ring should increase the $pK_a$ of the indole such that the $pK_a$ values could be comparable. If the carbamate nitrogen is deprototonated first, then subsequent deprotonation of the indole would not occur due to formation of an unstable dianion. Nearly all of the analogous addition/cyclization reactions in the literature utilized tertiary carbamates. The cyclization reported by Zhang *et al.* involved a secondary carbamate; however, this was conducted under acidic conditions.[217] We knew that this would not be an option in our case since under acidic conditions, the carbamate nitrogen atom would close down on the intermediate iminium ion and form the corresponding pyrroloindoline as has been shown previously in other systems. [207,214,215]

We then considered an indole-3-glyoxamide as a nucleophile in order to eliminate the problem of potential competing deprotonations. The electron-withdrawing carbonyl group at the C3-position of the indole ring should increase the acidity of the indole nitrogen

atom. Furthermore, use of a glyoxamide substituent at C3 would open up the possibility of exploring acidic conditions, as the ketoamide should not be able to act as a nucleophile and add into the intermediate iminium ion in the way that carbamates do to form pyrrloloindolines (see section **4.3.1**). We sought to use the *N*,*N*-dibenzyl glyoxamide **4.159** for this purpose (eq. 4.31).

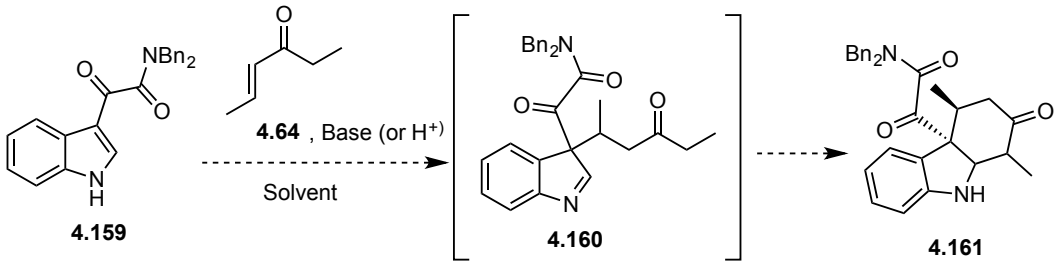


(4.31)

Indole derivative **4.56**, which was prepared previously by treatment of indole (**4.55**) with oxalyl chloride (see **Scheme 4.3**), was treated with dibenzyl amine to give **4.159** in 75% yield (eq. 4.32).

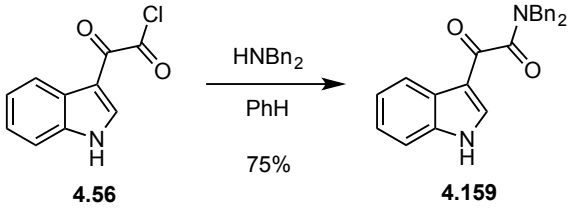


(4.32)

Indole **4.159** was then subjected to reactions with **4.64** analogous to those of the tryptamine derivatives **4.145** and **4.147** (Table **4.9**). Use of KH or KO*t*Bu as the base returned starting materials in both THF and MeCN, as did using several other solvents. However, the combination of KHMDS in THF led to the formation of the conjugate

addition adduct **1.160** in 48% yield. After optimization, we found that 1.2 equivalents of KHMDS and five equivalents of **4.64** generated **4.160** in 70% yield.

**Table 4.8**: Attempted Michael addition/cyclization reaction of **4.159** and **4.64**.

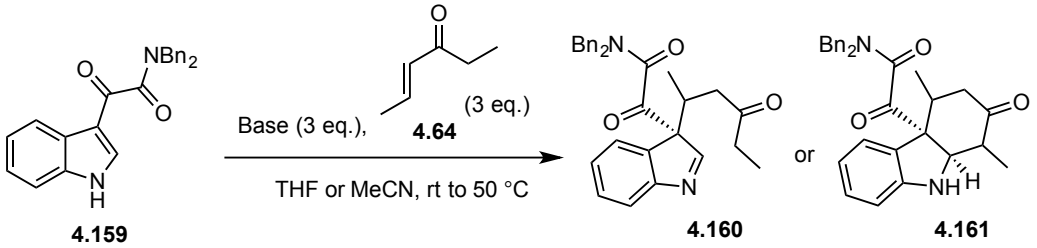


**4.159** **4.160** **4.161**

| Base | Solvent | Result |
|---|---|---|
| KH | THF | RSM |
| KH | MeCN | RSM |
| KOtBu | THF | RSM |
| KOtBu | MeCN | RSM |
| KHMDS | MeCN | RSM |
| KHMDS | PhMe | RSM |
| KHMDS | DMF | RSM |
| KHMDS | 1,4-dioxane | RSM |
| KHMDS | $CH_2Cl_2$ | RSM |
| KHMDS | THF | **4.160** (57%) |
| **KHMDS (1.2 eq)** | **THF** | **4.160 (70%)** |

With this exciting result in hand, we sought to identify methods to close the cyclohexanone ring and form the tricyclic compound **4.161** (Table **4.9**). We first attempted a L-proline-catalyzed ring closure similar to that reported by Cheng, [209] but these conditions returned starting material, even after multiple days of heating. Treatment of **4.160** with pyrrolidine surprisingly led to a 92:8 mixture of starting material and indole **4.159** after 24 h, presumable from a retro-Michael reaction. Addition of TFA shut down this degradation pathway, but cyclization of **4.160** was not observed. Use of a stronger base, such as KOtBu

completely consumed **4.160**, but again only the reto-Michael reaction was observed. Apparently, equilibration of the enolates eventually funneled the reaction to the enolate that undergoes a retro-Michael reaction. We then tried to use a stronger base, hoping that there would be a kinetic preference for the α-proton of the ethyl group that would lead to ring closure. We were disappointed to find that using LiTMP as the base, we obtained a 1:1 mixture of returned **4.160** and **4.159**. This suggested to us that there is no kinetic preference for the site of deprotonation.

**Table 4.9**: Attempted cyclization reaction of **4.160** (basic conditions).

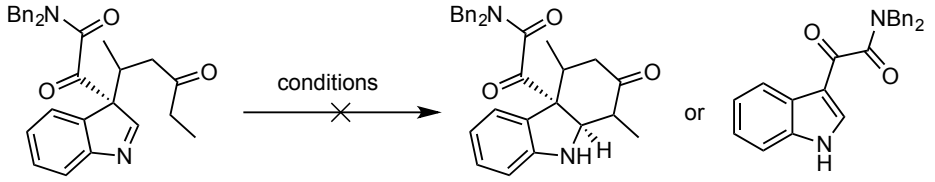


**4.160** **4.161** **4.159**

| Conditions | Solvent | Result |
|---|---|---|
| L-proline (20 mol%) | $CHCl_3$, rt to reflux | RSM |
| Pyrrolidine | THF, rt to reflux | RSM + **4.159** (92:8) |
| Pyrrolidine/TFA | THF | RSM |
| KOtBu | THF | **4.159** (80%) |
| LiTMP | THF | RSM + **4.159** (1:1) |

Based on the results obtained with LiTMP as the base, we speculated that the imine of **4.160** was not sufficiently reactive for ring closure to occur under basic conditions, so we examined reaction acidic conditions (eq. 4.33). Treatment of **4.160** with AcOH only returned starting material. Stronger acids such as TFA, HCl, or, as well as switching to toluene to achieve higher reaction temperatures all failed to induce a reaction.

.

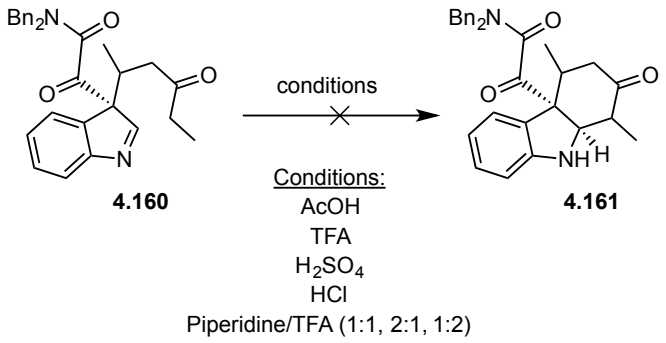


(4.33)

## 4.4 SUMMARY

Several concise, seven step syntheses of the pentacyclic indole alkaloid (±)-arboridinine were designed. The first approach featured the novel Diels-Alder cycloaddition of an indole-3-glyoxamide and a diene to form a key tricyclic intermediate, from which the final two rings would be installed via a double Mannich reaction. This approach was chosen because the stereospecific nature of the Diels-Alder reaction would allow for construction of three of the four stereocenters in a single step. We investigated a variety of conventional heating and microwave conditions were investigated to induce a cycloaddition, but unfortunately no reaction was observed, showcasing the difficulty to induce normal-demand Diels Alder reactions of indoles under normal pressure. Changing the protecting group on the indole nitrogen atom in order to make the dienophile more electrophilic and swapping the original diene **4.65** for the more electron-rich Danishefsky's diene (**4.37**) also failed to induce a reaction.

We investigated the possibility of inducing a conjugate addition/cyclization cascade to convert carbamates **4.145** and **4.147** into tricyclic indolines **4.157** and **4.158**, respectively. When no reaction was observed, the carbamates were replaced with indole-3-glyoxamides in order to increase the acidity of the indole proton prevent any issues with competing deprotonation of the carbamate. Upon reacting the *N,N*-dibenzyl glyoxamide **4.159** with enone **4.64**, the conjugate addition product **4.160** was isolated in 70% yield.

This represents the first report of an indole-3-glyoxamide as a nucleophile in a Michael addition. We found that the resulting 3,3-disubstituted indolenine was unreactive to ring closure under acidic conditions, and under basic conditions, a retro-Michael reaction was observed, to return the indole glyoxamide **4.159**. Without a straightforward method to remove this carbonyl group while preserving the integrity of other sensitive functionalities on the molecule, alternative strategies for formation of the key tricyclic intermediate need to be explored.

### 4.5 FUTURE DIRECTIONS

The conjugate addition product **4.160** proved to be remarkably stable to acid and labile under basic conditions. We speculated that this retro-Michael reaction would be difficult to stop with a carbonyl group at the C3 position of the indolenine, as the resonance-stability of the anion of **4.159** facilitates departure in the retro-Michael reaction (eq. 4.34).

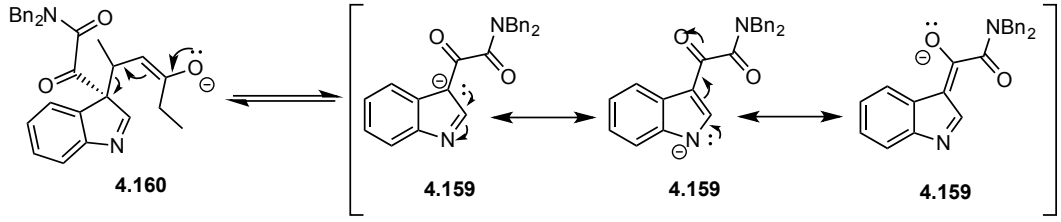


(4.34)

We felt that removal of the ketoamide group should stop this reaction; however, reductive conditions would also reduce the imine and the ketone as well. The number of protecting group manipulations and redox transformations required to preserve other functionalities while removing these carbonyl groups made this an unattractive prospect for us in terms of overall step count of the synthesis.

Given the very limited success of the conjugate addition/cyclization strategy with an indole-3-glyoxamide, we could then explore such a cascade with an unsubstituted indole

and install the ethylamine unit in a later step. The Lewis acid-catalyzed conjugate addition of indole (**4.54**) into enone **4.64** is known to proceed with good yield to give indole **4.162** (**Scheme 4.11**).[223] Unfortunately, this approach would generate a racemic mixture of indoles **4.162,** although exploration of chiral Lewis acids may provide some enantioselectivity. Rawal has reported a dearomative allylation of 3-substituted and 2,3-disubstituted indoles to give quaternary indolenines.[224] Use of this methodology could convert **4.162** to the 3,3-disubstituted indolenine **4.164**. From this compound, conversion to the silyl enol ether, followed by ozonolysis of the olefin, reductive amination, and oxidation to the α-silyloxyketone would give tricyclic compound **4.14**, the planned substrate for the double Mannich reaction.

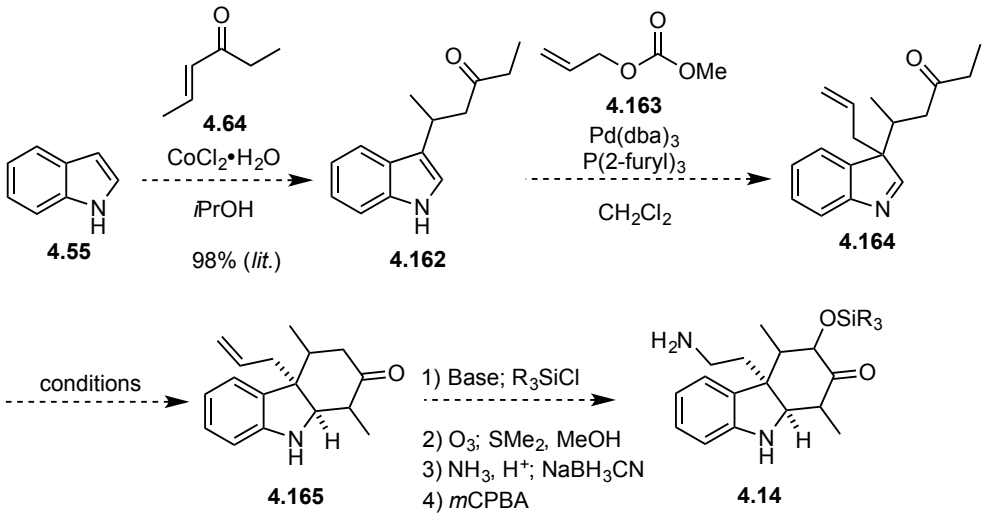


**Scheme 4.11:** Alternate conjugate/addition cyclization strategy to reach **4.14**.

In the case of the indole-3-glyoxamide we used previously, the ketone at the C3-position of the indole ring increases the acidity of the indole proton, which we believed to help facilitate the reaction under relatively mild conditions. However, this also worked to our disadvantage when we attempted the ring closure, as this resonance stabilization of the

anion between the indole nitrogen and the ketone makes this a suitable leaving group during the retro-Michael reaction. We speculate that without the additional electron withdrawing group at the C3 position of the indole ring, this retro-Michael reaction would be less likely to occur. Obtaining the relative stereochemistry of the adjacent stereocenters could be a major challenge in this synthesis, although a screen of chiral phosphine ligands could improve diastereoselectivity.

# Chapter 5. Experimental Procedures

## 5.1 Expression and Purification of HCV NS3 Protease

**Expression of HCV NS3 Protease:** BL21 (DE3) cells (Invitrogen) were transformed with the pET-29b vector containing the gene of the HCV NS3NS4A "sc protease"[155] inserted. Cells were plated on L. B. agar containing 0.030 g/L kanamycin and incubated overnight at 37 °C. A 30 mL L. B. culture containing 0.030 g/L kanamycin was then inoculated with a single colony and allowed to grow in a shaker at 150 rpm overnight at 37 °C. A 1 L L. B. culture containing 0.030 g/L kanamycin was inoculated with the 30 mL culture and allowed to grow in a shaker at 125 rpm at 37 °C until the $O.D._{\lambda 600}$ reached 0.6-0.9. The cultures were removed from the incubator, adjusted to 50 μM $Zn(OAc)_2$, and allowed to stand on ice for 30 min. The cultures were adjusted to 1 mM IPTG and expression was allowed to proceed overnight at 18 °C. Upon removal from the incubator cultures were centrifuged at 5,000 G for 20 min at 4 °C. The supernatant was discarded and cell pellets were stored at –78 °C until purification.

**Purification of HCV NS3 Protease:** One pellet (representing ~450 mL of bacteria broth) was suspended n 5 mL lysis buffer (25 mM $Na_2PO_4$, 10% (w/v) glycerol, 0.5% CHAPS, 100 mM NaCl, 2 mM TCEP, pH 7.5) and processed by passing the material through a French press (500 PSI, high pressure) twice. The resulting lysate was centrifuged at 10,000 G for 30 min at 4 °C. The supernatant was then loaded onto a 5 mL HiTrap Sepharose SP-HP column (GE Healthcare) and equilibrated with buffer A (50 mM $Na_2PO_4$, 5% (w/v) glycerol, pH 7.5). The column was then washed (3 mL/min) with buffer A until the $O.D._{\lambda 280}$ returned to baseline. The concentration of buffer B (buffer A + 1 M NaCl) was increased to 20% over a 70 mL volume. The concentration of buffer B was then increased to 30% over an additional 50 mL and 2 mL fractions were collected. The column was cleaned by raising the concentration of buffer B to 100% until the baseline was re-

established, followed by equilibration in 20% EtOH for a minimum of 30 min prior to storage. The fractions containing protein were combined, concentrated to a volume < 30 mL, and loaded onto a 5 mL HiTrap Hepatin column (GE Healthcare) equilibrated in buffer A. The column was washed with 10% buffer B (3 mL/min) until the $O.D._{\lambda 280}$ returned to baseline. The concentration of buffer B was increased to 30% over a 30 mL volume. The concentration of buffer B was then increased to 35% over an additional 90 mL volume and 2 mL fractions were collected. The column was cleaned by raising the concentration of buffer B to 100% until baseline was re-established, followed by equilibration in 20% EtOH for a minimum of 30 min prior to storage. The fractions containing protein were combined and dialyzed overnight (2 x 3 L) into the ITC buffer (50 mM HEPES, 3% (w/v) DMSO, pH 7.5) using 1,000 MWCO dialysis tubing. Upon removal from dialysis, protein solutions were stored at 4 °C until use. Approximately 250 mL dialysis buffer was saved and used to prepare the ligand solutions and to load the ITC reference cell. The protein was kept as a stock solution (~50 – 70 μM) at 4 °C and diluted as needed.

## 5.2 Isothermal Titration Calorimetry (ITC) Methods

### 5.2.1 Ligand Preparation

Upon purification by reverse-phase HPLC, fractions containing ligand were frozen in liquid $N_2$ and lyophilized for 24 h. Samples were dissolved in Millipore $H_2O$ (10 mL), frozen in liquid $N_2$ and lyophilized for 24 h. Once all solvent was removed, samples were again then dissolved in Millipore $H_2O$ (10 mL), frozen in liquid $N_2$, and lyophilized for an additional 24 h. Samples were then dissolved in Millipore $H_2O$ (5 mL) and HPLC-grade MeCN (10 mL), and lyophilized for a minimum of 24 h. Samples were removed from the lyophilizer, pulverized manually to break up solids, and subjected to an additional 6 h on the lyophilizer.

### 5.2.2 ITC Protocol[35,225]

The MicroCal™sample cell was soaked with CONTRAD™(5% solution) at 35 °C overnight, whereupon the cell was washed with MeOH (5 x 2.5 mL), Millipore $H_2O$ (5 x 2.5 mL), filtered ITC buffer (50 mM HEPES, 3% (w/v) DMSO, pH 7.5, obtained from the final round of dialysis, 5 x 2.5 mL), and protein solution in ITC buffer (1 x 0.5 mL). The protein solution was removed and replaced with a fresh 2.5 mL of protein solution in ITC buffer. The reference cell was washed with MeOH (5 x 2.5 mL), Millipore $H_2O$ (5 x 2.5 mL), and filtered ITC buffer (50 mM HEPES, 3% (w/v) DMSO, pH 7.5, obtained from the final round of dialysis, 5 x 2.5 mL) before being filled with fresh ITC buffer. The same reference solution was used for each batch of protein. The injection apparatus was cleaned by thorough rinsing alternating between MeOH and Millipore $H_2O$ before being dried by passing a stream of argon through the pipette.

Approximately 1 mL of ligand solution was prepared in the ITC buffer (50 mM HEPES, 3% (w/v) DMSO, pH 7.5, obtained from the final round of dialysis). Ligand concentrations were calculated from a Beer's Law determination using the experimentally determined molar extinction coefficient and $\lambda_{max}$ (Table **2.x**).

Both the ligand and protein solutions were degassed under reduced pressure for a minimum of 10 min. The protein solution transferred into the instrument cell. The ligand solution was loaded in a 250 μL injection syringe. An initial injection of 2 μL followed by 34 injections of 8 μL ligand solution into a solution of HCV NS3 were performed with a time delay of 220 sec per injection. Injections were performed until the final ratio of ligand to protein was between 2.5 and 3.0. The protein was diluted to *ca*. 0.050-0.070 mM and the ligand solutions were 0.400 mM – 0.500 mM to ensure that the Wiseman coefficient ($c$) was within the acceptable range of $10 < c < 1000$.

Raw data were integrated, background heats for injecting ligand into buffer were subtracted (by subtracting the heat of the final injection from all injections), and MicroCal graphing software (version 7.0) was used to determine the thermodynamic parameters *n* (number of binding sites), $K_a$ and $\Delta H°$.

### 5.2.3 Determination of Error (Prepared by Dr. John H. Clements)

Error from ITC measurements is random. That is, the sign of that error (+/-) is unknown. In such cases, it is customary to square any relations in which that error is employed in an effort to deal with absolute magnitude. Consider a function f in terms of the variables x, y, and z. That is, f(x,y,z). Infinitesimal changes in any of these variables produce changes in the function as a whole according to the following relation:

$$\partial f = \left(\frac{\partial f}{\partial x}\right)\partial x + \left(\frac{\partial f}{\partial y}\right)\partial y + \left(\frac{\partial f}{\partial z}\right)\partial z \tag{5.1}$$

If variations in x, y, and z are small but not infinitesimal, yet the values of the partial derivatives involved do not change considerably over the range of the variations, then we may write:

$$\Delta f = \left(\frac{\Delta f}{\Delta x}\right)\Delta x + \left(\frac{\Delta f}{\Delta y}\right)\Delta y + \left(\frac{\Delta f}{\Delta z}\right)\Delta z \tag{5.2}$$

Given that we must take into account the absolute magnitude of the variations, which themselves can be positive or negative, we must square both sides of the expression (5.2):

$$\Delta f^2 \cong \left(\frac{\Delta f}{\Delta x}\right)^2 \Delta x^2 + \left(\frac{\Delta f}{\Delta y}\right)^2 \Delta y^2 + \left(\frac{\Delta f}{\Delta z}\right)^2 \Delta z^2 + \text{(cross terms)} \tag{5.3}$$

In the above expression, the cross terms will be the terms that contain products such as this one: $\Delta x \Delta y$. For truly random errors, the average values of $\Delta x$ and $\Delta y$ are zero. As such, terms containing products of random errors tend toward zero and can be ignored such that expression (5.3) becomes:

$$\Delta f^2 \cong \left(\frac{\Delta f}{\Delta x}\right)^2 \Delta x^2 + \left(\frac{\Delta f}{\Delta y}\right)^2 \Delta y^2 + \left(\frac{\Delta f}{\Delta z}\right)^2 \Delta z^2 \tag{5.4}$$

Viewing $\Delta x$, $\Delta y$, and $\Delta z$ as the errors in x, y, and z, respectively, and $\Delta f$ as the total error in f, equation (5.4) may be used to determine the nature of error propagation in our experiments.

Error in concentration of a solute given errors in weight of solute and solution volume:

$$c = \frac{W}{MW} \times \frac{1}{V} \tag{5.5}$$

where c, W, and MW are molar concentration of solute, weight of solute, and volume of solution, respectively. Given c is a function of W and V, the error in c is given as follows:

$$\Delta c^2 \cong \left(\frac{\partial c}{\partial W}\right)^2 \Delta W^2 + \left(\frac{\partial c}{\partial V}\right)^2 \Delta V^2 \tag{5.6}$$

Hence,

$$\Delta c \cong \left\{\left(\frac{\partial c}{\partial W}\right)^2 \Delta W^2 + \left(\frac{\partial c}{\partial V}\right)^2 \Delta V^2\right\}^{\frac{1}{2}} \tag{5.7}$$

For cases in which concentrations were determined via application of a previously determined extinction coefficient, we will need to obtain the error in that extinction coefficient, which is equal to the error in the slope of a plot of optical density at the wavelength in question vs. concentration (as determined by weight and volume measurements). The error obtained from the slope of a line resulting from liner-regression analysis; $\Delta m$, is given as:

$$\Delta m^2 = \left[\frac{n \sum_i d_i}{(n-2)(n \sum_i x_i^2 - (\sum_i x_i)^2}\right]^2 \tag{5.8}$$

where n is the number of observations, $x_i$ is the ith observation of the x value, and $d_i$ is the residual of the ith observation defined as $d_i = y_i - (mx_i + b)$ where m and b are the slope and intercept from linear regression analysis, respectively.

Given the Beer-Lambert Law:

$$A=abc \tag{5.9}$$

in which A, a, and b are the optical density at a specific wavelength, molar extinction coefficient, and cell path length, respectively. This gives the error in concentration as:

$$\Delta c^2 = (A \ln a)^2 \Delta a^2 + \left(\frac{1}{a}\right)^2 \Delta A^2 \tag{5.10}$$

Recognizing that $\Delta a = \Delta m$ as given in equation (5.8), equation (5.10) becomes:

$$\Delta c^2 = (A \ln a)^2 \Delta m^2 + \left(\frac{1}{m}\right)^2 \Delta A^2 \tag{5.11}$$

From Whitesides *et al.*,[226] $\Delta c \approx \Delta H$. In other words, the error in the measurement of the change in enthalpy is almost entirely the result of error in the concentration of the titrant (ligand). Thus:

$$\Delta H \cong \left[(A \ln a)^2 \Delta m^2 + \left(\frac{1}{m}\right)^2 \Delta A^2\right]^{\frac{1}{2}} \tag{5.12}$$

for cases in which ligand concentration was determined by a previously measured extinction coefficient, or:

$$\Delta H \cong \left[\left(\frac{1}{V} \times \frac{1}{MW}\right)^2 \Delta w^2 + \left(\frac{W}{MW}\right)^2 \Delta V^2\right]^{\frac{1}{2}} \tag{5.13}$$

The error propagation through our other thermodynamic parameters is given below.

$$\Delta G^\circ = -RT \ln K_a \tag{5.14}$$

The error in $\Delta G^\circ$, $\Delta(\Delta G^\circ)$, can be expressed as follows:

$$\Delta(\Delta G^\circ)^2 \cong \left(\frac{\partial(\Delta G^\circ)}{\partial K_a}\right)^2 \Delta K_a{}^2 + \left(\frac{\partial(\Delta G^\circ)}{\partial T}\right)^2 \Delta T^2 \tag{5.15}$$

Given that:

$$\frac{\partial(\Delta G°)}{\partial K_a} = -\frac{RT}{K_a};\ \left(\frac{\partial(\Delta G°)}{\partial T}\right)^2 = -R\ln K_a \tag{5.16}$$

$$\Delta(\Delta G°)^2 \cong \left(\frac{RT}{K_a}\right)^2 (\Delta K)^2 + (R\ln K_a)^2(\Delta T)^2 \tag{5.17}$$

Equation (5.17) is appropriate for calculating the propagation of error in the determination of ΔG°. Although it won't be shown here, it can easily be seen that the resulting error has units of energy $mol^{-1}$ as it should.

Propagation of error in ΔS° can be shown similarly:

$$\Delta S° = \frac{\Delta H° - \Delta G°}{T} \tag{5.18}$$

$$\Delta(\Delta S°)^2 \cong \left(\frac{\partial(\Delta S°)}{\partial(\Delta(\Delta H°))}\right)^2 \Delta(\Delta H°)^2 + \left(\frac{\partial(\Delta S°)}{\partial(\Delta(\Delta H°))}\right)^2 \Delta(\Delta G°)^2 + \left(\frac{\partial(\Delta S°)}{\partial T}\right)^2 \Delta T^2 \tag{5.19}$$

*** Note ***

Equation (5.19) is only valid for cases in which each variable is independent. Since ΔG° depends on T, this equation is not valid. Instead, ΔG° must be expanded as such:

$$\Delta S° = \frac{\Delta H° - \Delta G°}{T} = \frac{\Delta H° - RT\ln K_a}{T} = \frac{\Delta H°}{T} + R\ln K_a \tag{5.20}$$

Representing $\Delta S°$ in this manner, the error in $\Delta S°$; $\Delta(\Delta S°)$, becomes:

$$\Delta(\Delta S°)^2 \cong \left(\frac{\partial(\Delta S°)}{\partial(\Delta H)°}\right)^2 \Delta(\Delta H°)^2 + \left(\frac{\partial(\Delta S°)}{\partial K_a}\right)^2 \Delta K_a{}^2 + \left(\frac{\partial(\Delta S°)}{\partial T}\right)^2 \Delta T^2 \qquad (5.21)$$

Given that:

$$\frac{\partial(\Delta S°)}{\partial(\Delta H)°} = \frac{1}{T};\ \frac{\partial(\Delta S°)}{\partial K_a} = \frac{R}{K_a};\ \frac{\partial(\Delta S°)}{\partial T} = -\frac{\Delta H°}{T^2} \qquad (5.22)$$

Substituting equation (5.22) into (5.21):

$$\Delta(\Delta S°)^2 = \frac{\partial(\Delta H°)^2}{T^2} + \left(\frac{R}{K_a}\right)^2 \Delta K_a{}^2 + \left(\frac{\Delta H°}{T^2}\right)^2 \Delta T^2 \qquad (5.23)$$

Again, it can be shown that the units of $\Delta(\Delta S°)$, are energy $mol^{-1}$ $temp^{-1}$, as they should be.

If taking averages of data, they too propagate error. Consider two measurements; $M_1$ and $M_2$, which have been taken and are to be averaged to obtain a final reportable value. The average of these; <M>; is:

$$<M> = \frac{1}{2}(M_1 + M_2) \qquad (5.24)$$

The error in <M>; $\Delta(<M>)$, is:

$$\Delta(<M>)^2 = \left(\frac{\partial<M>}{\partial M_1}\right)^2 \Delta M_1{}^2 + \left(\frac{\partial<M>}{\partial M_2}\right)^2 \Delta M_2{}^2 \qquad (5.25)$$

$$\frac{\partial <M>}{\partial M_1} = \frac{\partial <M>}{\partial M_2} = \frac{1}{2} \tag{5.26}$$

Substituting equation (5.26) into (5.25):

$$\Delta(<M>)^2 = \frac{1}{4}\left[\Delta M_1{}^2 + \Delta M_2{}^2\right] \tag{5.27}$$

In more general terms:

$$\Delta(<M>)^2 = \frac{1}{N^2}\sum_{1}^{N}(\Delta M_N)^2 \tag{5.28}$$

Where N is the number of data points being averaged, and $\Delta M_N$ refers to the error in each data point.

## 5.3 ORGANIC SYNTHESIS

### 5.3.1 General

Solvents and reagents were reagent grade and were used without purification unless otherwise noted. Methanol (MeOH) and *N*,*N*,-dimethylformamide (DMF) were dried by filtration through two columns of activated molecular sieves prior to use. Tetrahydrofuran (THF) and diethyl ether ($Et_2O$) were passed through two columns of activated neutral alumina prior to use. Toluene (PhMe) was dried by passage through a column of activated neutral alumina followed by passage through a column of Q5 reactant. *N*-methyl-2-pyrrolidone (NMP), diisopropylamine ($^iPr_2NH$), and *tert*-butyldimethylsilyl chloride (TBSCl) were distilled over $CaH_2$ prior to use. Grignard reagents were titrated with menthol using 1,10-phenanthroline as an indicator.[227] All reactions were performed under

an atmosphere of argon or nitrogen. Removal of solvent under reduced pressure was performed using a rotary evaporator. UV/vis absorbance measurements were determined using a Beckman Coulter DU Series 700 UV/vis scanning spectrophotometer. Microwave reactions were run in a sealed reaction vessel using a CEM Discover microwave. Thin layer chromatography (TLC) was performed on glass-backed pre-coated silica gel plates (0.25 mm thick with 60 $F_{254}$ indicator) and was visualized using one or both of the following methods: UV light (254 nm) and staining with p-anisaldehyde (PAA) or $KMnO_4$. Flash chromatography was performed using glass columns and SiliaFlash® F60 silica gel (Silicycle, 40-63 μM, 60 Å). Reverse-phase high performance liquid chromatography (RP HPLC) was conducted using a binary solvent system, where solvent A was 0.1% aqueous TFA and solvent B was 0.1% TFA in MeCN, with a Phenomenex Gemini C18 column (10 μM particle size, 300 Å pore size), 250 mm x 21.2 mm diameter (flow rate of 10 mL/min) being used for preparative work. Melting points were determined using a Thomas-Hoover Uni-melt capillary melting point apparatus and are uncorrected. Infrared (IR) spectra were obtained with a Nicolet IR 100 FT-IR spectrometer in $CH_2Cl_2$ on sodium chloride plates. Band positions are given in reciprocal centimeters ($cm^{-1}$). Proton nuclear magnetic resonance ($^1H$ NMR) spectra were obtained on a 400 MHz spectrometer as a solution in $CDCl_3$ unless otherwise indicated. Chemical shifts are reported in parts per million (ppm) downfield from tetramethylsilane (TMS) (δ 0.00) and referenced relative to the 7.24 ppm resonance of $CDCl_3$, the 7.15 ppm resonance of $C_6D_6$, the center of the 3.31 ppm quintet resonance of $CD_3OD$, or the center of the 2.49 ppm quintet resonance of DMSO-$d_6$. Carbon nuclear magnetic resonance ($^{13}C$ NMR) spectra were obtained using the above-mentioned instrument operating at 100 MHz and chemical shifts are reported in ppm relative to the center line of the multiplet for deuterium solvent peaks (δ 77.0 for $CDCl_3$, δ 49.0 for $CD_3OD$, δ 39.5 for DMSO-$d_6$, δ 128.6 for $C_6D_6$). Coupling constants (*J*) are reported in Hz

and the splitting abbreviations used are: s, singlet; d, doublet; t, triplet; q, quartet; dd, doublet of doublets; ddd, doublet of doublet of doublets; m, multiplet; comp, overlapping multiplets of magnetically non-equivalent protons; br, broad.

### 5.3.2 Compounds

**General procedure for the preparation of substituted 4-methoxyquinolines. Preparation of 3.18-3.20.** Sodium metal (675 mg, 29 mmol) was added portionwise to MeOH (12 mL) and stirred until dissolved. To the solution was added 4-chloroquinoline (2 mmol), and the mixture was heated under reflux for 1 h. The mixture was cooled to room temperature, whereupon saturated $NH_4Cl$ (10 mL) was added. The mixture was extracted with $CHCl_3$ (3 x 15 mL), and the combined organic layers were washed with brine (15 mL), dried ($MgSO_4$), and concentrated under reduced pressure.

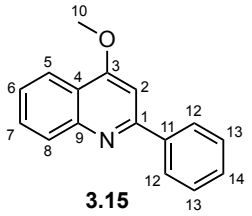

**3.15**

**4-Methoxy-2-phenylquinoline (3.15) (rmw_01_84).** The resulting yellow oil was purified by flash chromatography eluting with EtOAc/hexanes (1:5) to give 122 mg (50%) of **3.15** as a white solid (mp = 81-83 °C). $^1$H NMR (40 MHz, $C_6D_6$) δ 8.36-8.38 (m, 1 H), 8.31-833 (comp, 2 H), 8.27-8.29 (dd, $J$ = 6.4, 0.8 Hz, 1 H), 7.40-7.42 (ddd, $J$ = 6.8, 5.2, 1.2 Hz, 1 H), 7.32-7.36 (comp, 2 H), 7.20-7.24 (comp, 2 H), 6.83 (s, 1 H), 3.27 (s, 3 H); $^{13}$C NMR (100 MHz, $C_6D_6$) δ 162.9, 158.4, 150.0, 140.8, 131.0, 130.0, 129.4, 128.8, 128.3,

128.1, 127.9, 125.5, 121.8, 120.9, 97.7, 54.8. HRMS (ESI) *m/z* 236.1073 [$C_{16}H_{13}NO$ (M+H) requires 236.1070].

**NMR Assignments.** $^{1}$H NMR (400 MHz, $C_6D_6$) δ 8.36-8.38 (m, 1 H, C5-H), 8.31-833 (comp, 2 H, C12-H), 8.27-8.29 (dd, *J* = 6.4, 0.8 Hz, 1 H, C8-H), 7.40-7.42 (ddd, *J* = 6.8, 5.2, 1.2 Hz, 1 H, C6-H), 7.32-7.36 (comp, 2 H, C13-H), 7.20-7.24 (comp, 2 H, C7-H, C14-H), 6.83 (s, 1 H, C2-H), 3.27 (s, 3 H, C10-H); $^{13}$C NMR (100 MHz, $C_6D_6$) δ 162.9 (C3), 158.4 (C1), 150.0 (C9), 140.8 (C11), 131.0 (C5), 130.0 (C6), 129.4 (C14), 128.8 (C13), 128.3 (C13), 128.1 (C12), 127.9 (C12), 125.5 (C7), 121.8 (C8), 120.9 (C4), 97.7 (C2), 54.8 (C10).

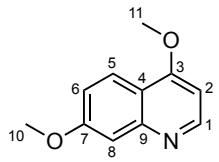


**3.16**

**4,7-Dimethoxyquinoline (3.16). (rmw_01_112).** The resulting yellow oil was washed with hexane to give 300 mg (54%) of **3.16** as an off-white solid. (mp = 81-83 °C). $^{1}$H NMR (400 MHz, $C_6D_6$) δ 8.71 (d, *J* = 5.1 Hz, 1 H), 8.16 (d, *J* = 9.4 Hz, 1 H), 7.64 (d, *J* = 2.7 Hz, 1 H), 7.16 (dd, *J* = 9.0, 2.4 Hz, 1 H), 5.98 (d, *J* = 5.1 Hz, 1 H), 3.31 (s, 3 H), 3.20 (s, 3 H). $^{13}$C NMR (100 MHz, $C_6D_6$) δ 162.2, 161.4, 152.2, 152.0, 123.2, 118.6, 116.4, 108.2, 98.9, 54.8; HRMS (ESI) *m/z* 190.0867 [$C_{11}H_{11}NO_2$ (M+H) requires 190.0863].

**NMR Assignments.** $^{1}$H NMR (400 MHz, $C_6D_6$) δ 8.71 (d, *J* = 5.1 Hz, 1 H, C1-H), 8.16 (d, *J* = 9.4 Hz, 1 H, C5-H), 7.64 (d, *J* = 2.7 Hz, 1 H, C8-H), 7.16 (dd, *J* = 9.0, 2.4 Hz, 1 H, C6-H), 5.98 (d, *J* = 5.1 Hz, 1 H, C2-H), 3.31 (s, 3 H, C10-H), 3.20 (s, 3 H, C-11-H).

$^{13}$C NMR (100 MHz, $C_6D_6$) δ 162.2 (C3), 161.4 (C7), 152.2 (C9), 152.0 (C1), 123.2 (C5), 118.6 (C6), 116.4 (C4), 108.2 (C8), 98.9 (C2), 54.8 (C10/C11).

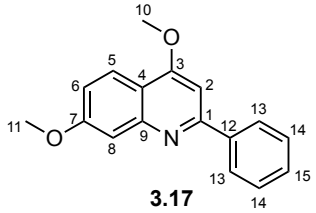


**3.17**

**4,7-Dimethoxy-2-phenylquinoline (3.17). (rmw_01_111).** The resulting yellow oil was recrystallized from hexanes to give 300 mg (54%) of **3.17** as an off-white solid. (mp = 75-77 °C). $^1$H NMR (400 MHz, $C_6D_6$) δ 8.34-8.38 (comp, 2 H), 8.17 (d, *J* = 9.0 Hz, 1 H), 7.68 (d, *J* = 2.7 Hz, 1 H), 7.35-7.39 (comp, 2 H), 7.24-7.28 (m, 1 H), 7.17 (dd, *J* = 9.0, 2.4 Hz, 1 H), 6.79 (s, 1 H), 3.38 (s, 3 H), 3.29 (s, 3 H). $^{13}$C NMR (100 MHz, $C_6D_6$) δ 163.0, 161.7, 158.9, 152.0, 141.1, 129.0, 128.5, 127.6, 123.1, 118.4, 115.2, 108.5, 96.3, 54.9, 54.8; HRMS (ESI) *m/z* 266.1177 [$C_{17}H_{15}NO_2$ (M+H) requires 266.1176].

**NMR Assignments.** $^1$H NMR (400 MHz, $C_6D_6$) δ 8.34-8.38 (comp, 2 H C13-H), 8.17 (d, *J* = 9.0 Hz, 1 H, C5-H), 7.68 (d, *J* = 2.7 Hz, 1 H, C8-H), 7.35-7.39 (comp, 2 H, C14-H), 7.24-7.28 (m, 1 H, C15-H), 7.17 (dd, *J* = 9.0, 2.4 Hz, 1 H, C6-H), 6.79 (s, 1 H, C2-H), 3.38 (s, 3 H, C11-H), 3.29 (s, 3 H, C10-H). $^{13}$C NMR (100 MHz, $C_6D_6$) δ 163.0 (C7), 161.7 (C3), 158.9 (C1), 152.0 (C9), 141.1 (C12), 129.0 (C15), 128.5 (C14), 127.6 (C13), 123.1 (C5), 118.4 (C6), 115.2 (C4), 108.5 (C8), 96.3 (C2), 54.9 (C11), 54.8 (C10).

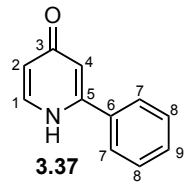

**3.37**

**2-Phenylpyridin-4(1*H*)-one (3.37) (rmw_02_43).** Prepared according to the method of Soni *et al*.[165] The crude oil was purified by flash chromatography eluting with $CH_2Cl_2$: MeOH (9:1) to give 71% of **3.37** as a tan solid. $^1$H NMR (600 MHz, $CDCl_3$) δ 6.31 (dd, *J* = 2.3, 7.0 Hz, 1 H), 6.55 (d, *J* = 1.9 Hz, 1 H), 7.36 (comp, 3 H), 7.58-7.57 (comp, 2 H), 7.65 (d, *J* = 7.0 Hz, 1 H); $^{13}$C NMR (150 MHz, $CDCl_3$) δ 178.8, 151.1, 139.7, 134.1, 130.2, 129.0, 126.9, 115.6, 114.7; HRMS (CI) *m/z* 171.0680 [$C_{11}H_9NO$ ($M^+$) requires 170.0684], 172.0764 [$C_{11}H_{10}NO$ (M+H) requires 172.0762].

**NMR Assignments.** $^1$H NMR (600 MHz, $CDCl_3$) δ 6.31 (dd, *J* = 2.3, 7.0 Hz, 1 H, C2-H), 6.55 (d, *J* = 1.9 Hz, 1 H, C4-H), 7.36 (comp, 3 H, C8-H, C9-H), 7.58-7.57 (comp, 2 H C7-H), 7.65 (d, *J* = 7.0 Hz, 1 H, C3-H); $^{13}$C NMR (150 MHz, $CDCl_3$) δ 178.8 (C3), 151.1 (C5), 139.7 (C1), 134.1 (C6), 130.2 (C9), 129.0 (C8), 126.9 (C7), 115.6 (C2), 114.7 (C4).

**General procedure for displacement of the tripeptide brosylate. Preparation of 3.29-3.32 and 3.44-3.45.** The tripeptide brosylate **3.27** (100 mg, 0.15 mmol) was dissolved in NMP (2 mL). The hydroxyquinoline (0.22 mmol) and $Cs_2CO_3$ (95 mh, 0.29 mmol) were added, and the mixture was heated at 70 °C until the brosylate was consumed by TLC (2-4 h). The mixture was cooled to room temperature and poured into EtOAc (10 mL). The

mixture was washed with $H_2O$ (3 x 10 mL), saturated $NaHCO_3$ (2 x 10 mL), 1 N NaOH (1 x 10 mL), $H_2O$ (2 x 10 mL), and brine (1 x 10 mL). The organic layer was dried over $MgSO_4$, filtered, and concentrated under reduced pressure. The crude residue was purified by flash chromatography eluting with $CH_2Cl_2$: MeOH (9:1).

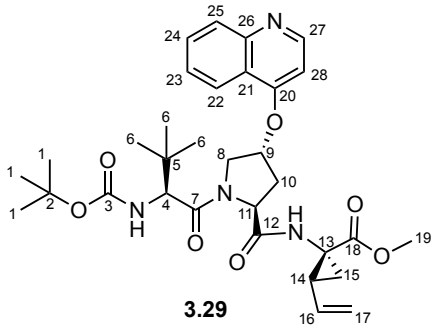

**3.29**

**Methyl (1*R*,2*R*)-1-((2*S*,4*R*)-1-((*S*)-2-((*tert*-butoxycarbonyl)amino)-3,3-dimethylbutanoyl)-4-(quinolin-4-yloxy)pyrrolidine-2-carboxamido)-2-vinylcyclopropane-1-carboxylate (3.29) (rmw_02_28).** Prepared according to the general procedure to give 74% of **3.29** as a colorless oil. $^1$H NMR (400 MHz, $CD_3OD$) δ 8.71 (d, *J* = 5.4 Hz, 1 H), 8.24 (d, *J* = 8.1 Hz, 1 H), 7.94 (d, *J* = 8.4 Hz, 1 H), 7.77-7.72 (m, 1 H), 7.50 (t, *J* = 7.6 Hz, 1 H), 7.07 (d, *J* = 5.5 Hz, 1 H), 5.80-5.71 (m, 1 H), 5.46 (br, 1 H), 5.28-5.23 (m, 1 H), 5.10-5.07 (m, 1 H), 4.63-4.56 (m, 2 H), 4.21 (s, 1 H), 4.05 (dd, *J* = 11.9, 3.2 Hz, 1 H), 3.71-3.63 (m, 3 H), 2.74-2.66 (m, 1 H), 2.45-2.37 (m, 1 H), 2.26-2.16 (m, 1 H), 1.73-1.69 (m, 1 H), 1.45-1.39 (m, 3 H), 1.27-1.22, comp, 9 H), 1.09 (s, 9 H).

**NMR Assignments.** $^1$H NMR (400 MHz, $CD_3OD$) δ 8.71 (d, *J* = 5.4 Hz, 1 H, C27-H), 8.24 (d, *J* = 8.1 Hz, 1 H, C25-H), 7.94 (d, *J* = 8.4 Hz, 1 H, C22-H), 7.77-7.72 (m, 1 H, C24-H), 7.50 (t, *J* = 7.6 Hz, 1 H, C23-H), 7.07 (d, *J* = 5.5 Hz, 1 H, C28-H), 5.80-5.71 (m,

1 H, C16-H), 5.46 (br, 1 H, C9-H), 5.28-5.23 (m, 1 H, C17-H), 5.10-5.07 (m, 1 H, C17-H), 4.63-4.56 (comp, 2 H, C8-H, C11-H), 4.21 (s, 1 H, C4-H), 4.05 (dd, *J* = 11.9, 3.2 Hz, 1 H, C8-H), 3.71-3.63 (comp, 3 H, C19-H), 2.74-2.66 (m, 1 H, C10-H), 2.45-2.37 (m, 1 H, C14-H), 2.26-2.16 (m, 1 H, C10-H), 1.73-1.69 (m, 1 H, C15-H), 1.45-1.39 (m, 3 H, C15-H), 1.27-1.22, comp, 9 H, C1-H), 1.09 (s, 9 H, C6-H).

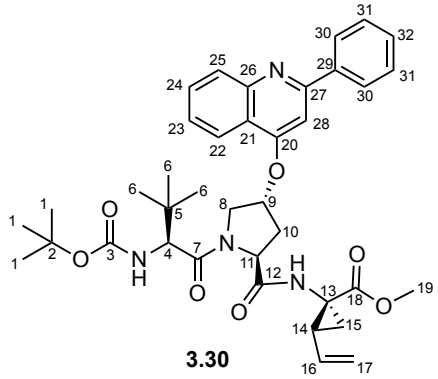

**3.30**

**Methyl (1*R*,2*R*)-1-((2*S*,4*R*)-1-((*S*)-2-((*tert*-butoxycarbonyl)amino)-3,3-dimethylbutanoyl)-4-((2-phenylquinolin-4-yl)oxy)pyrrolidine-2-carboxamido)-2-vinylcyclopropane-1-carboxylate (3.30) (rmw_01_119).** Prepared according to the general procedure to give 99% of **3.29** as a colorless oil. $^1$H NMR (400 MHz, $CD_3OD$) δ 8.40 (d, *J* = 8.0 Hz, 1 H), 8.18 (d, *J* = 8.1 Hz, 1 H), 8.10-8.08 (comp, 2 H), 8.05-8.02 (m, 1 H), 7.76-7.69 (comp, 5 H), 5.87-5.80 (comp, 2 H), 5.26 (dd, *J* = 1.5 Hz, 17.0 Hz, 1 H), 5.08 (dd, *J* = 2.5 Hz, 10.0 Hz, 1 H), 4.71-4.67 (comp, 2 H), 4.18 (s, 1 H), 4.09 (dd, *J* = 3.1 Hz, 12.2 Hz, 1 H), 3.68 (s, 3 H), 2.82-2.78 (m, 1 H), 2.63-2.55 (m, 1 H), 2.22-2.13 (m, 1 H), 1.71-1.68 (m, 1 H), 1.46-1.42 (comp, 3 H, 1.15 (s 9 H), 1.09 (s, 9 H).

**NMR Assignments.** $^1$H NMR (400 MHz, $CD_3OD$) δ 8.40 (d, *J* = 8.0 Hz, 1 H, C25-H), 8.18 (d, *J* = 8.1 Hz, 1 H, C22-H), 8.10-8.08 (comp, 2 H, C30-H), 8.05-8.02 (m, 1 H,

C23-H), 7.76-7.69 (comp, 5 H, C31-H, C32-H, C24-H, C28-H), 5.87-5.80 (comp, 2 H), 5.26 (dd, *J* = 1.5 Hz, 17.0 Hz, 1 H, C17-H), 5.08 (dd, *J* = 2.5 Hz, 10.0 Hz, 1 H, C17-H), 4.71-4.67 (comp, 2 H, C8-H, C11-H), 4.18 (s, 1 H, C4-H), 4.09 (dd, *J* = 3.1 Hz, 12.2 Hz, 1 H, C8-H), 3.68 (s, 3 H, C19-H), 2.82-2.78 (m, 1 H, C10-H), 2.63-2.55 (m, 1 H, C10-H), 2.22-2.13 (m, 1 H, C14-H), 1.71-1.68 (m, 1 H, C14-H), 1.46-1.42 (comp, 3 H, C15-H), 1.15 (s 9 H, C1-H), 1.09 (s, 9 H, C6-H).

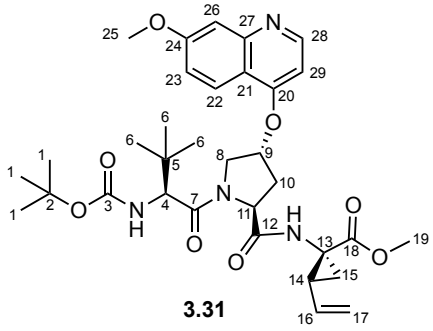

**3.31**

**Methyl (1*R*,2*R*)-1-((2*S*,4*R*)-1-((*S*)-2-((*tert*-butoxycarbonyl)amino)-3,3-dimethylbutanoyl)-4-((7-methoxyquinolin-4-yl)oxy)pyrrolidine-2-carboxamido)-2-vinylcyclopropane-1-carboxylate (3.31) (rmw_01_120).** Prepared according to the general procedure to give 90% of **3.31** as a colorless oil. $^{1}$H NMR (500 MHz, $CD_3OD$) δ 8.60 (d, *J* = 5.5 Hz, 1 H), 8.10 (d, *J* = 9.0 Hz, 1 H), 7.26 (d, *J* = 2.4 Hz, 1 H), 7.09 (dd, *J* = 2.3, 9.0 Hz, 1 H), 6.90 (d, *J* = 5.5 Hz, 1 H), 5.79-570 (m, 1 H), 5.41 (br, 1 H), 5.25 (dd, *J* = 1.57, 17.22 Hz, 1 H), 5.09 (dd, *J* = 1.57, 10.17 Hz, 1 H), 4.61-4.50 (comp, 2 H), 4.20 (s, 1 H), 4.02 (dd, *J* = 3.5, 12.1 Hz, 1 H), 3.92 (s, 3 H), 3.66 (s, 3 H), 2.68-2.63 (m, 1 H), 2.24-2.14 (m, 1 H), 1.74 (dd, *J* = 5.5, 8.2 Hz, 1 H), 1.46-1.40 (comp, 2 H), 1.26 (s, 9 H), 1.04 (s, 9 H). $^{13}$C NMR (125 MHz, $CD_3OD$) δ 174.6, 173.3, 172.0, 163.1, 161.9, 157.9, 152.1,

151.5, 135.1, 124.7, 119.8, 118.0, 117.5, 106.5, 101.8, 80.3, 78.4, 67.0, 60.9, 56.0, 55.1, 52.8, 40.9, 35.6, 35.0, 28.9, 28.7, 28.5, 26.9.

**NMR Assignments.** $^{1}$H NMR (500 MHz, $CD_3OD$) δ 8.60 (d, *J* = 5.5 Hz, 1 H, C28-H), 8.10 (d, *J* = 9.0 Hz, 1 H, C22-H), 7.26 (d, *J* = 2.4 Hz, 1 H, C26-H), 7.09 (dd, *J* = 2.3, 9.0 Hz, 1 H, C23-H), 6.90 (d, *J* = 5.5 Hz, 1 H, C29-H), 5.79-570 (m, 1 H, C16-H), 5.41 (br, 1 H, C9-H), 5.25 (dd, *J* = 1.57, 17.22 Hz, 1 H, C17-H), 5.09 (dd, *J* = 1.57, 10.17 Hz, 1 H, C17-H), 4.61-4.50 (comp, 2 H, C8-H, C11-H), 4.20 (s, 1 H, C4-H), 4.02 (dd, *J* = 3.5, 12.1 Hz, 1 H, C8-H), 3.92 (s, 3 H, C25-H), 3.66 (s, 3 H, C19-H), 2.68-2.63 (m, 1 H, C10-H), 2.24-2.14 (m, 1 H, C10-H), 1.74 (dd, *J* = 5.5, 8.2 Hz, 1 H, C15-H), 1.46-1.40 (comp, 2 H, C14-H, C15-H), 1.26 (s, 9 H, C1-H), 1.04 (s, 9 H, C6-H). $^{13}$C NMR (125 MHz, $CD_3OD$) δ 174.6 (C18), 173.3 (C7), 172.0 (C12), 163.1 (C24), 161.9 (C20), 157.9 (C3), 152.1 (C27), 151.5 (C28), 135.1 (C16), 124.7 (C22), 119.8 (C23), 118.0 (C21), 117.5 (C17), 106.5 (C26), 101.8 (C29), 80.3 (C9), 78.4 (C2), 67.0 (C11), 60.9 (C4), 56.0 (C25), 55.1 (C8), 52.8 (C19), 40.9 (C13), 35.6 (C10), 35.0 (C5), 28.9 (C14), 28.7 (C15), 28.5 (C1), 26.9 (C6).

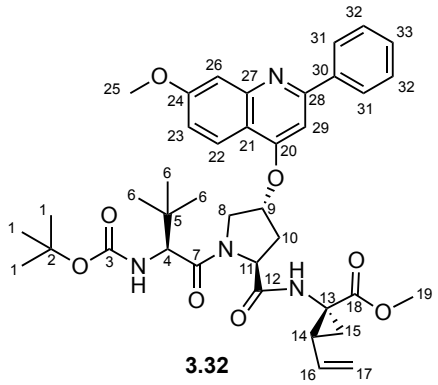

**3.32**

**Methyl (1*R*,2*R*)-1-((2*S*,4*R*)-1-((*S*)-2-((*tert*-butoxycarbonyl)amino)-3,3-dimethylbutanoyl)-4-((7-methoxy-2-phenylquinolin-4-yl)oxy)pyrrolidine-2-carboxamido)-2-vinylcyclopropane-1-carboxylate (3.32) (rmw_01_211).** Prepared according to the general procedure to give 90% of **3.32** as a colorless oil. $^{1}$H NMR (500 MHz, $CD_3OD$) δ 8.05-8.02 (comp, 3 H), 7.53-7.47 (comp, 3 H), 7.35 (d, *J* = 2.1 Hz, 1 H), 7.17 (s, 1 H), 7.02 (dd, *J* = 2.2 Hz, 9.0 Hz, 1 H), 5.77-5.70 (m, 1 H), 5.47 (br, 1 H), 5.24 (dd, *J* = 1.0 Hz, 17.2 Hz, 1 H), 5.07 (dd, *J* = 1.7 Hz, 10.2 Hz, 1 H), 4.61-4.57 (m, 1 H), 4.50 (d, *J* = 11.7 Hz, 1 H), 4.22 (s, 1 H), 4.04-4.01 (m, 1 H), 3.92 (s, 3 H), 3.63 (s, 3 H), 2.67-2.63 (m, 1 H), 2.41-2.36 (m, 1 H), 2.22-2.16 (m, 1 H), 1.73 (dd, *J* = 5.5, 8.2 Hz, 1 H), 1.44-1.38 (comp, 3 H), 1.27 (s, 9 H), 1.03 (s, 9 H); $^{13}$C NMR (125 MHz, $CD_3OD$) δ 174.2, 173.2, 172.0, 163.5, 161.7, 159.2, 157.1, 152.0, 151.5, 141.2, 136.2, 129.2, 128.0, 127.3, 124.7, 118.3, 117.9, 108.8, 96.0, 80.2, 79.0, 67.0, 60.6, 56.0, 55.3, 52.6, 41.2, 35.5, 35.3, 28.6, 27.8, 28.5, 26.4.

**NMR Assignments.** $^{1}$H NMR (500 MHz, $CD_3OD$) δ 8.505-8.02 (comp, 3 H, C22-H, C31-H), 7.53-7.47 (comp, 3 H, C32-H, C33-H), 7.35 (d, *J* = 2.1 Hz, 1 H, C26-H), 7.17 (s, 1 H, C29-H), 7.02 (dd, *J* = 2.2 Hz, 9.0 Hz, 1 H, C23-H), 5.77-5.70 (m, 1 H, C16-H),

5.47 (br, 1 H, C9-H), 5.24 (dd, *J* = 1.0 Hz, 17.2 Hz, 1 H, C17-H), 5.07 (dd, *J* = 1.7 Hz, 10.2 Hz, 1 H, C17-H), 4.61-4.57 (m, 1 H, C10-H), 4.50 (d, *J* = 11.7 Hz, 1 H, C11-H), 4.22 (s, 1 H, C4-H), 4.04-4.01 (m, 1 H, C8-H), 3.92 (s, 3 H, C25-H), 3.63 (s, 3 H C19-H), 2.67-2.63 (m, 1 H, C10-H), 2.41-2.36 (m, 1 H, C14-H), 2.22-2.16 (m, 1 H, C10-H), 1.73 (dd, *J* = 5.5, 8.2 Hz, 1 H, C15-H), 1.44-1.38 (comp, 3 H, C15-H), 1.27 (s, 9 H, C1-H), 1.03 (s, 9 H, C6-H); $^{13}$C NMR (125 MHz, $CD_3OD$) δ 174.2 (C18), 173.2 (C7), 172.0 (C12), 163.5 (C24), 161.7 (C20), 159.2 (C28), 157.4 (C3), 152.0 (C27), 141.2 (C30), 136.2 (C16), 129.2 (C33), 128.0 (C32), 127.3 (C31), 124.1 (C22), 118.3 (C23), 117.9 (C17), 108.5 (C26), 108.8 (C26), 96.0 (C29) 80.2 (C9), 79.0 (C2), 67.0 (C11), 60.6 (C4), 55.4 (C25), 55.3 (C8), 52.6 (C19), 41.2 (C13), 35.5 (C10), 35.3 (C5), 28.6 (C14), 27.8 (C15), 28.5 (C1), 26.4 (C6).

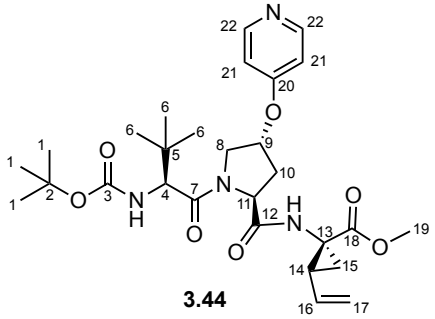

**3.44**

**Methyl (1*R*,2*R*)-1-((2*S*,4*R*)-1-((*S*)-2-((*tert*-butoxycarbonyl)amino)-3,3-dimethylbutanoyl)-4-(pyridin-4-yloxy)pyrrolidine-2-carboxamido)-2-vinylcyclopropane-1-carboxylate (3.44) (rmw_02_46).** Prepared according to the general procedure to give 95% of **3.44** as a colorless oil. $^1$H NMR (400 MHz, $CD_3OD$) δ 8.38-8.32 (comp, 2 H), 7.01-6.97 (comp, 2 H), 5.80-5.70 (m, 1 H), 5.32-5.23 (comp, 2 H), 5.10-5.05 (m, 1 H), 4.57-4.48 (m, 1 H), 4.29-4.23 (m, 1 H), 4.19 (m, 1 H), 4.00-3.93 (m, 1

H), 3.71-3.63 (comp, 3 H), 2.56-2.47 (m, 1 H), 2.36-2.28 (m, 1 H), 2.25-2.17 (m, 1 H), 1.71 (dt, *J* = 8.4, 3.4 Hz, 1 H), 1.43 (q, *J* = 9.6 Hz, 2 H), 1.31-1.27 (comp, 9 H), 1.07-0.85 (comp, 9 H).

**NMR Assignments.** $^1$H NMR (400 MHz, $CD_3OD$) δ 8.38-8.32 (comp, 2 H, C22-H), 7.01-6.97 (comp, 2 H, C21-H), 5.80-5.70 (m, 1 H, C16-H), 5.32-5.23 (comp, 2 H, C9-H, C17-H), 5.10-5.05 (m, 1 H, C17-H), 4.57-4.48 (m, 1 H, C11-H), 4.29-4.23 (m, 1 H, C8-H), 4.19 (m, 1 H), C4-H, 4.00-3.93 (m, 1 H, C8-H), 3.71-3.63 (comp, 3 H, C19-H), 2.56-2.47 (m, 1 H, C10-H), 2.36-2.28 (m, 1 H, C10-H), 2.25-2.17 (m, 1 H, C14-H), 1.71 (dt, *J* = 8.4, 3.4 Hz, 1 H, C15-H), 1.43 (q, *J* = 9.6 Hz, 2 H, C15-H), 1.31-1.27 (comp, 9 H, C1-H), 1.07-0.85 (comp, 9 H, C6-H).

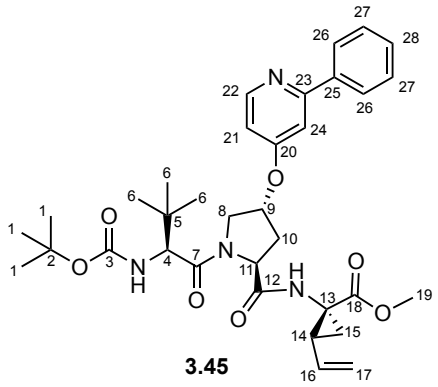

**3.45**

**Methyl (1*R*,2*R*)-1-((2*S*,4*R*)-1-((*S*)-2-((*tert*-butoxycarbonyl)amino)-3,3-dimethylbutanoyl)-4-((2-phenylpyridin-4-yl)oxy)pyrrolidine-2-carboxamido)-2-vinylcyclopropane-1-carboxylate (3.45) (rmw_02_46).** Prepared according to the general procedure to give 99% of **3.45** as a colorless oil. $^1$H NMR (400 MHz, $CD_3OD$) δ 8.44 (d, *J* = 5.7, 2.5 Hz, 1 H), 7.90-7.88 (comp, 2 H), 7.49-7.41 (comp, 3 H), 7.32 (dd, *J* = 9.2, 2.0 Hz, 1 H), 6.96 (dd, *J* = 5.6, 2.0 Hz, 1 H), 5.80-5.71 (m, 1 H), 5.34 (br, 1 H), 5.28-

5.23 (m, 1 H), 5.08 (dt, *J* = 10.2, 2.5 Hz, 1 H), 4.56 (t, *J* = 8.5 Hz, 1 H), 4.32 (d, *J* = 11.7 Hz, 1 H), 4.22-4.19 (m, 1 H), 4.00 (dd, *J* = 11.8, 3.1 Hz, 1 H), 3.67-3.64 (comp, 3 H), 2.54 (dd, *J* = 13.8, 7.6 Hz, 1 H), 2.39-2.30 (m, 1 H), 2.24-2.17 (m, 1 H), 1.71 (dt, *J* = 8.3, 4.2 Hz, 1 H), 1.45-1.40 (comp, 3 H), 1.34-1.24 (comp, 9 H), 1.02 (d, *J* = 25.6 Hz, 9 H).

**NMR Assignments**. $^{1}$H NMR (400 MHz, $CD_3OD$) δ 8.44 (d, *J* = 5.7, 2.5 Hz, 1 H, C22-H), 7.90-7.88 (comp, 2 H, C26-H), 7.49-7.41 (comp, 3 H, C27-H, C28-H), 7.32 (dd, *J* = 9.2, 2.0 Hz, 1 H, C24-H), 6.96 (dd, *J* = 5.6, 2.0 Hz, 1 H, C21-H), 5.80-5.71 (m, 1 H, C16-H), 5.34 (br, 1 H, C9-H), 5.28-5.23 (m, 1 H, C17-H), 5.08 (dt, *J* = 10.2, 2.5 Hz, 1 H, C17-H), 4.56 (t, *J* = 8.5 Hz, 1 H, C11-H), 4.32 (d, *J* = 11.7 Hz, 1 H, C8-H), 4.22-4.19 (m, 1 H, C4-H), 4.00 (dd, *J* = 11.8, 3.1 Hz, 1 H, C8-H), 3.67-3.64 (comp, 3 H, C19-H), 2.54 (dd, *J* = 13.8, 7.6 Hz, 1 H, C10-H), 2.39-2.30 (m, 1 H, C10-H), 2.24-2.17 (m, 1 H, C14-H), 1.71 (dt, *J* = 8.3, 4.2 Hz, 1 H, C15-H), 1.45-1.40 (comp, 3 H, C15-H), 1.34-1.24 (comp, 9 H, C1-H), 1.02 (d, *J* = 25.6 Hz, 9 H, C6-H).

**General procedure for hydrolysis of the tripeptide esters. Preparation of 3.1-3.6.** The tripeptide ester was dissolved in THF/MeOH (2:1) (3 mL) and 2 N NaOH (0.5 mL) was added. The mixture was stirred at room temperature overnight and concentrated to dryness. The residue was dissolved in EtOAc/$H_2O$ and adjusted to pH ~ 5 by addition of 1 N citric acid. The mixture was extracted with EtOAc (5 x 15 mL), washed with brine, dried ($MgSO_4$), filtered, and concentrated. Crude material was purified by RP HPLC with a gradient of 10% B to 100% B over 18 min.

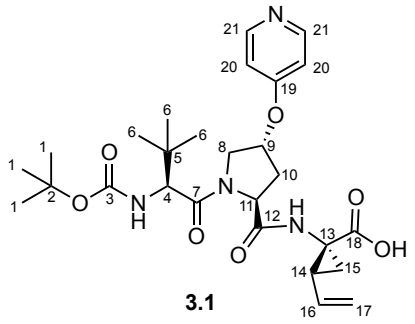

**3.1**

**(1*R*,2*R*)-1-((2*S*,4*R*)-1-((*S*)-2-((*tert*-butoxycarbonyl)amino)-3,3-dimethylbutanoyl)-4-(pyridin-4-yloxy)pyrrolidine-2-carboxamido)-2-vinylcyclopropane-1-carboxylic acid (3.1) (rmw_02_29).** Prepared according to the general procedure to yield 80% of **3.1** as a white powder. $^{1}$H NMR (600 MHz, $CD_3OD$) δ 8.55 (br, 2 H), 7.35 (br, 2 H), 5.86-5.79 (m, 1 H), 5.09-5.06 (m, 1 H), 4.55 (t, *J* = 8.7 Hz, 1 H), 4.34 (d, *J* = 12.3 Hz, 1 H), 4.12 (s, 1 H), 4.00 (dd, *J* = 3.6, 12.3 Hz, 1 H), 2.58-2.54 (m, 1 H), 2.46-2.43 (m, 1 H), 2.21-2.15 (m, 1 H), 1.69-1.67 (m, 1 H), 1.43-1.40 (comp, 3 H), 1.31 (s, 9 H), 1.01 (s, 9 H); $^{13}$C NMR (125 MHz, $CD_3OD$) δ 174.3, 173.4, 173.1, 157.9, 147.1, 135.6, 117.7, 114.3, 80.6, 80.5, 60.7, 60.3, 54.5, 40.7, 36.1, 35.6, 35.2, 28.6, 26.9, 23.4; HRMS (ESI) *m/z* 531.2816 [$C_{27}H_{38}N_4O_7$ (M+H) requires 531.2813].

**NMR Assignments.** $^{1}$H NMR (600 MHz, $CD_3OD$) δ 8.55 (br, 2 H, C21-H), 7.35 (br, 2 H, C20-H), 5.86-5.79 (m, 1 H, C16-H), 5.09-5.06 (m, 1 H, C9-H), 4.55 (t, *J* = 8.7 Hz, 1 H, C11-H), 4.34 (d, *J* = 12.3 Hz, 1 H, C8-H), 4.12 (s, 1 H, C4-H), 4.00 (dd, *J* = 3.6, 12.3 Hz, 1 H, C8-H), 2.58-2.54 (m, 1 H, C10-H), 2.46-2.43 (m, 1 H, C10-H), 2.21-2.15 (m, 1 H, C14-H), 1.69-1.67 (m, 1 H, C15-H), 1.43-1.40 (comp, 3 H, C15-H), 1.31 (s, 9 H, C6-H), 1.01 (s, 9 H, C1-H); $^{13}$C NMR (125 MHz, $CD_3OD$) δ 174.3 (C18), 173.4 (C7), 173.1 (C12), 157.9 (C3), 147.1 (C19), 135.6 (C16), 117.7 (C17), 114.3 (C20), 80.6 (C2), 80.5

(C9), 60.7 (C4), 60.3 (C11), 54.5 (C8), 40.7 (C13), 36.1 (C5), 35.6 (C10), 35.2 (C14), 28.6 (C1), 26.9 (C6), 23.4 (C15).

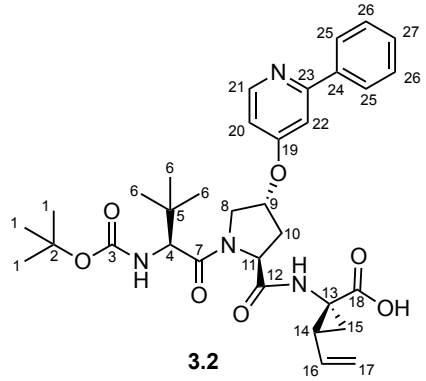

**3.2**

**(1*R*,2*R*)-1-((2*S*,4*R*)-1-((*S*)-2-((*tert*-butoxycarbonyl)amino)-3,3-dimethylbutanoyl)-4-((2-phenylpyridin-4-yl)oxy)pyrrolidine-2-carboxamido)-2-vinylcyclopropane-1-carboxylic acid (3.2) (rmw_02_45).** Prepared according to the general procedure to yield 74% of **3.2** as a white powder. $^{1}$H NMR (600 MHz, $CD_3OD$) δ 8.58 (d, *J* = 6.7 Hz, 1 H), 7.90-7.87 (comp, 3 H), 7.69 (d, *J* = 2.4 Hz, 1 H), 7.64-7.61 (comp, 2 H), 7.40 (dd, *J* = 2.1, 6.6 Hz, 1 H), 5.86-5.80 (m, 1 H), 5.54 (br, 1 H), 5.27-5.23 (m, 1 H), 5.09-5.05 (m, 1 H), 4.59 (t, *J* = 8.9 Hz, 1 H), 4.42 (d, *J* = 12.2 Hz, 1 H), 4.13 (s, 1 H), 4.02 (dd, *J* = 3.3, 12.2 Hz, 1 H), 2.64-2.60 (m, 1 H), 2.50-2.46 (m, 1 H), 2.21-2.15 (m, 1 H), 1.70-1.65 (m, 1 H), 1.45-1.41 (comp, 3 H), 1.26 (s, 9 H), 1.01 (s, 9 H); $^{13}$C NMR (125 MHz, $CD_3OD$) δ 174.3, 173.4, 173.2, 157.9, 146.7, 146.1, 135.6, 132.8, 130.6, 128.9, 117.7, 112.6, 80.5, 80.2, 60.7, 60.3, 54.6, 40.7, 36.1, 35.7, 35.2, 38.6, 26.9, 23.4; HRMS (ESI) *m/z* 607.3116 [$C_{33}H_{42}N_4O_7$ (M+H) requires 607.3126].

**NMR Assignments.** $^{1}$H NMR (600 MHz, $CD_3OD$) δ 8.58 (d, *J* = 6.7 Hz, 1 H, C21-H), 7.90-7.87 (comp, 3 H, C25-H), 7.69 (d, *J* = 2.4 Hz, 1 H, C22-H), 7.64-7.61 (comp, 2

H, C26-H, C27-H), 7.40 (dd, *J* = 2.1, 6.6 Hz, 1 H, C20-H), 5.86-5.80 (m, 1 H, C16-H), 5.54 (br, 1 H, C9-H, 5.27-5.23 (m, 1 H, C17-H), 5.09-5.05 (m, 1 H, C17-H), 4.59 (t, *J* = 8.9 Hz, 1 H, C11-H), 4.42 (d, *J* = 12.2 Hz, 1 H, C8-H), 4.13 (s, 1 H, C4-H), 4.02 (dd, *J* = 3.3, 12.2 Hz, 1 H, C8-H), 2.64-2.60 (m, 1 H, C10-H), 2.50-2.46 (m, 1 H, C10-H), 2.21-2.15 (m, 1 H, C14-H), 1.70-1.65 (m, 1 H, C15-H), 1.45-1.41 (comp, 3 H, C15-H), 1.26 (s, 9 H, C1-H), 1.01 (s, 9 H, C6-H); $^{13}$C NMR (125 MHz, $CD_3OD$) δ 174.3 (C18), 173.4 (C7), 173.2 (C12), 157.9 (C3), 146.7 (C19), 146.1 (C21), 135.6 (C16), 132.8 (C23), 130.6 (C26, C27), 128.9 (C25), 117.7 (C17), 112.6 (C20), 80.5 (C2), 80.2 (C9), 60.7 (C4), 60.3 (C11), 54.6 (C8), 40.7 (C13), 36.1 (C5), 35.7 (C10), 35.2 (C14), 38.6 (C1), 26.9 (C6), 23.4 (C5).

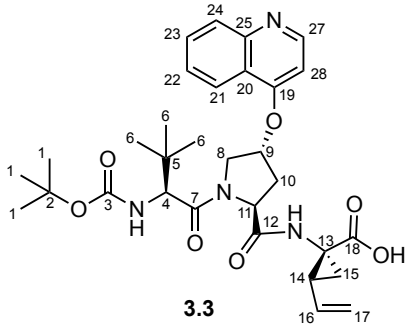


**3.3**

**(1*R*,2*R*)-1-((2*S*,4*R*)-1-((*S*)-2-((*tert*-butoxycarbonyl)amino)-3,3-dimethylbutanoyl)-4-(quinolin-4-yloxy)pyrrolidine-2-carboxamido)-2-vinylcyclopropane-1-carboxylic acid (3.3) (rmw_02_30).** Prepared according to the general procedure to yield 77% of **3.3** as a white powder. $^1$H NMR (400 MHz, $C_6D_6$) δ 8.98 (d, *J* = 6.3 Hz, 1 H), 8.45 (d, *J* = 8.5 Hz, 1 H), 8.07-8.02 (comp, 2 H), 7.78-7.75 (m, 1 H), 7.49 (d, *J* = 6.6 Hz, 1 H), 5.87-5.80 (m, 1 H), 5.68 (br, 1 H), 5.27-5.24 (m, 1 H), 5.10-5.07

(m, 1 H), 4.68-4.65 (comp, 2 H), 4.11 (s, 1 H), 4.07 (dd, *J* = 3.2, 12.2 Hz, 1 H), 2.78-2.74 (m, 1 H), 2.59-2.53 (m, 1 H), 2.21-2.16 (m, 1 H), 1.70-1.67 (m, 1 H). 1.45-1.42 (comp, 3 H), 1.14 (s, 9 H), 1.04 (s, 9 H).;$^{13}$C NMR (125 MHz, $CD_3OD$) δ 174.2, 173.6, 173.4, 167.5, 158.0, 148.4, 142.4, 135.6, 135.5, 129.6, 124.6, 122.8, 122.7, 117.8, 104.1, 81.2, 80.3, 61.1, 60.3, 54.7, 40.7, 36.7, 35.6, 35.3, 28.9, 28.5, 26.9; HRMS (ESI) *m/z* 581.2971 [$C_{31}H_{40}N_4O_7$ (M+H) requires 581.2970].

**NMR Assignments.** $^1$H NMR (400 MHz, $C_6D_6$) δ 8.98 (d, *J* = 6.3 Hz, 1 H, C26-H), 8.45 (d, *J* = 8.5 Hz, 1 H, C24-H), 8.07-8.02 (comp, 2 H, C21-H, C22-H), 7.78-7.75 (m, 1 H, C23-H), 7.49 (d, *J* = 6.6 Hz, 1 H, C27-H), 5.87-5.80 (m, 1 H, C16-H), 5.68 (br, 1 H, C9-H), 5.27-5.24 (m, 1 H, C17-H), 5.10-5.07 (m, 1 H, C17-H), 4.68-4.65 (comp, 2 H, C8-H, C11-H), 4.11 (s, 1 H, C4-H), 4.07 (dd, *J* = 3.2, 12.2 Hz, 1 H, C8-H), 2.78-2.74 (m, 1 H, C10-H), 2.59-2.53 (m, 1 H, C10-H), 2.21-2.16 (m, 1 H, C14-H), 1.70-1.67 (m, 1 H, C15-H). 1.45-1.42 (comp, 3 H, C15-H), 1.14 (s, 9 H, C1-H), 1.04 (s, 9 H, C6-H); $^{13}$C NMR (125 MHz, $CD_3OD$) δ 174.2 (C18), 173.6 (C7), 173.4 (C12), 167.5 (C19), 158.0 (C3), 148.4 (C19), 142.4 (C25), 135.6 (C22), 135.5 (C16), 129.6 (C23), 124.6 (C24), 122.8 (C21), 122.7 (C20), 117.8 (C17), 104.1 (C27), 81.2 (C2), 80.3 (C9), 61.1 (C4), 60.3 (C11), 54.7 (C8), 40.7 (C13), 36.7 (C5), 35.6 (C10), 35.3 (C14), 28.9 (C15), 28.5 (C1), 26.9 (C6).

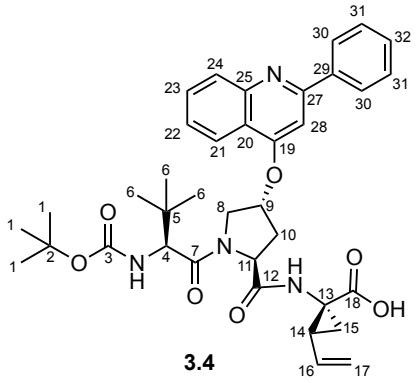

**3.4**

**(1*R*,2*R*)-1-((2*S*,4*R*)-1-((*S*)-2-((*tert*-butoxycarbonyl)amino)-3,3-Dimethylbutanoyl)-4-((2-phenylquinolin-4-yl)oxy)pyrrolidine-2-carboxamido)-2-vinylcyclopropane-1-carboxylic acid (3.4) (rmw_02_34).** Prepared according to the general procedure to yield 71% of **3.4** as a white powder. $^1$H NMR (400 MHz, $CD_3OD$) δ 8.43 (d, *J* = 8.3 Hz, 1 H), 8.16 (d, *J* = 8.5 Hz, 1 H), 8.10-8.08 (m, 2 H), 8.05-8.02 (m, 1 H), 7.76-7.69 (comp, 5 H), 5.87-5.80 (comp, 2 H), 5.26 (dd, *J* = 1.5 Hz, 17.2 Hz, 1 H), 5.08 (dd, *J* = 2.2 Hz, 10.4 Hz, 1 H), 4.71-4.67 (comp, 2 H), 4.15 (s, 1 H), 4.09 (dd, *J* = 3.1 Hz, 12.2 Hz, 1 H), 2.82-2.78 (m, 1 H), 2.60-2.54 (m, 1 H), 2.22-2.17 (m, 1 H), 1.71-1.68 (m, 1 H), 1.46-1.42 (comp, 3 H), 1.16 (s 9 H), 1.04 (s, 9 H); HRMS (ESI) *m/z* 655.3131 [$C_{37}H_{44}N_4O_7$ (M-H) requires 655.3137].

**NMR Assignments**. $^1$H NMR (400 MHz, $CD_3OD$) δ 8.43 (d, *J* = 8.3 Hz, 1 H, C24-H), 8.16 (d, *J* = 8.5 Hz, 1 H, C21-H), 8.10-8.08 (m, 2 H, C30-H), 8.05-8.02 (m, 1 H, C22-H), 7.76-7.69 (comp, 5 H, C23-H, C31-H, C32-H), 5.87-5.80 (comp, 2 H, C16-H, C9-H), 5.26 (dd, *J* = 1.5 Hz, 17.2 Hz, 1 H, C17-H), 5.08 (dd, *J* = 2.2 Hz, 10.4 Hz, 1 H, C17-H), 4.71-4.67 (comp, 2 H, C8-H, C11-H), 4.15 (s, 1 H, C4-H, C4-H), 4.09 (dd, *J* = 3.1 Hz, 12.2 Hz, 1 H, C8-H), 2.82-2.78 (m, 1 H, C10-H), 2.60-2.54 (m, 1 H, C10-H), 2.22-2.17 (m, 1

H, C14-H), 1.71-1.68 (m, 1 H, C14-H), 1.46-1.42 (comp, 3 H, C15-H), 1.16 (s 9 H, C1-H), 1.04 (s, 9 H, C6-H).

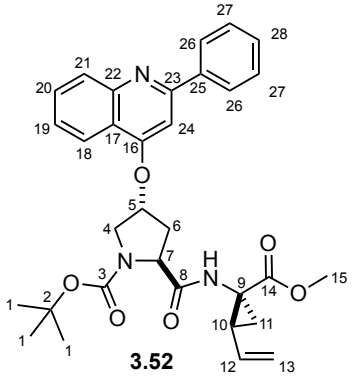

**3.52**

***tert*-Butyl (2*S*,4*R*)-2-(((1*R*,2*S*)-1-(methoxycarbonyl)-2-vinylcyclopropyl)carbamoyl)-4-((2-phenylquinolin-4-yl)oxy)pyrrolidine-1-carboxylate (3.52) (rmw_02_108).** Dipeptide brosylate **3.51** (589 mg, 1.02 mmol), was dissolved in 10 mL NMP. Hydroxyquinoline **3.23** (340 mg, 1.5 mmol) and $Cs_2CO_3$ (590 mg, 2.04 mmol) were added, and the mixture was heated at 70 °C until the brosylate was consumed by TLC (2 h). The mixture was cooled to room temperature and poured into EtOAc (30 mL). The mixture was washed with $H_2O$ (3 x 20 mL), saturated $NaHCO_3$ (2 x 20 mL), 1 N NaOH (1 x 20 mL), $H_2O$ (2 x 20 mL), and brine (1 x 20 mL). The organic layer was dried over $MgSO_4$, filtered, and concentrated under reduced pressure. The crude residue was purified by flash chromatography eluting with $CH_2Cl_2$: MeOH (9:1) to give 550 mg (96%) of **3.52** as an off-white solid. $^1$H NMR (400 MHz, $CD_3OD$) δ 8.65 (d, *J* = 8.2 Hz, 1 H), 8.10-8.09 (comp, 2 H), 8.06 (d, *J* = 8.5 Hz,1 H), 7.79-7.76 (m 1 H), 7.58-7.50 (comp, 4 H), 7.41 (s, 1 H), 5.78 (dt, *J* = 9.1 Hz, 17.5 Hz, 1 H), 5.53 (br, 1 H), 5.33 (d, *J* = 17.2 Hz, 1 H), 5.14 (t, *J* = 10.2 Hz, 1 H), 4.49-4.45 (m, 1 H), 4.02-3.95 (comp, 2 H), 3.69 (s, 3 H), 2.80-2.76 (m, 1 H),

2.50-2.46 (m, 1 H), 2.23 (q, $J$ = 8.86, 1 H), 2.16 1.47 (s, 9 H). $^{13}$C NMR (100 MHz, $CD_3OD$) δ 174.7, 170.7, 170.4, 160.6, 159.4, 155.0, 154.7, 148.9, 139.7, 133.7, 130.3, 129.3, 127.8, 127.6, 125.6, 121.3, 120.4, 116.9, 100.1, 80.7, 80.5, 59.2, 58.9, 52.2, 39.5, 35.3, 29.2, 27.2, 26.9.

**NMR Assignments.** $^1$H NMR (400 MHz, $CD_3OD$) δ 8.65 (d, $J$ = 8.2 Hz, 1 H, C21-H), 8.10-8.09 (comp, 2 H, C26-H), 8.06 (d, $J$ = 8.5 Hz, 1 H, C18-H), 7.79-7.76 (m 1 H, C19-H), 7.58-7.50 (comp, 4 H, C27-H, C28-H, C20-H), 7.41 (s, 1 H, C24-H), 5.78 (dt, $J$ = 9.1 Hz, 17.5 Hz, 1 H, C12-H), 5.53 (br, 1 H, C5-H), 5.33 (d, $J$ = 17.2 Hz, 1 H, C13-H), 5.14 (t, $J$ = 10.2 Hz, 1 H, C7-H), 4.49-4.45 (m, 1 H, C4-H), 4.02-3.95 (comp, 2 H, C4-H, C6-H), 3.69 (s, 3 H, C15-H), 2.80-2.76 (m, 1 H, C6-H), 2.50-2.46 (m, 1 H, C10-H), 2.23 (q, $J$ = 8.86, 1 H, C10-H), 2.16 (comp, 2 H, C11-H), 1.47 (s, 9 H, C1-H). $^{13}$C NMR (100 MHz, $CD_3OD$) δ 174.7 (C14), 170.7 (C16), 170.4 (C8), 160.6 (C16), 159.4 (C3), 155.0 (C23), 154.7 (C25), 148.9 (C22), 139.7 (C19), 133.7 (C12), 130.3 (C20), 129.3 (C27), 127.8 (C28), 127.6 (C26), 125.6 (C21), 121.3 (C18), 120.4 (C17), 116.9 (C13), 100.1 (C24), 80.7 (C2), 80.5 (C5), 59.2 (C7), 58.9 (C4), 52.2 (C15), 39.5 (C9), 35.3 (C6), 29.2 (C1), 27.2 (C11), 26.9 (C10).

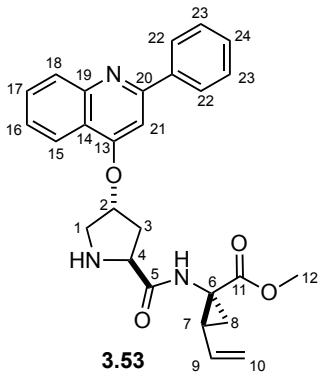

**3.53**

**Methyl (1*R*,2*S*)-1-((2*S*,4*R*)-4-((2-phenylquinolin-4-yl)oxy)pyrrolidine-2-carboxamido)-2-vinylcyclopropane-1-carboxylate (3.53) (rmw_02_109).** Boc-protected dipeptide **3.52** (550 mg, 0.98 mmol) was dissolved in neat TFA (5 mL) and stirred at room temperature until al starting material was consumed by TLC (~ 1 h). The mixture was concentrated under reduced pressure to half-volume and the concentrated mixture was neutralized with saturated $NaHCO_3$. The solution was extracted with $CH_2Cl_2$ (5 x 30 mL), dried ($MgSO_4$), filtered, and concentrated under reduced pressure to give 435 mg (93%) of **3.52** as an off-white solid that was used without further purification. $^1$H NMR (400 MHz, $CD_3OD$) δ; 8.27 (d, *J* = 8.2 Hz, 1 H), 8.07-8.00 (comp, 3 H), 7.72 (m, 1 H), 7.53-7.46 (comp, 4 H), 7.21 (s, 1 H), 5.85-5.76 (m, 1 H), 5.43 (d, *J* = 17.1 Hz, 1 H), 5.28 (br, 1 H), 5.20 (d, *J* = 10.4 Hz, 1 H), 4.16-4.07 (comp, 2 H), 3.69 (s, 3 H), 3.37-3.33 (comp, 2 H), 2.75-2.71 (m, 1 H), 2.51-2.40 (comp, 2 H), 2.15-2.11 (comp, 2 H).

**NMR Assignments.** $^1$H NMR (400 MHz, $CD_3OD$) δ; 8.27 (d, *J* = 8.2 Hz, 1 H, C18-H), 8.07-8.00 (comp, 3 H, C22-H, C15-H), 7.72 (m, 1 H, C16-H), 7.53-7.46 (comp, 4 H, C23-H, C24-H, C17-H), 7.21 (s, 1 H, C21-H), 5.85-5.76 (m, 1 H, C9-H), 5.43 (d, *J* = 17.1

Hz, 1 H, C10-H), 5.28 (br, 1 H, C2-H), 5.20 (d, $J$ = 10.4 Hz, 1 H, C10-H), 4.16-4.07 (comp, 2 H, C1-H), 3.69 (s, 3 H, C12-H), 3.37-3.33 (comp, 2 H, C6-H), 2.75-2.71 (m, 1 H, C4-H), 2.51-2.40 (comp, 2 H, C7-H), 2.15-2.11 (comp, 2 H, C8-H).

**General procedure for hydrolysis of the tripeptide esters. Preparation of 3.46-3.49.** The tripeptide ester was dissolved in THF/MeOH (2:1) (3 mL) and 2 N NaOH (0.5 mL) was added. The mixture was stirred at room temperature overnight and concentrated to dryness. The residue was dissolved in EtOAc/$H_2O$ and adjusted to pH ~ 5 by addition of 1 N citric acid. The mixture was extracted with EtOAc (5 x 15 mL), washed with brine, dried ($MgSO_4$), filtered, and concentrated. Crude material was purified by RP HPLC with a gradient of 10% B to 100% B over 18 min.

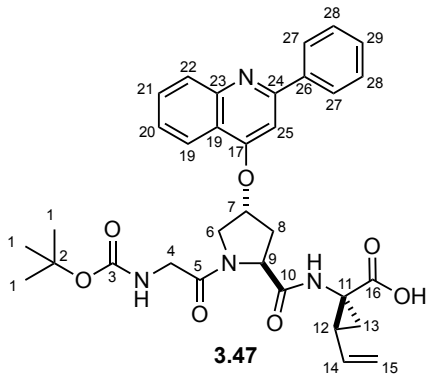

**3.47**

**(1*R*,2*S*)-1-((2*S*,4*R*)-1-((*tert*-Butoxycarbonyl)glycyl)-4-((2-phenylquinolin-4-yl)oxy)pyrrolidine-2-carboxamido)-2-vinylcyclopropane-1-carboxylic acid (3.47) (rmw_02_120).** Prepared according to the general procedure to yield 60% of **3.47** as a white powder. The crude material was purified by preparative RP HPLC with a gradient of 5% B to 95% B over 18 min. $^1$H NMR (600 MHz, $CD_3OD$) δ 8.45 (d, $J$ = 8.2 Hz, 1 H), 8.21-8.19 (m, 1 H), 8.10-8.07 (comp, 3 H), 7.85-7.82 (m, 1 H), 7.77-7.72 (comp, 4 H),

5.87-5.78 (comp, 2 H), 5.32-5.30 (m, 1 H), 5.12-5.09 (m, 1 H), 4.64 (t, *J* = 8.2 Hz, 1 H), 4.26 (d, *J* = 12.3 Hz, 1 H), 4.20 (dd, *J* = 3.8 Hz, 12.2 Hz, 1 H), 3.99-3.96 (m, 1 H), 3.80 (d, *J* = 16.9 Hz, 1 H), 2.85-2.80 (m, 1 H), 2.61-2.55 (m, 1 H), 2.29-2.25 (m, 1 H), 1.49-1.44 (comp, 2 H), 1.38 (s, 9 H); $^{13}$C NMR (150 MHz, $CD_3OD$) δ 174.4, 173.6, 173.4, 171.2, 159.1, 158.6, 135.8, 135.7, 134.0, 133.8, 130.7, 130.0, 129.7, 127.7, 124.5, 121.6, 117.8, 103.4, 81.0, 80.7, 60.7, 53.1, 43.8, 40.7, 35.8, 34.8, 28.6, 28.4; HRMS (ESI) *m/z* 601.2649 [$C_{33}H_{36}N_4O_7$ (M+H) requires 601.2657].

**NMR Assignments.** $^1$H NMR (600 MHz, $CD_3OD$) δ 8.45 (d, *J* = 8.2 Hz, 1 H, C22-H), 8.21-8.19 (m, 1 H, C20-H), 8.10-8.07 (comp, 3 H, C19-H, C27-H), 7.85-7.82 (m, 1 H, C21-H), 7.77-7.72 (comp, 4 H, C25-H, C28-H, C29-H), 5.87-5.78 (comp, 2 H, C14-H, C7-H), 5.32-5.30 (m, 1 H, C15-H), 5.12-5.09 (m, 1 H, C15-H), 4.64 (t, *J* = 8.2 Hz, 1 H, C9-H), 4.26 (d, *J* = 12.3 Hz, 1 H, C6-H), 4.20 (dd, *J* = 3.8 Hz, 12.2 Hz, 1 H, C6-H), 3.99-3.96 (m, 1 H, C8-H), 3.80 (d, *J* = 16.9 Hz, 1 H, C8-H), 2.85-2.80 (m, 1 H, C4-H), 2.61-2.55 (m, 1 H, C4-H), 2.29-2.25 (m, 1 H, C12-H), 1.49-1.44 (comp, 2 H, C13-H), 1.38 (s, 9 H, C1-H); $^{13}$C NMR (150 MHz, $CD_3OD$) δ 174.4 (C16), 173.6 (C5), 173.4 (C10), 171.2 (C17), 159.1 (C3), 158.6 (C24), 135.8 (C23), 135.7 (C14), 134.0 (C26), 133.8 (C19), 130.7 (C20), 130.0 (C29), 129.7 (C28), 127.7 (C27), 124.5 (C21), 121.6 (C22), 117.8 (C15), 103.4 (C25), 81.0 (C2), 80.7 (C7), 60.7 (C9), 53.1 (C6), 43.8 (C4), 40.7 (C11), 35.8 (C8), 34.8 (C12), 28.6 (C1), 28.4 (C13).

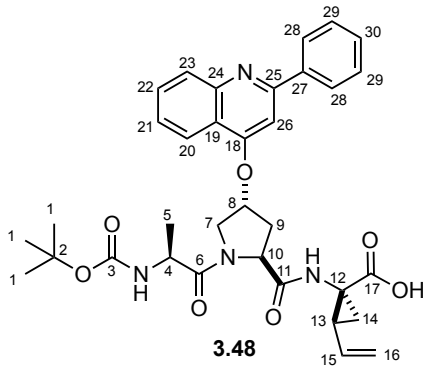

**3.48**

**(1*R*,2*S*)-1-((2*S*,4*R*)-1-((*tert*-Butoxycarbonyl)-*L*-alanyl)-4-((2-phenylquinolin-4-yl)oxy)pyrrolidine-2-carboxamido)-2-vinylcyclopropane-1-carboxylic acid (3.48) (rmw_02_121).** Prepared according to the general procedure to yield 88% of **3.48** as a white powder. The crude material was purified by preparative RP HPLC with a gradient of 5% B to 95% B over 18 min. $^{1}$H NMR (600 MHz, $CD_3OD$) δ 8.48 (d, *J* = 8.3 Hz 1 H), 8.19-8.17 (m, 1 H), 8.09-8.04 (comp, 2 H), 7.80-7.78 (m, 1 H), 7.75-7.70 (comp, 5 H), 5.86-5.79 (comp, 2 H), 5.30 (dd, *J* = 2.4 Hz, 17.2 Hz, 1 H), 5.10 (dd, *J* = 2.3 Hz, 10.4 Hz, 1 H), 4.70-4.66 (comp, 2 H), 4.35 (q, *J* = 6.9 Hz, 1 H), 4.11 (dd, *J* = 3.5 Hz, 12.3 Hz, 1 H), 2.85-2.81 (m, 1 H), 2.59-2.55 (m, 1 H), 2.21 (q, *J* = 8.8 Hz, 1 H), 1.73-1.69 (m, 1 H), 1.44-1.41 (comp, 2.48 H), 1.31-1.26 (comp, 3.27 H), 1.20 (s, 6 H); $^{13}$C NMR (150 MHz, $CD_3OD$) δ 175.3, 174.3, 173.4, 171.0, 159.2, 157.7, 135.6, 133.6, 130.6, 129.9, 124.7, 122.4, 121.7, 117.8, 103.4, 81.1, 80.2, 60.4, 53.7, 40.7, 35.7, 34.9, 35.7, 34.9, 30.7, 28.7, 28.5, 23.3, 17.0; HRMS (ESI) *m/z* 615.2807 [$C_{33}H_{36}N_4O_7$ (M+H) requires 615.2813].

**NMR Assignments.** $^{1}$H NMR (600 MHz, $CD_3OD$) δ 8.48 (d, *J* = 8.3 Hz, 1 H, C23-H), 8.19-8.17 (m, 1 H, C20-H), 8.09-8.04 (comp, 2 H, C28-H), 7.80-7.78 (m, 1 H, C21-H), 7.75-7.70 (comp, 5 H, C22-H, C26-H, C29-H, C30-H), 5.86-5.79 (comp, 2 H, C15-H, C8-

H), 5.30 (dd, *J* = 2.4 Hz, 17.2 Hz, 1 H, C16-H), 5.10 (dd, *J* = 2.3 Hz, 10.4 Hz, 1 H, C16-H), 4.70-4.66 (comp, 2 H, C7-H, C10-H), 4.35 (q, *J* = 6.9 Hz, 1 H, C4-H), 4.11 (dd, *J* = 3.5 Hz, 12.3 Hz, 1 H, C7-H), 2.85-2.81 (m, 1 H, C9-H), 2.59-2.55 (m, 1 H, C9-H), 2.21 (q, *J* = 8.8 Hz, 1 H, C13-H), 1.73-1.69 (m, 1 H, C14-H), 1.44-1.41 (comp, 3 H, C5-H), 1.31-1.26 (comp, 3 H, C14-H), 1.20 (s, 9 H, C1-H);

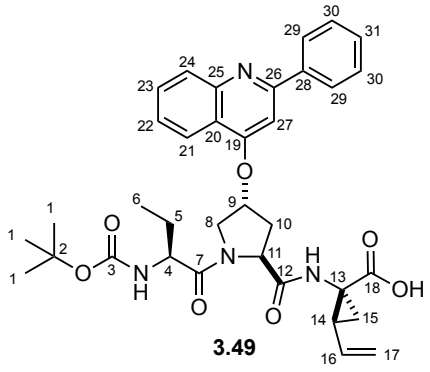

**3.49**

**(1*R*,2*S*)-1-((2*S*,4*R*)-1-((*S*)-2-((*tert*-Butoxycarbonyl)amino)butanoyl)-4-((2-phenylquinolin-4-yl)oxy)pyrrolidine-2-carboxamido)-2-vinylcyclopropane-1-carboxylic acid (3.49) (rmw_02_122).** Prepared according to the general procedure to yield 90% of **3.49** as a white powder. The crude material was purified by preparative RP HPLC with a gradient of 5% B to 95% B over 18 min. $^{1}$H NMR (600 MHz, $CD_3OD$) δ 8.45 (d, *J* = 8.0 Hz, 1 H), 8.16 (d, *J* = 8.5 Hz, 1 H), 8.09-8.08 (comp, 2 H), 8.04-8.01 (m, 1 H), 7.77-7.74 (m, 1 H), 7.73-7.66 (comp, 4 H), 5.86-5.80 (comp, 2 H), 5.28 (dd, *J* = 1.8 Hz, 17.2 Hz, 1 H), 5.10 (dd, *J* = 1.8 Hz, 10.3 Hz, 1 H), 4.72-4.68 (comp, 2 H), 4.18 (t, *J* = 7.2 Hz, 1 H), 4.12-4.09 (dd, *J* = 3.4 Hz, 12.3 Hz, 1 H), 2.84-2.80 (m, 1 H), 2.59-2.54 (m, 1 H), 2.22 (q, *J* = 8.8 Hz, 1 H), 1.77-1.73 (m, 1 H), 1.71-1.69 (m, 1 H), 1.65-1.58 (m, 1 H), 1.46-1.42 (comp, 2.85 H), 1.18 (s, 9 H), 0.98 (t, *J* = 7.4 Hz, 3 H); $^{13}$C NMR (150 MHz, $CD_3OD$)

δ 174.6, 174.3, 173.4, 159.4, 157.9, 135.6, 135.2, 133.3, 130.6, 129.9, 129.3, 124.5, 121.7, 117.8, 103.3, 80.9, 80.2, 60.4, 55.5, 53.9,, 38.0, 35.8, 35.0, 32.9, 32.9, 28.7, 28.4, 25.7, 23.3, 10.6; HRMS (ESI) *m/z* 615.2807 [$C_{33}H_{36}N_4O_7$ (M+H) requires 615.2813].

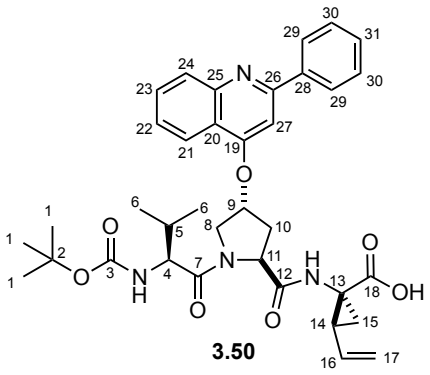

**3.50**

**(1*R*,2*S*)-1-((2*S*,4*R*)-1-((*tert*-butoxycarbonyl)-*L*-valyl)-4-((2-phenylquinolin-4-yl)oxy)pyrrolidine-2-carboxamido)-2-vinylcyclopropane-1-carboxylic acid (3.50) (rmw_02_123).** Prepared according to the general procedure to yield 85% of **3.50** as a white powder. The crude material was purified by preparative RP HPLC with a gradient of 5% B to 95% B over 18 min. $^1$H NMR (600 MHz, $CD_3OD$) δ 8.45 (d, *J* = 7.9 Hz, 1 H), 8.17 (d, *J* = 8.4 Hz, 1 H), 8.09-8.08 (comp, 2 H), 8.07-8.04 (m, 1 H), 7.79-7.77 (m, 1 H), 7.74-7.69 (comp, 4 H), 5.86-5.80 (comp, 2 H), 5.27 (dd, *J* = 2.4 Hz, 16.9 Hz, 1 H), 5.09 (dd, *J* = 1.8 Hz, 10.3 Hz, 1 H), 4.80 (d, *J* = 11.5 Hz, 1 H), 4.70-4.68 (m, 1 H), 4.12 (dd, *J* = 3.4 Hz, 12.3 Hz, 1 H), 3.96 (d, *J* = 9 Hz, 1 H), 2.85-2.80 (m, 1 H), 2.59-2.55 (m, 1 H), 2.24-2.19 (q, *J* = 8.8 Hz, 1 H), 2.00-1.95 (m, 1 H), 1.70 (dd, *J* = 5.2 Hz, 8.0 Hz, 1 H), 1.47-1.44 (m, 1 H?), 1.12 (s, 9 H), 1.00 (d, *J* = 6.7 Hz, 3 H), 0.97 (d, *J* = 6.7 Hz, 3 H); $^{13}$C NMR (150 MHz, $CD_3OD$) δ 174.3, 174.3, 173.5, 160.7, 159.3, 158.0, 135.6, 133.6, 130.7, 130.0, 129.9, 129.5, 124.6, 121.7, 117.8, 103.5, 81.3, 80.1, 60.4, 59.9, 54.1, 43.8, 40.7, 35.9, 35.2,

31.6, 28.7, 28.5, 28.3, 23.3, 19.7, 19.5, 19.2; HRMS (ESI) *m/z* 643.3117 [$C_{36}H_{42}N_4O_7$ (M+H) requires 643.3126].

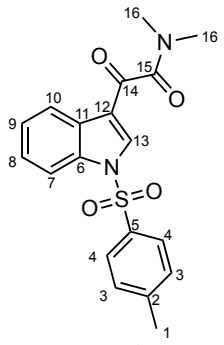

**4.58**

***N*,*N*-Dimethyl-2-oxo-2-(1-tosyl-1*H*-indol-3-yl)acetamide (4.58) (rmw_03_257).** Indole glyoxamide **4.57** (200 mg, 0.92 mmol) was dissolved in 5 mL DMF and cooled to 0 °C. NaH (55 mg, 1.39 mmol) was added and the mixture was stirred at 0 °C for 30 min. TsCl (264 mg, 1.38 mmol) was added and the mixture was allowed to warm to room temperature with stirring overnight. The solution was quenched with 2 N HCl (10 mL), extracted with EtOAc (3 x 20 mL), dried over $MgSO_4$, filtered, and concentrated under reduced pressure. The crude residue was purified by flash chromatography eluting with 2:1 hexanes/EtOAc to give 171 mg (50%) of **4.58** as a white solid. $^1$H NMR (400 MHz, DMSO-$d_6$) δ 8.55 (s, 1 H), 8.17 (d, *J* = 7.7 Hz, 1 H), 8.08 (d, *J* = 8.4 Hz, 2 H), 7.99 (d, *J* = 8.7 Hz, 1 H), 7.51-7.42 (comp, 4 H), 3.04 (s, 3 H), 2.94 (s, 3 H), 235 (s, 3 H). $^{13}$C NMR (125 MHz, DMSO-$d_6$) δ 187.6, 166.1, 147.2, 136.5, 134.5, 133.6, 131.1, 128.0, 126.8, 125.8, 122.4, 117.3, 113.8, 37.2, 34.3, 21.6. HRMS (ESI) *m/z* 393.0880 [$C_{19}H_{18}N_2O_4$ (M+Na) requires 393.0879].

**NMR Assignments**. $^{1}$H NMR (400 MHz, DMSO-$d_6$) δ 8.55 (s, 1 H, C13-H), 8.17 (d, $J$ = 7.7 Hz, 1 H, C10-H), 8.08 (d, $J$ = 8.4 Hz, 2 H, C4-H, C8-H, C9-H), 7.99 (d, $J$ = 8.7 Hz, 1 H, C7-H), 7.51-7.42 (comp, 4 H, C3-H, ), 3.04 (s, 3 H, C16-H), 2.94 (s, 3 H, C16-H), 235 (s, 3 H, C1-H). $^{13}$C NMR (125 MHz, DMSO-$d_6$) δ 187.6 (C14), 166.1 (C15), 147.2 (C5), 136.5 (C13), 134.5 (C6), 133.6 (C2), 131.1 (C3), 128.0 (C4), 126.8 (C8), 125.8 (C9), 122.4 (C10), 117.3 (C12), 113.8 (C7), 37.2 (C16), 34.3 (C16), 21.6 (C1).

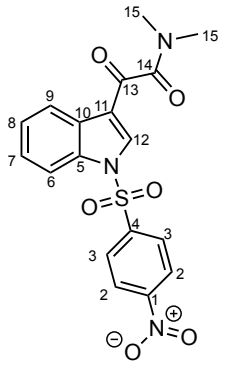

**4.59**

***N*,*N*-Dimethyl-2-(1-((4-nitrophenyl)sulfonyl)-1*H*-indol-3-yl)-2-oxoacetamide (4.59) (rmw_04_23)** Indole glyoxamide **4.57** (1.00 g, 4.62 mmol) was dissolved in 20 mL $CH_2Cl_2$. DMAP (28 mg, 0.23 mmol) and DIPEA (1.19g, 9.24 mmol) were added and the mixture was stirred at room temperature overnight. The mixture was washed with bring (3 x 30 mL), dried over $MgSO_4$, filtered, and concentrated under reduced pressure. The crude residue was purified by flash chromatography eluting with a gradient of 3:1 Hex/EtOAc to 100% EtOAc to give 1.42g (77%) of **4.59** as a yellow solid. $^{1}$H NMR (400 MHz, DMSO-$d_6$) δ 8.64 (s, 1 H), 8.51-8.47 (comp, 2 H), 8.44-8.41 (comp, 2 H), 8.18 (d, $J$ = 7.8 Hz, 1 H), 8.04 (d, $J$ = 8.3 Hz, 1 H), 7.55-7.45 (comp, 2 H), 3.05 (s, 3 H), 2.95 (s, 3 H). $^{13}$C NMR (125 MHz, DMSO-$d_6$) δ 187.6, 165.9, 151.8, 141.3, 136.5, 134.5, 129.7, 127.2, 126.9,

126.2, 125.9, 122.6, 118.0, 113.7, 37.2, 34.3. HRMS (ESI) *m/z* 424.0574 [$C_{18}H_{15}N_3O_6$ (M+Na) requires 424.0574].

**NMR Assignments**. $^1$H NMR (400 MHz, DMSO-$d_6$) δ 8.64 (s, 1 H, C12-H), 8.51-8.47 (comp, 2 H, C2-H), 8.44-8.41 (comp, 2 H, C3-H), 8.18 (d, $J$ = 7.8 Hz, 1 H, C6-H), 8.04 (d, $J$ = 8.3 Hz, 1 H, C9-H), 7.55-7.45 (comp, 2 H, C7-H, C8-H), 3.05 (s, 3 H, C15-H), 2.95 (s, 3 H, C15-H). $^{13}$C NMR (125 MHz, DMSO-$d_6$) δ 187.6 (C13), 165.9 (C14), 151.8 (C1), 141.3 (C4), 136.5 (C12), 134.5 (C5), 129.7 (C2), 127.2 (C8), 126.9 (C10), 126.2 (C7), 125.9 (C3), 122.6 (C6), 118.0 (C11), 113.7 (C9), 37.2 (C15), 34.3 (C15).

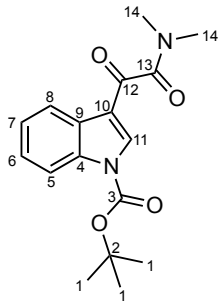


**4.60**

***tert*-Butyl 3-(2-(dimethylamino)-2-oxoacetyl)-1*H*-indole-1-carboxylate (4.60) (rmw_03_272).** Indole glyoxamide **4.57** (100 mg, 0.46 mmol) was dissolved in 3 mL $CH_2Cl_2$. DMAP (2.8 mg, 0.023 mmol) and $Et_3N$ (84 mg, 0.83 mmol) was added and the mixture was cooled to 0 °C. $Boc_2O$ (121 mg, 0.46 mmol) was added dropwise and the mixture was allowed to warm to room temperature over 72 h with stirring. The mixture was diluted with saturated $NaHCO_3$ (5 mL) and $CH_2Cl_2$ (10 mL). The layers were separated and the aqueous layer was extracted with $CH_2Cl_2$ (2 x 10 mL). The organic layers were combined, dried over $MgSO_4$, filtered, and concentrated under reduced pressure to give

120 mg (82%) of **4.60** as a yellow solid. The crude material was used without further purification. $^{1}$H NMR (500 MHz, $CDCl_3$) δ 8.28 (d, *J* = 6.8 Hz, 1 H), 8.25 (s, 1 H), 8.09 (d, *J* = 8.2 Hz, 1 H), 7.37-7.30 (comp, 2 H), 3.05 (s, 3 H), 2.99 (s, 3 H), 1.63 (s, 9 H). $^{13}$C NMR (125 MHz, $CDCl_3$) δ 186.9, 166.6, 148.8, 135.9, 135.7, 126.9, 125.9, 124.8, 122.3, 116.9, 115.2, 85.6, 37.4, 34.5, 28.0. HRMS (ESI) *m/z* 339.1321 [$C_{17}H_{20}N_2O_4$ (M+Na) requires 339.1315].

**NMR Assignments**. $^{1}$H NMR (500 MHz, $CDCl_3$) δ 8.28 (d, *J* = 6.8 Hz, 1 H, C5-H), 8.25 (s, 1 H, C11-H), 8.09 (d, *J* = 8.2 Hz, 1 H, C8-H), 7.37-7.30 (comp, 2 H, C6-H, C7-H), 3.05 (s, 3 H, C14-H), 2.99 (s, 3 H, C14-H), 1.63 (s, 9 H, C1-H). $^{13}$C NMR (125 MHz, $CDCl_3$) δ 186.9 (C12), 166.6 (C13), 148.8 (C3), 135.9 (C11), 135.7, 126.9, 125.9 (C7), 124.8 (C6), 122.3 (C5), 116.9, 115.2 (C8), 85.6, 37.4 (C14), 34.5 (C14), 28.0 (C1).

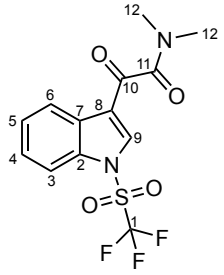


**4.61**

***N*,*N*-Dimethyl-2-oxo-2-(1-((trifluoromethyl)sulfonyl)-1*H*-indol-3-yl)acetamide (4.61) (rmw_xx_xx)** $^{1}$H NMR (400 MHz, DMSO-$d_6$) δ 8.56 (s, 1 H), 8.31 (d, *J* = 8.0 Hz, 1 H), 7.91 (d, *J* = 8.1 Hz, 1 H), 7.61 (ddd, *J* = 14.2, 7.8, 4.1 Hz, 2 H), 7.25-7.12 (comp, 3 H), 3.02 (s, 3 H), 2.98 (s, 3 H). $^{13}$C NMR (125 MHz, DMSO-$d_6$) δ 187.4,

165.5, 136.8, 135.5, 128.1, 127.2, 127.1, 123.0, 120.3, 118.0, 113.8, 37.2, 34.4. HRMS (ESI) *m/z* 371.0284 [$C_{13}H_{11}F_3N_2O_4$ (M+Na) requires 371.0284].

**NMR Assignments**. $^1$H NMR (400 MHz, DMSO-$d_6$) δ 8.56 (s, 1 H, C9-H), 8.31 (d, *J* = 8.0 Hz, 1 H, C3-H), 7.91 (d, *J* = 8.1 Hz, 1 H C6-H), 7.61 (ddd, *J* = 14.2, 7.8, 4.1 Hz, 2 H, C4-H, C5-H), 3.02 (s, 3 H, C12-H), 2.98 (s, 3 H, C12-H). $^{13}$C NMR (125 MHz, DMSO-$d_6$) δ 187.4 (C10), 165.5 (C11), 136.8 (C9), 135.5 (C2), 128.1 (C5), 127.2 (C4), 127.1 (C7), 123.0 (C3), 120.3 (C7), 118.0 (C1), 113.8 (C8), 37.2 (C12), 34.4 (C12).

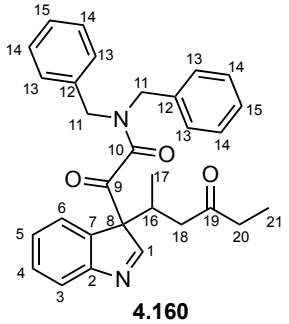

**4.160**

***N*,*N*-Dibenzyl-2-oxo-2-(3-(4-oxohexan-2-yl)-3*H*-indol-3-yl)acetamide (4.160) (rmw_04_141).** $^1$H NMR (400 MHz, DMSO-$d_6$) δ 8.34 (d, *J* = 8.1 Hz, 1 H), 7.96 (s, 1 H), 7.46 (dd, *J* = 6.9 Hz, 1.6 Hz, 1 H), 7.42-7.25 (comp, 12 H), 5.16-5.07 (m, 1 H), 4.62 (s, 2 H), 4.45 (s, 2 H), 3.02 (dd, *J* = 17.3, 5.3 Hz, 1 H), 2.90 (dd, *J* = 17.3, 7.8 Hz, 1 H), 2.45-2.31 (comp, 2 H), 2.04, 1.60 (d, *J* = 6.8 Hz, 3 H), 1.02 (t, *J* = 7.2 Hz, 3 H); 208.8, 184.9, 168.4, 137.0, 136.4, 135.0, 128.7, 127.2, 126.9, 126.0, 125.6, 122.6, 114.6, 60.2, 50.4, 48.6, 48.3, 46.2, 36.7, 20.6, 7.5; HRMS (ESI) *m/z* 527.1727 [$C_{32}H_{28}N_2O_3$ (M+K) requires 527.1732].

**NMR Assignments.** $^{1}$H NMR (400 MHz, DMSO-$d_6$) δ 8.34 (d, $J$ = 8.1 Hz, 1 H, C3-H), 7.96 (s, 1 H, C1-H), 7.49-7.43 (m, 1 H, C6-H), 7.42-7.25 (comp, 12 H, C13-H, C14-H, C15-H, C4-H, C5-H), 5.16-5.07 (m, 1 H, C16-H), 4.62 (s, 2 H, C11-H), 4.45 (s, 2 H, C11-H), 3.02 (dd, $J$ = 17.3, 5.3 Hz, 1 H, C18-H), 2.90 (dd, $J$ = 17.3, 7.8 Hz, 1 H, C18-H), 2.45-2.31 (comp, 2 H, C20-H), 1.60 (d, $J$ = 6.8 Hz, 3 H, C17-H), 1.02 (t, $J$ = 7.2 Hz, 3 H, C21-H); $^{13}$C NMR (100 MHz, DMSO-$d_6$) δ 208.8 (C19), 184.9 (C9), 168.4 (C10), 137.0 (C2), 136.4 (C12), 135.0 (C1), 128.7 (C14), 127.2 (C13), 126.9 (C7), 126.0 (C15), 125.6 (C4), 122.6 (C3), 114.6 (C6), 60.2 (C8), 50.4 (C11), 48.6 (C18), 48.3 (C16), 46.2 (C11), 36.7 (C20), 20.6 (C17), 7.5 (C21).

# Chapter 6. Appendix

## 6.1 Determination of Extinction Coefficients

**General Procedure:** EtOH was filtered by passing through a 0.22 μm syringe filter prior to use. Blank samples were prepared using filtered EtOH. Dry samples (~ 1.5-2 mg) were weighed into oven-dried 10 mL volumetric flasks and diluted to the mark with EtOH. Solutions were capped and mixed for 3-5 min with sonication as necessary to ensure complete dissolution, then passed through a 0.22 μm syringe filter before absorbance measurements were collected. Three independent solutions of different concentrations were prepared and diluted as necessary until absorbance measurements at $\lambda_{max}$ fell within the acceptable Beer's Law range ($0.000 < OD_{\lambda_{max}} < 1.000$). The cuvette was rinsed twice with the blank solution and dried prior to each measurement.

UV absorbance for each sample was measured from 200 nm – 500 nm, with recorded absorbance measurements every 0.5 nm. The longest wavelength in the spectrum for which a local maximum was observed for the sample was taken as $\lambda_{max}$. Absorbance measurements at 500 nm and 400 nm were also noted for corrections regarding baseline absorbance and light scattering, respectively. Absorbance at $\lambda_{max}$ was corrected according to Equation 5.1.

$$A_{\lambda max,corr} = A_{max} - A_{500} - \left[\left(\frac{\lambda_{max}}{400}\right)^4 \times (A_{400} - A_{500})\right] \quad (6.1)$$

## 6.2 UV/VIS SPECTRA

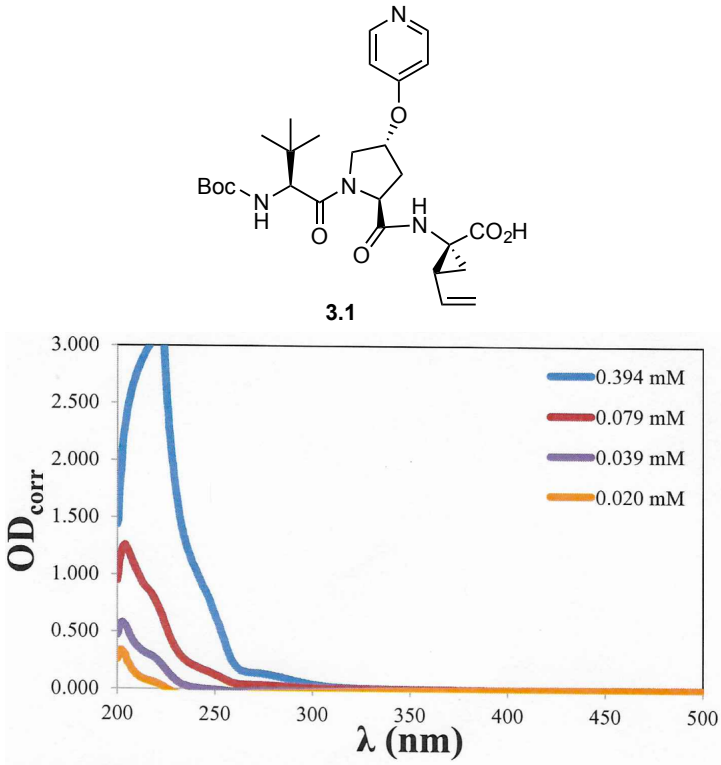


**Figure 6.1:** UV Spectrum of ligand **3.1**.

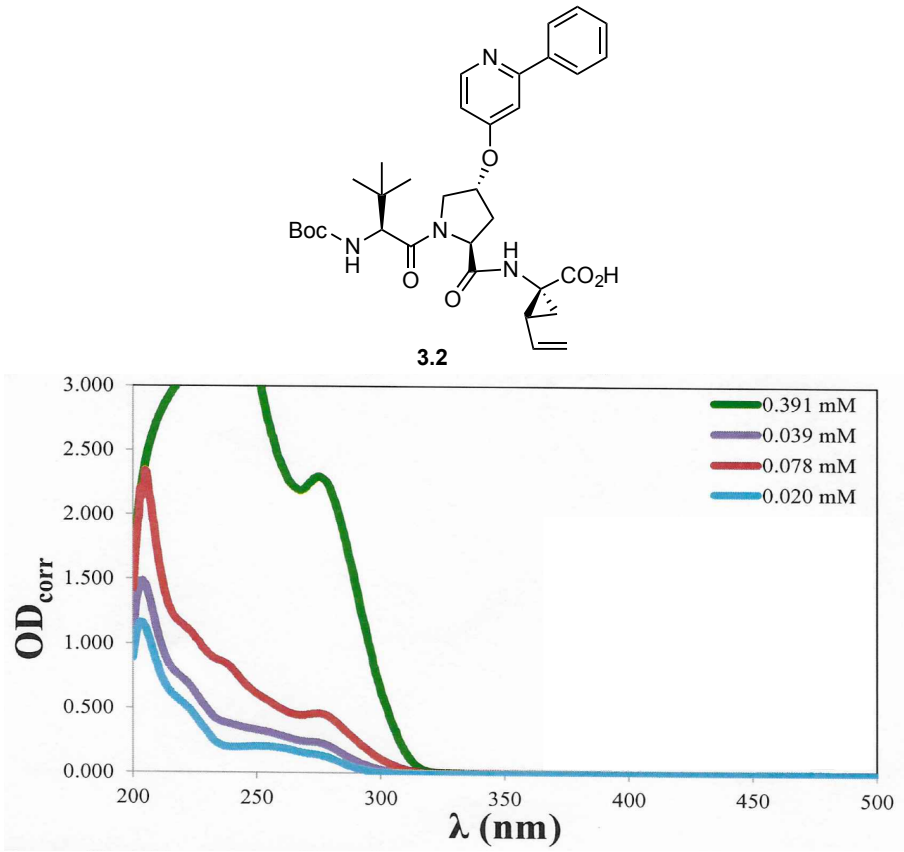


**Figure 6.2a:** UV Spectrum of ligand **3.2**.

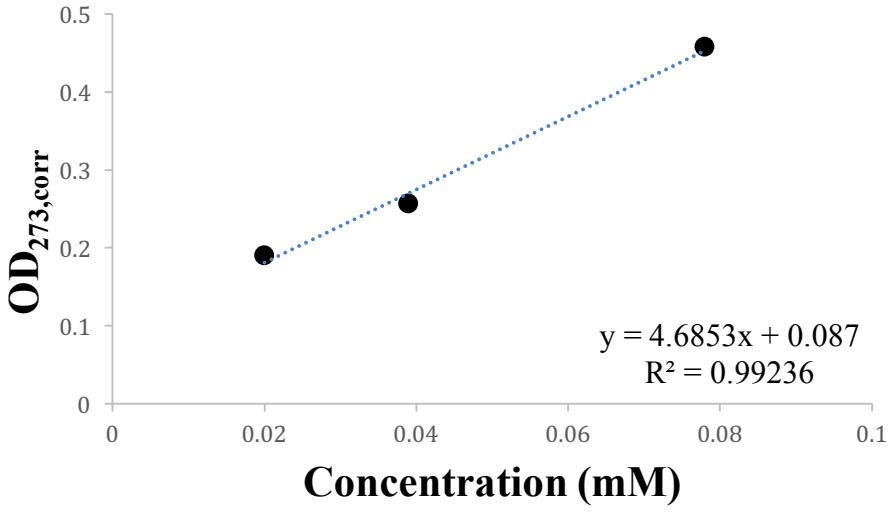


**Figure 6.2b:** Beer's Law standard curve for ligand **3.2**.

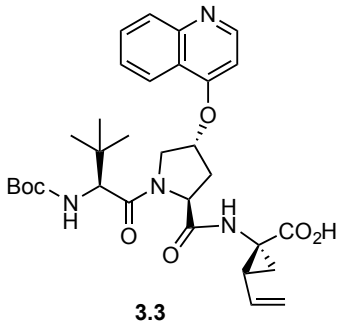


**3.3**

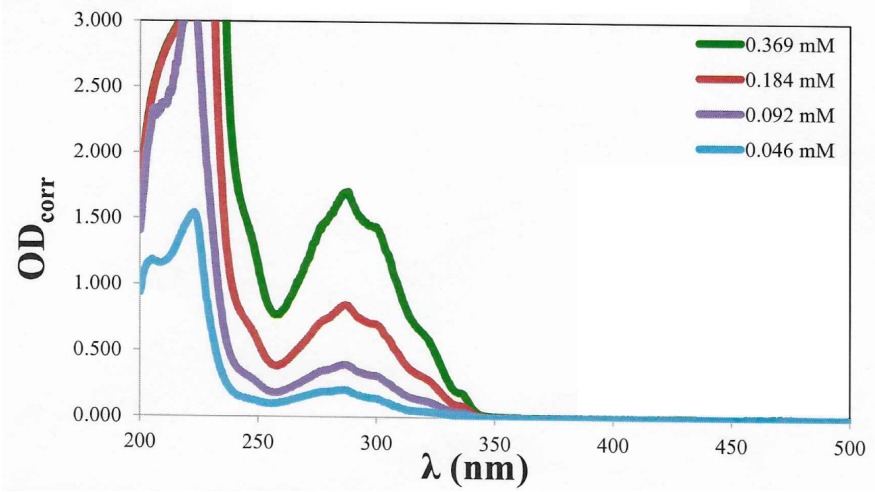


**Figure 6.3a:** UV Spectrum of ligand **3.3**.

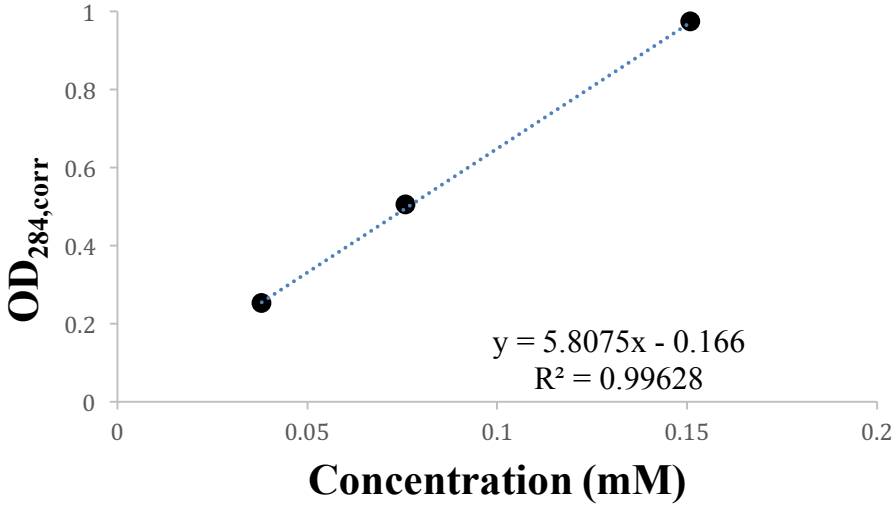


**Figure 6.3b:** Beer's Law standard curve for ligand **3.3**.

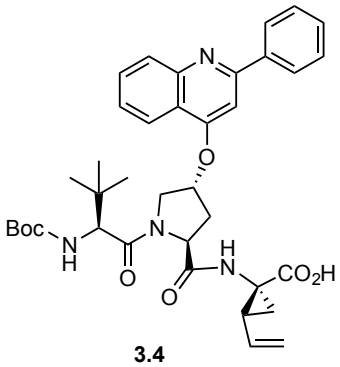


3.4

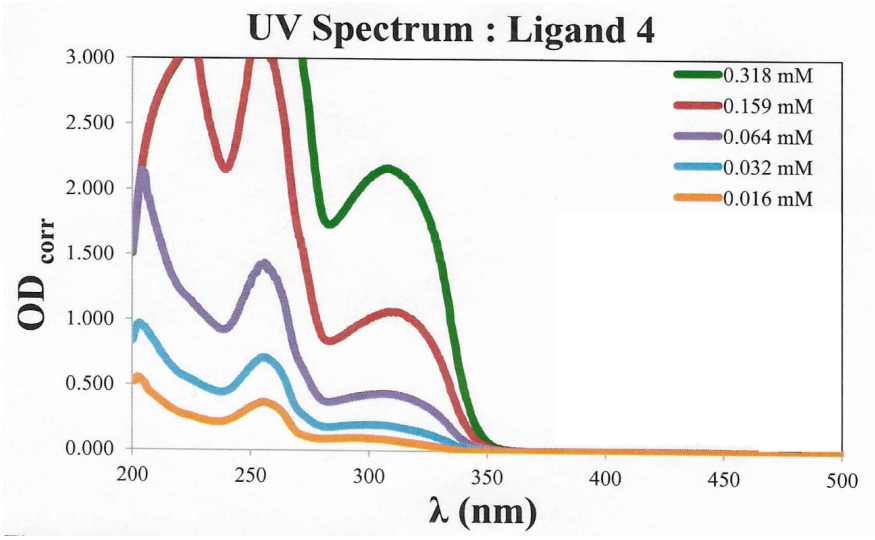


**Figure 6.4a:** UV Spectrum of ligand **3.4**.

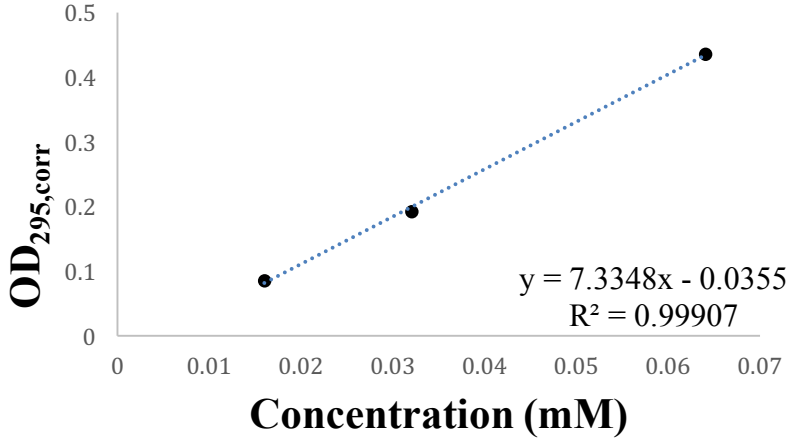


**Figure 6.5b:** Beer's Law standard curve for ligand **3.5**.

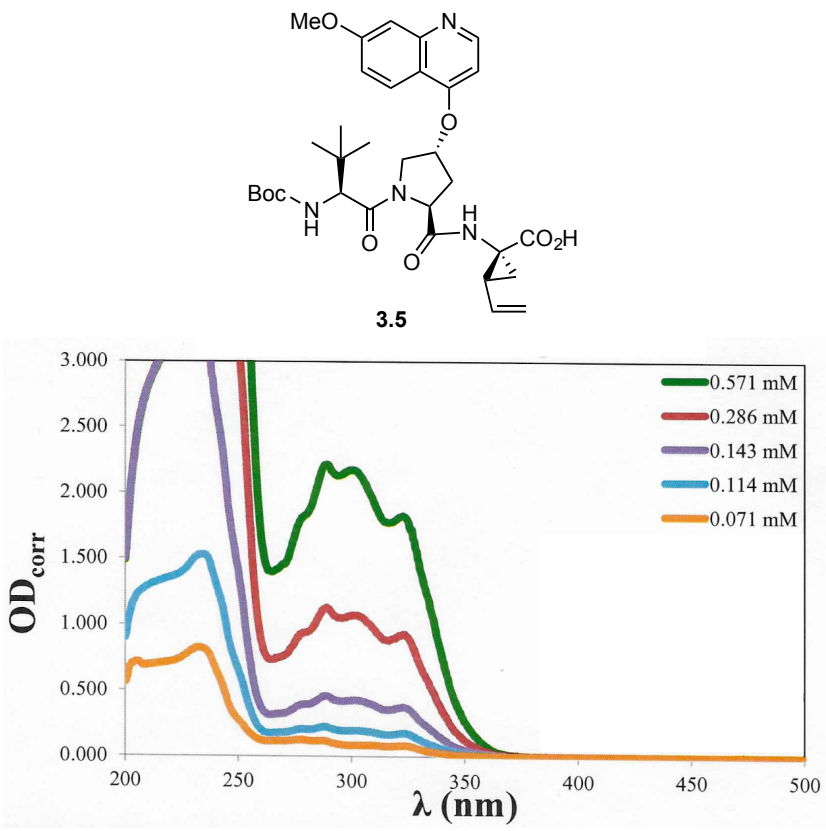


**Figure 6.5a:** UV Spectrum of ligand **3.5**.

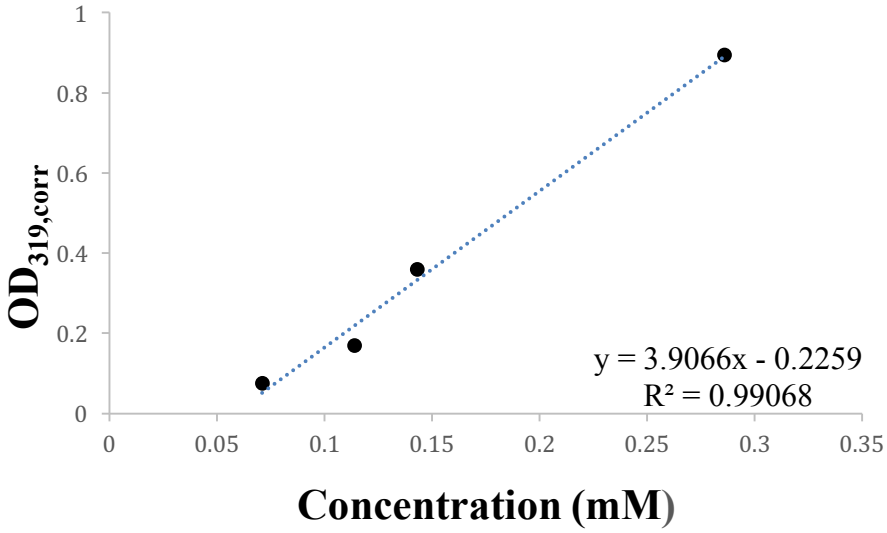

**Figure 6.5b:** Beer's Law standard curve for ligand **3.5**.

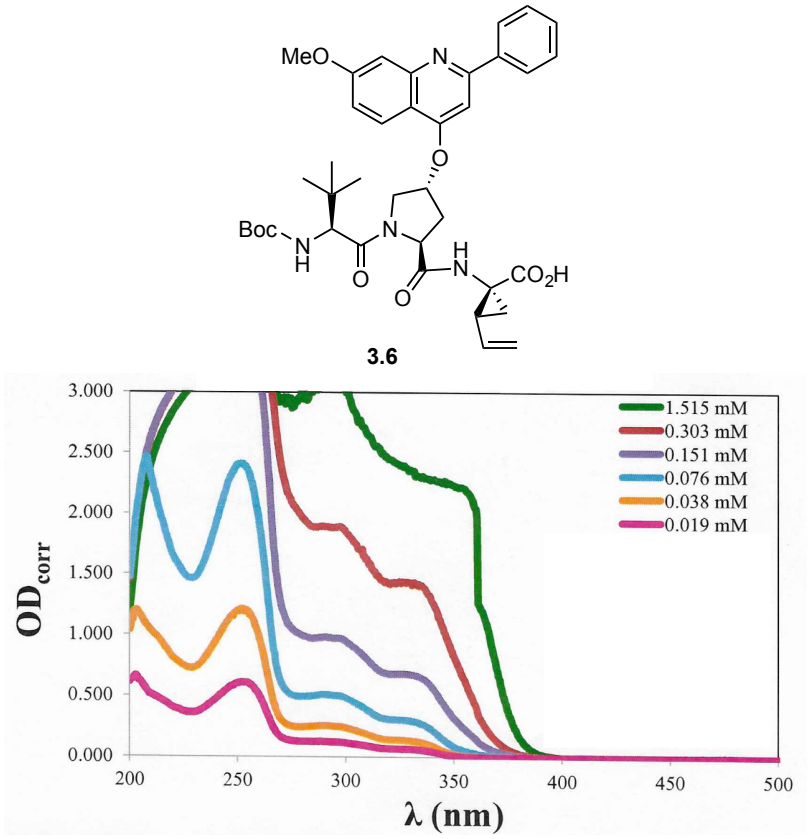


**Figure 6.6a:** UV Spectrum of ligand **3.6**.

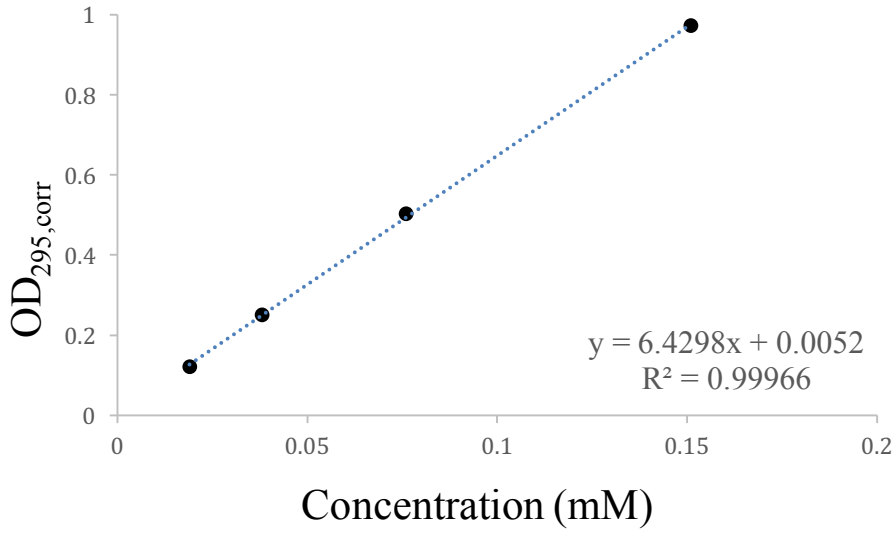

**Figure 6.6b:** Beer's Law standard curve for ligand **3.6**.

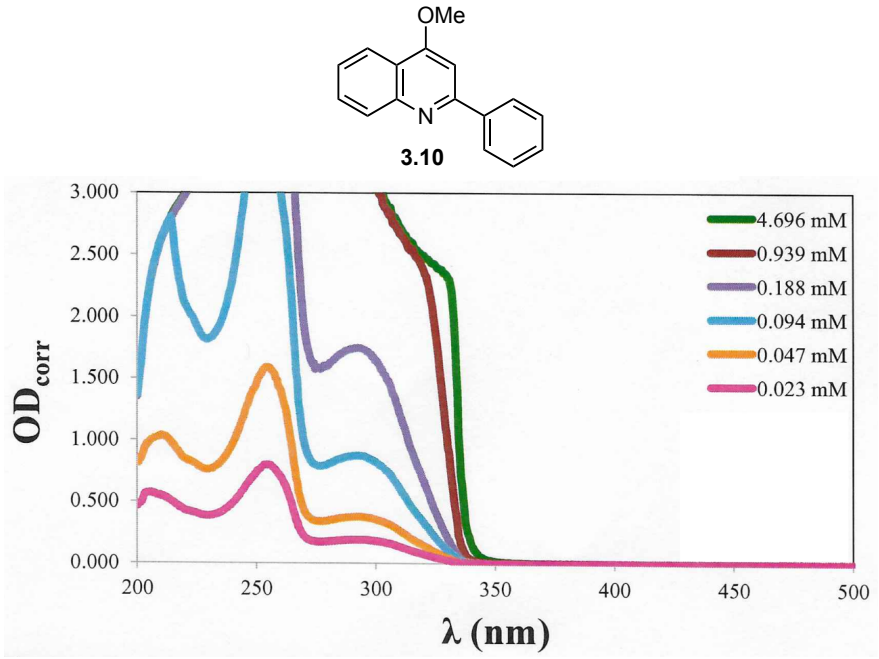


**Figure 6.7a:** UV Spectrum of **3.10**.

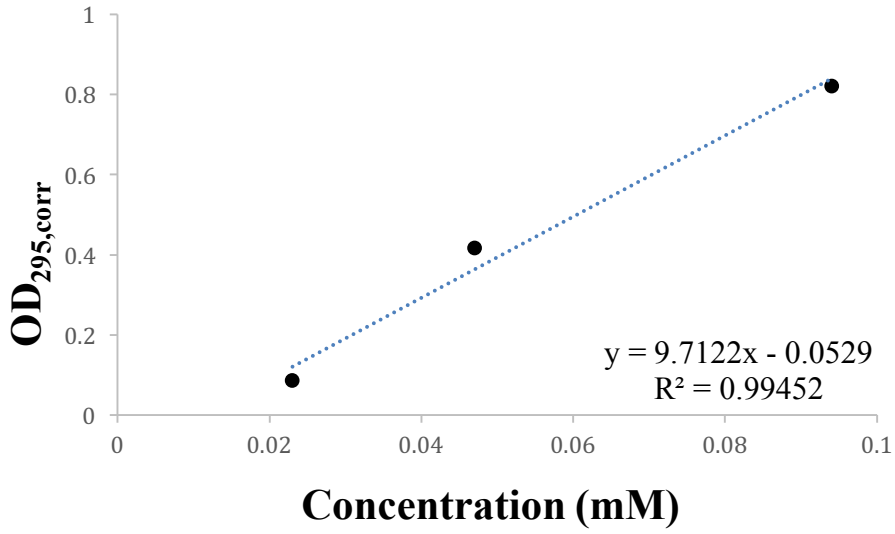


**Figure 6.7b:** Beer's Law standard curve for **3.10** in EtOH.

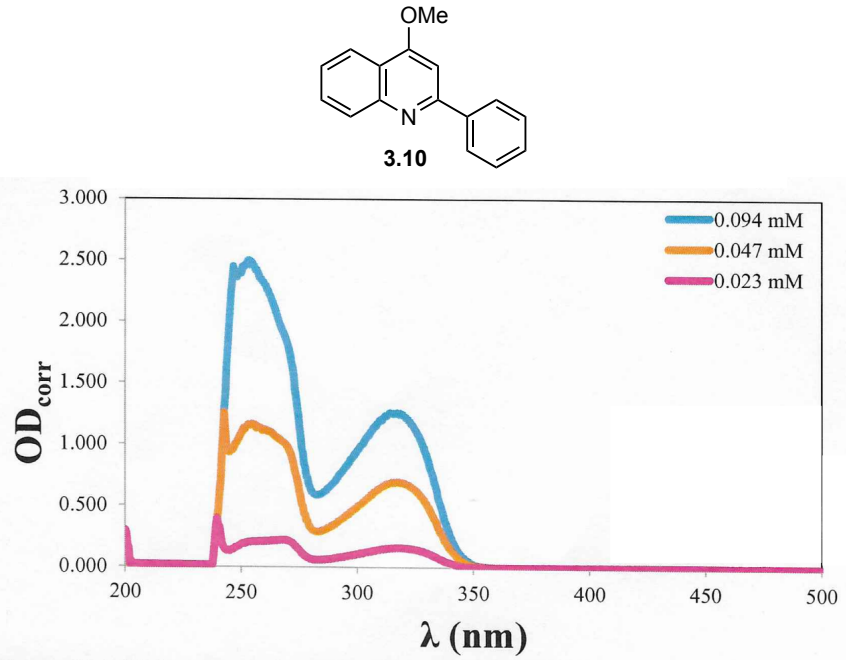


**Figure 6.8a:** UV Spectrum of **3.10** in 10% AcOH/EtOH.

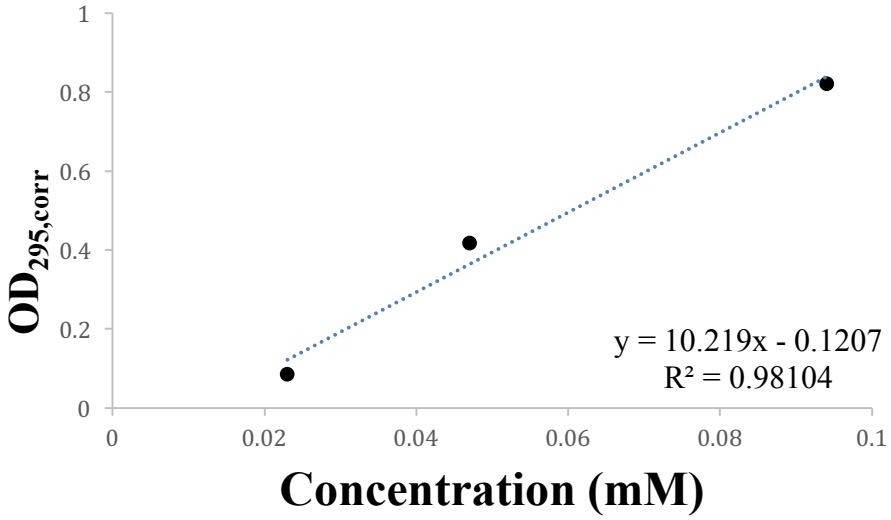


**Figure 6.8b:** Beer's Law standard curve for **3.10** in 10% AcOH/EtOH.

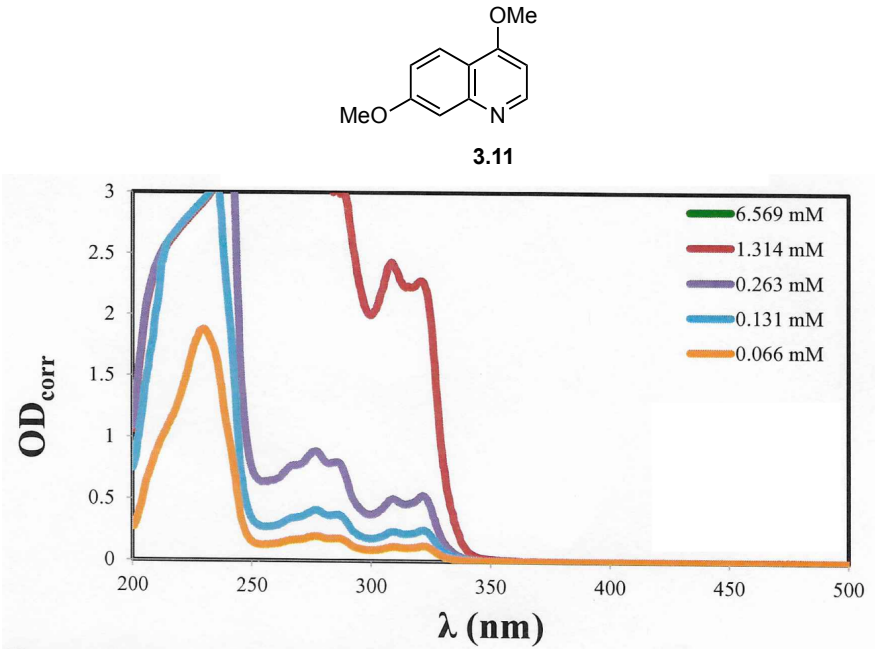


**Figure 6.9a:** UV Spectrum of **3.11** in EtOH.

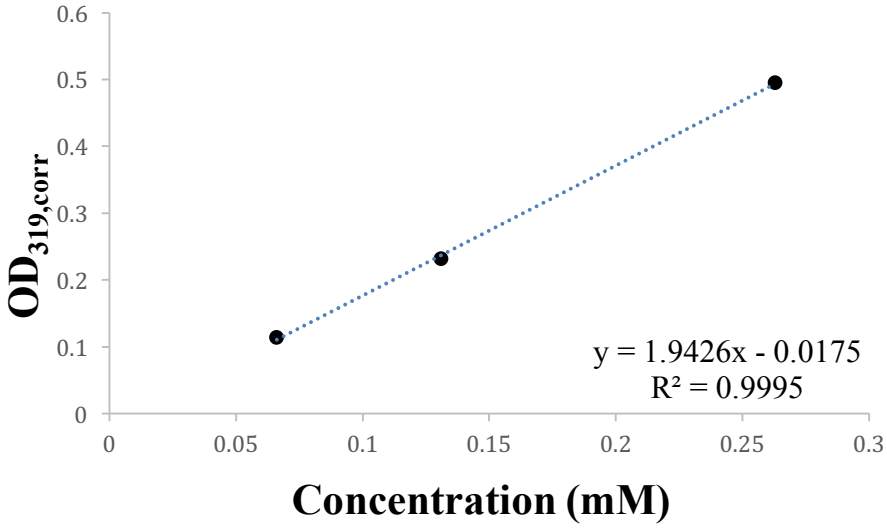


**Figure 6.9b:** Beer's Law standard curve for **3.11** in EtOH.

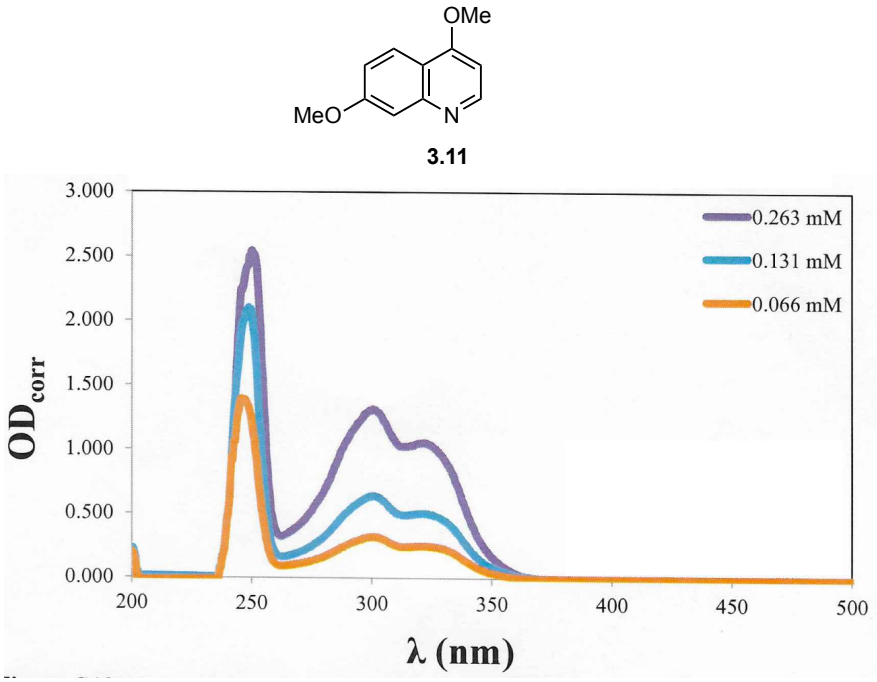


**Figure 6.10a:** UV Spectrum of **3.11** in 10% AcOH/EtOH.

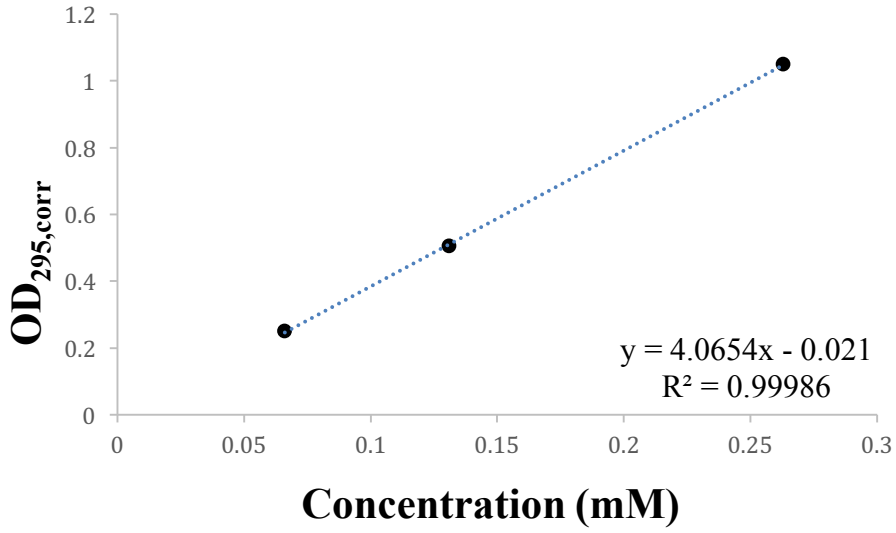


**Figure 6.10b:** Beer's Law standard curve for **3.11** in 10% AcOH/EtOH.

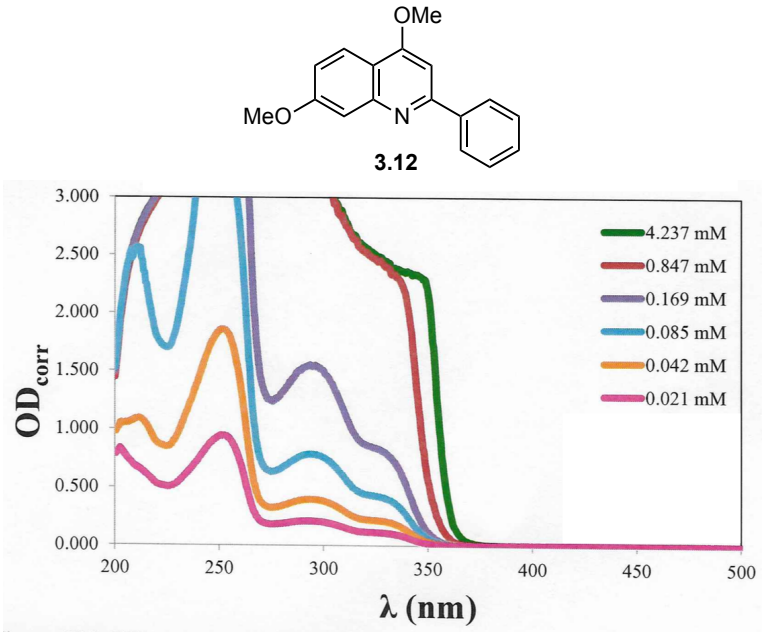


**Figure 6.11a:** UV Spectrum of **3.12** in EtOH.

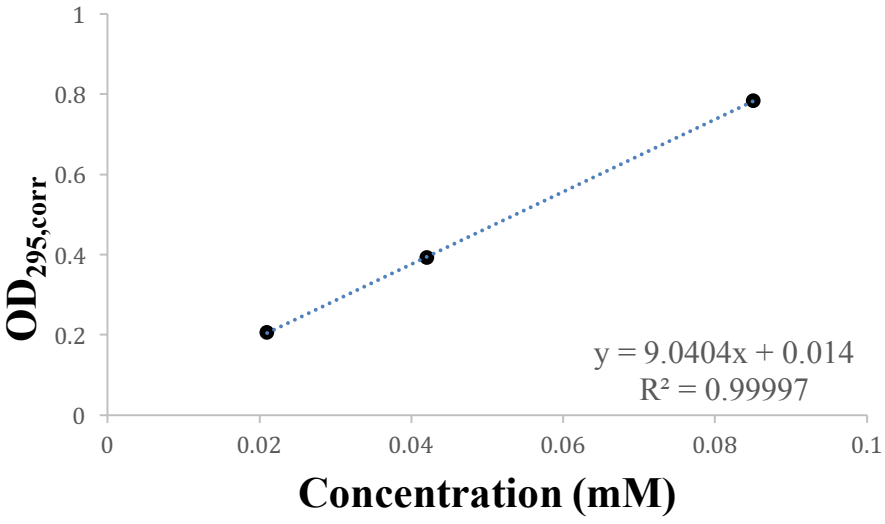


**Figure 6.11b:** Beer's Law standard curve for **3.12** in EtOH.

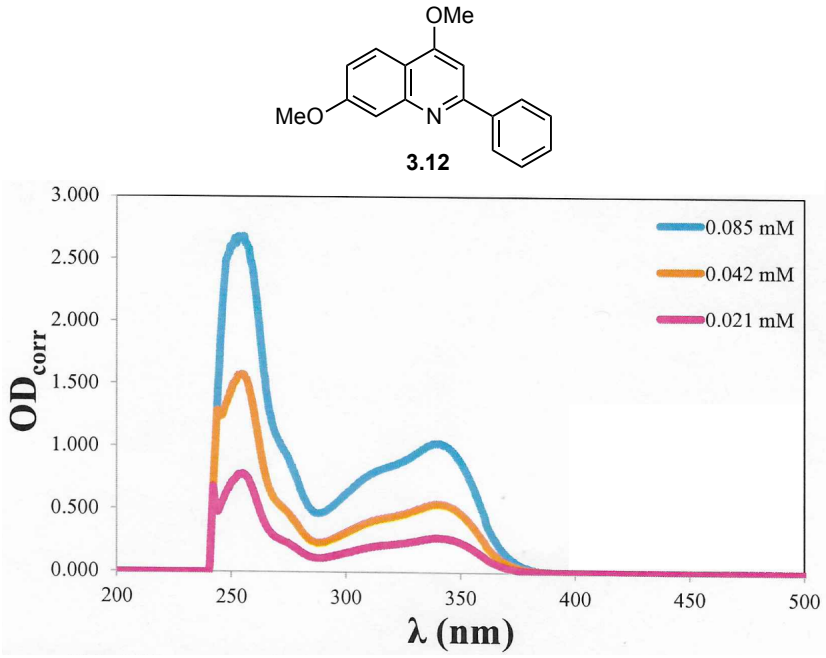


**Figure 6.12a:** UV Spectrum of **3.12** in 10% AcOH/EtOH.

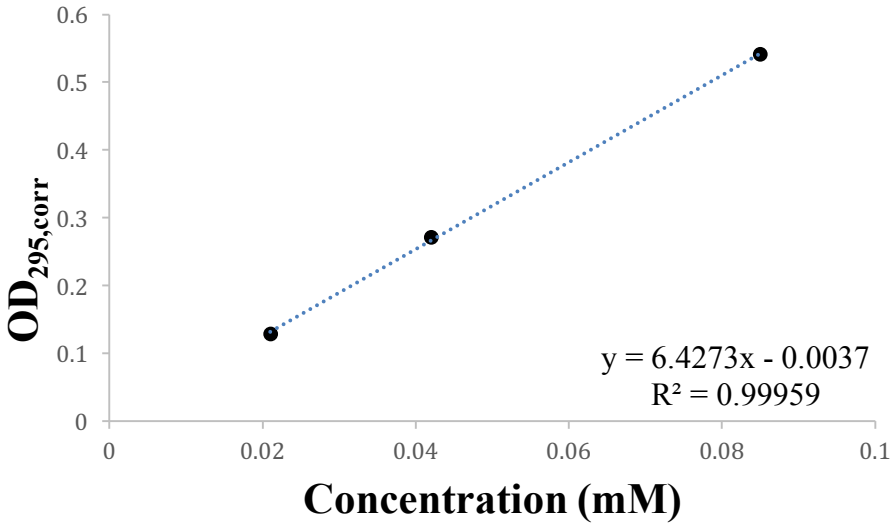


**Figure 6.12b:** Beer's Law standard curve for **3.12** in 10% AcOH/EtOH.

## 6.3 ISOTHERMAL TITRATION CALORIMETRY DATA AND REPRESENTATIVE TRACES

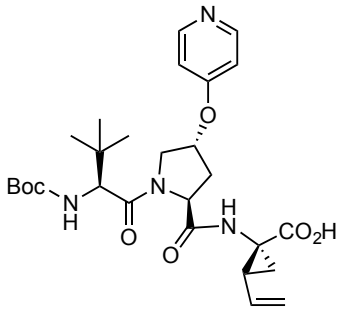


**3.1**

| | | |
|---|---|---|
| $n$ = 1.00 | $n$ = 1.00 | $n$ = 0.901 |
| $K_a$ = 5.99 x $10^4$ $M^{-1}$ | $K_a$ = 6.78 x $10^4$ $M^{-1}$ | $K_a$ = 9.87 x $10^4$ $M^{-1}$ |
| $\Delta G°$ = –6.52 kcal $mol^{-1}$ | $\Delta G°$ = –6.59 kcal $mol^{-1}$ | $\Delta G°$ = –6.81 kcal $mol^{-1}$ |
| $\Delta H°$ = –1.27 kcal $mol^{-1}$ | $\Delta H°$ = –1.40 kcal $mol^{-1}$ | $\Delta H°$ = –1.42 kcal $mol^{-1}$ |
| $-T\Delta S°$ = –5.25 kcal $mol^{-1}$ | $-T\Delta S°$ = –5.19 kcal $mol^{-1}$ | $-T\Delta S°$ = –5.39 kcal $mol^{-1}$ |

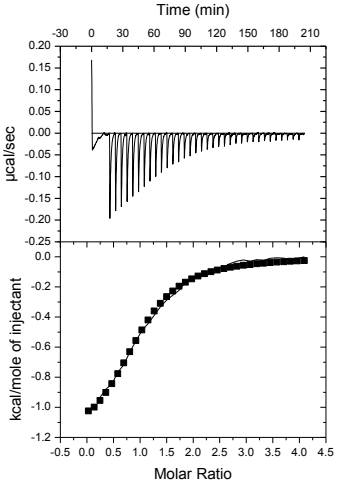


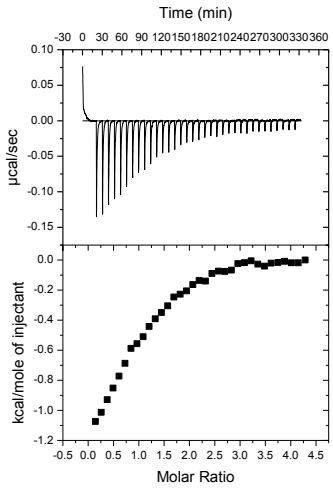


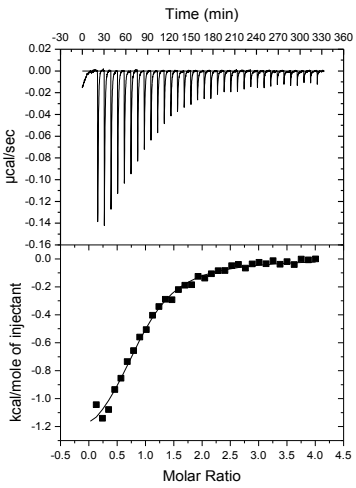

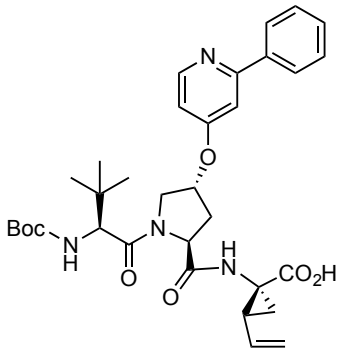


**3.2**

| | | |
|---|---|---|
| $n$ = 0.99 | $n$ = 0.95 | $n$ = 1.09 |
| $K_a$ = 1.58 x $10^6$ $M^{-1}$ | $K_a$ = 1.11 x $10^6$ $M^{-1}$ | $K_a$ = 8.63 x $10^5$ $M^{-1}$ |
| $\Delta G°$ = –8.46 kcal $mol^{-1}$ | $\Delta G°$ = –8.25 kcal $mol^{-1}$ | $\Delta G°$ = –8.10 kcal $mol^{-1}$ |
| $\Delta H°$ = –2.17 kcal $mol^{-1}$ | $\Delta H°$ = –2.21 kcal $mol^{-1}$ | $\Delta H°$ = –2.00 kcal $mol^{-1}$ |
| $-T\Delta S°$ = –6.29 kcal $mol^{-1}$ | $-T\Delta S°$ = –6.04 kcal $mol^{-1}$ | $-T\Delta S°$ = –6.10 kcal $mol^{-1}$ |

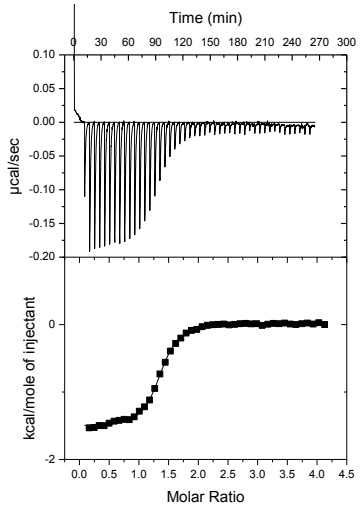


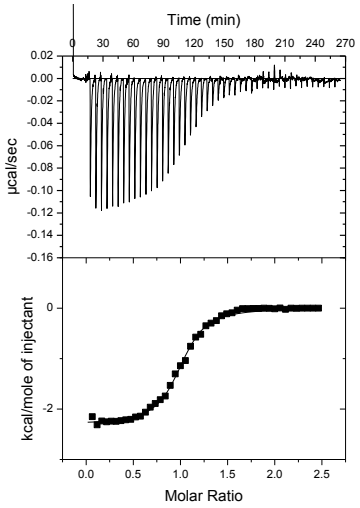


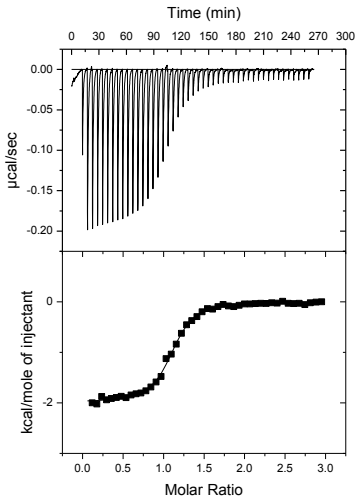

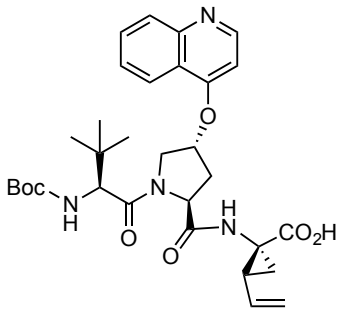

**3.3**

| | | |
|---|---|---|
| $n$ = 1.00 | $n$ = 1.00 | $n$ = 0.92 |
| $K_a$ = 5.41 x $10^6$ $M^{-1}$ | $K_a$ = 5.28 x $10^6$ $M^{-1}$ | $K_a$ = 5.02 x $10^6$ $M^{-1}$ |
| $\Delta G°$ = –9.19 kcal $mol^{-1}$ | $\Delta G°$ = –9.17 kcal $mol^{-1}$ | $\Delta G°$ = –9.14 kcal $mol^{-1}$ |
| $\Delta H°$ = –5.39 kcal $mol^{-1}$ | $\Delta H°$ = –5.34 kcal $mol^{-1}$ | $\Delta H°$ = –5.39 kcal $mol^{-1}$ |
| $-T\Delta S°$ = –3.80 kcal $mol^{-1}$ | $-T\Delta S°$ = –3.83 kcal $mol^{-1}$ | $-T\Delta S°$ = –3.75 kcal $mol^{-1}$ |

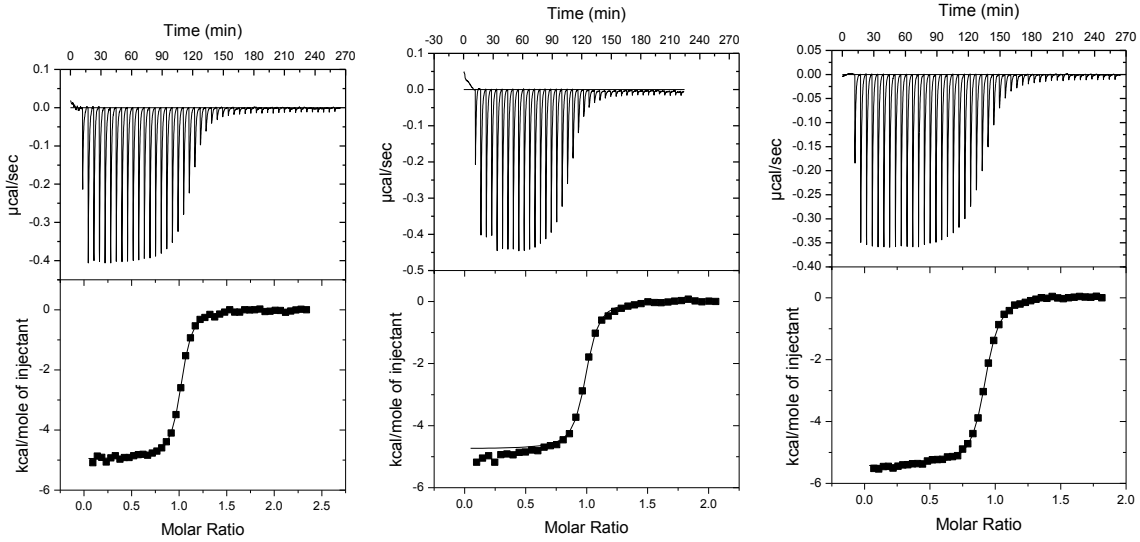

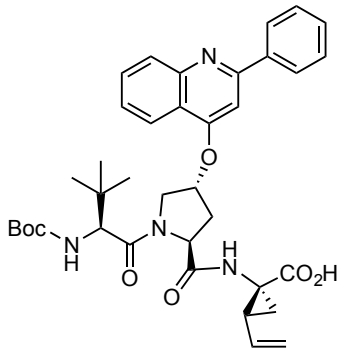

**3.4**

$n$ = 0.98
$K_a$ = 9.99 x $10^6$ $M^{-1}$
$\Delta G°$ = –9.55 kcal $mol^{-1}$
$\Delta H°$ = –2.72 kcal $mol^{-1}$
–T$\Delta S°$ = –6.83 kcal $mol^{-1}$

$n$ = 1.05
$K_a$ = 1.01 x $10^7$ $M^{-1}$
$\Delta G°$ = –9.56 kcal $mol^{-1}$
$\Delta H°$ = –2.57 kcal $mol^{-1}$
–T$\Delta S°$ = –6.99 kcal $mol^{-1}$

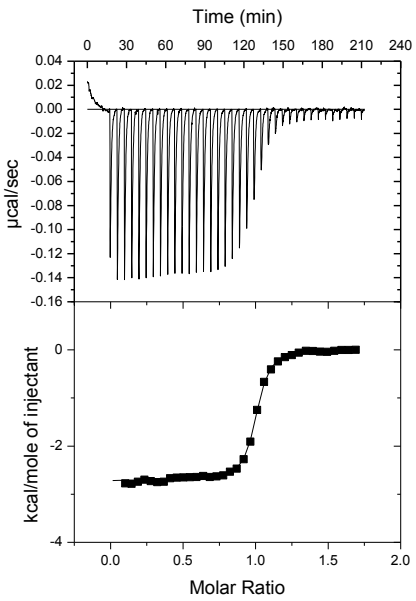


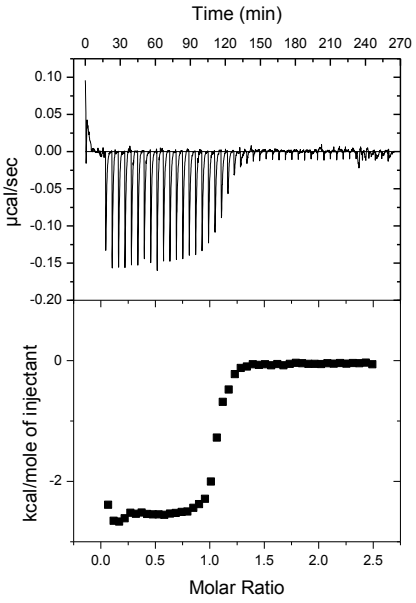

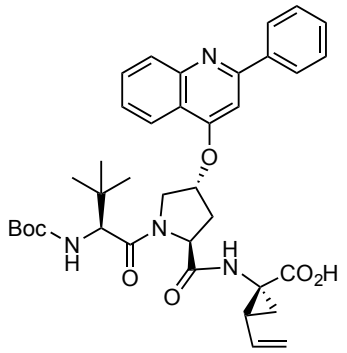

**3.4**

(continued)

| | |
|---|---|
| $n$ = 1.17 | $n$ = 1.11 |
| $K_a$ = 1.11 x $10^7$ $M^{-1}$ | $K_a$ = 1.01 x $10^7$ $M^{-1}$ |
| $\Delta G°$ = –9.61 kcal $mol^{-1}$ | $\Delta G°$ = –9.58 kcal $mol^{-1}$ |
| $\Delta H°$ = –2.52 kcal $mol^{-1}$ | $\Delta H°$ = –2.62 kcal $mol^{-1}$ |
| $-T\Delta S°$ = –7.09 kcal $mol^{-1}$ | $-T\Delta S°$ = –6.96 kcal $mol^{-1}$ |

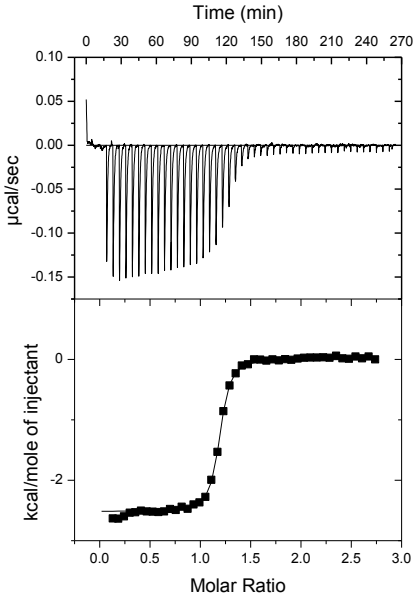


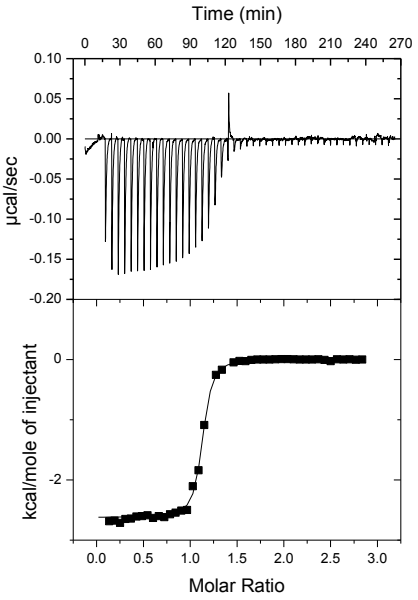

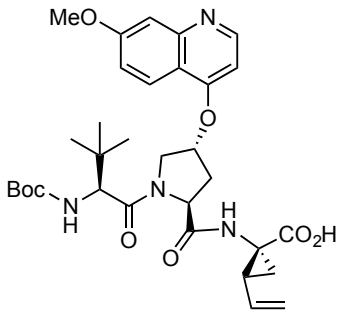


**3.5**

| | | |
|---|---|---|
| $n$ = 1.03 | $n$ = 0.98 | $n$ = 1.00 |
| $K_a$ = 5.47 x $10^6$ $M^{-1}$ | $K_a$ = 5.95 x $10^6$ $M^{-1}$ | $K_a$ = 1.66 x $10^7$ $M^{-1}$ |
| $\Delta G°$ = –9.19 kcal $mol^{-1}$ | $\Delta G°$ = –9.24 | $\Delta G°$ = –9.85 kcal $mol^{1}$ |
| $\Delta H°$ = –8.52 kcal $mol^{-1}$ | $\Delta H°$ = –7.81 | $\Delta H°$ = –8.19 kcal $mol^{-1}$ |
| $-T\Delta S°$ = –0.67 kcal $mol^{-1}$ | $-T\Delta S°$ = –1.43 | $-T\Delta S°$ = –1.66 kcal $mol^{-1}$ |

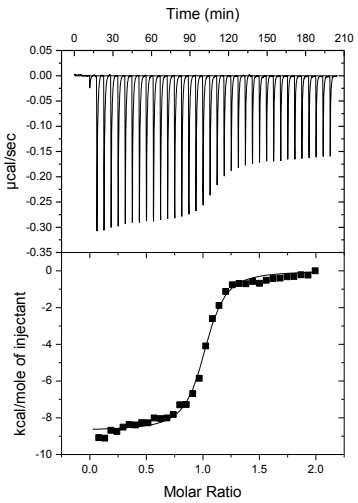


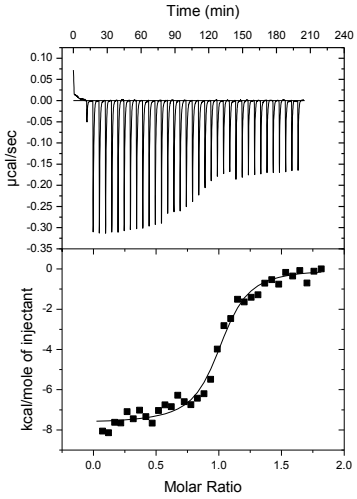


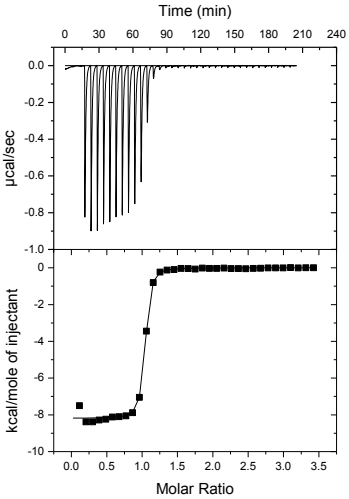

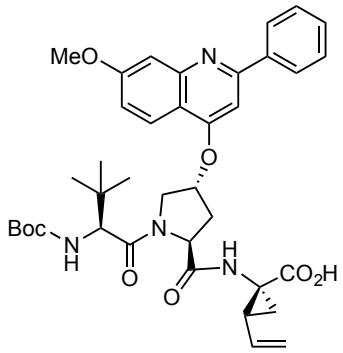


**3.6**

| | |
|---|---|
| $n$ = 1.02 | $n$ = 1.00 |
| $K_a$ = 4.87 x $10^7$ $M^{-1}$ | $K_a$ = 5.62 x $10^7$ $M^{-1}$ |
| $\Delta G°$ = –10.49 kcal $mol^{-1}$ | $\Delta G°$ = –10.57 kcal $mol^{-1}$ |
| $\Delta H°$ = –3.29 kcal $mol^{-1}$ | $\Delta H°$ = –3.96 kcal $mol^{-1}$ |
| $-T\Delta S°$ = –6.50 kcal $mol^{-1}$ | $-T\Delta S°$ = –6.61 kcal $mol^{-1}$ |

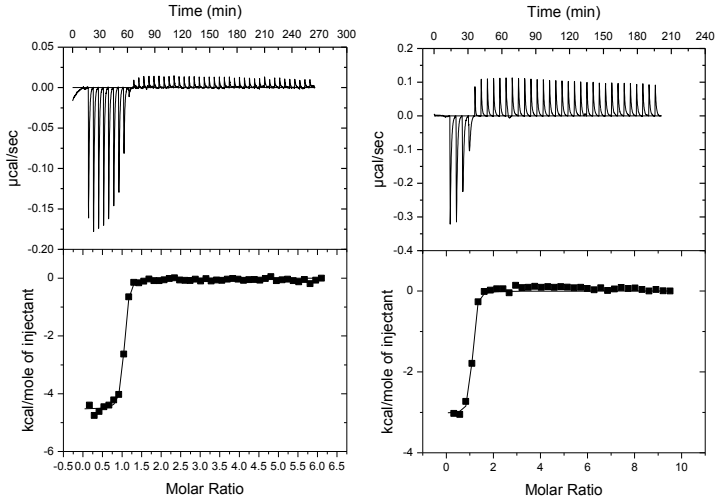

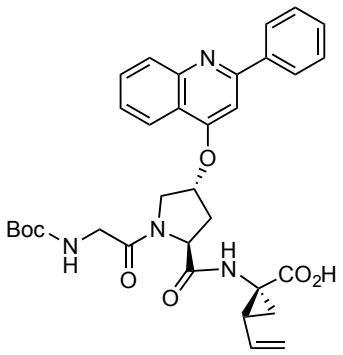


**3.49**

$n$ = 1.00

$K_a$ = 1.28 x $10^4$ $M^{-1}$

$\Delta G°$ = –5.60

$\Delta H°$ = –1.01

–T$\Delta S°$ = –4.59

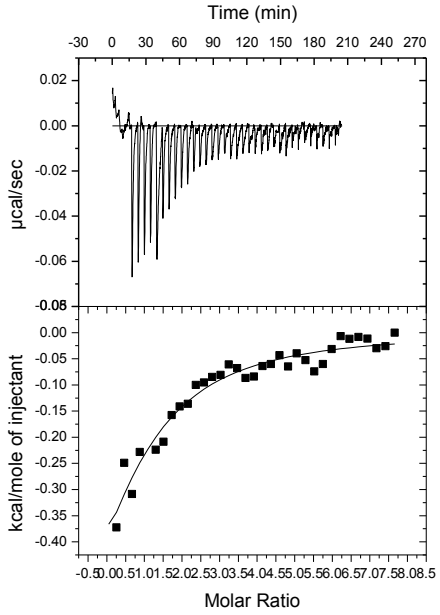

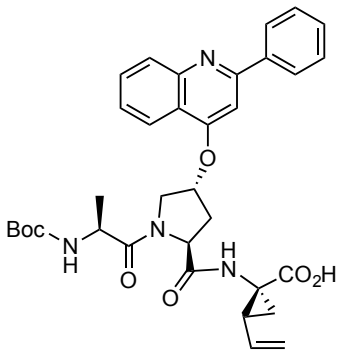


**3.50**

$n = 0.97$

$K_a = 4.62 \times 10^5\ M^{-1}$

$\Delta G° = -7.73$

$\Delta H° = -1.10$

$-T\Delta S° = -6.63$

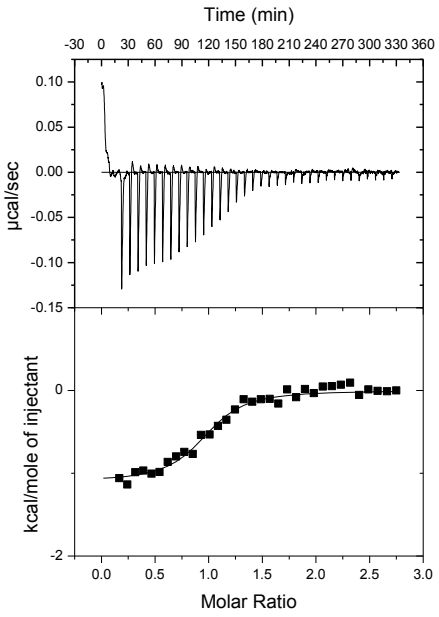

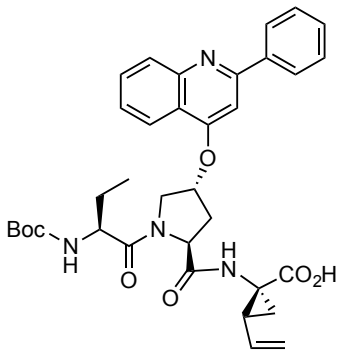

**3.x**

| | | |
|---|---|---|
| $n$ = 0.96 | $n$ = 0.96 | $n$ = 0.93 |
| $K_a$ = 9.89 x $10^5$ $M^{-1}$ | $K_a$ = 1.22 x $10^6$ $M^{-1}$ | $K_a$ = 1.12 x $10^6$ $M^{-1}$ |
| $\Delta G°$ = –8.18 kcal $mol^{-1}$ | $\Delta G°$ = –8.30 kcal $mol^{-1}$ | $\Delta G°$ = –8.25 kcal $mol^{1}$ |
| $\Delta H°$ = –1.76 kcal $mol^{-1}$ | $\Delta H°$ = –1.69 kcal $mol^{-1}$ | $\Delta H°$ = –1.83 kcal $mol^{-1}$ |
| $-T\Delta S°$ = –6.42 kcal $mol^{1}$ | $-T\Delta S°$ = –6.61 kcal $mol^{-1}$ | $-T\Delta S°$ = –6.42 kcal $mol^{1}$ |

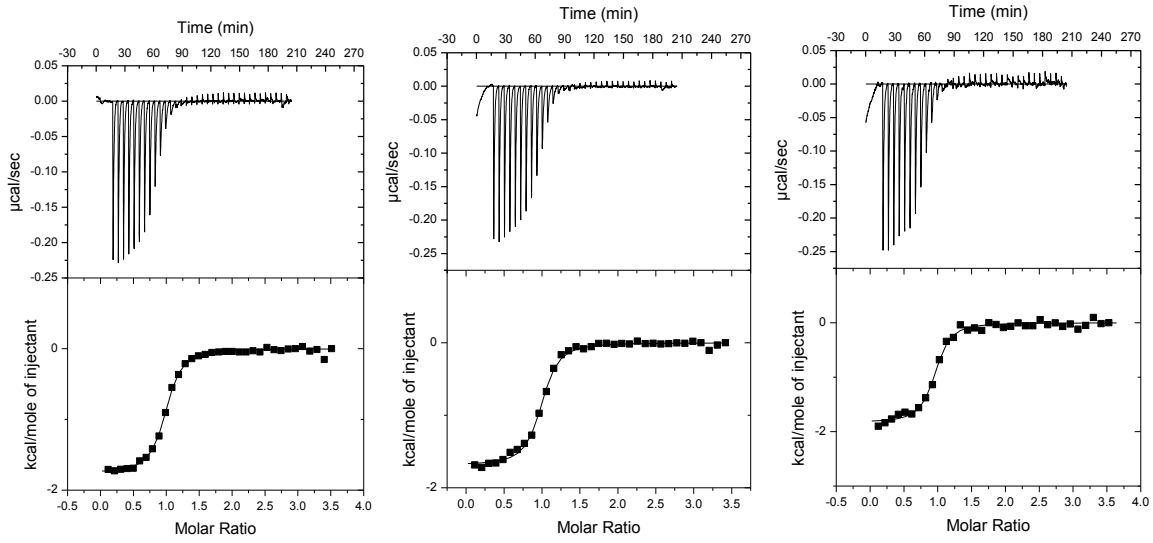

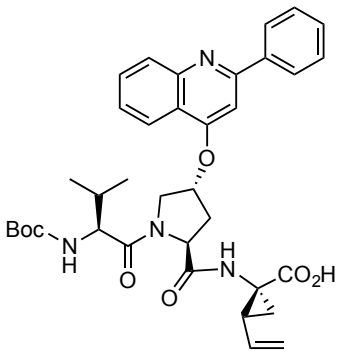

**3.x**

| | | |
|---|---|---|
| $n$ = 0.94 | $n$ = 0.98 | $n$ = 0.98 |
| $K_a$ = 4.06 x $10^6$ $M^{-1}$ | $K_a$ = 3.84 x $10^6$ $M^{-1}$ | $K_a$ = 4.36 x $10^6$ $M^{-1}$ |
| $\Delta G°$ = –9.02 kcal $mol^1$ | $\Delta G°$ = –8.98 kcal $mol^{-1}$ | $\Delta G°$ = –9.06 kcal $mol^{-1}$ |
| $\Delta H°$ = –2.31 kcal $mol^{-1}$ | $\Delta H°$ = –2.16 kcal $mol^{-1}$ | $\Delta H°$ = –2.10 kcal $mol^{-1}$ |
| $-T\Delta S°$ = –6.71 kcal $mol^{-1}$ | $-T\Delta S°$ = –6.82 kcal $mol^{-1}$ | $-T\Delta S°$ = –6.96 kcal $mol^{-1}$ |

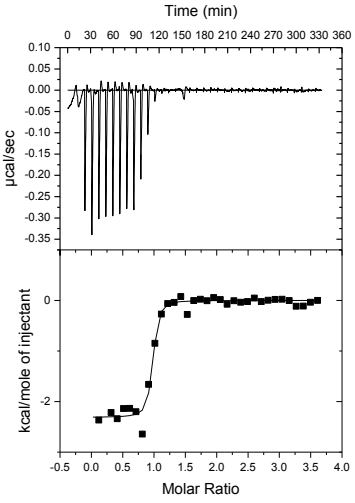


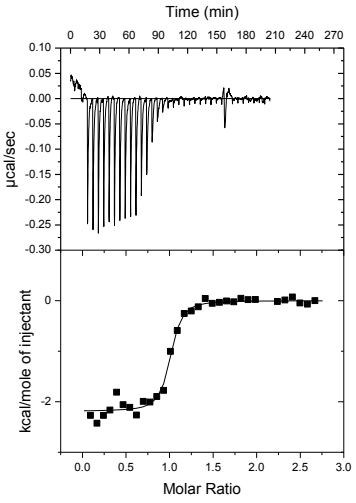


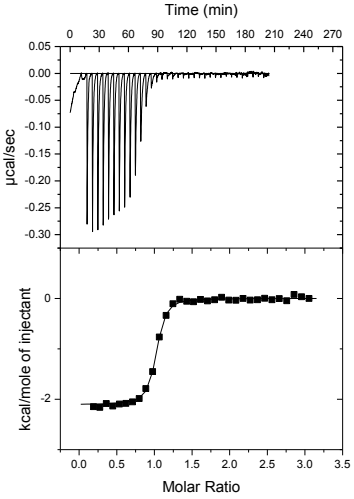

## References


(1) Hertzberg, R. P.; Pope, A. J. High-Throughput Screening: New Technology for the 21st Century Robert P Hertzberg* and Andrew J Pope. *Current Opinion in Chemical Biology* **2000**, *4*, 445–451.

(2) Baig, M.; Ahmad, K.; Roy, S.; Ashraf, J.; Adil, M.; Siddiqui, M.; Khan, S.; Kamal, M.; Provazník, I.; Choi, I. Computer Aided Drug Design: Success and Limitations. *Current Pharmaceutical Design* **2016**, *22*, 572–581.

(3) Lionta, E.; Spyrou, G.; Vassilatis, D.; Cournia, Z. Structure-Based Virtual Screening for Drug Discovery: Principles, Applications and Recent Advances. *Curr. Top. Med. Chem.* **2014**, *14*, 1923–1938.

(4) Warren, G. L.; Andrews, C. W.; Capelli, A.-M.; Clarke, B.; LaLonde, J.; Lambert, M. H.; Lindvall, M.; Nevins, N.; Semus, S. F.; Senger, S.; Tedesco, G.; Wall, I. D.; Woolven, J. M.; Peishoff, C. E.; Head, M. S. A Critical Assessment of Docking Programs and Scoring Functions. *J. Med. Chem.* **2006**, *49*, 5912–5931.

(5) Babine, R. E.; Bender, S. L. Molecular Recognition of Protein-Ligand Complexes: Applications to Drug Design. *Chem. Rev.* **1997**, *97*, 1359–1472.

(6) Martin, S. F.; Clements, J. H. Correlating Structure and Energetics in Protein-Ligand Interactions: Paradigms and Paradoxes. *Annu. Rev. Biochem.* **2013**, *82*, 267–293.

(7) Reichelt, A.; Martin, S. F. Synthesis and Properties of Cyclopropane-Derived Peptidomimetics. *Acc. Chem. Res.* **2006**, *39*, 433–442.

(8) Li, T.; Saro, D.; Spaller, M. R. Thermodynamic Profiling of Conformationally Constrained Cyclic Ligands for the PDZ Domain. *Bioorg. Med. Chem. Lett.* **2004**, *14*, 1385–1388.

(9) DeLorbe, J. E.; Clements, J. H.; Teresk, M. G.; Benfield, A. P.; Plake, H. R.; Millspaugh, L. E.; Martin, S. F. Thermodynamic and Structural Effects of Conformational Constraints in Protein−Ligand Interactions. Entropic Paradoxy Associated with Ligand Preorganization. *J. Am. Chem. Soc.* **2009**, *131*, 16758–16770.

(10) DeLorbe, J. E.; Clements, J. H.; Whiddon, B. B.; Martin, S. F. Thermodynamic and Structural Effects of Macrocyclic Constraints in

Protein−Ligand Interactions. *ACS Med. Chem. Lett.* **2010**, *1*, 448–452.

(11) Myslinski, J. M.; DeLorbe, J. E.; Clements, J. H.; Martin, S. F. Protein–Ligand Interactions: Thermodynamic Effects Associated with Increasing Nonpolar Surface Area. *J. Am. Chem. Soc.* **2011**, *133*, 18518–18521.

(12) Myslinski, J. M.; Clements, J. H.; DeLorbe, J. E.; Martin, S. F. Protein–Ligand Interactions: Thermodynamic Effects Associated with Increasing the Length of an Alkyl Chain. *ACS Med. Chem. Lett.* **2013**, *4*, 1048–1053.

(13) Myslinski, J. M.; Clements, J. H.; Martin, S. F. Protein-Ligand Interactions: Probing the Energetics of a Putative Cation-Pi Interaction. *Bioorg. Med. Chem. Lett.* **2014**, *24*, 3164–3167.

(14) Bingham, R. J.; Findlay, J. B. C.; Hsieh, S.-Y.; Kalverda, A. P.; Kjellberg, A.; Perazzolo, C.; Phillips, S. E. V.; Seshadri, K.; Trinh, C. H.; Turnbull, W. B.; Bodenhausen, G.; Homans, S. W. Thermodynamics of Binding of 2-Methoxy-3-Isopropylpyrazine and 2-Methoxy-3-Isobutylpyrazine to the Major Urinary Protein. *J. Am. Chem. Soc.* **2004**, *126*, 1675–1681.

(15) Malham, R.; Johnstone, S.; Bingham, R. J.; Barratt, E.; Phillips, S. E. V.; Laughton, C. A.; Homans, S. W. Strong Solute-Solute Dispersive Interactions in a Protein-Ligand Complex. *J. Am. Chem. Soc.* **2005**, *127*, 17061–17067.

(16) Davidson, J. P.; Lubman, O.; Rose, T.; Waksman, G.; Martin, S. F. Calorimetric and Structural Studies of 1,2,3-Trisubstituted Cyclopropanes as Conformationally Constrained Peptide Inhibitors of Src SH2 Domain Binding. *J. Am. Chem. Soc.* **2002**, *124*, 205–215.

(17) Udugamasooriya, D. G.; Spaller, M. R. Conformational Constraint in Protein Ligand Design and the Inconsistency of Binding Entropy. *Biopolymers* **2008**, *89*, 653–667.

(18) Homans, S. W. Water, Water Everywhere — Except Where It Matters? *Drug Discovery Today* **2007**, *12*, 534–539.

(19) Gilli, P.; Ferretti, V.; Gilli, G.; Borea, P. A. Enthalpy-Entropy Compensation in Drug-Receptor Binding. *J. Phys. Chem. A* **1994**, *98*, 1515–1518.

(20) Ford, D. M. Enthalpy−Entropy Compensation Is Not a General Feature of Weak Association. *J. Am. Chem. Soc.* **2005**, *127*, 16167–16170.

(21) Sharp, K. Entropy–Enthalpy Compensation: Fact or Artifact? *Protein Sci.*

**2001**, *10*, 661–667.

(22) Dunitz, J. D. Win Some, Lose Some: Enthalpy-Entropy Compensation in Weak Intermolecular Interactions. *Current Biology* **1995**, *2*, 709–712.

(23) Grunwald, E.; Steel, C. Solvent Reorganization and Thermodynamic Enthalpy-Entropy Compensation. *J. Am. Chem. Soc.* **1995**, *117*, 5687–5692.

(24) Yang, D.; Kay, L. E. Contributions to Conformational Entropy Arising From Bond Vector Fluctuations Measured From NMR-Derived Order Parameters: Application to Protein Folding. *Journal of Molecular Biology* **1996**, *263*, 369–382.

(25) Li, Z.; Raychaudhuri, S.; Wand, J. Insights Into the Local Residual Entropy of Proteins Provided by NMR Relaxation. *Protein Sci.* **1996**, *5*, 2647–2650.

(26) Ward, J. M.; Gorenstein, N. M.; Tian, J.; Martin, S. F.; Post, C. B. Constraining Binding Hot Spots: NMR and Molecular Dynamics Simulations Provide a Structural Explanation for Enthalpy−Entropy Compensation in SH2−Ligand Binding. *J. Am. Chem. Soc.* **2010**, *132*, 11058–11070.

(27) Harris, T. K.; Mildvan, A. S. High-Precision Measurement of Hydrogen Bond Lengths in Proteins by Nuclear Magnetic Resonance Methods. *Proteins* **1999**, *35*, 275–282.

(28) Brown, S. P.; Pérez-Torralba, M.; Sanz, D.; Claramunt, R. M.; Emsley, L. Determining Hydrogen-Bond Strengths in the Solid State by NMR: the Quantitative Measurement of Homonuclear J Couplings. *Chem. Commun.* **2002**, *120*, 1852–1853.

(29) Cheng, Y.-C.; Prusoff, W. H. Relationship Between the Inhibition Constant ($K_I$) And the Concentration of Inhibitor Which Causes 50 Percent Inhibition ($IC_{50}$) Of an Enzymatic Reaction. *Biochemical Pharmacology* **1973**, *22*, 3099–3108.

(30) Munson, P. J.; Rodbard, D. An Exact Correction to the "Cheng-Prusoff" Correction. *Journal of Receptor Research* **2008**, *8*, 533–546.

(31) Tellinghuisen, J. Van't Hoff Analysis of K°(T): How Good…or Bad? *Biophysical Chemistry* **2006**, *120*, 114–120.

(32) Naghibi, H.; Tamura, A.; Sturtevant, J. M. Significant Discrepancies Between Van't Hoff and Calorimetric Enthalpies. *Proc. Natl. Acad. Sci. USA* **1995**, *92*, 5597–5599.

(33) Wiseman, T.; Williston, S.; Brandts, J. F.; Lin, L.-N. Rapid Measurement of Binding Constants and Heats of Binding Using a New Titration Calorimeter. *Anal. Biochem.* **1989**, *179*, 1–131–137.

(34) Turnbull, W. B.; Daranas, A. H. On the Value of C: Can Low Affinity Systems Be Studied by Isothermal Titration Calorimetry? *J. Am. Chem. Soc.* **2003**, *125*, 14859–14866.

(35) Delorbe, J. Design, Synthesis, and Evaluation of Conformationally-Constrained Grb2 SH2 Ligands and a Concise Total Synthesis of Lycopladine A, 2010, pp 1–490.

(36) Gravensteter, A. Design and Synthesis of Conformationally Constrained Src SH2 Ligands for Protein–Ligand Thermodynamic Evaluation, 2016, pp 1–146.

(37) Momoki, K.; Sekino, J.; Sato, H.; Yamaguchi, N. Theory of Curved Molar Ratio Plots and a New Linear Plotting Method. *Anal. Chem.* **1969**, *41*, 1286–1299.

(38) Tellinghuisen, J. A Study of Statistical Error in Isothermal Titration Calorimetry. *Anal. Biochem.* **2003**, *321*, 79–88.

(39) Hansen, L. D.; Fellingham, G. W.; Russell, D. J. Simultaneous Determination of Equilibrium Constants and Enthalpy Changes by Titration Calorimetry: Methods, Instruments, and Uncertainties. *Anal. Biochem.* **2011**, *409*, 220–229.

(40) Broecker, J.; Vargas, C.; Keller, S. Revisiting the Optimal C Value for Isothermal Titration Calorimetry. *Anal. Biochem.* **2011**, *418*, 307–309.

(41) Williams, D. H.; Cox, J. P. L.; Doig, A. J.; Gardner, M.; Gerhard, U.; Kaye, P. T.; Lal, A. R.; Nicholls, I. A.; Salter, C. J.; Mitchell, R. C. Toward the Semiquantitative Estimation of Binding Constants. Guides for Peptide-Peptide Binding in Aqueous Solution. *J. Am. Chem. Soc.* **1991**, *113*, 7020–7030.

(42) Anslyn, E. V.; Dougherty, D. A. *Modern Physical Organic Chemistry*; University Science Books: Sausalito, 2006; pp 1–1099.

(43) Mathews, C. K.; van Holde, K. E.; Appling, D. R.; Anthony-Cahill, S. J. *Biochemistry*, 4 ed.; Pearson Education: Toronto, 2013.

(44) Kuntz, I. D.; Chen, K.; Sharp, K. A.; Kollman, P. A. The Maximal Affinity of

Ligands. *Proc. Natl. Acad. Sci. USA* **1999**, *96*, 9997–10002.

(45) Velazquez-Campoy, A.; Todd, M. J.; Freire, E. HIV-1 Protease Inhibitors: Enthalpic Versus Entropic Optimization of the Binding Affinity †. *Biochemistry* **2000**, *39*, 2201–2207.

(46) Ruben, A. J.; Kiso, Y.; Freire, E. Overcoming Roadblocks in Lead Optimization: a Thermodynamic Perspective. *Chem Biol Drug Design* **2006**, *67*, 2–4.

(47) Homans, S. W. Dynamics and Thermodynamics of Ligand–Protein Interactions. *Top. Curr. Chem.* **2007**, *272*, 51–82.

(48) Pitzer, K. S.; Gwinn, W. D. Energy Levels and Thermodynamic Functions for Molecules with Internal Rotation I. Rigid Frame with Attached Tops. *The Journal of Chemical Physics* **1942**, *10*, 428–440.

(49) Bracken, C.; Carr, P. A.; Cavanagh, J.; Palmer, A. G., III. Temperature Dependence of Intramolecular Dynamics of the Basic Leucine Zipper of GCN4: Implications for the Entropy of Association with DNA. *Journal of Molecular Biology* **1999**, *285*, 2133–2146.

(50) Lee, A. L.; Kinnear, S. A.; Wand, J. Redistribution and Loss of Side Chain Entropy Upon Formation of a Calmodulin–Peptide Complex. *Nat. Struct. Biol.* **2000**, *7*, 72–77.

(51) Zidek, L.; Novotny, M. V.; Stone, M. J. Increased Protein Backbone Conformational Entropy Upon Hydrophobic Ligand Binding. *Nat. Struct. Biol.* **1999**, *6*, 1118–1121.

(52) Mäller, L.; Blankenship, J.; Rance, M.; Chazin, W. J. Site–Site Communication in the EF-Hand Ca2+-Binding Protein Calbindin D9k. *Nat. Struct. Biol.* **2000**, *7*, 245–250.

(53) Loh, A. P.; Pawley, N.; Nicholson, L. K.; Oswald, R. E. An Increase in Side Chain Entropy Facilitates Effector Binding: NMR Characterization of the Side Chain Methyl Group Dynamics in Cdc42Hs †. *Biochemistry* **2001**, *40*, 4590–4600.

(54) Hanessia, S.; McNaughton-Smith, G.; Lombart, H.-G.; Lubell, W. D. Design and Synthesis of Conformationally Constrained Amino Acids as Versatile Scaffolds and Peptide Mimetics. *Tetrahedron* **1997**, *53*, 12789–12854.

(55) Searle, M. S.; Williams, D. H. The Cost of Conformational Order: Entropy Cbanges in Molecular Associations. *J. Am. Chem. Soc.* **1992**, *114*, 10690–10697.

(56) Smith, W. W.; Bartlett, P. A. Macrocyclic Inhibitors of Penicillopepsin. 3. Design, Synthesis, and Evaluation of an Inhibitor Bridged Between P2 and P1'. *J. Am. Chem. Soc.* **1998**, *120*, 4622–4628.

(57) Gerhard, U.; Searle, M. S.; Williams, D. H. The Free Energy Change of Restricting a Bond Rotation in the Binding of Peptide ANalogues to Vancomycin Group Antibiotics. *Bioorg. Med. Chem. Lett.* **1993**, *3*, 803–808.

(58) Searle, M. S.; Williams, D. H.; Gerhard, U. Partitioning of Free Energy Contributions in the Estimation of Binding Constants: Residual Motions and Consequences for Amide-Amide Hydrogen Bond Strengths. *J. Am. Chem. Soc.* **1992**, *114*, 10697–10704.

(59) Martin, R. S.; Henningsen, R. A.; Suen, A.; Apparsundaram, S.; Leung, B.; Jia, Z.; Kondru, R. K.; Milla, M. E. Kinetic and Thermodynamic Assessment of Binding of Serotonin Transporter Inhibitors. *J. Pharmacol. Exp. Ther.* **2008**, *327*, 991–1000.

(60) Boström, J.; Hogner, A.; Schmitt, S. Do Structurally Similar Ligands Bind in a Similar Fashion? *J. Med. Chem.* **2006**, *49*, 6716–6725.

(61) Talhout, R.; Villa, A.; Mark, A. E.; Engberts, J. B. F. N. Understanding Binding Affinity: a Combined Isothermal Titration Calorimetry/Molecular Dynamics Study of the Binding of a Series of Hydrophobically Modified Benzamidinium Chloride Inhibitors to Trypsin. *J. Am. Chem. Soc.* **2003**, *125*, 10570–10579.

(62) Williams, D. H.; Stephens, E.; Zhou, M. Ligand Binding Energy and Catalytic Efficiency From Improved Packing Within Receptors and Enzymes. *Journal of Molecular Biology* **2003**, *329*, 389–399.

(63) MacRaild, C. A.; Daranas, A. H. N.; Bronowska, A.; Homans, S. W. Global Changes in Local Protein Dynamics Reduce the Entropic Cost of Carbohydrate Binding in the Arabinose-Binding Protein. **2007**, *368*, 822–832.

(64) Stone, M. J. NMR Relaxation Studies of the Role of Conformational Entropy in Protein Stability and Ligand Binding. *Acc. Chem. Res.* **2001**, *34*, 379–388.

(65) Hruby, V. J. Designing Peptide Receptor Agonists and Antagonists. *Net. Rev.*

*Drug Discov.* **2002**, *1*, 847–858.

(66) Avan, I.; Hall, C. D.; Katritzky, A. R. Peptidomimetics via Modifications of Amino Acids and Peptide Bonds. *Chem. Soc. Rev.* **2014**, *43*, 3575–20.

(67) Tsantrizos, Y. S.; Bolger, G.; Bonneau, P.; Cameron, D. R.; Goudreau, N.; Kukolj, G.; LaPlante, S. R.; Llinàs-Brunet, M.; Nar, H.; Lamarre, D. Macrocyclic Inhibitors of the NS3 Protease as Potential Therapeutic Agents of Hepatitis C Virus Infection. *Angew. Chem. Int. Ed.* **2003**, *42*, 1356–1360.

(68) Reichelt, A.; Gaul, C.; Frey, R. R.; Kennedy, A.; Martin, S. F. Design, Synthesis, and Evaluation of Matrix Metalloprotease Inhibitors Bearing Cyclopropane-Derived Peptidomimetics as P1‘ and P2‘ Replacements. *J. Org. Chem.* **2002**, *67*, 4062–4075.

(69) Hillier, M. C.; Davidson, J. P.; Martin, S. F. Cyclopropane-Derived Peptidomimetics. Design, Synthesis, and Evaluation of Novel Ras Farnesyltransferase Inhibitors. *J. Org. Chem.* **2001**, *66*, 1657–1671.

(70) Martin, S. F.; Dorsey, G. O.; Gane, T.; Hillier, M. C. Cyclopropane-Derived Peptidomimetics. Design, Synthesis, Evaluation, and Structure of Novel HIV-1 Protease Inhibitors. *J. Med. Chem.* **1998**, *41*, 1581–1597.

(71) Martin, S. F.; Austin, R. E.; Oalmann, C. J.; Baker, W. R.; Condon, S. L.; deLara, E.; Rosenberg, S. H.; Spina, K. P.; Stein, H. H.; Cohen, J.; Kleinert, H. D. 1,2,3-Trisubstituted Cyclopropanes as Conformationally Restricted Peptide Isosteres: Application to the Design and Synthesis of Novel Renin Inhibitors. *J. Med. Chem.* **1992**, *35*, 1710–1721.

(72) Plake, H. R.; Sundberg, T. B.; Woodward, A. R.; Martin, S. F. Design and Synthesis of Conformationally Constrained, Extended and Reverse Turn Pseudopeptides as Grb2-SH2 Domain Antagonists. *Tetrahedron Lett.* **2003**, *44*, 1571–1574.

(73) Momany, F. A. Conformational Energy Analysis of the Molecule, Luteinizing Hormone-Releasing Hormone. 1. Native Decapeptide. *J. Am. Chem. Soc.* **1976**, *98*, 2990–2996.

(74) Freidinger, R.; Veber, D.; Perlow, D.; Brooks; Saperstein, R. Bioactive Conformation of Luteinizing Hormone-Releasing Hormone: Evidence From a Conformationally Constrained Analog. *Science* **1980**, *210*, 656–658.

(75) LaPlante, S. R.; Cameron, D. R.; Aubry, N.; Lefebvre, S.; Kukolj, G.; Maurice,

R.; Thibeault, D.; Lamarre, D.; Llinas-Brunet, M. Solution Structure of Substrate-Based Ligands When Bound to Hepatitis C Virus NS3 Protease Domain. *Journal of Biological Chemistry* **1999**, *274*, 18618–18624.

(76) Llinàs-Brunet, M.; Bailey, M. D.; Fazal, G.; Ghiro, E.; Gorys, V.; Goulet, S.; Halmos, T.; Maurice, R.; Poirier, M.; Poupart, M.-A.; Rancourt, J.; Thibeault, D.; Wernic, D.; Lamarre, D. Highly Potent and Selective Peptide-Based Inhibitors of the Hepatitis C Virus Serine Protease: Towards Smaller Inhibitors. *Bioorg. Med. Chem. Lett.* **2000**, *10*, 2267–2270.

(77) Martin, S. F.; Dwyer, M. P.; Hartmann, B.; Knight, K. S. Cyclopropane-Derived Peptidomimetics. Design, Synthesis, and Evaluation of Novel Enkephalin Analogues. *J. Org. Chem.* **2000**, *65*, 1305–1318.

(78) Shakespeare, W.; Yang, M.; Bohacek, R.; Cerasoli, F.; Stebbins, K.; Sundaramoorthi, R.; Azimioara, M.; Vu, C.; Pradeepan, S.; Metcalf, C.; Haraldson, C.; Merry, T.; Dalgarno, D.; Narula, S.; Hatada, M.; Lu, X.; van Schravendijk, M. R.; Adams, S.; Violette, S.; Smith, J.; Guan, W.; Bartlett, C.; Herson, J.; Iuliucci, J.; Weigele, M.; Sawyer, T. Structure-Based Design of an Osteoclast-Selective, Nonpeptide Src Homology 2 Inhibitor with I*N Vivo* Antiresorptive Activity. *Proceedings of the National Academy of Sciences* **2000**, *97*, 9373–9378.

(79) Charifson, P. S.; Shewchuk, L. W.; Rocque, W.; Hummel, C. W.; Jordan, S. R.; Mohr, C.; Pacofsky, G. J.; Peel, M. R.; Rodriguez, M.; Sternbach, D. D.; Consler, T. G. Peptide Ligands of $Pp60^{C\text{-}Src}$ SH2 Domains: a Thermodynamic and Structural Study. *Biochemistry* **1997**, *36*, 6283–6293.

(80) Bradshaw, J. M.; Grucza, R. A.; Bradbury, J. E.; Waksman, G. Probing the "Two-Pronged Plug Two-Holed Socket" Model for the Mechanism of Binding of the Src SH2 Domain to Phosphotyrosyl Peptides: a Thermodynamic Study. *Biochemistry* **1998**, *37*, 9083–9090.

(81) Waksman, G.; Shoelson, S. E.; Pant, N.; Cowburn, D.; Kuriyan, J. Binding of a High Affinity Phosphotyrosyl Peptide to the Src SH2 Domain: Crystal Structures of the Complexed and Peptide-Free Forms. *Cell* **1993**, *72*, 779–790.

(82) Songyang, Z.; Shoelson, S. E.; Chaudhuri, M.; Gish, G.; Pawson, T.; Haser, W. G.; King, F.; Roberts, T.; Ratnofsky, S.; LEchleider, R. J.; Neel, B. G.; Birge, R. B.; Fajardo, J. E.; Chou, M. M.; Hanafusa, H.; Schaffhausen, B.; Cantley, L. C. SH2 Domains Recognize Specific Phosphopeptide Sequences. *Cell* **1993**, *72*, 767–778.

(83) Bradshaw, J. M.; Waksman, G. Calorimetric Examination of High-Affinity Src SH2 Domain-Tyrosyl Phosphopeptide Binding:? Dissection of the Phosphopeptide Sequence Specificity and Coupling Energetics ? *Biochemistry* **1999**, *38*, 5147–5154.

(84) Bradshaw, J. M.; Mitaxov, V.; Waksman, G. Investigation of Phosphotyrosine Recognition by the SH2 Domain of the Src Kinase. *Journal of Molecular Biology* **1999**, *293*, 971–985.

(85) Davidson, J. P. Calorimetric and Structural Studies of 1,2,3-Trisubstituted Cyclopropanes as Conformationally Constrained Peptide Miimcs, 2001, pp 1–304.

(86) Bonaparte, A. C. Synthesis of B-Heteroaryl Propionates via Trapping of Carbocations with Π-Nucleophiles, Efforts Towards the Total Synthesis of Acutumine, and the Design, Synthesis, and Thermodynamics of Protein-Ligand Interactions at the Src SH2 Domain, 2013, pp 1–398.

(87) Shi, Y.; Zhu, C. Z.; Martin, S. F.; Ren, P. Probing the Effect of Conformational Constraint on Phosphorylated Ligand Binding to an SH2 Domain Using Polarizable Force Field Simulations. *J. Phys. Chem. B* **2012**, *116*, 1716–1727.

(88) Ettmayer, P.; France, D.; Gounarides, J.; Jarosinski, M.; Martin, M.-S.; Rondeau, J.-M.; Sabio, M.; Topiol, S.; Weidmann, B.; Zurini, M.; Bair, K. W. Structural and Conformational Requirements for High-Affinity Binding to the SH2 Domain of Grb2. *J. Med. Chem.* **1999**, *42*, 971–980.

(89) Rahuel, J.; Gay, B.; Erdmann, D.; Strauss, A.; García-Echeverría, C.; Furet, P.; Caravatti, G.; Fretz, H.; Schoepfer, J.; Grütter, M. G. Structural Basis for Specificity of GRB2-SH2 Revealed by a Novel Ligand Binding Mode. *Nat. Struct. Biol.* **1996**, *3*, 586–589.

(90) Eley, D. D. On the Solubility of Gases. Part I.—the Inert Gases in Water. *Trans. Faraday Soc.* **1939**, *35*, 1281–1293.

(91) Frank, H. S. Free Volume and Entropy in Condensed Systems I. General Principles. Fluctuation Entropy and Free Volume in Some Monatomic Crystals. *The Journal of Chemical Physics* **1945**, *13*, 478–492.

(92) Setny, P.; Baron, R.; McCammon, J. A. How Can Hydrophobic Association Be Enthalpy Driven? *J. Chem. Theory Comput.* **2010**, *6*, 2866–2871.

(93) Cheng, Y.-K.; Rossky, P. J. Surface Topography Dependence of Biomolecular

Hydrophobic Hydration. *Nature* **1998**, *392*, 696–699.

(94) Cheng, Y.-K.; Sheu, W.-S.; Rossky, P. J. Hydrophobic Hydration of Amphipathic Peptides. *Biophys. J.* **1999**, *76*, 1734–1743.

(95) Houk, K. N.; Leach, A. G.; Kim, S. P.; Zhang, X. Binding Affinities of Host–Guest, Protein–Ligand, and Protein–Transition-State Complexes. *Angew. Chem. Int. Ed.* **2003**, *42*, 4872–4897.

(96) Mirejovsky, D.; Arnett, E. M. Heat Capacities of Solution for Alcohols in Polar Solvents and the New View of Hydrophobic Effects. *J. Am. Chem. Soc.* **1983**, *105*, 1112–1117.

(97) García-Echeverría, C.; Gay, B.; Rahuel, J.; Furet, P. Mapping the X+1 Binding Site of the Grb2-SH2 Domain with a,a-Disubstituted Cyclic a-Amino Acids. *Bioorg. Med. Chem. Lett.* **1999**, *9*, 2915–2920.

(98) Schoepfer, J.; Gay, B.; Caravatti, G.; García-Echeverría, C.; Fretz, H.; Rahuel, J.; Furet, P. Structure-Based Design of Peptidomimetic Ligands of the Grb2-SH2 Domain. *Bioorg. Med. Chem. Lett.* **1998**, *8*, 2865–2870.

(99) Sharrow, S. D.; Novotny, M. V.; Stone, M. J. Thermodynamic Analysis of Binding Between Mouse Major Urinary Protein-I and the Pheromone 2- Sec-Butyl-4,5-Dihydrothiazole, *Biochemistry* **2003**, *42*, 6302–6309.

(100) Wang, L.; Berne, B. J.; Friesner, R. A. Ligand Binding to Protein-Binding Pockets with Wet and Dry Regions. *Proceedings of the National Academy of Sciences* **2011**, *108*, 1326–1330.

(101) Gerlach, C.; Smolinski, M.; Steuber, H.; Sotriffer, C. A.; Heine, A.; Hangauer, D. G.; Klebe, G. Thermodynamic Inhibition Profile of a Cyclopentyl and a Cyclohexyl Derivative Towards Thrombin: the Same but for Different Reasons. *Angew. Chem. Int. Ed.* **2007**, *46*, 8511–8514.

(102) Englert, L.; Biela, A.; Zayed, M.; Heine, A.; Hangauer, D.; Klebe, G. Displacement of Disordered Water Molecules From Hydrophobic Pocket Creates Enthalpic Signature: Binding of Phosphonamidate to the S1'-Pocket of Thermolysin. *BBA - General Subjects* **2010**, *1800*, 1192–1202.

(103) Myslinski, J. M.; DeLorbe, J. E.; Clements, J. H.; Martin, S. F. Protein–Ligand Interactions: Thermodynamic Effects Associated with Increasing Nonpolar Surface Area. *J. Am. Chem. Soc.* **2011**, *133*, 18518–18521.

(104) Llinàs-Brunet, M.; Bailey, M. D.; Goudreau, N.; Bhardwaj, P. K.; Bordeleau, J.; Bös, M.; Bousquet, Y.; Cordingley, M. G.; Duan, J.; Forgione, P.; Garneau, M.; Ghiro, E.; Gorys, V.; Goulet, S.; Halmos, T.; Kawai, S. H.; Naud, J.; Poupart, M.-A.; White, P. W. Discovery of a Potent and Selective Noncovalent Linear Inhibitor of the Hepatitis C Virus NS3 Protease (BI 201335). *J. Med. Chem.* **2010**, *53*, 6466–6476.

(105) Lauer, G. M.; Walker, B. D. Hepatitis C Virus Infection. *N. Engl. J. Med.* **2001**, *345*, 41–52.

(106) Alter, M. J.; Kruszon-Moran, D.; Nainan, O. V.; McQuillan, G. M.; Gao, F.; Moyer, L. A.; Kaslow, R. A.; Margolis, H. S. The Prevalence of Hepatitis C Virus Infection in the United States, 1988 Through 1994. *N. Engl. J. Med.* **1999**, *341*, 556–562.

(107) Grakoui, A.; Wychowski, C.; Lin, C.; Feinstone, S. M.; Rice, C. M. Expression and Identification of Hepatitis C Virus Polyprotein Cleavage Products. *J. Virol.* **1993**, *67*, 1385–1395.

(108) Bartenschlager, R.; Ahlborn-Laake, L.; Mous, J.; Jacobsen, H. Nonstructural Protein 3 of the Hepattis C Virus Encodes a Serine-Type PRoteinase Required for Cleavage at the NS3/4 and NS4/5 Junctions. *J. Virol.* **1993**, *67*, 3835–3844.

(109) Tomei, L.; Failla, C.; Santolini, E.; de Francesco, R.; La Monica, N. NS3 Is a Serine Protease Required for Processing of Hepatitis C Virus Polyprotein. *J. Virol.* **1993**, *67*, 4017–4026.

(110) Grakoui, A.; McCourt, D. W.; Wychowski, C.; Feinstone, S. M.; Rice, C. M. Characterization of the Hepatitis C Virus-Encoded Serine Proteinase: Determination of the Proteinase-Dependent Polyprotein Cleavage Sites. *J. Virol.* **1993**, *67*, 2832–2843.

(111) Simmonds, P.; Holmes, E. C.; Cha, T. A.; Chan, S. W.; McOmish, F.; Irvine, B.; Beall, E.; Yap, P. L.; Kolberg, J.; Urdea, M. S. Classification of Hepatitis C Virus Into Six Major Genotypes and a Series of Subtypes by Phylogenetic Analysis of the NS-5 Region. **1993**, 2391–2399.

(112) Hoofnagle, J. H.; Mullen, K. D.; Jones, B.; Rustgi, V.; Di Bisceglie, A.; Peters, M.; Waggoner, J. G.; Park, Y.; Jones, E. A. Treatment of Chronic Non-a, Non-B Hepatitis with Recombinant Human Alpha Interferon. *N. Engl. J. Med.* **1986**, *315*, 1575–1578.

(113) Di Bisceglie, A. M.; Martin, P.; Kassianides, C.; Lisker-Melman, M.; Murray,

L.; Waggoner, J. G.; Goodman, Z. D.; Banks, S. M.; Hoofnagle, J. H. Recombinant Interferon Alfa Therapy for Chronic Hepatitis C. *N. Engl. J. Med.* **1989**, *321*, 1506–1510.

(114) Davis, G. L.; Balart, L. A.; Schiff, E. R.; Lindsay, K.; Bodenheimer, H. C.; Perrillo, R. P.; Carey, W.; Jacobson, I. M.; Payne, J.; Dienstag, J. L.; VanThiel, D. H.; Tamburro, C.; Lefkowitch, J.; Albrecht, J.; Meschievitz, C.; Ortego, T. J.; Gibas, A. Treatment of Chronic Hepatitis C with Recombinant Interferon Alfa. *N. Engl. J. Med.* **1989**, *321*, 1501–1506.

(115) Jacobson, I. M.; McHutchison, J. G.; Dusheiko, G.; Di Bisceglie, A. M.; Reddy, K. R.; Bzowej, N. H.; Marcellin, P.; Muir, A. J.; Ferenci, P.; Flisiak, R.; George, J.; Rizzetto, M.; Shouval, D.; SOla, R.; Terg, R. A.; Yoshida, E. M.; Adda, N.; Bengtsson, L.; Sankoh, A. J.; Kieffer, T. L.; GEorge, S.; Kauffman, R. S.; Zeuzem, S. Telaprevir for Previously Untreated Chronic Hepatitis C Virus Infection. *N. Engl. J. Med.* **2011**, *364*, 2405–2416.

(116) Poordad, F.; McCone, J., Jr; Bacon, B. R.; Savino, B.; Manns, M. P.; Sulkowski, M. S.; Jacobson, I. M.; Reddy, K. R.; Goodman, Z. D.; Boparai, N.; DiNubile, M. J.; Sniukiene, V.; Brass, C. A.; Albrecht, J. K.; Bronowicki, J.-P. Boceprevir for Untreated Chronic HCV Genotype 1 Infection. *N. Engl. J. Med.* **2011**, *364*, 1195–1206.

(117) Tanwar, S.; Trembling, P. M.; Dusheiko, G. M. TMC435 for the Treatment of Chronic Hepatitis C. *Expert Opin. Investig. Drugs* **2012**, *21* (8), 1193–1209.

(118) Rolland, S.; Vachon, M.-L. Sofosbuvir for the Treatment of Hepatitis C Virus Infection. *Can. Med. Assoc. J.* **2015**, *187*, 203–204.

(119) Younossi, Z. M.; Stepanova, M.; Afdhal, N.; Kowdley, K. V.; Zeuzem, S.; Henry, L.; Hunt, S. L.; Marcellin, P. Improvement of Health-Related Quality of Life and Work Productivity in Chronic Hepatitis C Patients with Early and Advanced Fibrosis Treated with Ledipasvir and Sofosbuvir. *Journal of Hepatology* **2015**, *63*, 337–345.

(120) Zeng, Q.-L.; Xu, G.-H.; Zhang, J.-Y.; Li, W.; Zhang, D.-W.; Li, Z.-Q.; Liang, H.-X.; Li, C.-X.; Yu, Z.-J. Generic Ledipasvir-Sofosbuvir for Patients with Chronic Hepatitis C: a Real-Life Observational Study. *Journal of Hepatology* **2017**, 1–7.

(121) Ohara, E.; Hiraga, N.; Imamura, M.; Iwao, E.; Kamiya, N.; Yamada, I.; Kono, T.; Onishi, M.; Hirata, D.; Mitsui, F.; Kawaoka, T.; Tsuge, M.; Takahashi, S.; Abe, H.; Hayes, C. N.; Ochi, H.; Tateno, C.; Yoshizato, K.; Tanaka, S.; Chayama, K. Elimination of Hepatitis C Virus by Short Term NS3-4A and

NS5B Inhibitor Combination Therapy in Human Hepatocyte Chimeric Mice. *Journal of Hepatology* **2011**, *54*, 872–878.

(122) Shi, N.; Hiraga, N.; Imamura, M.; Hayes, C. N.; Zhang, Y.; Kosaka, K.; Okazaki, A.; Murakami, E.; Tsuge, M.; Abe, H.; Aikata, H.; Takahashi, S.; Ochi, H.; Tateno-Mukaidani, C.; Yoshizato, K.; Matsui, H.; Kanai, A.; Inaba, T.; McPhee, F.; Gao, M.; Chayama, K. Combination Therapies with NS5A, NS3 and NS5B Inhibitors on Different Genotypes of Hepatitis C Virus in Human Hepatocyte Chimeric Mice. *Gut* **2013**, *62*, 1055–1061.

(123) Kolykhalov, A. A.; Mihalik, K.; Feinstone, S. M.; Rice, C. M. Hepatitis C Virus-Encoded Enzymatic Activities and Conserved RNA Elements in the 3 Nontranslated Region Are Essential for Virus Replication in Vivo. *J. Virol.* **2000**, *74*, 2046–2051.

(124) Failla, C.; Tomei, L.; de Francesco, R. Both NS3 and NS4A Are Required for Proteolytic Processing of Hepatitis C Virus Nonsructural Proteins. *J. Virol.* **1994**, *68*, 3753–3760.

(125) Love, R. A.; Parge, H. E.; Wickersham, J. A.; Hostomsky, Z.; Habuka, N.; Moomaw, E. W.; Adachi, T.; Hostomska, Z. The Crystal Structure of Hepatitis C Virus NS3 Proteinase Reveals a Trypsin-Like Fold and a Structural Zinc Binding Site. *Cell* **1996**, *87*, 331–342.

(126) Abian, O.; Vega, S.; Neira, J. L.; Velazquez-Campoy, A. Conformational Stability of Hepatitis C Virus NS3 Protease. *Biophys. J.* **2010**, *99*, 3811–3820.

(127) Bartenschlager, R.; Lohmann, V.; Wilkinson, T.; Koch, J. O. Complex Formation Between the NS3 Serine-Type Proteinase of the Hepatitis C Virus and NS4A and Its Importance for Polyprotein Maturation. *J. Virol.* **1995**, *69*, 7519–7528.

(128) Failla, C.; Tomei, L.; de Francesco, R. An Amino-Terminal Domain of the Hepatitis C Virus NS3 Protease Is Essential for Interaction with NS4A. *J. Virol.* **1995**, *69*, 1769–1777.

(129) Kolykhalov, A. A.; Agapov, E. V.; Rice, C. M. Specificity of the Hepatitis C Virus NS3 Serine Protease: Effects of Substitutions at the 3/4A, 4A/4B, 4B/5A, and 5A/5B Cleavage Sites on Polyprotein Processing. *J. Virol.* **1994**, *68*, 7525–7533.

(130) Di Marco, S.; Rizzi, M.; Volpari, C.; Walsh, M. A.; Narjes, F.; Colarusso, S.; de Francesco, R.; Matassa, V. G.; Sollazzo, M. Inhibition of the Hepatitis C

Virus NS3/4A Protease. *Journal of Biological Chemistry* **2000**, *275*, 7152–7157.

(131) Llinàs-Brunet, M.; Bailey, M. D.; Fazal, G.; Goulet, S.; Halmos, T.; LaPlante, S. R.; Maurice, R.; Poirier, M.; Poupart, M.-A.; Thibeault, D.; Wernic, D.; Lamarre, D. Peptide-Based Inhibitors of the Hepatitis C Virus Serine Protease. *Bioorg. Med. Chem. Lett.* **1998**, *8*, 1713–1718.

(132) Llinàs-Brunet, M.; Bailey, M. D.; Déziel, R.; Fazal, G.; Gorys, V.; Goulet, S.; Halmos, T.; Maurice, R.; Poirier, M.; Poupart, M.-A.; Rancourt, J.; Thibeault, D.; Wernic, D.; Lamarre, D. Studies on the C-Terminal of Hexapeptide Inhibitors of the Hepatitis C Virus Serine Protease. *Bioorg. Med. Chem. Lett.* **1998**, *8*, 2719–2724.

(133) Poupart, M.-A.; Cameron, D. R.; Chabot, C.; Ghiro, E.; Goudreau, N.; Goulet, S.; Poirier, M.; Tsantrizos, Y. S. Solid-Phase Synthesis of Peptidomimetic Inhibitors for the Hepatitis C Virus NS3 Protease. *J. Org. Chem.* **2001**, *66*, 4743–4751.

(134) Pause, A.; Kukolj, G.; Bailey, M.; Brault, M.; Dô, F.; Halmos, T.; Lagacé, L.; Maurice, R.; Marquis, M.; McKercher, G.; Pellerin, C.; Pilote, L.; Thibeault, D.; Lamarre, D. An NS3 Serine Protease Inhibitor Abrogates Replication of Subgenomic Hepatitis C Virus RNA. *Journal of Biological Chemistry* **2003**, *278*, 20374–20380.

(135) Lamarre, D.; ANderson, P. C.; Bailey, M.; Beaulieu, P.; Bolger, G.; Bonneau, P.; Bös, M.; Cameron, D. R.; Cartier, M.; Cordingley, M. G.; Faucher, A.-M.; Goudreau, N.; Kawai, S. H.; Kukolj, G.; Legacé, L.; LaPlante, S. R.; Narjes, H.; Poupart, M.-A.; Rancourt, J.; Sentjens, R. E.; George, R. S.; Simoneau, B.; Steinmann, G.; Thibeault, D.; Tsantrizos, Y. S.; Welcond, S. M.; Yong, C.-L.; Llinàs-Brunet, M. An NS3 Protease Inhibitor with Antiviral Effects in Humans Infected with Hepatitis C Virus. *Nature* **2003**, *426*, 186–189.

(136) Goudreau, N.; Cameron, D. R.; Bonneau, P.; Gorys, V.; Plouffe, C.; Poirier, M.; Lamarre, D.; Llinàs-Brunet, M. NMR Structural Characterization of Peptide Inhibitors Bound to the Hepatitis C Virus NS3 Protease: Design of a New P2 Substituent. *J. Med. Chem.* **2004**, *47*, 123–132.

(137) Llinàs-Brunet, M.; Bailey, M. D.; Bolger, G.; Brochu, C.; Faucher, A.-M.; Ferland, J. M.; Garneau, M.; Ghiro, E.; Gorys, V.; Grand-Maître, C.; Halmos, T.; Lapeyre-Paquette, N.; Liard, F.; Poirier, M.; Rhéaume, M.; Tsantrizos, Y. S.; Lamarre, D. Structure−Activity Study on a Novel Series of Macrocyclic Inhibitors of the Hepatitis C Virus NS3 Protease Leading to the Discovery of

BILN 2061. *J. Med. Chem.* **2004**, *47*, 1605–1608.

(138) Rancourt, J.; Cameron, D. R.; Gorys, V.; Lamarre, D.; Poirier, M.; Thibeault, D.; Llinàs-Brunet, M. Peptide-Based Inhibitors of the Hepatitis C Virus NS3 Protease: Structure−Activity Relationship at the C-Terminal Position. *J. Med. Chem.* **2004**, *47*, 2511–2522.

(139) Faucher, A.-M.; Bailey, M. D.; Beaulieu, P. L.; Brochu, C.; Duceppe, J.-S.; Ferland, J. M.; Ghiro, E.; Gorys, V.; Halmos, T.; Kawai, S. H.; Poirier, M.; Simoneau, B.; Tsantrizos, Y. S.; Llinàs-Brunet, M. Synthesis of BILN 2061, an HCV NS3 Protease Inhibitor with Proven Antiviral Effect in Humans. *Org. Lett.* **2004**, *6*, 2901–2904.

(140) Llinàs-Brunet, M.; Bailey, M. D.; Ghiro, E.; Gorys, V.; Halmos, T.; Poirier, M.; Rancourt, J.; Goudreau, N. A Systematic Approach to the Optimization of Substrate-Based Inhibitors of the Hepatitis C Virus NS3 Protease: Discovery of Potent and Specific Tripeptide Inhibitors. *J. Med. Chem.* **2004**, *47*, 6584–6594.

(141) Kawai, S. H.; Bailey, M. D.; Halmos, T.; Forgione, P.; LaPlante, S. R.; Llinàs-Brunet, M.; Naud, J.; Goudreau, N. The Use of Chemical Double-Mutant Cycles in Biomolecular Recognition Studies: Application to HCV NS3 Protease Inhibitors. *ChemMedChem* **2008**, *3*, 1654–1657.

(142) Kakiuchi, N.; Hijikata, M.; Komoda, Y.; Tanji, Y.; Hirowatari, Y.; Shimotohno, K. Bacterial Expression and Analysis of Cleavage Activity of HCV Serine Proteinase Using Recombinant and Synthetic Substrate. *Biochemical and Biophysical Research Communications* **1995**, *210*, 1059–1065.

(143) Steinkühler, C.; Biasiol, G.; Brunetti, M.; Urbani, A.; Koch, U.; Cortese, R.; Pessi, A.; de Francesco, R.; Raffae. Product Inhibition of the Hepatitis C Virus NS3 Protease. *Biochemistry* **1998**, *37*, 8899–8905.

(144) Kim, J. L.; Morgenstern, K. A.; Lin, C.; Fox, T.; Dwyer, M. D.; Landro, J. A.; Chambers, S. P.; Markland, W.; Lepre, C. A.; OMalley, E. T.; Harbeson, S. L.; Rice, C. M.; Murcko, M. A.; Caron, P. R.; Thomson, J. A. Crystal Structure of the Hepatitis C Virus NS3 Protease Domain Complexed with a Synthetic NS4A Cofactor Peptide. *Cell* **1996**, *87*, 343–355.

(145) Mehdi, S. Synthetic and Naturally Occurring Protease Inhibitors Containing an Electophilic Carbonyl Group. *Bioorganic Chemistry* **1993**, *21*, 249–259.

(146) Stoltz, J. H.; Stern, J. O.; Huang, Q.; Seidler, R. W.; Pack, F. D.; Knight, B. L. A Twenty-Eight-Day Mechanistic Time Course Study in the Rhesus Monkey with Hepatitis C Virus Protease Inhibitor BILN 2061. *Toxicologic Pathology* **2011**, *39*, 496–501.

(147) Carter, P. J.; Winter, G.; Wilkinson, A. J.; Fersht, A. R. The Use of Double Mutants to Detect Structural Changes in the Active Site of the Tyrosyl-tRNA Synthetase (Bacillus Stearothermophilus). *Cell* **1984**, *38*, 835–840.

(148) Aoyama, Y.; Asakawa, M.; Matsui, Y.; Ogoshi, H. Molecular Recognition of Quinones: Two-Point Hydrogen-Bonding Strategy for the Construction of Face-to-Face Porphyrin-Quinone Architectures'. *J. Am. Chem. Soc.* **1991**, *113*, 6233–6240.

(149) Kato, Y.; Conn, M. M.; Rebek, J., Jr. Water-Soluble Receptors for Cyclic-AMP and Their Use for Evaluating Phosphate-Guanidinium Interactions. *J. Am. Chem. Soc.* **1994**, *116*, 3279–3284.

(150) Bisson, A. P.; Carver, F. J.; Hunter, C. A.; Waltho, J. Molecular Zippers. *J. Am. Chem. Soc.* **1994**, *116*, 10292–10293.

(151) Bisson, A. P.; Carver, F. J.; Eggleston, D. S.; Haltiwanger, R. C.; Hunter, C. A.; Livingstone, D. L.; McCabe, J. F.; Rotger, C.; Rowan, A. E. Synthesis and Recognition Properties of Aromatic Amide Oligomers: Molecular Zippers. *J. Am. Chem. Soc.* **2000**, *122*, 8856–8868.

(152) Adams, H.; Hunter, C. A.; Lawson, K. R.; Perkins, J.; Spey, S. E.; Urch, C. J.; Sanderson, J. M. A Supramolecular System for Quantifying Aromatic Stacking Interactions. *Chem. Eur. J.* **2001**, *7*, 4863–4877.

(153) Hunter, C. A.; Low, C. M. R.; Vinter, J. G.; Zonta, C. Quantification of Functional Group Interactions in Transition States. *J. Am. Chem. Soc.* **2003**, *125*, 9936–9937.

(154) Cockroft, S. L.; Hunter, C. A. Chemical Double-Mutant Cycles: Dissecting Non-Covalent Interactions. *Chem. Soc. Rev.* **2007**, *36*, 172–188.

(155) Thibeault, D.; Massariol, M.-J.; Zhao, S.; Welchner, E.; Goudreau, N.; Gingras, R.; Llinàs-Brunet, M.; White, P. W. Use of the Fused NS4A Peptide−NS3 Protease Domain to Study the Importance of the Helicase Domain for Protease Inhibitor Binding to Hepatitis C Virus NS3-NS4A. *Biochemistry* **2009**, *48*, 744–753.

(156) Lemke, C. T.; Goudreau, N.; Zhao, S.; Hucke, O.; Thibeault, D.; Llinas-Brunet, M.; White, P. W. Combined X-Ray, NMR, and Kinetic Analyses Reveal Uncommon Binding Characteristics of the Hepatitis C Virus NS3-NS4A Protease Inhibitor BI 201335. *Journal of Biological Chemistry* **2011**, *286*, 11434–11443.

(157) Nsumiwa, S.; Kuter, D.; Wittlin, S.; Chibale, K.; Egan, T. J. Structure–Activity Relationships for Ferriprotoporphyrin IX Association and B-Hematin Inhibition by 4-Aminoquinolines Using Experimental and Ab Initio Methods. *Bioorg. Med. Chem.* **2013**, *21*, 3738–3748.

(158) Beak, P.; Fry, F. S., Jr; Lee, J.; Steele, F. Equilibration Studies. Protomeric Equilibria of 2- and 4-Hydroxypyridines, 2- and 4-Hydroxypyrimidines, 2- and 4-Mercaptopyridines, and Structurally Related Compounds in the Gas Phase. *J. Am. Chem. Soc.* **1976**, *98*, 171–179.

(159) Desjardins, S. Y.; Cavell, K. J.; Hoare, J. L.; Skelton, B. W.; Sobolev, A. N.; White, A. H.; Keim, W. Single Component N-O Chelated Arylnickel(II) Complexes as Ethene Polymerisation and CO/Ethene Copolymerisation Catalysts. Examples of Ligand Induced Changes to the Reaction Pathway. *Journal of Organometallic Chemistry* **1997**, *544*, 163–174.

(160) Connon, S. J.; Hegarty, A. F. Stabilised 2,3-Pyridyne Reactive Intermediates of Exceptional Dienophilicity. *Eur. J. Org. Chem.* **2004**, *2004*, 3477–3483.

(161) Andersson, H.; Sainte-Luce Banchelin, T.; Das, S.; Olsson, R.; Almqvist, F. Efficient, Mild and Completely Regioselective Synthesis of Substituted Pyridines. *Chem. Commun.* **2010**, *46*, 3384–3.

(162) van Bergen, T. J.; Kellogg, R. M. Reactions of Aryl Grignard Reagents with Pyridine 1-Oxide. the Structure of the Addition Products. *J. Org. Chem.* **1971**, *36*, 1705–1708.

(163) Sieburth, S. M.; Lin, C.-H.; Rucando, D. Selective Intermolecular Photo-[4 + 4]-Cycloaddition with 2-Pyridone Mixtures. 2. Preparation of (1α,2β,5β,6α)-3-Butyl- 9-Methoxy-3,7-Diazatricyclo[4.2.2.2 2,5]Dodeca-9,11-Diene-4,8-Dione. *J. Org. Chem.* **1999**, *64*, 950–953.

(164) Yang, J.; Liu, S.; Zheng, J.-F.; Zhou, J. S. Room-Temperature Suzuki-Miyaura Coupling of Heteroaryl Chlorides and Tosylates. *Eur. J. Org. Chem.* **2012**, *2012*, 6248–6259.

(165) Soni, A.; Dutt, A.; Sattigeri, V.; Cliffe, I. A. Efficient and Selective

Demethylation of Heteroaryl Methyl Ethers in the Presence of Aryl Methyl Ethers. *Synthetic Communications* **2011**, *41*, 1852–1857.

(166) Liao, S.-M.; Du, Q.-S.; Meng, J.-Z.; Pang, Z.-W.; Huang, R.-B. The Multiple Roles of Histidine in Protein Interactions. *Chemistry Central Journal* **2013**, *7*, 1–12.

(167) Wheeler, S. E.; Bloom, J. W. G. Toward a More Complete Understanding of Noncovalent Interactions Involving Aromatic Rings. *J. Phys. Chem. A* **2014**, *118*, 6133–6147.

(168) Sörme, P.; Arnoux, P.; Kahl-Knutsson, B.; Leffler, H.; Rini, J. M.; Nilsson, U. J. Structural and Thermodynamic Studies on Cation−Π Interactions in Lectin−Ligand Complexes: High-Affinity Galectin-3 Inhibitors Through Fine-Tuning of an Arginine−Arene Interaction. *J. Am. Chem. Soc.* **2005**, *127*, 1737–1743.

(169) Meyer, E. A.; Castellano, R. K.; Diederich, F. Interactions with Aromatic Rings in Chemical and Biological Recognition. *Angew. Chem. Int. Ed.* **2003**, *42*, 1210–1250.

(170) Churchill, C. D. M.; Wetmore, S. D. Noncovalent Interactions Involving Histidine: the Effect of Charge on Π−Π Stacking and T-Shaped Interactions with the DNA Nucleobases. *J. Phys. Chem. B* **2009**, *113*, 16046–16058.

(171) Middleton, D. J. 2004; Vol. 9, pp 89–142.

(172) Lim, K.-H.; Hiraku, O.; Komiyama, K.; Koyano, T.; Hayashi, M.; Kam, T.-S.; Zhou, H.; Hua, Z.; He, H.-P.; Kong, N.-C.; Liu, X.-D.; Wang, Y.-H.; Hao, X.-J. Biologically Active Indole Alkaloids From Kopsia Arborea. *Helvetica Chimica Acta* **2007**, *70*, 1302–1307.

(173) Zhou, H.; He, H. P.; Kong, N. C.; Wang, Y. H. Three New Indole Alkaloids From the Leaves of Kopsia Officinalis. *Helvetica chimica ...* **2006**.

(174) Kam, T.-S.; Sim, K.-M.; Koyano, T.; Komiyama, K. Leishmanicidal Alkaloids From *Kopsia Griffithii*. *Phytochemistry* **1999**, *50*, 75–79.

(175) Tan, M. J.; Yin, C.; Tang, C. P.; Ke, C. Q.; Lin, G.; Ye, Y. *Antitussive Indole Alkaloids From Kopsia Hainanensis*; 2011; Vol. 77, pp 939–944.

(176) Wong, S.-P.; Gan, C.-Y.; Lim, K.-H.; Ting, K.-N.; Low, Y.-Y.; Kam, T.-S. Arboridinine, a Pentacyclic Indole Alkaloid with a New Cage Carbon–Nitrogen Skeleton Derived From a Pericine Precursor. *Org. Lett.* **2015**, *17*,

3628–3631.

(177) Diels, O.; Alder, K. Synthesen in Der Hydroaromatischen Reihe. *Justus Liebigs Annalen der Chemie* **1928**, *460*, 98–122.

(178) Nicolaou, K. C.; Snyder, S. A.; Montagnon, T.; Vassilikogiannakis, G. The Diels-Alder Reaction in Total Synthesis. *Angew. Chem. Int. Ed.* **2002**, *4*, 1668–1698.

(179) Juhl, M.; Tanner, D. Recent Applications of Intramolecular Diels-Alder Reactions to Natural Product Synthesis. *Chem. Soc. Rev.* **2009**, *38*, 2983–11.

(180) Takahashi, M.; Ishida, H.; Kohmoto, M. The Cycloaddition of 1,2,4,5-Tetrazines with Indoles. the Formation of 5*H*-Pyridazino[4,5-*B*]Indoles. *Bulletin of the Chemical Society of Japan* **1976**, *49*, 1725–1726.

(181) Raasch, M. S. Annelations with Tetrachlorothiophene 1,1-Dioxide. *J. Org. Chem.* **1980**, *45*, 856–867.

(182) Benson, S. C.; Palabrica, C. A.; Snyder, J. K. 5*H*-Pyridazine[4,5-*B*]Indoles as Cycloadducts with 3,6-Dicarbomethoxy1,2,4,5-Tetrazine. *J. Org. Chem.* **1987**, *52*, 4610–4614.

(183) Bäckvall, J. E.; Plobeck, N. A. New Synthesis of the 6*H*-Pyrido-[4,3-*B*]Carbazoles Ellipticine and Olivacine via Cycloaddition of 2-Phenylsulfonyl 1,3-Dienes to Indoles. *J. Org. Chem.* **1990**, *55*, 4528–4531.

(184) Gieseler, A.; Steckhan, E.; Wiest, O.; Knoch, F. Photochemically Induced Radical Cation Diels-Alder Reactions Fo Indole and Electron-Rich Dienes. *J. Org. Chem.* **1991**, *56*, 1405–1411.

(185) Bodwell, G. J.; Li, J. Concise Synthesis and Transannular Inverse Electron Demand Diels-Alder Reaction of [3](3,6)Pyridazino[3](1,3)Indolophane. Rapid Access to a Pentacyclic Indoloid System. **2017**, 1–4.

(186) Wenkert, E.; Moeller, P. D. R.; Piettre, S. R. Five-Membered Aromatic Heterocycles as Dienophiles in Diels-Alder Reactions. Furan, Pyrrole, and Indole. *J. Am. Chem. Soc.* **1988**, *110*, 7188–7194.

(187) Dauben, W. G.; Kozikowski, A. P. Organic Reactions at High Pressure. Cycloadditions of Enamines and Dienamines. *J. Am. Chem. Soc.* **1974**, *96*, 3664–3666.

(188) Walling, C.; Schugar, H. J. Organic Reactions Under High Pressure. VII. Volumes of Activation for Some Diels-Alder Reactions. *J. Am. Chem. Soc.* **1963**, *85*, 607–612.

(189) Biolatto, B.; Kneeteman, M.; Paredes, E.; Mancini, P. M. E. Reactions of 1-Tosyl-3-Substituted Indoles with Conjugated Dienes Under Thermal and/or High-Pressure Conditions. *J. Org. Chem.* **2001**, *66*, 3906–3912.

(190) Keana, J. F. W.; Eckler, P. E. A New Furan and Dihydro-4-Pyrone Synthesis via Diels-Alder Reactions Between MEthyl 2-[2'-Acetamido-4'(1"*H)*-Pyrimidon-6-"Yl]Glyoxylate and Diethyl Oxomalonate and Oxygenated 1,3-Dienes. **2017**, 1–5.

(191) Sano, T.; Toda, J.; Kashiwaba, N.; Ohshima, T.; Tsuda, Y. Synthesis of *Erythrina* And Related Alkaloids. XVI. Diels-Alder Approach: Total Synthesis of *Di*-Erysotrine, *Di*-Erythraline, *Di*-Erysotramidine, *Di*-8-Oxoerythraline and Their 3-Epimers. *Chem. Pharm. Bull.* **1987**, *35*, 479–500.

(192) Chrétien, A.; Chataigner, I.; L'Hélia, N.; Piettre, S. R. Complete and Remarkable Reversal of Chemoselectivity in [4 + 2] Cycloadditions Involving Electron-Poor Indoles as Dienophiles. Diels−Alder Versus Hetero-Diels−Alder Processes. *J. Org. Chem.* **2003**, *68*, 7990–8002.

(193) Chu, U. B.; Vorperian, S. K.; Satyshur, K.; Eickstaedt, K.; Cozzi, N. V.; Mavlyutov, T.; Hajipour, A. R.; Ruoho, A. E. Noncompetitive Inhibition of Indolethylamine- N-Methyltransferase by N, N-Dimethyltryptamine and N, N-Dimethylaminopropyltryptamine. *Biochemistry* **2014**, *53*, 2956–2965.

(194) Speeter, M. E.; Anthony, W. C. The Action of Oxalyl Chloride on Indoles - a New Approach to Tryptamines. *J. Am. Chem. Soc.* **1954**, *76*, 6208–6210.

(195) Pérez, E. G.; Cassels, B. K.; Eibl, C.; Gündisch, D. Synthesis and Evaluation of N1-Alkylindole-3-Ylalkylammonium Compounds as Nicotinic Acetylcholine Receptor Ligands. *Bioorg. Med. Chem.* **2012**, *20*, 3719–3727.

(196) Cheng, Y.-S.; Liu, W.-L.; Chen, S.-H. Pyridinium Chlorochromate Adsorbed on Alumina as a Selective Oxidant for Primary and Secondary Alcohols. *Synthesis* **1980**, *1980*, 223–224.

(197) Yamamoto, Y.; Yamamoto, H. Catalytic Asymmetric Nitroso-Diels-Alder Reaction with Acyclic Dienes. *Angew. Chem. Int. Ed.* **2005**, *44*, 7082–7085.

(198) Lidström, P.; Tierney, J.; Wathey, B.; Westman, J. Microwave Assisted

Organic Synthesis - a Review. *Tetrahedron* **2001**, *57*, 9225–9283.

(199) Pindur, U.; Lutz, G.; Otto, C. Acceleration and Selectivity Enhancement of Diels-Alder Reactions by Special and Catalytic Methods. *Chem. Rev.* **1993**, *93*, 741–761.

(200) Rideout, D. C.; Breslow, R. Hydrophobic Acceleration of Diels-Alder Reactions. *J. Am. Chem. Soc.* **1980**, *102*, 7817–7818.

(201) Kagan, H. B.; Riant, O. Catalytic Asymmetric Diels-Alder Reactions. *Chem. Rev.* **1992**, *92*, 1007–1019.

(202) Fringuelli, F.; Piermatti, O.; Pizzo, F.; Vaccaro, L. Recent Advances in Lewis Acid Catalyzed Diels-Alder Reactions in Aqueous Media. *Eur. J. Org. Chem.* **2001**, 439–455.

(203) Szczésniak, P.; Stecko, S.; Maziarz, E. B.; Staszewska-Krajewska, O.; Furman, B. O. Synthesis of Polyhydroxylated Quinolizidine and Indolizidine Scaffolds From Sugar-Derived Lactams via a One-Pot Reduction/Mannich/Michael Sequence. *J. Org. Chem.* **2014**, *79*, 10487–10503.

(204) Sundberg, R. J. Electrophilic Substitution Reactions of Indoles. In *Heterocyclic Scaffolds II:*; Topics in Heterocyclic Chemistry; Springer Berlin Heidelberg: Berlin, Heidelberg, 2010; Vol. 26, pp 47–115.

(205) Liu, K. G.; Robichaud, A. J.; Lo, J. R.; Mattes, J. F.; Cai, Y. Rearrangement of 3,3-Disubstituted Indolenines and Synthesis of 2,3-Substituted Indoles. *Org. Lett.* **2006**, *8*, 5769–5771.

(206) Pictet, A.; Spengler, T. Über Die Bildung Von Isochinolin-Derivaten Durch Einwirkung Von Methylal Auf Phenyl-Äthylamin, Phenyl-Alanin Und Tyrosin. *Berichte der deutschen chemischen Gesellschaft* **1911**, *44*, 2030–2036.

(207) Marsden, S. P.; Depew, K. M.; Danishefsky, S. J. Stereoselective Total Syntheses of Amauromine and 5-*N*-Acetylardeemin. a Concise Route to the Family of "Reverse Prenylated" Hexahydropyrroloindole Alkaloids. *J. Am. Chem. Soc.* **1994**, *116*, 11143–11144.

(208) He, F.; Bo, Y.; Altom, J. D.; Corey, E. J. Enantioselective Total Synthesis of Aspidophytine. *J. Am. Chem. Soc.* **1999**, *121*, 6771–6772.

(209) Cheng, D.-J.; Tian, S.-K. A Highly Enantioselective Catalytic Mannich Reaction of Indolenines with Ketones. *Adv. Synth. Catal.* **2013**, *355*, 1715–1718.

(210) Dhankher, P.; Benhamou, L.; Sheppard, T. D. Rapid Assembly of Functionalised Spirocyclic Indolines by Palladium-Catalysed Dearomatising Diallylation of Indoles with Allyl Acetate. *Chem. Eur. J.* **2014**, *20*, 13375–13381.

(211) Shao, Y.-D.; Tian, S.-K. A Highly Enantioselective Catalytic Strecker Reaction of Cyclic (Z)-Aldimines. *Chem. Commun.* **2012**, *48*, 4899–3.

(212) Moriyama, K.; Sugiue, T.; Saito, Y.; Katsuta, S.; Togo, H. 2,6-Bis(Amido)Benzoic Acid with Internal Hydrogen Bond as Brønsted Acid Catalyst for Friedel-Crafts Reaction of Indoles. *Adv. Synth. Catal.* **2015**, *357*, 2143–2149.

(213) Garnick, R. L.; Levery, S. B.; Le Quesne, P. W. Addition and Annulation Reactions Between Indoles and a,B-Unsaturated Ketones. *J. Org. Chem.* **1978**, *43*, 1226–1229.

(214) Austin, J. F.; Kim, S.-G.; Sinz, C. J.; Xiao, W.-J.; MacMillan, D. W. C. Enantioselective Organocatalytic Construction of Pyrroloindolines by a Cascade Addition–Cyclization Strategy: Synthesis of (–)-Flustramine B. *Proc. Natl. Acad. Sci. USA* **2004**, *101*, 5482–5487.

(215) Lucarini, S.; Bartoccini, F.; Battistoni, F.; Diamantini, G.; Piersanti, G.; Righi, M.; Spadoni, G. A Novel One-Pot Approach of Hexahydropyrrolo[2,3-*B*]Indole Nucleus by a Cascade Addition/Cyclization Strategy: Synthesis of (±)-Esermethole. *Org. Lett.* **2010**, *12*, 3844–3847.

(216) Cai, Q.; Zheng, C.; Zhang, J.-W.; You, S.-L. Enantioselective Michael/Mannich Polycyclization Cascade of Indolyl Enones Catalyzed by Quinine-Derived Primary Amines. *Angew. Chem. Int. Ed.* **2011**, *50*, 8665–8669.

(217) Zhang, Z.-W.; Yang, J. Synthesis of the Polycyclic Core of Vincorine via Cascade Reactions. *Tetrahedron Lett.* **2014**, *55*, 761–763.

(218) Turet, L.; Markó, I. E.; Tinant, B.; Declercq, J.-P.; Touillaux, R. Novel Anionic Polycyclisation Cascade. Highly Stereocontrolled Assembly of Functionalised Tetracycles Akin to the Middle Core of the Manzamines. *Tetrahedron Lett.* **2002**, *43*, 6591–6595.

(219) Heureux, N.; Wouters, J.; Mark, I. N. E. Sequential Acid/Base-Catalyzed Polycyclization of Tryptamine Derivatives. a Rapid Access to B?Chi's Ketone ? *Org. Lett.* **2005**, *7*, 5245–5248.

(220) Zuo, Z.; Xie, W.; Ma, D. Total Synthesis and Absolute Stereochemical Assignment of (–)-Communesin F. *J. Am. Chem. Soc.* **2010**, *132*, 13226–13228.

(221) Feldman, K. S.; Ngernmeesri, P. Dragmacidin E Synthesis Studies. Preparation of a Model Heptacyclic Core Structure. *Org. Lett.* **2010**, *12*, 4502–4505.

(222) Yadav, V. K.; Kapoor, K. K. $Al_2O3$ Supported KF: an Efficient Mediator in the Epoxidation of Electron Deficient Alkenes with T-BuOOH. *Tetrahedron Lett.* **1994**, *35*, 9481–9484.

(223) Schwalm, C. S.; Ceschi, M. A.; Russowsky, D. Metal Halide Hydrates as Lewis Acid Catalysis for the Conjugated Friedel-Crafts Reactions of Indoles and Activated Olefins. *Journal of the Brazilian Chemical Society* **2011**, *22*, 623–636.

(224) Kagawa, N.; Malerich, J. P.; Rawal, V. H. Palladium-Catalyzed B-Allylation of 2,3-Disubstituted Indoles. *Org. Lett.* **2008**, *10*, 2381–2384.

(225) Myslinski, J. *Design, Synthesis, and Calorimetric Studies on Protein-Ligand Interactions: Apolar Surface Area, Conformational Constraints, and Cation-Π Interactions*; Ph.D. Dissertation, University of Texas at Austin, 2013; pp 1–305.

(226) Krishnamurthy, V. M.; Bohall, B. R.; Semetey, V.; Whitesides, G. M. The Paradoxical Thermodynamic Basis for the Interaction of Ethylene Glycol, Glycine, and Sarcosine Chains with Bovine Carbonic Anhydrase II: an Unexpected Manifestation of Enthalpy/Entropy Compensation. *J. Am. Chem. Soc.* **2006**, *128*, 5802–5812.

(227) Lin, H.-S.; Paquette, L. A. A Convenient Method for Determining the Concentration of Grignard Reagents. *Synthetic Communications* **1994**, *24*, 2503–2506.